Advanced bronchoscopic techniques for diagnosing interstitial lung disease



KIRSTEN KALVERDA

Stellingen behorende bij het proefschrift

Advanced bronchoscopic techniques for diagnosing interstitial lung disease

1. In patients suspected of sarcoidosis stage I/II, intrathoracic lymphnode sampling with the EBUS scope can be performed trans- esophageal or bronchial with similar granuloma detection rate. (this thesis)

2. Starting lung tissue sampling for ILD diagnosis with transbronchial cryobiopsy leads to similar diagnostic yield but less pain, in hospital stay and serious adverse events over immediate surgical lung biopsy. (this thesis)

3. Transbronchial cryobiopsy as the initial tissue sampling test for ILD diagnosis reduces healthcare costs by half over immediate surgical lung biopsy. (this thesis)

4. Interobserver agreement for ILD histopathological pattern of lung biopsies is similar for both transbronchial cryobiopsies and surgical lung biopsies. (this thesis)

5. Endobronchial PS-OCT enables quantification of fibrotic changes in ILD patients. (this thesis)

6. Endobronchial CLE is feasible and safe in mechanically ventilated patients with respiratory failure. (this thesis)

7. HHG microscopy of transbronchial cryobiopsies allows for rapid recognition of adequate tissue samples, with a sensitivity of 86.1%. (this thesis)

8. The whole is greater than the sum of its parts. (Aristotle)

9. Take a walk on the wild side. (Lou Reed)

10. Keep your heels, head and standards high. (Coco Chanel)

Kirsten Kalverda
Amsterdam, 8 juni 2026

Advanced bronchoscopic techniques for diagnosing interstitial lung disease

Kirsten Alexandra Kalverda

© copyright Kirsten Kalverda, 2026

Printing: ProefschriftMaken || www.proefschriftmaken.nl
Cover Design: Erwin Timmerman || DTPservice

ISBN 978 94 6534 443 0

All rights reserved. No part of this publication may be reproduced, stored in a retrieval system or transmitted, in any form or by any means, electronic, mechanical, photocopying, recording or otherwise, without prior permission of the author or the copyright-owning journals for previous published chapters.

Financial support for the publication of this thesis is provided by:
Educontent BV
Amsterdam UMC
Boehringer Ingelheim
Chiesi
Erbe
Chipsoft

Advanced bronchoscopic techniques for diagnosing interstitial lung disease

ACADEMISCH PROEFSCHRIFT

ter verkrijging van de graad van doctor
aan de Universiteit van Amsterdam
op gezag van de Rector Magnificus
prof. dr. ir. P.P.C.C. Verbeek
ten overstaan van een door het College voor Promoties ingestelde commissie,
in het openbaar te verdedigen in de Agnietenkapel
op maandag 8 juni 2026, te 16.00 uur

door Kirsten Alexandra Kalverda
geboren te UTRECHT

Promotiecommissie

Promotor:	prof. dr. J.T. Annema	AMC-UvA
Co-promotor:	dr. P.I. Bonta	AMC-UvA
Overige leden:	dr. S. Tomassetti	University of Florence
	prof. dr. M.S. Wijsenbeek-Lourens	Erasmus Universiteit
	prof. dr. J. Braun	Universiteit Leiden
	prof. dr. A.G.J.M. van Leeuwen	AMC-UvA
	prof. dr. O.M. van Delden	AMC-UvA
	prof. dr. M.J. Schultz	AMC-UvA

Faculteit der Geneeskunde

TABLE OF CONTENT

Introduction

Chapter 1	General introduction and outline of the thesis	9
Part I	**Bronchoscopic sampling techniques for diagnosing interstitial lung disease**	29
Chapter 2	Crombag LMM, **Kalverda KA,** Szlubowski A, Gnass M, Tournoy KG, Sun J, Oki M, Ninaber MK, Steinfort DP, Jennings BR, Liberman M, Bilaceroglu S, Bonta PI, Korevaar DA, Trisolini R, Annema JT. EBUS versus EUS-B for diagnosing sarcoidosis: The International Sarcoidosis Assessment (ISA) randomized clinical trial. Respirology 2022 Feb;27(2):152-160.	31
Chapter 3	**Kalverda KA**, Ninaber MK, Wijmans L, von der Thüsen J, Jonkers RE, Daniels JM, Miedema JR, Dickhoff C, Hölters J, Heineman D, Kant M, Radonic T, Shahin G, Cohen D, Boerrigter B, Nijman S, Nossent E, Braun J, Mathot B, Poletti V, Hetzel J, Dijkgraaf M, Korevaar DA, Bonta PI, Annema JT. Transbronchial cryobiopsy followed by as-needed surgical lung biopsy versus immediate surgical lung biopsy for diagnosing interstitial lung disease (the COLD study): a randomised controlled trial. Lancet Respir Med. 2024 Jul;12(7):513-522	53
Chapter 4	**Kalverda KA**, M van Barreveld, PI Bonta, J Daniels, C Dickhoff, DA Korevaar, JT Annema, MG Dijkgraaf. Transbronchial cryobiopsy followed by as-needed surgical lung biopsy versus immediate surgical lung biopsy for diagnosing interstitial lung disease; a cost utility analysis. ERJ Open Research. 2026;12(1):00629–2025.	83
Part II	**Bronchoscopic imaging techniques for the assessment of interstitial lung disease and ARDS**	107
Chapter 5	**Kalverda KA**, Goorsenberg A, Annema J, Bonta P. Advances in Optical Coherence Tomography and Confocal Laser Endomicroscopy in Pulmonary Diseases. Respiration 2020;99(3):190-205	109

Chapter 6	**Kalverda KA,** Vaselli M, Thunnissen E, Tanck MWT, Mets OM, van den Berk IAH, Annema JT, Bonta PI, de Boer JF. In vivo polarisation sensitive optical coherence tomography for fibrosis assessment in interstitial lung disease: a prospective, exploratory, observational study. BMJ Open Respir Res. 2023 Aug;10(1):e001628	143
Chapter 7	**Kalverda KA,** Vaselli M, Wijmans L, de Bruin DM, Jonkers RE, Poletti V, de Boer J, Annema JT, Bonta PI. Endobronchial Optical Coherence Tomography: Shining New Light on Diagnosing Usual Interstitial Pneumonitis? Am J Respir Crit Care Med. 2022 Apr 15;205(8):967-968	177
Chapter 8	**Kirsten A Kalverda**, Lizzy Wijmans, Lieuwe D.J. Bos, Mary R. Smit, Inge A.H. van de Berk, Daniel M. de Bruin, Paul Bloemen, Teodora Radonic, Marcus J. Schultz, Peter I. Bonta, Jouke T. Annema. Confocal laser endomicroscopy in patients with acute respiratory failure. Submitted for publication	183
Part III	**Novel imaging technique for rapid assessment of lung tissue in interstitial lung disease**	207
Chapter 9	**KA Kalverda**, LMG van Huizen, J von der Thüsen, V Poletti, T Radonic, C Dickhoff, JMA Daniels, PI Bonta, JT Annema, ML Groot. Rapid on-site histology of lung biopsies in ILD using higher harmonic generation microscopy: a proof of concept and image atlas. Submitted for publication	209
Chapter 10	**Kalverda KA,** van Huizen LMG, von der Thüsen J, Poletti V, Radonic T, Dickhoff C, Daniels JMA, Bonta PI, Annema JT, Groot ML. Rapid On-Site Evaluation of Cryobiopsies in Interstitial Lung Disease Using Higher Harmonic Generation Microscopy. Am J Respir Crit Care Med. 2025 Oct;211(10):1876-1879	235
Chapter 11	van Huizen LMG, **Kalverda KA,** Bugiani M, Poletti V, Bonta PI, Annema JT, Groot ML. Rapid On-Site Pathology Visualization of COVID-19 Characteristics Using Higher Harmonic Generation Microscopy. Am J Respir Crit Care Med. 2023 Jul 15;208(2):199-200	245

Part IV **Discussion** 251

Chapter 12 General discussion 253

Chapter 13 English summary 273

Chapter 14 Nederlandse samenvatting 279

Appendices 285

PhD portfolio

Curriculum vitae

Dankwoord

Chapter 1

General introduction

GENERAL INTRODUCTION

This thesis evolves on bronchoscopic techniques within the diagnostic pathway for interstitial lung disease (ILD). ILDs comprise a heterogeneous group of more than 100 diffuse parenchymal lung disorders that can present with overlapping symptoms, imaging abnormalities, and physiological impairment, yet different ILD subtypes may require distinct treatments and carry markedly different prognoses (1, 2). This thesis focuses on three complementary approaches to improve bronchoscopic diagnostics in patients with suspected ILD: (1) optimizing bronchoscopic sampling strategies when tissue is required; (2) investigating bronchoscopic imaging techniques that provide tissue specific information in vivo; and (3) exploring ex vivo imaging of lung biopsy specimens to provide immediate feedback on sample representativeness and complement routine histopathology.

INTERSTITIAL LUNG DISEASE

ILD is not a single disease entity but refers to a broad category of over 200 disorders characterized by inflammation, fibrosis or both, of the lung parenchyma. This leads to impaired gas exchange, which results in dyspnea, reduced exercise capability and quality of life. Prognosis vary across ILDs, but not rarely ILD leads to respiratory failure and ultimately death (3). Although many ILDs are individually rare, ILD as a group is common, with an estimated 3,500–5,000 new cases annually in the Netherlands, and incidence is rising (4-6). Sarcoidosis is the most common of interstitial lung diseases. It is a systemic disorder that can involve virtually any organ, but most frequently affects the lungs; when the lung parenchyma is involved, sarcoidosis is classified as an ILD (7). Other ILDs include idiopathic ILD (i.e. idiopathic pulmonary fibrosis and idiopathic nonspecific interstitial pneumonia), auto-immune related ILD (i.e. connective tissue disease associated ILD), exposure related ILD (i.e. drug induced ILD, hypersensitivity pneumonitis), ILD with cysts or airspace filling (i.e. Langerhans cell histiocytosis, pulmonary alveolar proteinosis) and some others such as eosinophilic pneumonia (3).

The importance of early and precise diagnosis is fundamental given the variation in treatment strategies and prognosis between the different ILD subtypes. Correct and effective classification can guide specific treatments, such as immunosuppression for certain inflammatory forms or

antifibrotic strategies for progressive fibrosis(1, 8). Over the past decade, the therapeutic landscape for ILD has evolved substantially, particularly for progressive fibrosing phenotypes. Two antifibrotic agents, Nintedanib and Pirfenidone, originally approved for idiopathic pulmonary fibrosis (IPF), have become central to management by slowing the rate of lung function decline (9) (10, 11). While these drugs do not reverse fibrosis, they can substantially impact disease trajectory and quality of life, making timely and accurate phenotyping increasingly important. Moreover, with the introduction of a new antifibrotic agent (Nerandomilast) which is currently under evaluation by the European Medicines Agency (EMA) for registration, the need for precise patient identification becomes even more critical (12, 13). As these medications require specialized care and are expensive, ensuring the correct patient selection for these treatments is a clinical and economic priority.

However, diagnosing ILD can be challenging due to the overlapping clinical symptoms and radiological features among subtypes. No single test serves as a gold standard for diagnosis. Instead, accurate diagnosis relies on integrating clinical data, including medical history, laboratory tests, high-resolution computed tomography (HRCT), bronchoalveolar lavage (BAL), and, in some cases, lung biopsy. This multidisciplinary approach involves input from at least pulmonologists, thoracic radiologists, and pathologists specialized in ILD (8, 14).

Although HRCT plays a central role in the initial evaluation of suspected ILD, it has limitations. Radiological patterns on HRCT are sometimes unclassifiable, or different ILD subtypes may present with similar CT patterns, complicating the diagnostic process. Additionally, HRCT may have reduced sensitivity for detecting early fibrosis. It has been estimated that in 10–40% of newly diagnosed cases, a lung biopsy may be necessary to further confirm the diagnosis, especially when radiological and clinical findings are insufficiently clear (15–18). However, biopsies are invasive and are only performed in selected cases due to the associated risks. This highlights the need for more refined and less invasive diagnostic tools, which are further explored in this thesis.

When lung tissue is deemed necessary, the optimal approach depends on the suspected disease and procedural risk. In stage I–II pulmonary sarcoidosis, mediastinal and hilar lymph nodes provide an accessible target. Diagnostic sampling of lymph nodes has shifted to minimally

invasive endosonography, which is now recommended in international guidelines(19).

Yet, endosonography can be performed via a transbronchial (EBUS) or transesophageal (EUS-B) route, and the preferred approach remains debated in terms of practicality and performance. In other ILDs, surgical lung biopsy is considered the reference standard when histology is indicated, but transbronchial lung cryobiopsy has emerged as a less invasive technique and is now used in selected cases(8, 20, 21). Nevertheless, uncertainty towards transbronchial cryobiopsy persists regarding the balance between diagnostic yield, safety, and resource use remains a key challenge, particularly in vulnerable ILD populations.

ADULT RESPIRATORY DISTRESS SYNDROME (ARDS)

Acute respiratory distress syndrome (ARDS) is a clinical syndrome of acute, diffuse, inflammatory lung injury (direct or indirect) that results in hypoxemic respiratory failure and bilateral opacities on chest imaging not fully explained by cardiac failure or fluid overload (22). ARDS is not typically classified within the interstitial lung diseases (ILDs). However it can be viewed pathobiologically as an acute diffuse parenchymal lung disease, because the injury involves the alveolar–capillary unit with interstitial and intra-alveolar damage. The histopathological pattern most strongly associated with ARDS is diffuse alveolar damage (DAD), often described as its histopathological hallmark. Importantly, DAD is also the defining histopathologic pattern of what has historically been called acute interstitial pneumonia (AIP) in the idiopathic interstitial pneumonias. In the recent ERS/ATS update, AIP is explicitly renamed by the term "idiopathic diffuse alveolar damage" to reflect the underlying pathology more precisely(1). The shared histopathologic substrate (DAD) in both ARDS (typically with an identifiable precipitating insult) and idiopathic DAD (by definition without one) underscores that the distinction between these entities depends largely on clinical context rather than histology alone.

ARDS is a frequent cause of respiratory failure in the ICU. Among mechanically ventilated ICU patients, approximately one in four meets the criteria for ARDS, and outcomes remain poor, with an in-hospital mortality of around 40%(23) . Efforts are being made to identify clinically

meaningful ARDS phenotypes, because prognosis and treatment response may differ between subgroups. Phenotyping can be approached across multiple domains, including biological, radiological, and physiological characteristics (24). Histopathology is usually not incorporated into phenotyping because lung tissue is rarely obtained in these critically ill patients, given the risks associated with biopsy in this setting. However, since diffuse alveolar damage (DAD) is present in only ~50% of clinically defined ARDS cases, histologic heterogeneity may be clinically relevant(25). This is further supported by reports showing that lung biopsy can lead to changes in clinical management in a substantial proportion of cases(26). This suggest that histopathologic information could add value to ARDS phenotyping, but would likely need to be obtained through approaches other than conventional lung biopsy in the critically ill.

BRONCHOSCOPIC SAMPLING TECHNIQUES FOR DIAGNOSING ILD

Sarcoidosis and Endosonography for intrathoracic Lymph Node Sampling

Sarcoidosis is a multisystem granulomatous disease and is classified within the ILD spectrum as a granulomatous ILD. Pulmonary sarcoidosis frequently affects both the lungs and intrathoracic lymph nodes. Diagnosis relies on a compatible clinical-radiological presentation, blood biomarkers, non-caseating granulomas in tissue, and the exclusion of alternative granulomatous diseases. Histological confirmation is often required due to the nonspecific nature of symptoms and imaging findings (19). Confirmation of the presence of non-caseating granulomas typically requires tissue sampling, but biopsy sites in sarcoidosis are not always easily accessible. Given that over 90% of patients have pulmonary involvement, tissue is usually sampled from the thorax. Granulomas can be detected from different intra-thoracic sites using different bronchoscopic techniques: airway wall (mucosa biopsies); mediastinal and hilar lymphnodes (endosonography using needle aspiration or cryobiopsy) or lung parenchyma (transbronchial forceps or cryobiopsies) (19). Ultrasound-guided needle aspiration of lymphnodes is a endoscopic procedure in which the endoscope has an ultrasound probe at its distal tip, allowing real-time visualization of intrathoracic lymph nodes and needle guidance through the airway wall to obtain diagnostic material. It offers a sensitivity for diagnosing sarcoidosis of ~85% with minimal

complication risk, combining efficiency, accuracy, and safety in a single procedure (19, 27).

Ultrasound guided lymph node sampling can be performed via endobronchial ultrasound (EBUS)-TBNA or, alternatively, through transesophageal sampling using endoscopic ultrasound (EUS), with the latter referred to as EUS-B when the EBUS-scope is used. Even though some lymphnodes can only be sampled from the endobronchial route, it has been suggested that the sensitivity for diagnosing sarcoidosis through the esophageal route may be higher(27). **Chapter 2** addresses the clinical question of whether the sampling route (EUS-B versus EBUS) impacts granuloma detection rates in suspected sarcoidosis, considering that sampling from the esophagus may be better tolerated (e.g., avoiding coughing) and has a different reach (Figure 1). Additionally, **Chapter 2** evaluates the performance of two different needle designs, the standard baffle shaped for cytology vs a needle with a beveled side opening aiming for tissue cores, as cytological aspirates can be difficult to interpret, and larger tissue samples may improve diagnostic accuracy.

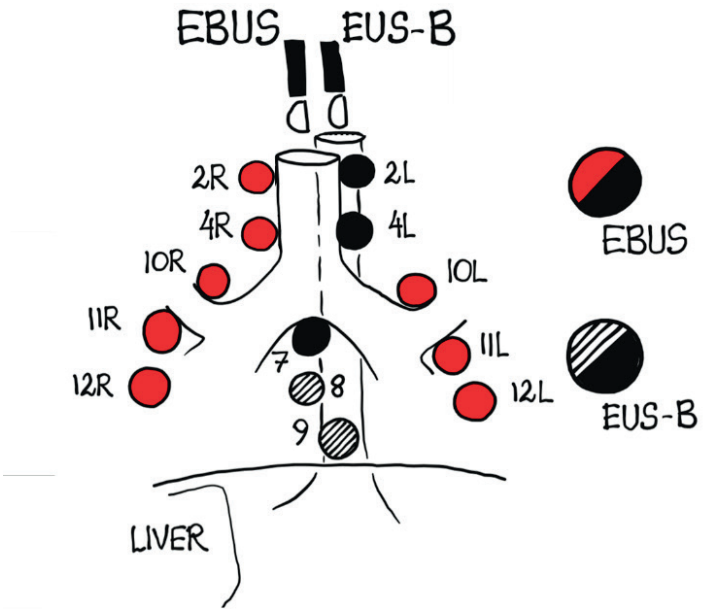


Figure 1. Schematic overview of mediastinal and hilar lymph node stations that can be sampled using endobronchial ultrasound (EBUS) or transoesophageal endoscopic ultrasound with the EBUS scope (EUS-B). Red (solid) indicates stations accessible only by EBUS; black (hatched) indicates stations accessible only by EUS-B; black (solid) indicates stations accessible by both techniques. (Adapted from images of P. Clementsen)

Transbronchial cryobiopsy for diagnosing ILD

In ILD, diagnosis is generally established in a multidisciplinary discussion (MDD), integrating clinical context, pulmonary physiology, serology, and HRCT, with lung biopsy reserved for selected cases in which non-invasive data do not allow a sufficiently confident classification. Although many ILD patients can be diagnosed without tissue, lung biopsy is still considered beneficial in an estimated 10–40% of newly evaluated ILD cases to secure the diagnosis or to increase diagnostic confidence when considering specific treatment decisions (15, 16, 28).

When tissue is required, surgical lung biopsy is considered the reference standard because of its high diagnostic yield. It is usually performed by video-assisted thoracoscopic surgery (VATS), but is associated with substantial morbidity, routine hospital admission with chest tube drainage, and a procedure-related mortality of approximately 2% (29, 30).

In transbronchial cryobiopsy, a flexible cryoprobe is advanced through the bronchoscope to the subpleural area of the lung. Brief freezing (typically 5–8 seconds) adheres surrounding tissue to the probe, after which the bronchoscope and probe are withdrawn '*en bloc*' to retrieve the specimen. Compared with conventional forceps biopsies, cryobiopsy specimens are larger and typically better preserve alveolar architecture. This can improve pathological interpretation by avoiding the alveolar collapse that is common in forceps-derived samples(31). Because ILD can be spatially heterogeneous, multiple biopsies from different segments are commonly obtained to reduce sampling error. The main complications are bleeding and pneumothorax, which may require chest tube drainage (32). Procedure related mortality is rare, but has been reported at 0.3% (33).

Considering the advantages of the transbronchial cryobiopsy procedure but recognizing its lower diagnostic yield, a clinical guideline from an European Respiratory Society Taskforce proposed a diagnostic step-up strategy. This step-up strategy means when tissue sampling in ILD is indicated, it is recommended to start with transbronchial cryobiopsy, and pursue for an additional surgical lung biopsy procedure when the cryobiopsy is insufficient informative for a classifying ILD diagnosis. However the supporting evidence for this diagnostic strategy was judged to be of very low quality and prospective comparisons across the full diagnostic pathway were lacking (32). To address this evidence gap, the COLD trial (**Chapter 3**) compared a step-up strategy with immediate surgical lung

biopsy, focusing on patient burden, length of hospital stay, and multidisciplinary diagnostic yield. In addition, implementation of the proposed step-up strategy also depends on whether it is an efficient use of healthcare resources at the pathway level. Therefore, **Chapter 4** complements the clinical trial by evaluating the cost–utility of the step-up strategy versus immediate surgical lung biopsy.

NOVEL IN-VIVO BRONCHOSCOPIC IMAGING TECHNIQUES

High-resolution CT provides an essential overview of the lungs, but its spatial resolution is limited to approximately 1mm and it cannot directly visualize microstructural changes at a histological level (34). In recent years, bronchoscopic optical imaging techniques have emerged that can provide real-time "in vivo microscopy" during a standard bronchoscopy, thereby bridging the gap between HRCT and tissue sampling. Optical coherence tomography (OCT) and confocal laser endomicroscopy (CLE) are two such techniques, offering complementary information at different imaging depths and resolutions(35, 36). **Chapter 5**, provides a thematic overview of OCT and CLE across pulmonary medicine, outlining their underlying principles, practical integration into conventional bronchoscopy, and potential clinical applications.

Optical coherence tomography

OCT uses near-infrared light to generate cross-sectional images of tissue microstructure, conceptually comparable to ultrasound but based on light rather than sound waves. Bronchoscopic endobronchial OCT (EB-OCT) is performed by advancing a thin, flexible OCT probe through the working channel of the bronchoscope towards the region of interest, after which adjacent cross-sectional images can be acquired during pullback and reconstructed into volumetric datasets. EB-OCT achieves a resolution in the order of 10–15 µm with an imaging depth of approximately 2–3 mm, enabling visualization of airway wall layers and peripheral lung microstructure (figure 2).

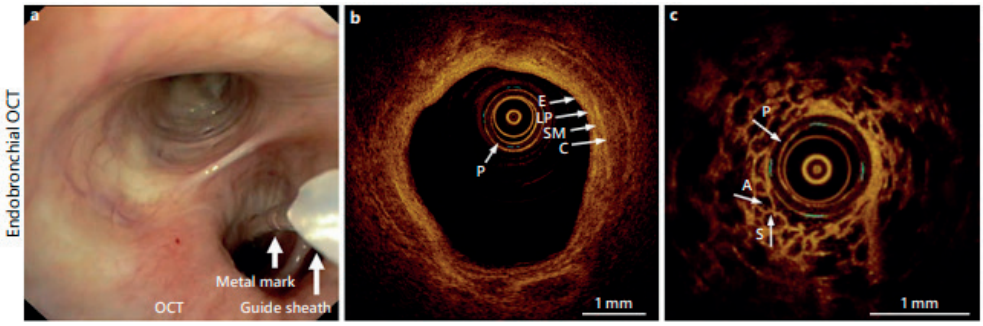


Figure 2. OCT imaging airway wall and alveolar compartment. A: Bronchoscopic view while the OCT probe is advanced through the guide sheath towards the right lower lobe. The metal mark on the probe is used to maintain a standard pullback of 5.4cm. B: OCT image of a normal segmental airway wall showing the OCT-probe (P) in the lumen of the airway, epithelium (E), lamina propria (LP), submucosa (SM) and cartilage(C) as different layers of the airwaywall. OCT image of the alveolar compartment showing normal alveoli(A) and septae (S). This image is adapted from Goorsenberg et al., Respiration 2020;99:190–205 (Chapter 5 in this thesis)

Polarization-sensitive EB-OCT

Polarization-sensitive OCT (PS-EB-OCT) extends conventional OCT by adding tissue-specific contrast based on birefringence. Birefringence is an optical property that is strongly associated with the presence of collagen, which in the healthy lung is a key structural component of the extracellular matrix in both the alveolar interstitium and the airway wall, including the connective tissue surrounding airway smooth muscle. In fibrotic lung disease, collagen accumulates as a hallmark of fibrotic remodeling, providing a biological rationale for PS-EB-OCT to detect increased birefringence in ILD. Endobronchial PS-OCT (PS-EB-OCT) is performed in a similar bronchoscopic workflow as conventional OCT. In addition to detecting birefringent tissue, PS-EB-OCT can provide information on fiber orientation (optic axis), which may help characterize and differentiate birefringent microstructural patterns in the airway wall and distal lung parenchyma (37, 38).

Confocal laser endomicroscopy

Confocal laser endomicroscopy (CLE) is a fiber-optic imaging technique that can be performed during bronchoscopy to obtain real-time microscopic images. Similar to EB-OCT, a thin probe is advanced through the working channel of the bronchoscope and positioned at the site of interest. The probe illuminates tissue with laser light, most commonly at

488 nm, and detects the resulting autofluorescence signal, which in the distal lung predominantly comes from elastin(39). Because the alveolar scaffold is rich in elastin fibers, CLE enables in vivo visualization of alveolar architecture (40). In addition, auto fluorescent cellular elements, including inflammatory cells such as alveolar macrophages, may also be detected (41, 42). In pulmonary applications, CLE provides a lateral resolution of up to 3.5 µm, an imaging depth of up to 70 µm, and a field of view of up to 600 µm. CLE can be performed as probe-based CLE (pCLE), in which the probe is placed directly onto the target tissue, or as needle-based CLE (nCLE), in which the probe is introduced through the lumen of a needle to access targets such as lymph nodes or masses. In this thesis, only pCLE was used (Figure 3). In gastroenterology, nCLE is approved to characterize pancreatic cystic lesions by imaging the cyst wall in vivo. pCLE has also been applied during Endoscopic Retrograde Cholangiopancreatography to help characterize biliary strictures (43).

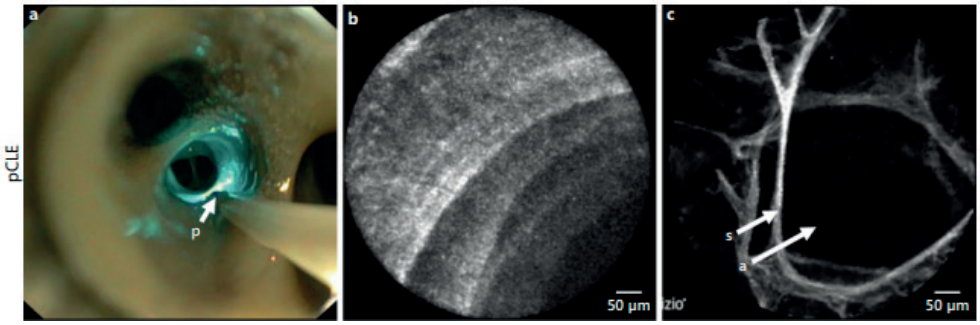


Figure 3. pCLE imaging procedure in vivo with images of the normal alveolar and airway wall compartment (a–c); A: bronchoscopic view of the CLE probe (P) and blue laser light at the tip. B: CLE image of the distal airway wall showing a helical ring-like pattern of the terminal bronchiole. C: CLE image of the alveolar compartment showing air-filled alveoli (a) and thin alveolar septae (s). This image is adapted from Goorsenberg et al., Respiration 2020;99:190–205 (Chapter 5 in this thesis)

Novel bronchoscopic imaging techniques in ILD and acute respiratory distress syndrome (ARDS)

HRCT is central to ILD assessment, but it cannot directly visualize microscopic changes at histological level. Specificity may be limited when radiological patterns overlap, are inconclusive or when early remodeling is subtle (34, 44, 45). Tissue sampling can add decisive information for ILD classification, but it is invasive. In ARDS, tissue acquisition is rarely feasible because lung biopsy procedures carry substantial risk in

mechanically ventilated patients. However, histopathologic findings in clinically defined ARDS are heterogeneous, suggesting that tissue-level information could add value to phenotyping. Moreover, when tissue is obtained, biopsy results have been reported to influence clinical management, indicating that histopathological information can be clinically informative (25, 46). Bronchoscopic optical imaging aims to fill this diagnostic gap by providing in vivo microscopic tissue specific information during routine bronchoscopy. In ILD, **Chapter 6** investigates whether in vivo EB-PS-OCT can detect and quantify fibrosis with histology as reference, and further explores whether OCT-derived microscopic features correspond to histopathological hallmarks. **Chapter 7** comments on (through correspondence) key requirements for EB-PS-OCT on clinical translation, including reproducible acquisition and probe positioning. In acute respiratory failure, **Chapter 8** assesses the feasibility and safety of bedside CLE in mechanically ventilated ICU patients and explores whether CLE can distinguish patterns of alveolar filling and architectural alteration. Together, these studies address how bronchoscopic tissue-level microscopic information may contribute to a more precise and less invasive diagnostic pathway in diffuse parenchymal lung disease.

NOVEL EX-VIVO IMAGING TECHNIQUE

Higher harmonic generation (HHG) microscopy

HHG microscopy is a laser-based imaging technique that can be used on fresh, unprocessed biopsy tissue. In practical terms: it allows on-site evaluation of histological tissue within minutes, without fixation, embedding, sectioning or staining. HHG combines three complementary optical signals that each highlight different tissue components: THG (third-harmonic generation) emphasizes cellular detail and tissue boundaries, SHG (second-harmonic generation) highlights collagen, and 2PEF (two-photon excited autofluorescence) visualizes auto- fluorescence in tissue, mostly elastin in the lung. After sampling, the biopsy is placed in a glass holder and inserted into the transportable microscope. The system scans the specimen and generates images rapidly (Figure 4). Because the microscope is transportable, it can be used not only in the lab, but also in the operating room or bronchoscopy suite. In a lung cancer cohort, HHG microscopy has shown to reliably visualize key parenchymal structures in both normal and diseased lung tissue(47). In **Chapter 9**, we introduce HHG microscopy as an ex vivo imaging approach for biopsies from ILD patients. We focus on whether the technique is

feasible and how HHG images relates to standard histology. Based on the speed of HHG microscopy and the ability to recognize important lung structures in biopsies, we then hypothesized that HHG could be used as a rapid on-site evaluation (ROSE)-like tool to judge whether a biopsy is adequate, similar to how ROSE is used in procedures that rely on cytology. This is the rationale for **Chapter 10**, where two pathologists assess transbronchial cryobiopsy adequacy using HHG images. Finally, **Chapter 11** explores HHG microscopy in post-mortem lung tissue from COVID-19-related ARDS, using the same rapid, label-free workflow enabled by the availability of autopsy material.

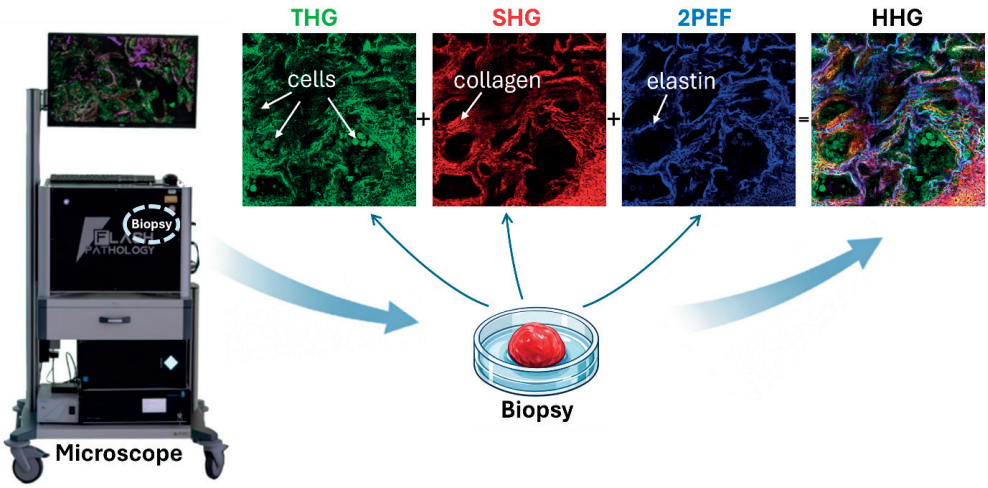


Figure 4. Higher harmonic generation (HHG) microscopy workflow. A freshly excised, unprocessed lung biopsy is placed in a glass sample holder and inserted into a transportable HHG microscope. The specimen is raster-scanned with a laser, producing three complementary imaging signals that are detected simultaneously: third-harmonic generation (THG; green), highlighting tissue interfaces and cellular morphology; second-harmonic generation (SHG; red), highlighting collagen; and two-photon excited autofluorescence (2PEF; blue), capturing autofluorescent signals, in lungs mostly elastin. The three channels are combined into a single composite HHG image, providing rapid, label-free visualization of tissue architecture and extracellular matrix components without fixation or staining. (Courtesy of L.M.G. van Huizen)

OUTLINE OF THIS THESIS

Aims and research questions of this thesis:

At the start of this PhD trajectory, several key questions regarding the bronchoscopic diagnosis and assessment of interstitial lung disease (ILD) remained unresolved. The overarching aim of this thesis was to evaluate how diagnostic bronchoscopic techniques, including novel imaging, can optimize the diagnostic work-up and assessment of parenchymal lung disorders, including ILD and ARDS. To this end, the thesis consists of three parts addressing the following research questions:

1. **Bronchoscopic sampling techniques for diagnosing ILD**

    - In patients undergoing diagnostic evaluation for sarcoidosis stage I/II, does the lymph node sampling approach: esophageal (EUS-B) versus tracheobronchial (EBUS) influence granuloma detection rate? (Chapter 2)

    - Does the use of a core biopsy needle (ProCore) compared with a standard 22G needle influence granuloma detection rates in mediastinal lymph node sampling for suspected sarcoidosis stage I/II? (Chapter 2)

    - In patients with suspected ILD in whom a lung biopsy is indicated, what is the optimal diagnostic strategy: transbronchial cryobiopsy followed by surgical lung biopsy when needed versus immediate surgical lung biopsy (Chapter 3)

    - Is a diagnostic strategy starting with transbronchial cryobiopsy cost-effective compared with immediate surgical lung biopsy? (Chapter 4)

2. **Bronchoscopic imaging techniques for the assessment of ILD and ARDS**

    - In patients with ILD, can bronchoscopic in vivo PS-OCT assess pulmonary fibrosis and characterize distinct microscopic imaging features relevant to ILD evaluation? (Chapter 6)

- In ICU patients with respiratory failure, is bronchoscopic CLE feasible and safe, and can it characterize patterns of alveolar filling and detect alterations in alveolar architecture (Chapter 8)

3. Novel imaging technique for rapid assessment of lung tissue in ILD

- Is HHG microscopy feasible for imaging fresh, unprocessed lung biopsies from ILD patients; can it identify ILD-relevant anatomical features that correlate with conventional histopathology; and what additional value might HHG provide beyond standard histopathological assessment? (Chapter 9)

- Can HHG microscopy assess the adequacy of transbronchial cryobiopsy specimens? (Chapter 10)

REFERENCES

1. Ryerson CJ, Adegunsoye A, Piciucchi S, Hariri LP, Khor YH, Wijsenbeek MS, et al. Update of the international multidisciplinary classification of the interstitial pneumonias: an ERS/ATS statement. Eur Respir J. 2025;66(6).
2. Travis WD, Costabel U, Hansell DM, King TE, Jr., Lynch DA, Nicholson AG, et al. An official American Thoracic Society/European Respiratory Society statement: Update of the international multidisciplinary classification of the idiopathic interstitial pneumonias. Am J Respir Crit Care Med. 2013;188(6):733–48.
3. Wijsenbeek M, Suzuki A, Maher TM. Interstitial lung diseases. Lancet. 2022;400(10354):769–86.
4. Duchemann B, Annesi-Maesano I, Jacobe de Naurois C, Sanyal S, Brillet PY, Brauner M, et al. Prevalence and incidence of interstitial lung diseases in a multi-ethnic county of Greater Paris. Eur Respir J. 2017;50(2).
5. Kaul B, Cottin V, Collard HR, Valenzuela C. Variability in Global Prevalence of Interstitial Lung Disease. Front Med (Lausanne). 2021;8:751181.
6. Maher TM, Bendstrup E, Dron L, Langley J, Smith G, Khalid JM, et al. Global incidence and prevalence of idiopathic pulmonary fibrosis. Respir Res. 2021;22(1):197.
7. Van Woensel J, Koopman B, Schiefer M, van Kan C, Janssen M, Ramiro S, et al. Organ involvement in newly diagnosed sarcoidosis patients in the Netherlands: The first large European multicentre prospective study. Respir Med. 2024;226:107608.
8. Raghu G, Remy-Jardin M, Richeldi L, Thomson CC, Inoue Y, Johkoh T, et al. Idiopathic Pulmonary Fibrosis (an Update) and Progressive Pulmonary Fibrosis in Adults: An Official ATS/ERS/JRS/ALAT Clinical Practice Guideline. Am J Respir Crit Care Med. 2022;205(9):e18–e47.
9. Richeldi L, du Bois RM, Raghu G, Azuma A, Brown KK, Costabel U, et al. Efficacy and safety of nintedanib in idiopathic pulmonary fibrosis. N Engl J Med. 2014;370(22):2071–82.
10. Noble PW, Albera C, Bradford WZ, Costabel U, Glassberg MK, Kardatzke D, et al. Pirfenidone in patients with idiopathic pulmonary fibrosis (CAPACITY): two randomised trials. Lancet. 2011;377(9779):1760–9.
11. Flaherty KR, Wells AU, Cottin V, Devaraj A, Walsh SLF, Inoue Y, et al. Nintedanib in Progressive Fibrosing Interstitial Lung Diseases. N Engl J Med. 2019;381(18):1718–27.
12. Maher TM, Assassi S, Azuma A, Cottin V, Hoffmann-Vold AM, Kreuter M, et al. Nerandomilast in Patients with Progressive Pulmonary Fibrosis. N Engl J Med. 2025;392(22):2203–14.
13. Richeldi L, Azuma A, Cottin V, Kreuter M, Maher TM, Martinez FJ, et al. Nerandomilast in Patients with Idiopathic Pulmonary Fibrosis. N Engl J Med. 2025;392(22):2193–202.
14. Cottin V, Hirani NA, Hotchkin DL, Nambiar AM, Ogura T, Otaola M, et al. Presentation, diagnosis and clinical course of the spectrum of progressive-fibrosing interstitial lung diseases. Eur Respir Rev. 2018;27(150).

15. Walsh SLF, Lederer DJ, Ryerson CJ, Kolb M, Maher TM, Nusser R, et al. Diagnostic Likelihood Thresholds That Define a Working Diagnosis of Idiopathic Pulmonary Fibrosis. Am J Respir Crit Care Med. 2019;200(9):1146–53.
16. Hetzel J, Wells AU, Costabel U, Colby TV, Walsh SLF, Verschakelen J, et al. Transbronchial cryobiopsy increases diagnostic confidence in interstitial lung disease: a prospective multicentre trial. Eur Respir J. 2020;56(6).
17. Poletti V, Ravaglia C, Gurioli C, Piciucchi S, Dubini A, Cavazza A, et al. Invasive diagnostic techniques in idiopathic interstitial pneumonias. Respirology. 2016;21(1):44–50.
18. Radu D, Freynet O, Kambouchner M, Boubaya M, Nunes H, Uzunhan Y, et al. Diagnosis Yield and Safety of Surgical Biopsy in Interstitial Lung Diseases: A Prospective Study. Ann Thorac Surg. 2022;114(5):1911–7.
19. Crouser ED, Maier LA, Wilson KC, Bonham CA, Morgenthau AS, Patterson KC, et al. Diagnosis and Detection of Sarcoidosis. An Official American Thoracic Society Clinical Practice Guideline. Am J Respir Crit Care Med. 2020;201(8):e26–e51.
20. Raghu G, Remy-Jardin M, Myers JL, Richeldi L, Ryerson CJ, Lederer DJ, et al. Diagnosis of Idiopathic Pulmonary Fibrosis. An Official ATS/ERS/JRS/ALAT Clinical Practice Guideline. Am J Respir Crit Care Med. 2018;198(5):e44–e68.
21. Raghu G, Remy-Jardin M, Ryerson CJ, Myers JL, Kreuter M, Vasakova M, et al. Diagnosis of Hypersensitivity Pneumonitis in Adults. An Official ATS/JRS/ALAT Clinical Practice Guideline. Am J Respir Crit Care Med. 2020;202(3):e36–e69.
22. Ranieri VM, Rubenfeld GD, Thompson BT, Ferguson ND, Caldwell E, Fan E, et al. Acute respiratory distress syndrome: the Berlin Definition. Jama. 2012;307(23):2526–33.
23. Bellani G, Laffey JG, Pham T, Fan E, Brochard L, Esteban A, et al. Epidemiology, Patterns of Care, and Mortality for Patients With Acute Respiratory Distress Syndrome in Intensive Care Units in 50 Countries. Jama. 2016;315(8):788–800.
24. Bos LDJ, Ware LB. Acute respiratory distress syndrome: causes, pathophysiology, and phenotypes. Lancet. 2022;400(10358):1145–56.
25. Thille AW, Penuelas O, Lorente JA, Fernandez-Segoviano P, Rodriguez JM, Aramburu JA, et al. Predictors of diffuse alveolar damage in patients with acute respiratory distress syndrome: a retrospective analysis of clinical autopsies. Crit Care. 2017;21(1):254.
26. Mir T, Regmi N, Saydain G, Kaul V, Soubani AO, Qureshi WT. Outcome and Post-Surgical Lung Biopsy Change in Management of ARDS: A Proportional Prevalence Meta-Analysis. Adv Respir Med. 2022;90(4):267–78.
27. von Bartheld MB, Dekkers OM, Szlubowski A, Eberhardt R, Herth FJ, in 't Veen JC, et al. Endosonography vs conventional bronchoscopy for the diagnosis of sarcoidosis: the GRANULOMA randomized clinical trial. Jama. 2013;309(23):2457–64.
28. Tomassetti S, Ravaglia C, Puglisi S, Ryu JH, Colby TV, Cavazza A, et al. Impact of Lung Biopsy Information on Treatment Strategy of Patients with Interstitial Lung Diseases. Ann Am Thorac Soc. 2022;19(5):737–45.

29. Hutchinson JP, McKeever TM, Fogarty AW, Navaratnam V, Hubbard RB. Surgical lung biopsy for the diagnosis of interstitial lung disease in England: 1997–2008. Eur Respir J. 2016;48(5):1453–61.
30. Fisher JH, Shapera S, To T, Marras TK, Gershon A, Dell S. Procedure volume and mortality after surgical lung biopsy in interstitial lung disease. Eur Respir J. 2019;53(2).
31. Ganganah O, Guo SL, Chiniah M, Li YS. Efficacy and safety of cryobiopsy versus forceps biopsy for interstitial lung diseases and lung tumours: A systematic review and meta-analysis. Respirology. 2016;21(5):834–41.
32. Korevaar DA, Colella S, Fally M, Camuset J, Colby TV, Hagmeyer L, et al. European Respiratory Society guidelines on transbronchial lung cryobiopsy in the diagnosis of interstitial lung diseases. Eur Respir J. 2022;60(5).
33. Sethi J, Ali MS, Mohananey D, Nanchal R, Maldonado F, Musani A. Are Transbronchial Cryobiopsies Ready for Prime Time?: A Systematic Review and Meta-Analysis. J Bronchology Interv Pulmonol. 2019;26(1):22–32.
34. Verleden SE, Vanstapel A, Jacob J, Goos T, Hendriks J, Ceulemans LJ, et al. Radiologic and Histologic Correlates of Early Interstitial Lung Changes in Explanted Lungs. Radiology. 2023;307(1):e221145.
35. Wijmans L, d'Hooghe JN, Bonta PI, Annema JT. Optical coherence tomography and confocal laser endomicroscopy in pulmonary diseases. Curr Opin Pulm Med. 2017;23(3):275–83.
36. Wijmans L, Kalverda K, de Bruin D, Brinkman P, van den Berk I, Roelofs J, et al. Bronchoscopic Journey of in vivo Real-Time Microscopic Imaging in ILD: A Case Series. Respiration. 2022;101(11):1006–14.
37. Nandy S, Raphaely RA, Muniappan A, Shih A, Roop BW, Sharma A, et al. Diagnostic Accuracy of Endobronchial Optical Coherence Tomography for the Microscopic Diagnosis of Usual Interstitial Pneumonia. Am J Respir Crit Care Med. 2021;204(10):1164–79.
38. Vaselli M, Wijsman PC, Willemse J, Goorsenberg AWM, Feroldi F, d'Hooghe JNS, et al. Polarization Sensitive Optical Coherence Tomography for Bronchoscopic Airway Smooth Muscle Detection in Bronchial Thermoplasty-Treated Patients With Asthma. Chest. 2021;160(2):432–5.
39. Thiberville L, Moreno-Swirc S, Vercauteren T, Peltier E, Cavé C, Bourg Heckly G. In vivo imaging of the bronchial wall microstructure using fibered confocal fluorescence microscopy. Am J Respir Crit Care Med. 2007;175(1):22–31.
40. Toshima M, Ohtani Y, Ohtani O. Three-dimensional architecture of elastin and collagen fiber networks in the human and rat lung. Arch Histol Cytol. 2004;67(1):31–40.
41. Thiberville L, Salaün M, Lachkar S, Dominique S, Moreno-Swirc S, Vever-Bizet C, et al. Human in vivo fluorescence microimaging of the alveolar ducts and sacs during bronchoscopy. Eur Respir J. 2009;33(5):974–85.
42. Wijmans L, Bonta PI, Rocha-Pinto R, de Bruin DM, Brinkman P, Jonkers RE, et al. Confocal Laser Endomicroscopy as a Guidance Tool for Transbronchial Lung Cryobiopsies in Interstitial Lung Disorder. Respiration. 2019;97(3):259–63.
43. Facciorusso A, Crino SF, Gkolfakis P, Spadaccini M, Arvanitakis M, Beyna T, et al. Diagnostic work-up of bile duct strictures: European Society of Gastrointestinal Endoscopy (ESGE) Guideline. Endoscopy. 2025;57(2):166–85.

44. Hatabu H, Hunninghake GM, Richeldi L, Brown KK, Wells AU, Remy-Jardin M, et al. Interstitial lung abnormalities detected incidentally on CT: a Position Paper from the Fleischner Society. Lancet Respir Med. 2020;8(7):726–37.
45. Elicker BM, Kallianos KG, Henry TS. The role of high-resolution computed tomography in the follow-up of diffuse lung disease: Number 2 in the Series "Radiology" Edited by Nicola Sverzellati and Sujal Desai. Eur Respir Rev. 2017;26(144).
46. Thompson BT, Chambers RC, Liu KD. Acute Respiratory Distress Syndrome. N Engl J Med. 2017;377(6):562–72.
47. van Huizen LMG, Radonic T, van Mourik F, Seinstra D, Dickhoff C, Daniels JMA, et al. Compact portable multiphoton microscopy reveals histopathological hallmarks of unprocessed lung tumor tissue in real time. Transl Biophotonics. 2020;2(4):e202000009.

PART I

Bronchoscopic sampling techniques for diagnosing ILD

Chapter 2

EBUS versus EUS-B for diagnosing sarcoidosis: The International Sarcoidosis Assessment (ISA) randomized clinical trial

Laurence M. M. Crombag[1], Kirsten Mooij-Kalverda[1], Artur Szlubowski[2], Maciej Gnass[3], Kurt G. Tournoy[4,5], Jiayuan Sun[6], Masahide Oki[7], Maarten K. Ninaber[8], Daniel P. Steinfort[9], Barton R. Jennings[10], Moishe Liberman[11], Semra Bilaceroglu[12,13], Peter I. Bonta[1], Daniël A. Korevaar[1], Rocco Trisolini[14], Jouke T. Annema[1]

1 Department of Respiratory Medicine, Amsterdam UMC, University of Amsterdam, Amsterdam, The Netherlands
2 Endoscopy Unit, Pulmonary Hospital, Zakopane, Poland
3 Endoscopy Unit, John Paul II Hospital, Kraków, Poland
4 Department of Respiratory Medicine, Onze-Lieve-Vrouw Ziekenhuis, Aalst, Belgium
5 Faculty of Medicine and Health Sciences, Ghent University, Ghent, Belgium
6 Department of Respiratory Endoscopy and Interventional Pulmonology, Shanghai Chest Hospital, Shanghai Jiao Tong University, Shanghai, China
7 Department of Respiratory Medicine, National Hospital Organization Nagoya Medical Center, Nagoya, Japan
8 Department of Respiratory Medicine, Leiden University Medical Center, Leiden, The Netherlands
9 Department of Respiratory Medicine, Royal Melbourne Hospital, Parkville, Victoria, Australia
10 Department of Respiratory Medicine, Monash Health, Clayton, Victoria, Australia
11 Division of Thoracic Surgery, University of Montreal, CR-CHUM, Montreal, Québec, Canada
12 Department of Respiratory Medicine, Health Sciences University, Izmir, Turkey
13 Dr. Suat Seren Training and Research Hospital for Thoracic Medicine and Surgery, Yenişehir Mahallesi, Izmir, Turkey
14 Interventional Pulmonology Unit, Fondazione Policlinico Universitario A. Gemelli IRCCS, Università Cattolica del Sacro Cuore, Rome, Italy

Respirology. 2022;27:152–160

ABSTRACT

Background and objective

Endosonography with intrathoracic nodal sampling is proposed as the single test with the highest granuloma detection rate in suspected sarcoidosis stage I/II. However, most studies have been performed in limited geographical regions. Studies suggest that oesophageal endosonographic nodal sampling has higher diagnostic yield than endobronchial endosonographic nodal sampling, but a head-to-head comparison of both routes has never been performed.

Methods

Global (14 hospitals, nine countries, four continents) randomized clinical trial was conducted in consecutive patients with suspected sarcoidosis stage I/II presenting between May 2015 and August 2017. Using an endobronchial ultrasound (EBUS) scope, patients were randomized to EBUS or endoscopic ultrasound (EUS)-B-guided nodal sampling, and to 22- or 25-G ProCore needle aspiration (2 × 2 factorial design). Granuloma detection rate was the primary study endpoint. Final diagnosis was based on cytology/pathology outcomes and clinical/radiological follow-up at 6 months.

Results

A total of 358 patients were randomized: 185 patients to EBUS transbronchial needle aspiration (EBUS-TBNA) and 173 to EUS-B-fine-needle aspiration (FNA). Final diagnosis was sarcoidosis in 306 patients (86%). Granuloma detection rate was 70% (130/185; 95% CI, 63–76) for EBUS-TBNA and 68% (118/173; 95% CI, 61–75) for EUS-B-FNA (p = 0.67). Sensitivity for diagnosing sarcoidosis was 78% (129/165; 95% CI, 71–84) for EBUS-TBNA and 82% (115/141; 95% CI, 74–87) for EUS-B-FNA (p = 0.46). There was no significant difference between the two needle types in granuloma detection rate or sensitivity.

Conclusion

Granuloma detection rate of mediastinal/hilar nodes by endosonography in patients with suspected sarcoidosis stage I/II is high and similar for EBUS and EUS-B. These findings imply that both diagnostic tests can be safely and universally used in suspected sarcoidosis patients.

Keywords: bronchoscopy and interventional techniques, diagnostic accuracy, EBUS, endoscopic ultrasound using the EBUS scope, endosonography, EUS-B, sarcoidosis

SUMMARY AT A GLANCE

This global RCT in patients with suspected sarcoidosis stage I/II with an indication for endosonographic nodal sampling showed a similarly high granuloma detection rate and sensitivity for diagnosing sarcoidosis with endobronchial ultrasound versus endoscopic ultrasound-B. The findings imply that both diagnostic tests (endobronchial/oesophageal) can be used safely and universally in suspected sarcoidosis patients.

INTRODUCTION

Sarcoidosis is a systemic disease of unknown cause that is characterized by the formation of immune granulomas in various organs, mainly the lungs and the lymphatic system.[1] Given that the clinical manifestations of sarcoidosis are often non-specific, demonstration of tissue granulomas is often required to establish the diagnosis.[2] Transoesophageal endoscopic ultrasound-guided fine-needle aspiration (EUS-FNA) of mediastinal lymph nodes has a high diagnostic yield in patients with suspected sarcoidosis.[3–5] Since the development of endobronchial ultrasound-transbronchial needle aspiration (EBUS-TBNA) using a bronchoscope in 2004, this procedure has also proved to be successful for granuloma detection. Besides, EBUS-TBNA has a higher diagnostic yield compared to conventional bronchoscopic techniques including (trans)bronchial lung biopsies (TBLB).[6–8] Frequently, both the hilar and mediastinal lymph nodes are affected in sarcoidosis, with the mean number of affected lymph nodes of 8, including the subcarinal lymph nodes in all cases.[9] Therefore, affected sarcoid lymph nodes can be sampled from both the oesophagus and the airways. EUS-B-guided nodal sampling is better tolerated by patients (no cough/shortness of breath) and often easier to perform in comparison to EBUS (absence of cartilage rings).[10,11] Several previous studies have compared endobronchial (EBUS-TBNA) and transoesophageal (EUS-FNA) approaches for indications such as undiagnosed mediastinal lymphadenopathy[10] or mediastinal staging of lung cancer,[12] but no such head-to-head comparisons have been performed in patients with suspected sarcoidosis.

Granuloma assessment on cytological specimens obtained by conventional FNAs can be challenging for pathologists. It is postulated that biopsy needles (ProCore) allow tissue acquisition including core biopsies—in

addition to the cytological aspirates—thereby increasing the granuloma detection rate compared to conventional needles.

We performed a randomized clinical trial, comparing intrathoracic nodal sampling from the airways (EBUS) with an oesophageal (EUS-B) approach, for the detection of non-caseating granulomas in patients with suspected pulmonary sarcoidosis stage I/II using an EBUS scope. Additionally, patients were also randomized between the conventional 22-G needle (EchoTip® Ultra Endobronchial HD Ultrasound Needle, Cook Medical, Limerick, Ireland) or the thinner 25-G biopsy needle (EchoTip ProCore® Endobronchial HD Biopsy Needle, Cook Medical).[13] Based on previous studies, we hypothesized that EUS-B sampling of intrathoracic lymph nodes has a higher granuloma detection rate compared to EBUS-guided nodal sampling in patients with suspected sarcoidosis stage I/II.

METHODS

Study design

The International Sarcoidosis Assessment (ISA) trial is a prospective investigator-initiated, unblinded, randomized clinical trial using a 2 × 2 factorial design. In this global study (14 hospitals, nine countries, four continents), patients were included in both university and general hospitals. Data were entered with web-based case report forms. The study was registered under number NCT02540694 at ClinicalTrials.gov. This manuscript is reported according to the STARD 2015 (Standards for Reporting Diagnostic Accuracy studies) statement[14] and CONSORT (Consolidated Standards of Reporting Trials) statement.

Study participants

Consecutive patients, 18 years or older, with a clinical and radiological suspicion of sarcoidosis stage I (mediastinal or hilar lymphadenopathy) or stage II (lymphadenopathy and parenchymal abnormalities) and an indication for tissue verification of non-caseating granulomas were eligible. Patients meeting any of the following criteria were excluded from participation in this study: obvious organ involvement of sarcoidosis with the possibility to confirm granulomas with a minimally invasive diagnostic procedure (e.g., skin lesion or superficial lymph node), pregnancy, a positive acid-fast bacilli sputum test, contra-indication for endosonography or a life expectancy of less than 6 months. Patients were recruited in outpatient clinics of respiratory medicine departments of participating

hospitals. Diagnostic work-up consisted of a conventional clinical evaluation (including medical history, physical examination and laboratory tests) with radiography and contrast-enhanced computed tomography (CT) of the chest. The decision to obtain tissue for diagnostic purposes versus a clinical and radiological followup was made in dialogue between the treating physician and the patient, weighing the risks and benefits of biopsy. The indication to obtain tissue was either to confirm sarcoidosis, to rule out other diseases, or before the start of treatment. Candidates for study participation were identified in 14 university and regional hospitals in the Netherlands, Belgium, Italy, Poland, Turkey, China, Japan, Canada and Australia. This investigator-initiated trial was approved by the human research ethics committee or local institutional review board at each centre. This study was conducted in accordance with the amended Declaration of Helsinki. Written informed consent was obtained from every participant before randomization.

Study endpoints

The pre-specified primary endpoint was the granuloma detection rate of EBUS-guided sampling of intrathoracic lymph nodes compared to EUS-B (using the EBUS scope)-guided sampling, defined as the number of patients with granulomas detected relative to the total number of patients tested.

The pre-specified secondary study endpoints were: (1) sensitivity of EBUS-TBNA and EUS-B-FNA for diagnosing sarcoidosis, defined as the proportion of patients with granulomas relative to the total number of patients who received a final diagnosis of sarcoidosis; (2) granuloma detection rate of conventional 22-G needle versus 25-G ProCore needle in the overall population and in the EBUS and EUS-B subgroups; (3) complication rate; (4) procedure duration (in minutes); and (5) sample quality of conventional 22-G needle versus 25-G ProCore needle in the overall population, defined as representative (i.e., [non-] caseating granulomas, reactive lymph node or malignant disease) versus non-representative samples (i.e., blood, squamous cells and bronchial epithelium).

Randomization

Both endoscopic procedures (EBUS and EUS-B) were performed using a linear EBUS scope. Prior to endoscopy, patients were randomized using web-based randomization software to an endobronchial (EBUS) or an oesophageal (EUS-B) approach. In addition, patients in each arm were also randomized between the standard 22-G COOK needle and the 25-G

bevel-tipped COOK ProCore needle. We performed block randomization stratified by centre.

Endosonography

Sedation was performed following institutional practices; commonly, either deep sedation with propofol or mild sedation with low-dose midazolam with or without opioids was used. All patients randomized to EBUS underwent a systematic endosonographic evaluation of accessible mediastinal/hilar nodes using the EBUS Assessment Tool (EBUSAT).[15] For patients randomized to EUS-B, nodes were systematically assessed using the EUS Assessment Tool (EUSAT).[16] Endosonographic nodal characteristics were scored. Following endosonographic inspection, the most suspected, prominent and easily accessible nodes were selected for tissue sampling. In total, at least five nodal samples were taken per patient (at least four samples were sent in for cytology and one for microbiology). After insertion of the needle into the target lymph node, the stylet was pulled out slowly (slow pull technique). In case no or limited material was retrieved, suction using a 10-ml syringe during the aspirations was advised for the next samples. Rapid on-site cytological evaluation (ROSE) was available in some of the participating centres. In the absence of ROSE, it was advised to sample at least two different nodal stations, as this increases the diagnostic yield.[7,17] The aspirates were processed for both cytologic smears and cell block analysis. Cytology staining (Papanicolaou or Giemsa) and cell block preparation were performed following local practice. The local pathologist analysed nodal aspirates for clinical purposes. In addition, tissue samples were sent in routinely for Auramine/Ziehl–Neelsen staining, as well as culture and PCR testing (where available) for *Mycobacterium tuberculosis.*

Reference standard

Following endosonography—in the absence of granulomas—it was left to the local treating physician on how to proceed. A non-diagnostic EBUS could be followed by EUS-B or vice versa in the same session. Also, conventional bronchoscopy including TBLBs and biopsies of the bronchial mucosa could be performed in the same session.

Detection of granulomas does not equal diagnosing sarcoidosis, which also requires a compatible clinical and radiological manifestation and exclusion of other diseases capable of presenting similarly such as tuberculosis (TB) and lymphoma.[1,2,18] The diagnosis sarcoidosis was made by the (unblinded) treating physician based on the findings of the local

pathologist and other available clinical information using the ERS/ATS/WASOG consensus statement.[19] The diagnosis of TB required a positive microbiology (PCR and/or culture) or a compatible clinic on baseline or follow-up (worsening of typical clinical features, radiological features of progressive TB on CT) plus the resolution/ improvement of clinical radiological findings during antimycobacterial treatment. Clinical and radiological follow-up was performed in all patients 6 months after inclusion to reassess the diagnosis. The diagnosis after 6 months as determined by the treating physician was considered the reference standard for the diagnosis of sarcoidosis.

Statistical analysis

Based on previous studies, we assumed that the sensitivity for granuloma detection of EBUS-TBNA and EUS-B-FNA would be 75% and 90%,[8,20] respectively, and the sarcoidosis prevalence would be 90%. This would result in a granuloma detection rate of 67% (0.75 × 0.90) in the EBUS arm and of 81% (0.9× 0.9) in the EUS-B arm. This required a sample size of 167 patients per group with a power of 1- B= 0.80, α = 0.05, two-sided testing. Compensating for 5% drop-outs, we aimed to include 350 patients. Chi-square tests were used for the comparison of categorical data between EBUS and EUS-B, including comparison of the detection rate and sensitivity. Patients in whom endosonography was initiated but in whom a complete procedure could not be performed were also included in the analysis. Analysis were performed with SPSS statistical package version 24.0 (IBM corporation). A p value of <0.05 was considered statistically significant.

RESULTS

Between May 2015 and August 2017, 381 consecutive patients with suspected sarcoidosis stage I/II were assessed for eligibility. Ultimately, 358 patients were included and randomized: 185 patients for EBUS (n = 96 standard 22 G needle; n = 89 25 G ProCore needle) and 173 patients for EUS-B (n = 82 standard 22 G needle; n = 91 ProCore 25 G needle). In four patients, a different needle type or size was used. According to the protocol, these patients were analysed in the group into which they were randomized. At baseline, patients in both groups were well balanced for the major clinical characteristics (Table 1). Fatigue (in 49%) and cough (in 41%) were the most prevalent symptoms. Study flow of enrolled patients is presented in Figure 1.

Table 1. Clinical characteristics

Characteristics	EBUS (*n* = 185)	EUS-B (*n* = 173)
Age, median (IQR), years	49 (39–60)	50 (41–61)
Sex, no. (%)		
Male	112 (61)	96 (56)
Race, no. (%)		
Caucasian	138 (75)	137 (78.5)
Asian	30 (16)	25 (15)
African	12 (6.5)	10 (6)
Other	4 (2)	1 (0.5)
Unknown	1 (0.5)	0 (0)
Symptoms, no. (%)		
Fatigue	86 (47)	91 (53)
Cough	78 (42)	67 (39)
Dyspnoea	56 (30)	52 (30)
Weight loss	25 (14)	28 (16)
Night sweats	30 (16)	35 (20)
Laboratory		
ACE, median (IQR), U/L[a]	53 (34–76)	54 (28–82)
Radiology, no. (%)		
Sarcoidosis stage based on chest radiograph		
Stage I	97 (52)	95 (55)
Stage II	48 (26)	32 (18)
Stage III	2 (1)	0 (0)
No enlarged LNs	9 (5)	8 (5)
No chest radiograph performed	29 (16)	38 (22)
Sarcoidosis stage based on chest CT		
Stage I	89 (48)	87 (50)
Stage II	92 (50)	84 (49)
Stage IV	1 (0.5)	0 (0)
No enlarged LNs	3 (1.5)	1 (0.5)
No chest CT performed	0 (0)	1 (0.5)
Short axis of the largest LN on chest CT, median (IQR), mm	19 (15–23)	18 (15–22)
Enlarged LN in reach of EBUS resp. EUS-B, no. (%)		
Yes	179 (97)	165 (95)

Table 1. Continued

Characteristics	EBUS (n = 185)	EUS-B (n = 173)
No	3 (1.5)	5 (3)
Unknown	3 (1.5)	3 (2)

Abbreviations: ACE, serum angiotensin-converting enzyme; CT, computed tomography; EBUS, endobronchial ultrasound; EUS, endoscopic ultrasound; IQR, interquartile range; LN, lymph node.

[a]ACE (U/L) was determined in 69 patients in the EBUS group and 57 patients in the EUS-B group, respectively.

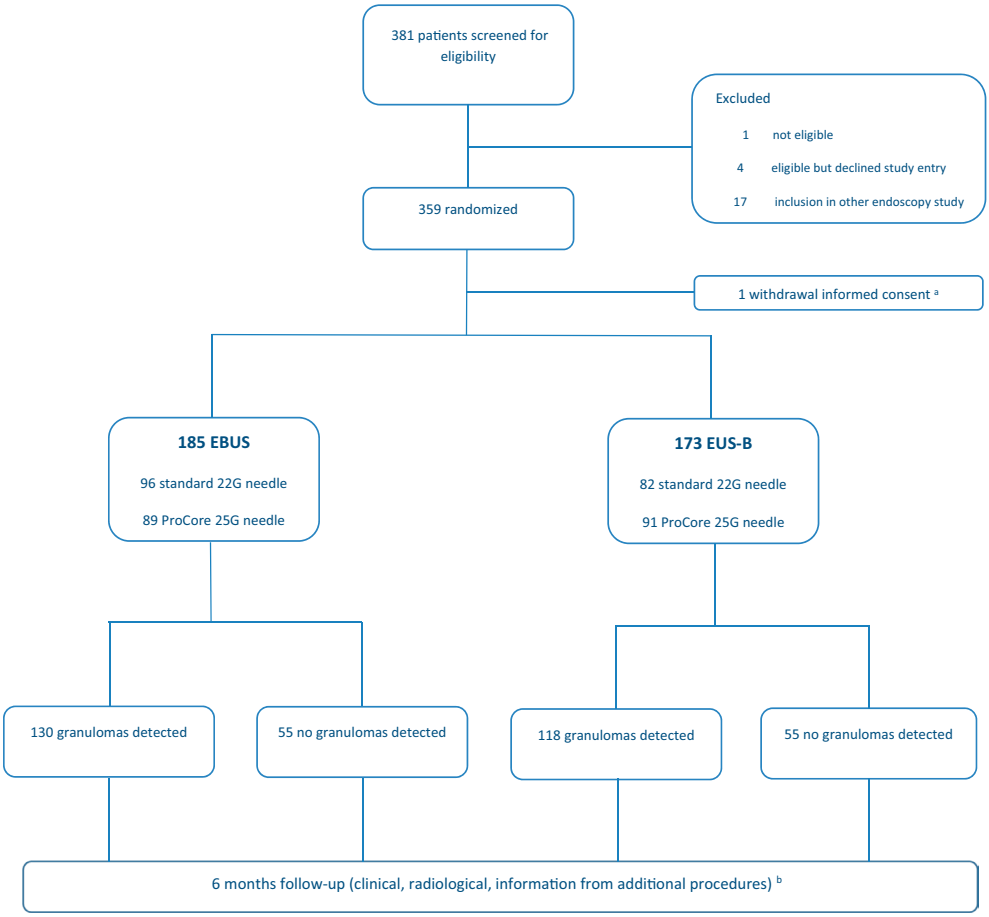


Figure 1. Flow diagram of enrolment and intervention in the International Sarcoidosis Assessment (ISA) trial. [a]One patient refused endoscopy after randomization and was excluded from analysis. [b]Seventeen patients did not complete the study: three due to death and 14 lost to follow-up

EBUS group

Among 185 patients undergoing an endobronchial procedure, the vast majority (179/185, 97%) of enlarged lymph nodes were located within the reach of EBUS, with a median short axis of the largest lymph node of 19 mm (interquartile range [IQR], 15–23). In 179 of 185 (97%) patients, the endoscopist was able to perform a complete systematic endosonographic evaluation of accessible mediastinal and hilar nodes using the EBUSAT[15] and perform five or more lymph node needle aspirations. The most prevalent ultrasound B-mode characteristics identified for the lymph nodes in patients with a final diagnosis of sarcoidosis were hypervascularization in 43% (71/165), node clustering in 64% (105/165), oval shaped in 70% (115/165), homogeneity in 75% (123/165), distinct margins in 86% (142/165), absence of coagulation necrosis sign in 81% (134/165) and absence of central hilar structure in 70% (115/165) of patients. The mean number of sampled lymph node stations per patient was 2.2 (range, 1–4). Median procedure time was 20 min (IQR, 17–25). Prophylactic antibiotics were used in 31 (17%) of 185 patients. Further procedural endoscopy details are provided in Table 2. Of the 185 patients, 37 (20%) underwent an additional (endoscopy) procedure (e.g., EUS-B [n = 25], bronchoscopy [n = 37], mediastinoscopy [n = 5]), resulting in granuloma detection in three additional patients not found by EBUS (one by EUS-B, one by bronchoscopy and one by mediastinoscopy).

EUS-B group

Among 173 patients undergoing an oesophageal procedure, the vast majority (165/173, 95%) of enlarged lymph nodes were located within the reach of EUS-B, with a median short axis of the largest lymph node of 18 mm (IQR, 15–22). In 164 of 173 (94%) patients, the endoscopist was able to perform a complete systematic endosonographic evaluation of accessible mediastinal nodes using the EUSAT[16] and perform at least five lymph node needle aspirations. Common B-mode findings for the lymph nodes of patients with a final diagnosis of sarcoidosis were hypervascularization in 43% (61/141), node clustering in 67% (95/141), oval shaped in 74% (104/141), homogeneity in 83% (117/141), distinct margins in 90% (127/141), absence of coagulation necrosis sign in 89% (125/141) and absence of central hilar structure in 79% (111/141) of patients. The mean number of sampled lymph node stations per patient was 1.8 (range, 0–3). Median procedure time was 18 min (IQR, 14–24). Prophylactic antibiotics were used in 77 (45%) of 173 patients. Further procedural endoscopy details are provided in Table 2. Of the 173 patients, 48 (28%) underwent an additional (endoscopy) procedure (e.g., EBUS [n = 35], bronchoscopy

[*n* = 4], mediastinoscopy [*n* = 4]) resulting in granuloma detection in six additional patients not found by EUS-B.

Table 2. Endosonography findings

Characteristics	EBUS (*n* = 185)	EUS-B (*n* = 173)
Sedation, no. (%)[a]		
None	1 (0.5)	2 (1)
Propofol	74 (40)	54 (31)
Midazolam	117 (63)	120 (69)
Opioid	97 (52)	90 (52)
General anaesthesia	0	0
Prophylactic antibiotics use, no. (%)	31 (17)	77 (45)
Endosonographic characteristics of sampled LNs with final diagnosis of sarcoidosis, no (%)[b]		
Hypervascularized LN	71 (43)	61 (43)
Multiple clustered LN	105 (64)	95 (67)
Oval-shaped LN	115 (70)	104 (74)
Homogeneous LN	123 (75)	117 (83)
Distinct margin LN	142 (86)	127 (90)
Absence of coagulation necrosis sign	134 (81)	125 (89)
Absence of hilar structure	115 (70)	111 (79)
Needle use randomization		
Standard 22 G, no. (%)	96 (52)	82 (47)
ProCore 25 G, no. (%)	89 (48)	91 (53)
No. of sampled LN stations, mean (range)	2.2 (1–4)	1.8 (0–3)
On-site cytological evaluation, no. (%)	76 (41)	67 (39)
Procedure time, median (IQR), min[c]	20 (17–25)	18 (14–24)
LN station (%) [median number of needle passes]		
2R	2 (1) [1]	2 (1) [3]
2L	1 (1) [3]	0 (0)
4R	105 (57) [3]	1 (1) [5]
4L	20 (11) [2]	91 (53) [3]
5	0 (0)	0 (0)
6	1 (1) [5]	0 (0)
7	155 (84) [3]	168 (97) [3]
8	0 (0)	48 (28) [3]
9	0 (0)	1 (1) [2]

Table 2. Continued

Characteristics	EBUS (*n* = 185)	EUS-B (*n* = 173)
10R	13 (7) [3]	0 (0)
10L	1 (1) [1]	0 (0)
11R	46 (25) [2.5]	0 (0)
11L	66 (36) [3]	0 (0)

Abbreviations: EBUS, endobronchial ultrasound; EUS, endoscopic ultrasound; IQR, interquartile range; LN, lymph node.
[a]Patients could receive a combination of benzodiazepines with opioids, or propofol and opioids. [b]In the EBUS group, 165 patients had a final diagnosis of sarcoidosis, and in the EUS-B group 141 patients had a final diagnosis of sarcoidosis. [c]Procedure time not recorded for 24 patients in the EBUS-group, and for 12 patients in the EUS-B group.

Final diagnoses

Final diagnoses determined at 6 months after randomization were sarcoidosis in 306 patients (86%), malignancy in 16 patients (4%), TB in two patients (0.5%) or another diagnosis in 34 patients (9.5%). The diagnosis of sarcoidosis was supported by the presence of granulomas in 280 of 306 patients, whereas in the remaining 26 patients it was based on clinical and radiological findings at baseline and during follow-up or on the results of additional (endoscopy) procedures (other than the randomization arm procedure) (Table 3).

Study outcomes

The granuloma detection rate was 70% (130/185; 95% CI, 63–76) for EBUS, and 68% (118/173; 95% CI, 61–75) for EUS-B (p = 0.67; Table 3) and independent of the geographic localization. Sensitivity for diagnosing sarcoidosis was 78% (129/165; 95% CI, 71–84) for EBUS, and 82% (115/141; 95% CI, 74–87) for EUS-B (p = 0.46; Table 3).

In the overall study population, the percentage of representative TBNA/FNA samples defined as (non-)caseating granulomas, reactive lymph node or malignant disease was 90.4% (161/178; 95% CI, 85–94) in the standard 22-G needle group and 91.1% (164/180; 95% CI, 86–94) in the 25-G ProCore needle group (p = 0.829). Among patients in whom a standard 22-G needle was used, granuloma detection rate was 70% (125/178; 95% CI, 63–76) in the overall study population, 70% (67/96; 95% CI, 60–78) in the EBUS procedural subgroup and 71% (58/82; 95% CI, 60–79) in the EUS-B procedural subgroup (p = 0.89). Among patients in whom a 25-G ProCore needle was used, granuloma detection

rate was 68% (123/180; 95% CI, 61–75) in the overall study population, 71% (63/89; 95% CI, 61–79) in the EBUS procedural subgroup and 66% (60/91; 95% CI, 56–75) in the EUS-B procedural subgroup (p = 0.48).

One serious adverse event was reported: a patient with a final diagnosis of sarcoidosis developed mediastinitis 10 weeks after an EBUS procedure with a standard 22-G needle, requiring antibiotics; no prophylactic antibiotics had been administered in this patient prior to the endoscopy procedure. The patient recovered completely. No serious adverse events were reported in the EUS-B group.

Table 3. Granuloma detection rate, sensitivity and final diagnoses by group

	EBUS (*n* = 185)	**EUS-B (*n* = 173)**
Granuloma detection rate, no. (%, 95% CI)	130 (70, 63–76)	118 (68, 61–75)
Sensitivity for diagnosing sarcoidosis, % (95% CI)	78 (71–84)	82 (74–87)
Final diagnosis at 6 months after randomization, no. (%)		
Sarcoidosis	165 (89)	141 (82)
Lymphoma	4 (2)	3 (2)
Lung cancer	2 (1)	5 (3)
Post-inflammation/reactive nodal disease	8 (4.5)	13 (7)
Tuberculosis	0	2 (1)
Other	6 (3.5)	5 (3)
Unknown	0	4 (2)

Abbreviations: EBUS, endobronchial ultrasound; EUS, endoscopic ultrasound; 95%CI, 95% confidence interval

DISCUSSION

In this randomized clinical trial, we found that endobronchial (EBUS) and oesophageal (EUS-B) sampling of intrathoracic lymph nodes have a similar granuloma detection rate and sensitivity in patients with presumed sarcoidosis stage I and II, irrespective of the needle type used. Adverse events were rare for both procedures, indicating that they can both be safely applied in this clinical setting. Procedure time of both approaches was in the same range.

Some of our findings are in line with the results of previous, non-randomized, studies on the diagnostic accuracy of endosonography in

granuloma detection in patients with suspected sarcoidosis. Two systematic reviews showed a diagnostic yield of EBUS-TBNA ranging from 33% to 100% in individual studies, with a pooled diagnostic accuracy of 79% (95% CI, 71–86).[20,21] Multiple studies evaluated the diagnostic yield of transoesophageal EUS-FNA using the conventional EUS scope, which ranged from 82% to 100% in patients with a final diagnosis of sarcoidosis.[3–5] A study on transoesophageal bronchoscopic ultrasound-guided FNA using the EBUS scope (EUS-B-FNA) showed granulomas in 86% of patients with the final diagnosis of sarcoidosis.[22]

To the best of our knowledge, EBUS-TBNA and EUS-B-FNA have not been directly compared previously among patients with suspected sarcoidosis. The granuloma randomized clinical trial compared conventional bronchoscopy (with TBLB and endobronchial lung biopsies) with endosonography (EBUS or conventional EUS) and showed that the use of endosonographic nodal aspiration resulted in greater diagnostic yield for a tissue confirmation of sarcoidosis. In contrast to our findings, the authors reported in the endosonography group that EUS-FNA (with a conventional EUS scope) seemed to have a higher diagnostic yield than EBUS-TBNA (88% vs. 66%; $p < 0.01$).[8] However, patient selection bias can possibly explain this difference, as the decision to perform an oesophageal or endobronchial procedure was left to the local investigator. In sarcoidosis, the mean number of affected intrathoracic lymph node stations can be as high as 8 per patient and the subcarinal station (that can be reached both endobronchially and oesophageally) is affected in almost all patients with stage I/II.[9] This seems a likely explanation for the similar granuloma detection rate of both routes (EBUS and EUS-B) that was found in the current trial.

EBUS-TBNA and EUS-B-FNA are safe procedures. Mediastinitis/mediastinal abscess is described in 1% of patients after an EUS-FNA procedure in sarcoidosis.[5] Mediastinitis as a complication of EBUS-TBNA is described in 0.10% (95% CI, 0.02–0.17) of procedures for evaluation of mediastinal or hilar lymph node lesions,[23] although bacteraemia without clinically significant infection was found in 7% of patients.[24] In the present study, a single patient developed mediastinitis after an EBUS-TBNA of a mediastinal lymph node (after 10 weeks).

Several limitations apply to the present study. The final diagnosis was sarcoidosis in the vast majority of cases as the majority of the participating centres were not located in a region with high prevalence of TB.

Therefore, the results may not be reproducible to such settings. The diagnosis after 6 months as determined by the treating physician was considered the reference standard in this study. Although this strategy has been used in other studies on sarcoidosis diagnosis, we acknowledge that this contains a level of subjectivity. Based on previous literature, we assumed granuloma detection rates of 75% for EBUS-TBNA and 90% for EUS-B- FNA in our sample size calculation. However, these were only 70% and 68%, respectively, in our study. Most likely, the retrospective nature of most previous studies resulted in selected patients and an overestimation of diagnostic yield, which cannot be extrapolated to a consecutive unselected sample of patients with suspected sarcoidosis. The outcomes of this study demonstrate that it is important to conduct multicentre, prospective, international studies as the results are likely to be a better reflection of the true diagnostic value than single-centre retrospective studies.

To the best of our knowledge this is the largest randomized clinical trial on diagnostic approaches for sarcoidosis. Strong points of the study are its randomized design, multicentre and global setting. The current study was performed in a well-defined study population, and endosonography procedures were performed with a structured and well-documented approach. Patients were included in both general and university hospitals of four continents in the world.

There is an ongoing clinical debate whether it is essential to establish a pathological diagnosis in all patients with suspected sarcoidosis, as a clinical presentation of stage I/II disease can be characteristic based on clinical presentation and imaging only, and invasive diagnostic testing may be unnecessary.[25,26] However, sarcoidosis can mimic serious disorders which, if undiagnosed and untreated, may be associated with significant morbidity or mortality. In our study population, over 15% of patients had a final diagnosis other than sarcoidosis including lymphoma and lung cancer, underlining the need for appropriate and careful patient selection for invasive nodal sampling, both in a clinical setting and for study participation. In clinical practice, endoscopists may be inclined to initiate the endobronchial procedure with standard bronchoscopy, followed by EBUS. In our study, we only evaluated EBUS, and adding bronchoscopy with mucosal and transbronchial biopsies could increase granuloma detection rate. However, this added value is likely to be limited, as of the 37 patients in the EBUS group who underwent subsequent bronchoscopy, granulomas were found in only one patient. Our findings also imply that

adding EBUS to EUS-B (or the other way around) is not likely to improve granuloma detection rate to a considerable extent: 25 patients (14%) in the EBUS group underwent subsequent EUS-B, revealing granulomas not detected by EBUS in only one patient. Of the 35 patients (20%) in the EUS-B group who underwent subsequent EBUS, no additional granulomas not already detected by EUS-B were found. These findings imply that performing additional endoscopic techniques may only be useful in selected patients, for example, in case lymph nodes cannot be sampled during the initial diagnostic procedure.

Despite a similar granuloma detection rate identified between EBUS and EUS-B in the current trial, parameters affecting the choice of a diagnostic procedure for confirming sarcoidosis include endoscopists' competence, and availability of the diagnostic test and availability of moderate/deep sedation. An advantage of EBUS is that hilar (station #10) and inter-lobar (station #11) lymph nodes, which are very commonly involved in sarcoidosis, can be sampled from the airways and not from the oesophagus. Besides, the endobronchial route allows to perform, in a single session, both EBUS-TBNA and additional sampling procedures such as bronchoalveolar lavage and endobronchial and transbronchial biopsies. This strategy has been shown to optimize the diagnostic yield in sarcoidosis, especially in stage II disease.[6,27] On the other hand, lymph nodes more difficult to sample (station #4L) or inaccessible (station #8L) from the airways can be sampled from the oesophagus through EUS-B. Other advantages of an EUS-B procedure are the fewer doses of anaesthetics and sedatives generally needed, and fewer oxygen desaturations.[11]

In conclusion, granuloma detection rate of mediastinal/hilar nodes by endosonography in patients suspected of sarcoidosis stage I/II is high, geographic independent and does not significantly differ for endobronchial versus transoesophageal sampling routes. Parameters affecting the choice of a diagnostic procedure for confirming sarcoidosis include endoscopists' competence, patient's general status, availability of bronchoscopy/endosonography equipment and availability of sedation.

CONFLICT OF INTEREST

This is an investigator-initiated study. The institution received a financial contribution for the database and a PhD student from Cook Medical. The institutions purchased the needles used in this study for a reduced

fee. The complete design, execution, analysis and presentation of results were performed by the investigators without any input from Cook Medical or any other external party. The individual investigators made no other disclosures.

AUTHOR CONTRIBUTION

Kirsten Kalverda: Data curation (supporting); formal analysis (supporting); investigation (supporting); project administration (supporting); software (supporting); writing – review and editing (supporting). **Artur Szlubowski:** Investigation (equal); project administration (equal). **Maciej Gnass:** Investigation (equal); project administration (supporting). **Kurt G. Tournoy:** Conceptualization (supporting); investigation (equal); project administration (equal). **Jiayuan Sun:** Investigation (equal); project administration (supporting). **Masahide Oki:** Investigation (equal); project administration (supporting). **Maarten K. Ninaber:** Investigation (equal); project administration (supporting). **Daniel Steinfort:** Investigation (equal); project administration (equal). **Barton Jennings:** Investigation (equal); project administration (equal). **Moishe Liberman:** Investigation (equal); project administration (equal). **Semra Bilaceroglu:** Investigation (equal); project administration (equal). **Peter I. Bonta:** Conceptualization (supporting); investigation (equal); methodology (supporting); project administration (equal); writing – review and editing (supporting). **Daniël A. Korevaar:** Conceptualization (supporting); data curation (equal); formal analysis (equal); methodology (equal); writing – review and editing (equal). **Rocco Trisolini:** Investigation (equal); project administration (equal); supervision (equal); writing – review and editing (equal). **Jouke T. Annema:** Conceptualization (equal); data curation (equal); formal analysis (equal); funding acquisition (lead); investigation (equal); methodology (equal); project administration (equal); resources (equal); software (supporting); supervision (lead); validation (equal); writing – original draft (supporting); writing – review and editing (equal). **Laurence M. M. Crombag:** Conceptualization (lead); data curation (lead); formal analysis (lead); funding acquisition (supporting); investigation (lead); methodology (lead); project administration (lead); resources (equal); software (lead); supervision (supporting); validation (lead); writing – original draft (lead); writing – review and editing (equal).

DATA AVAILABILITY STATEMENT

The study protocol including the statistical analysis plan is available. The (deidentified) data that underlie the results reported in this article are available on request. The corresponding author will decide, depending on the type of planned analysis, whether these data will be shared.

HUMAN ETHICS APPROVAL DECLARATION

This study was performed in accordance with the Declaration of Helsinki and approved by the Medical Ethical Committee of Amsterdam University Medical Centers. All adult participants provided written informed consent to participate in this study (Clinical trial registration: NCT02540694 at ClinicalTrials.gov). Participant registration took place from May 2015 to Aug 2017.

REFERENCES

1. Valeyre D, Prasse A, Nunes H, Uzunhan Y, Brillet PY, Muller- Quernheim J. Sarcoidosis. Lancet (London, England). 2014;383(9923): 1155–67.
2. Crouser ED, Maier LA, Wilson KC, Bonham CA, Morgenthau AS, Patterson KC, et al. Diagnosis and detection of sarcoidosis. An official American Thoracic Society clinical practice guideline. Am J Respir Crit Care Med. 2020;201(8):e26–51.
3. Annema JT, Veseliç M, Rabe KF. Endoscopic ultrasound-guided fine-needle aspiration for the diagnosis of sarcoidosis. Eur Respir J. 2005; 25(3):405–9.
4. Fritscher-Ravens A, Sriram PV, Topalidis T, Hauber HP, Meyer A, Soehendra N, et al. Diagnosing sarcoidosis using endosonography-guided fine-needle aspiration. Chest. 2000;118(4):928–35.
5. von Bartheld MB, Veseliç-Charvat M, Rabe KF, Annema JT. Endoscopic ultrasound-guided fine-needle aspiration for the diagnosis of sarcoidosis. Endoscopy. 2010;42(3):213–7.
6. Gupta D, Dadhwal DS, Agarwal R, Gupta N, Bal A, Aggarwal AN. Endobronchial ultrasound-guided transbronchial needle aspiration vs conventional transbronchial needle aspiration in the diagnosis of sarcoidosis. Chest. 2014;146(3):547–56.
7. Tremblay A, Stather DR, MacEachern P, Khalil M, Field SK. A randomized controlled trial of standard vs endobronchial ultrasonography-guided transbronchial needle aspiration in patients with suspected sarcoidosis. Chest. 2009;136(2):340–6.
8. von Bartheld MB, Dekkers OM, Szlubowski A, Eberhardt R, Herth FJ, in 't Veen JC, et al. Endosonography vs conventional bronchoscopy for the diagnosis of sarcoidosis: the GRANULOMA randomized clinical trial. JAMA. 2013;309(23):2457–64.
9. Trisolini R, Anevlavis S, Tinelli C, Orlandi P, Patelli M. CT pattern of lymphadenopathy in untreated patients undergoing bronchoscopy for suspected sarcoidosis. Respir Med. 2013;107(6):897–903.
10. Madan K, Mittal S, Madan NK, Tiwari P, Jain D, Arava S, et al. EBUS-TBNA versus EUS-B-FNA for the evaluation of undiagnosed mediastinal lymphadenopathy: the TEAM randomized controlled trial. Clin Respir J. 2020;14(11):1076–82.
11. Oki M, Saka H, Ando M, Tsuboi R, Nakahata M, Oka S, et al. Transbronchial vs transesophageal needle aspiration using an ultrasound bronchoscope for the diagnosis of mediastinal lesions: a randomized study. Chest. 2015;147(5):1259–66.
12. Korevaar DA, Crombag LM, Cohen JF, Spijker R, Bossuyt PM, Annema JT. Added value of combined endobronchial and oesophageal endosonography for mediastinal nodal staging in lung cancer: a systematic review and meta-analysis. Lancet Respir Med. 2016;4(12):960–8.
13. Dhooria S, Sehgal IS, Prasad KT, Muthu V, Gupta N, Bal A, et al. Diagnostic yield and safety of the ProCore versus the standard EBUS-TBNA needle in subjects with suspected sarcoidosis. Expert Rev Med Devices. 2021;18(2):211–6.

14. Bossuyt PM, Reitsma JB, Bruns DE, Gatsonis CA, Glasziou PP, Irwig L, et al. STARD 2015: an updated list of essential items for reporting diagnostic accuracy studies. BMJ. 2015;351:h5527.
15. Konge L, Clementsen PF, Ringsted C, Minddal V, Larsen KR, Annema JT. Simulator training for endobronchial ultrasound: a randomised controlled trial. Eur Respir J. 2015;46(4):1140–9.
16. Konge L, Vilmann P, Clementsen P, Annema JT, Ringsted C. Reliable and valid assessment of competence in endoscopic ultrasonography and fine-needle aspiration for mediastinal staging of non-small cell lung cancer. Endoscopy. 2012;44(10):928–33.
17. Trisolini R, Tinelli C, Cancellieri A, Paioli D, Alifano M, Boaron M, et al. Transbronchial needle aspiration in sarcoidosis: yield and predictors of a positive aspirate. J Thorac Cardiovasc Surg. 2008;135(4):837–42.
18. Spagnolo P, Rossi G, Trisolini R, Sverzellati N, Baughman RP, Wells AU. Pulmonary sarcoidosis. Lancet Respir Med. 2018;6(5):389–402.
19. Costabel U, Hunninghake GW. ATS/ERS/WASOG statement on sarcoidosis. Sarcoidosis Statement Committee. American Thoracic Society. European Respiratory Society. World Association for Sarcoidosis and Other Granulomatous Disorders. Eur Respir J. 1999;14(4):735–7.
20. Agarwal R, Srinivasan A, Aggarwal AN, Gupta D. Efficacy and safety of convex probe EBUS-TBNA in sarcoidosis: a systematic review and meta-analysis. Respir Med. 2012;106(6):883–92.
21. Trisolini R, Lazzari Agli L, Tinelli C, De Silvestri A, Scotti V, Patelli M. Endobronchial ultrasound-guided transbronchial needle aspiration for diagnosis of sarcoidosis in clinically unselected study populations. Respirology (Carlton, Vic). 2015;20(2):226–34.
22. Oki M, Saka H, Kitagawa C, Kogure Y, Murata N, Adachi T, et al. Transesophageal bronchoscopic ultrasound-guided fine needle aspiration for diagnosis of sarcoidosis. Respiration. 2013;85(2):137–43.
23. Asano F, Aoe M, Ohsaki Y, Okada Y, Sasada S, Sato S, et al. Complications associated with endobronchial ultrasound-guided transbronchial needle aspiration: a nationwide survey by the Japan Society for Respiratory Endoscopy. Respir Res. 2013;14:50.
24. Steinfort DP, Johnson DF, Irving LB. Incidence of bacteraemia following endobronchial ultrasound-guided transbronchial needle aspiration. Eur Respir J. 2010;36(1):28–32.
25. Mehta AC, Almeida FA. Choose wisely: endobronchial ultrasound-guided transbronchial needle aspiration for sarcoidosis. Chest. 2014; 146(3):530–2.
26. Ribeiro Neto ML, Culver DA, Mehta AC. Sarcoidosis – no business of the bronchoscopist. J Thorac Cardiovasc Surg. 2012;144(5):1276–7; author reply 1277.
27. Trisolini R, Lazzari Agli L, Cancellieri A, Poletti V, Candoli P, Paioli D, et al. Transbronchial needle aspiration improves the diagnostic yield of bronchoscopy in sarcoidosis. Sarcoidosis Vasc Diffuse Lung Dis. 2004;21(2):147–51.

Chapter 3

Transbronchial cryobiopsy followed by as-needed surgical lung biopsy versus immediate surgical lung biopsy for diagnosing interstitial lung disease (the COLD study): a randomised controlled trial

Kirsten A. Kalverda[1] MD, Maarten K. Ninaber[2] PhD, Lizzy Wijmans[1] PhD, Jan von der Thüsen[3] PhD, René E. Jonkers[1] PhD, Johannes M. Daniels[4] PhD, Jelle R. Miedema[5] MD, Chris Dickhoff[6] PhD, Jürgen Hölters[7] PhD, David Heineman[6] PhD, Merijn Kant[8] MD, Teodora Radonic[9] PhD, Ghada Shahin[10] PhD, Danielle Cohen[11] PhD, Bart Boerrigter[4] PhD, Suzan Nijman[4] MD, Esther Nossent[4] MD, prof Jerry Braun[10] PhD, Bas Mathot[5] MD, Prof Venerino Poletti[12,13] PhD, Jürgen Hetzel[14,15] PhD, prof Marcel Dijkgraaf[16] PhD, Daniel A. Korevaar[4] PhD, Peter I. Bonta[1] PhD, prof Jouke T. Annema[1] PhD

1. Department of respiratory diseases, Amsterdam University Medical centers, location AMC, Meibergdreef 9, Amsterdam
2. Department of respiratory diseases, Leiden University Medical Center, Leiden
3. Department of Pathology and Clinical Bioinformatics, Erasmus Medical Center, Rotterdam
4. Department of Respiratory diseases, Amsterdam University Medical centers, location VUMC, Boelelaan 1117, Amsterdam
5. Department of Respiratory diseases, Erasmus Medical Center, Rotterdam
6. Department of Cardiothoracic Surgery, Amsterdam University Medical centers, location VUMC, Boelelaan 1117, Amsterdam
7. Department of Respiratory diseases, Canisius Wilhelmina Ziekenhuis, Nijmegen
8. Department of Respiratory diseases, Amphia Hospital, Breda
9. Department of Pathology, Amsterdam University Medical centers, location VUMC, Boelelaan 1117, Amsterdam
10. Department of Surgery, Leiden University Medical Center, Leiden
11. Department of Pathology, Leiden University Medical Center, Leiden
12. Department of Medical Specialities. GB Morgagni Hospital/DIMEC University of Bologna-Forlì, Italy
13. Department of Respiratory Diseases and Allergy, Aarhus University Hospital, Aarhus, Denmark
14. Department of Medical Oncology and Pneumology, Eberhard Karls University, Tübingen
15. Department of Pneumology, Cantonal Hospital of Winterthur, Winterthur, Switzerland
16. Department of Epidemiology and Data Science, Amsterdam University Medical Centers, University of Amsterdam, Amsterdam

Lancet Respir Med 2024; 12: 513–22

SUMMARY

Background

An adequate diagnosis for interstitial lung disease (ILD) is important for clinical decision making and prognosis. In most patients with ILD, an accurate diagnosis can be made by clinical and radiological data assessment, but in a considerable proportion of patients, a lung biopsy is required. Surgical lung biopsy (SLB) is the most common method to obtain tissue, but it is associated with high morbidity and even mortality. More recently, transbronchial cryobiopsy has been introduced, with fewer adverse events but a lower diagnostic yield than SLB. The aim of this study is to compare two diagnostic strategies: a step-up strategy (transbronchial cryobiopsy, followed by SLB if the cryobiopsy is insufficiently informative) versus immediate SLB.

Methods

The COLD study was a multicentre, randomised controlled trial in six hospitals across the Netherlands. We included patients with ILD with an indication for lung biopsy as assessed by a multidisciplinary team discussion. Patients were randomly assigned in a 1:1 ratio to the step-up or immediate SLB strategy, with follow-up for 12 weeks from the initial procedure. Patients, clinicians, and pathologists were not masked to the study treatment. The primary endpoint was unexpected chest tube drainage, defined as requiring any chest tube after transbronchial cryobiopsy, or prolonged (>24 h) chest tube drainage after SLB. Secondary endpoints were diagnostic yield, in-hospital stay, pain, and serious adverse events. A modified intention-to-treat analysis was performed. This trial is registered with the Dutch Trial Register, NL7634, and is now closed.

Findings

Between April 8, 2019, and Oct 24, 2021, 122 patients with ILD were assessed for study participation; and 55 patients were randomly assigned to the step-up strategy (n=28) or immediate SLB (n=27); three patients from the immediate SLB group were excluded. Unexpected chest tube drainage occurred in three of 28 patients (11%; 95% CI 4–27%) in the step-up group, and the number of patients for whom the chest tube could not be removed within 24 h was 11 of 24 patients (46%; 95% CI 28–65%) in the SLB group, with an absolute risk reduction of 35% (11–56%; p=0·0058). In the step-up strategy, the multidisciplinary team diagnostic yield after transbronchial cryobiopsy alone was 82% (64–92%), which increased to 89% (73–96%) when subsequent SLB was performed after inconclusive

transbronchial cryobiopsy. In the immediate surgery strategy, the multidisciplinary team diagnostic yield was 88% (69–97%). Total in-hospital stay was 1 day (IQR 1–1) in the step-up group versus 5 days (IQR 4–6) in the SLB group. One (4%) serious adverse event occurred in step-up strategy versus 12 (50%) in the immediate SLB strategy.

Interpretation

In ILD diagnosis, if lung tissue assessment is required, a diagnostic strategy starting with transbronchial cryobiopsy, followed by SLB when transbronchial cryobiopsy is inconclusive, appears to result in a significant reduction of patient burden and in-hospital stay with a similar diagnostic yield versus immediate SLB.

Funding

Netherlands Organisation for Health Research and Development (ZonMW) and Amsterdam University Medical Centers.

RESEARCH IN CONTEXT

Evidence before this study

Transbronchial cryobiopsy is a relatively new bronchoscopic technique to obtain lung tissue for diagnosing interstitial lung disease (ILD). Compared with surgical lung biopsy (SLB), transbronchial cryobiopsy appears to have a favourable safety profile. Because the diagnostic yield of transbronchial cryobiopsy is estimated to be less than that of SLB, it might be beneficial to start with the less invasive transbronchial cryobiopsy and to revert to SLB only in the case of inconclusive transbronchial cryobiopsy for ILD diagnosis (step-up strategy). We searched PubMed on May 2, 2023, using the terms “cryobiopsy” or “cryo probe” and “interstitial lung disease” or “diffuse parenchymal disease” for all reports from database inception without restrictions to language. No studies were found in which a step-up diagnostic strategy was compared with immediate SLB. Studies in which transbronchial cryobiopsy alone was compared with SLB were mostly indirect or retrospective. A few studies focused on a direct comparison of transbronchial cryobiopsy and SLB in the same patient, but because of the design of those studies, safety aspects and patient-related outcomes of either technique could not be assessed.

Added value of this study

The COLD study is the first randomised study comparing two strategies for diagnosing ILD (step-up strategy of transbronchial cryobiopsy only followed by SLB in the case of an inconclusive transbronchial cryobiopsy *vs* immediate SLB). The diagnostic strategy starting with transbronchial cryobiopsy resulted in a reduction of chest tube drainage, in-hospital stay, pain, and serious adverse events, whereas the diagnostic yield of both strategies was similar.

Implications of all the available evidence

Current guidelines recommend SLB for tissue acquisition for ILD diagnosis with a conditional recommendation of a first step of transbronchial cryobiopsy in centres with bronchoscopists experienced in transbronchial cryobiopsy. The results of the COLD study justify starting with transbronchial cryobiopsy and pursuing additional surgical tissue sampling in the case that transbronchial cryobiopsy is inconclusive for classifying ILD diagnosis. Widespread implementation of the transbronchial cryobiopsy technique in centres with less experience warrants more insight in the requirements for transbronchial cryobiopsy training, which should include all stakeholders such as interventional pulmonologists and pathologists.

INTRODUCTION

Interstitial lung diseases (ILDs) comprise a wide variety of disease entities. Treatment and prognosis vary across different ILDs, and establishing a correct diagnosis is therefore clinically important. A multidisciplinary team discussion, resulting in a consensus diagnosis, is considered the reference standard for diagnosing ILD.[1] In most cases, a high-confidence diagnosis can be established from clinical and radiological data, yet it is estimated that in 10–40% of newly diagnosed ILD, a lung biopsy is deemed necessary to establish a diagnosis or improve diagnostic confidence.[2–5] The addition of histopathology to clinical and radiological data has been shown to change the treatment strategy in a third of cases.[6]

Historically, lung biopsies for an ILD diagnosis have been obtained through surgical lung biopsy (SLB). Adding SLB findings to a multidisciplinary team discussion results in a diagnostic yield of approximately 90%, but is associated with considerable procedure-related morbidity and even mortality of approximately 2%.[7–10] In addition, patients undergoing SLB require hospital admission for post-surgical chest tube drainage, resulting in a high patient and health-care burden. More recently, transbronchial cryobiopsy has been introduced as a less invasive alternative technique to obtain lung tissue. Major advantages of transbronchial cryobiopsy include that post-procedure chest tube drainage is usually not needed and the procedure is therefore associated with a short in-hospital stay and a less than 1% procedure-related mortality rate.[9,11,12] However, the diagnostic yield of transbronchial cryobiopsy is lower than that of SLB, and varies between 70–80%.[12]

In a 2022 clinical guideline on the role of transbronchial cryobiopsy in the diagnostic tests of ILD, a step-up strategy is proposed: patients initially undergo transbronchial cryobiopsy and, if insufficiently informative, it is followed by a subsequent SLB.[12] However, the quality of the evidence was deemed very low for this guideline outcome, and so far no studies have been published that directly compare the outcomes of immediate SLB with the step-up strategy. The available studies that were considered in the guidelines were either single-arm or retrospective.[5,7–9,13–15] The only prospective studies in which transbronchial cryobiopsy was compared with SLB were those in which patients underwent both transbronchial cryobiopsy and SLB during the same procedure.[16–19] Additionally, most studies focused mainly on adverse events and the diagnostic yield of transbronchial cryobiopsy and SLB as single procedures, whereas studies

on patient-related outcomes of the entire diagnostic strategy were scarce. This is of importance, because shared decision making regarding diagnostic tests should be based on both patients' preferences and evidence.[20] In addition, there is wide variability in the applied diagnostic strategies used to obtain lung tissue in patients with ILD. Therefore, direct comparative studies across diagnostic strategies are needed.

The aim of the COLD study was to compare two diagnostic strategies (step-up strategy *vs* immediate SLB) in terms of the patient burden (with the primary outcome being unexpected chest tube drainage), in-hospital stay, and diagnostic yield.

METHODS

Study design and participants

We performed a randomised clinical trial in six hospitals across the Netherlands, including academic and general hospitals. In the Netherlands, ILD care is embedded in expertise centres and affiliated treatment centres. All patients newly diagnosed with ILD are discussed in a multidisciplinary team that includes at least two pulmonologists, a chest radiologist, and a pathologist, all with ILD expertise.[1,21–23] In the present study, the need for a biopsy was assessed at the local multidisciplinary team discussion and was part of standard care. Patients were consecutively recruited from the respiratory outpatient clinic of participating hospitals. Patients were eligible for inclusion when their clinical and radiological data were insufficient for the establishment of a classifying ILD diagnosis and the multidisciplinary team discussion advice was to obtain lung tissue for an ILD diagnosis. A full list of inclusion and exclusion criteria is presented in the appendix (p 1). The follow-up time was 12 weeks. The trial was approved by the Medical Ethics Committee of the Academic Medical Center Amsterdam (identifier number 2018_224), and was performed in accordance with Good Clinical Practice guidelines and the Declaration of Helsinki. All patients provided written informed consent before random assignment. The study was sponsored by the Netherlands Organisation for Health Research and Development (ZonMW) and was prospectively registered at the Dutch Trial Register (number NL7634).

Randomisation and masking

Included patients were randomly assigned in a 1:1 ratio either to the step-up strategy (starting with transbronchial cryobiopsy, followed by

SLB if the cryobiopsy was insufficiently informative) or to an immediate SLB. Random assignment was performed by the local study coordinator using the Castor Electronic Data Capturing System using variable block sizes (4 and 6), stratified by participating centre. Patients and clinicians were not masked to the diagnostic strategy.

Procedures

Transbronchial cryobiopsy was performed in accordance with a published consensus statement, including secured airway, prophylactic endobronchial balloon placement, and fluoroscopy guidance.[24] A minimum of two biopsies were obtained from two different segments using the 1·9 mm reusable cryoprobe (Erbe Elektromedizin, Tübingen, Germany).[14] After transbronchial cryobiopsy, patients received a chest x-ray to screen for pneumothorax. The need for chest tube insertion, in the case of a pneumothorax, was assessed by the treating physician. Patients were not given pain medication routinely. All participating bronchoscopists were experienced interventional pulmonologists but not necessarily experienced in transbronchial cryobiopsy. To train and to secure the harmonisation of the transbronchial cryobiopsy procedure, all participating bronchoscopists attended a 2-day international workshop at the University Hospital of Tübingen, Germany, before study initiation, which included live demonstrations and a training session of transbronchial cryobiopsy on a porcine model.

Patients were considered for a subsequent SLB if the results were insufficient for a classifying diagnosis as assessed by the multidisciplinary team. SLBs were obtained through standard local procedures, allowing uni-portal and multi-portal video-assisted thoracoscopic surgery or thoracotomy at the discretion of the thoracic surgeon. At least two biopsies were obtained from two lobes. In all cases a prophylactic chest tube was placed after lung biopsies. In the case of an uncomplicated surgical procedure, the chest tube could be removed within 24 h.[25] Patients received an erector spinae block and a combination of analgesics, including opioids, as needed (appendix p 2).

Criteria for chest tube removal were prespecified and protocolised in the standard operation procedure. Twice per day, whether the chest tube could be removed was evaluated, which was considered to be the case in the absence of an air leak, and less than 125 cc pleural effusion per 12 h.

All biopsies were evaluated by a local pathologist with expertise in ILD, in accordance with international guidelines for diagnosing idiopathic pulmonary fibrosis and idiopathic interstitial pneumonia.[21,23,26] Biopsy results were discussed during the multidisciplinary team discussions. Both a histopathological and a multidisciplinary team diagnosis were recorded after a multidisciplinary team discussion. Pathologists and other multidisciplinary team participants were not masked to the randomisation group.

After study completion, all biopsies were reviewed by a reference pathologist (JvdT) with specific ILD expertise who was masked to clinical multidisciplinary team results and initial histology reports. The time between local evaluation and this repeated evaluation was at least 12 months. The reference pathologist recorded histopathological diagnosis and diagnostic confidence (high, low, or unclassifiable; definitions for histopathological confidence are described in the appendix [p 3]). In case a patient underwent both transbronchial cryobiopsy and SLB in the step-up strategy, the overall histopathological pattern and diagnostic confidence was obtained.

Outcomes

The primary outcome was unexpected chest tube drainage, defined as the proportion of patients in need of any chest tube drainage after transbronchial cryobiopsy, or prolonged (>24 h) chest tube drainage after SLB. This primary outcome was chosen after a consultation with patients' representatives and in discussion with the medical ethical committee, and was considered to best reflect patient burden.

The prespecified secondary outcomes were: diagnostic yield, length of hospital stay, pain, and serious adverse events. Diagnostic yield was defined as the proportion of patients with a classifying multidisciplinary team diagnosis after a procedure and diagnostic strategy. Length of hospital stay was recorded in days, starting with the day of hospital admission and adding 1 day per overnight stay covering the total number of admitted days during 3 months of follow-up (including hospital admittance due to a second procedure or adverse event). Post-procedural pain was measured with a visual analogue scale for pain, ranging from 0 (no pain) to 100 (worst pain imaginable). Pain scores exceeding 30 were considered clinically relevant.[27] Pain scores were recorded at baseline, once per day during the first week after the biopsy procedure, and once at 2, 4, 6, 8, and 12 weeks after the procedure. In case a patient underwent a

second procedure, this procedure had to be performed within 6 weeks of the first procedure.

Adverse events were defined as any untoward medical events that occurred during the study period. When adverse events resulted in death, were life-threatening, or required admission to hospital or an increase in the length of stay of an existing inpatient hospital stay, an adverse event was classified as a serious adverse event. On the basis of local protocols and the available literature, the increase of an in-hospital stay due to a serious adverse event was defined as longer than 2 days (one overnight stay) for transbronchial cryobiopsy and 4 days (three overnight stays) for SLB.[15] The agreement of histopathology results between the reference pathologist and local pathologist was a post-hoc analysis.

Statistical analysis

A sample size calculation was performed before study initiation. On the basis of previous literature and our own expertise, we expected that less than 10% of patients would require unexpected chest tube drainage in the step-up strategy,[14,15] versus 50% after immediate SLB.[25] We calculated that two groups of 23 patients would achieve 81% power to detect such a difference, using a two-sided Fisher's exact test at a significance level of 0·05. Therefore, we aimed to include at least 50 patients, anticipating a 10% dropout rate. The analysis for primary and secondary outcomes was performed on patients who were randomly assigned and who underwent the allocated study procedure (modified intention-to-treat analysis). Because a high dropout rate in one of the two groups could lead to a major underestimation of unexpected chest tube drainage in that group, a modified intention-to-treat analysis was considered more appropriate than overall intention-to-treat analysis. However, the robustness of the main treatment effect on the primary outcome was assessed in a worst-case scenario. Hereby, patients who were randomly assigned to transbronchial cryobiopsy but did not undergo the procedure were assumed to have had unexpected chest tube drainage, whereas patients who were randomly assigned to immediate SLB but did not undergo SLB were assumed not to have had unexpected chest tube drainage. Baseline demographic variables were reported as absolute numbers with proportions for categorical data, and as means with SDs or medians with IQRs for continuous variables. A Fisher's exact test was used for the between-group comparison of categorical data, with the Wilson score method to report 95% CIs. A Student's *t* test and Mann-Whitney *U* test were used for continuous outcomes in the case of parametric or

non-parametric distributions, respectively. Visual analogue scale pain scores were reported as median (IQR) and as number (proportion) of patients with clinically relevant pain scores, with the between-group differences in pain scores at distinct points in time compared using Mann-Whitney *U* tests and the differences in proportions compared using Fisher's exact tests. For interobserver variability for histopathological diagnosis, Cohens κ was used.

After peer review, a post-hoc logistic regression on unexpected chest tube drainage (dependent variable) was applied with random assignment as the independent variable (reference group: SLB) and unevenly distributed baseline percentage of predicted forced vital capacity and percentage of predicted Hb-corrected diffusion capacity of the lungs for carbon monoxide as covariates. An odds ratio (OR) of less than 1 would indicate a lower odds of unexpected chest tube drainage in the step-up strategy compared with immediate SLB, and vice versa for an OR of more than 1. An OR of exactly 1 indicated that the odds of unexpected chest tube drainage were similar for both diagnostic strategies. A p value of less than 0·05 was considered statistically significant. Analyses were performed in IBM SPSS version 28.0.1.1 or WinPepi version 11.65.

Role of the funding source

The funder of the study had no role in study design, data collection, data analysis, data interpretation, or writing of the report.

RESULTS

Between April 8, 2019, and Oct 24, 2021, 122 patients with ILD were assessed for study participation after multidisciplinary team discussions from participating centres advised a lung biopsy. 66 patients (54%) were excluded for various reasons and 56 patients (46%) signed informed consent (figure 1). After informed consent, one patient was excluded because they showed sudden rapid lung function decline. The remaining 55 patients were randomly assigned to the step-up strategy (n=28) or immediate SLB (n=27). In the step-up strategy, all patients underwent transbronchial cryobiopsy, but in the immediate SLB group, three did not undergo SLB and were excluded from the analysis. Therefore, a total of 52 patients (step-up strategy n=28 *vs* immediate SLB n=24) were included in the modified intention-to-treat analysis.

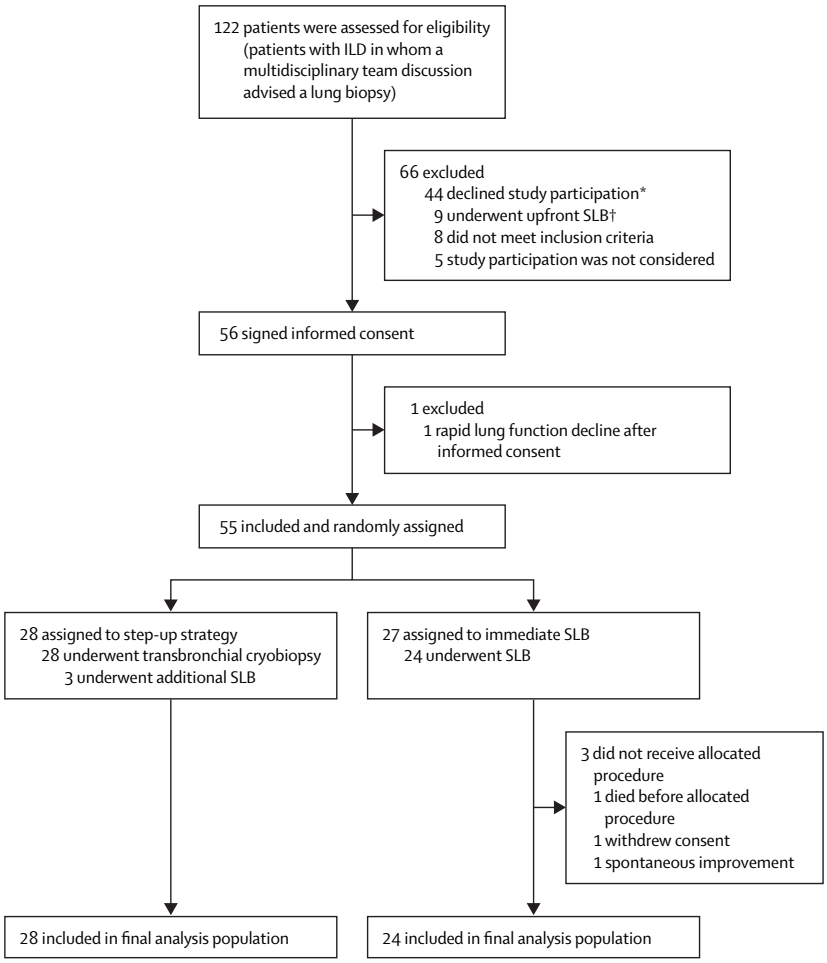


Figure 1. Trial profile
ILD=interstitial lung disease. SLB=surgical lung biopsy. *Reasons for declining participation were: patients preferred SLB (n=13), patients preferred transbronchial cryobiopsy (n=21), patients declined any lung biopsy procedure (n=5), patient did not want to participate in a clinical trial (n=1), and no reason provided (n=5). †Patient underwent upfront SLB as indicated by their physician due to suspicion of lung cancer in addition to underlying ILD (n=7), it was expected that large lung biopsies were needed and transbronchial cryobiopsy would be too small (n=1), or patient underwent upfront SLB because this was considered to be a maximally controlled setting for a very frail patient (n=1).

Baseline characteristics (table 1) were evenly distributed between the two groups except for percentage of predicted forced vital capacity and percentage of predicted Hb-corrected diffusion capacity of the lungs for carbon monoxide, which were higher in the step-up group (by 13% and

11%, respectively). Patients had moderate comorbidities as shown by a median Charlson comorbidity index of 3 (IQR 2–5) for both groups. Final multidisciplinary team diagnoses after lung biopsy included chronic hypersensitivity pneumonitis (n=27/52; 52%), idiopathic non-specific interstitial pneumonia (n=7; 13%), and idiopathic pulmonary fibrosis (n=4; 8%). Details on the number of biopsies, maximum diameter, and technical aspects of biopsy procedures are provided in the appendix (p 4).

In the step-up strategy group, one patient (4%) of 28 needed chest tube drainage after transbronchial cryobiopsy due to a pneumothorax. In addition, three patients underwent step-up SLB after inconclusive transbronchial cryobiopsy; the chest tube could not be removed within 24 h in two of these patients. Thus, in total, three of 28 patients (11%; 95% CI 4–27%) received an unexpected chest tube. In the immediate SLB group, the chest tube could not be removed within 24 h in 11 of 24 patients (46%; 28–65%). The difference in primary outcome was 35% (11–56%) in favour of the step-up approach (p=0·0058), with a corresponding OR for unexpected chest tube drainage of 0·14 (0·03–0·60). Patients randomly assigned to the step-up group had a median in situ chest tube duration of 25 h (IQR 25–170), versus 30 h (IQR 24–66; n=11) for the immediate SLB group. Adjusted for baseline forced vital capacity and the Hb-corrected diffusion capacity of the lungs for carbon monoxide values, the OR of 0·18 (0·04–0·87) was in favour of the step-up approach (p=0·033). The worst-case scenario with the three patients who dropped out in the immediate SLB group assumed not to have had unexpected chest tube drainage showed a difference in the primary outcome of 30% percentage points (7–50%) in favour of the step-up approach (p=0·014); after adjustment for baseline forced vital capacity values, the OR of 0·22 (0·05–0·99) was in favour of the step-up approach (p=0·048).

Table 1. Baseline characteristics

	Total (N=52)	**Step-up strategy (n=28)**	**Immediate SLB (n=24)**
Age, years	66 (59–72)	68 (61–73)	65 (57–70)
Sex			
Male	42 (81%)	22 (79%)	20 (83%)
Female	10 (19%)	6 (21%)	4 (17%)
BMI, kg/m^2	28 (26–30)	28 (26–30)	28 (25–30)

Table 1. Continued

	Total (N=52)	Step-up strategy (n=28)	Immediate SLB (n=24)
Smoking status			
Never	7 (13%)	2 (7%)	5 (21%)
Former	40 (77%)	23 (82%)	17 (71%)
Current	5 (10%)	3 (11%)	2 (8%)
Pulmonary function test			
Forced vital capacity, % predicted value	84 (16)	90 (14)	77 (15)
Hb-corrected diffusion capacity of the lungs for carbon monoxide, % predicted value	56 (16)	61 (15)	50 (16)
Charlson comorbidity index	3 (2–5)	3 (2–5)	3 (2–5)
Visual analogue scale pain	0 (0–26)	0 (0–19)	0 (0–44)
Final multidisciplinary team discussion diagnosis			
Hypersensitivity pneumonitis	27 (52%)	12 (43%)	15 (63%)
Idiopathic non-specific interstitial pneumonia	7 (13%)	5 (18%)	2 (8%)
Idiopathic pulmonary fibrosis	4 (8%)	3 (11%)	1 (4%)
Sarcoidosis	2 (4%)	1 (4%)	1 (4%)
Unclassifiable	6 (12%)	3 (11%)	3 (13%)
Other*	6 (12%)	4 (14%)	2 (8%)

Data are n (%), median (IQR), or mean (SD). ILD=interstitial lung disease. SLB=surgical lung biopsy. *Other included: respiratory bronchiolitis-associated ILD (n=2), connective tissue disease-related ILD (n=2), organising pneumonia with small airway disease in patient with common variable immunodeficiency (n=1), and drug-related ILD (n=1).

Diagnostic yield and patient-related outcomes are summarised in table 2. In the step-up strategy group, after transbronchial cryobiopsy alone, the multidisciplinary team reached a classifying diagnosis in 23 of 28 patients, resulting in a diagnostic yield of 82% (95% CI 64–92%). The other five patients were all discussed in a second multidisciplinary team discussion and considered for subsequent SLB. Three of them underwent subsequent SLB, reaching a classifying diagnosis in two patients, resulting in a diagnostic yield of the step-up strategy of 89% (73–96%). Two patients did not undergo subsequent SLB, although a classifying diagnosis was not reached after transbronchial cryobiopsy. In these cases, integration of the transbronchial cryobiopsy results during multidisciplinary team

discussion limited the differential diagnosis sufficiently to decide on the first-line treatment. In the immediate SLB group, a multidisciplinary team discussion after SLB reached a classifying diagnosis in 21 of 24 patients, resulting in a diagnostic yield of 88% (69–97%; figure 2).

Table 2. Diagnostic yield for ILD diagnosis and patient-centred outcomes

	Step-up strategy (n=28)	Immediate SLB (n=24)	p value
Diagnostic yield	89% (73–96)	88% (69–97)	0·841
Diagnostic yield after transbronchial cryobiopsy alone	82% (64–92)	..	..
Total need for a chest tube	4 (14%)	24 (100%)	<0·0001
After transbronchial cryobiopsy	1 (4%)	..	..
After SLB	3 (11%)	24 (100%)	..
Unexpected chest tube*	3 (11%)	11 (46%)	0·0058
After transbronchial cryobiopsy	1 (4%)	..	..
After SLB	2 (7%)	11 (46%)	..
Chest tube in situ			
<24 h	1 (4%)	13 (54%)	..
24–36 h	2 (7%)	7 (29%)	..
36–48 h	0	1 (4%)	..
>48 h	1 (4%)	3 (13%)	..
Total in-hospital stay	1 (1–1)	5 (4–6)	<0·0001
Completed visual analogue scale pain score on day 1	25 (89%)	20 (83%)	..
Visual analogue scale pain score	15 (0–38)	45 (21–50)	0·0057
Visual analogue scale pain score >30	7/25 (28%)	14/20 (70%)	0·0073
Completed visual analogue scale pain score on day 4	25 (89%)	21 (88%)	..
Visual analogue scale pain score	1 (1–21)	20 (6–30)	0·056
Visual analogue scale pain score >30	3/25 (12%)	4/21 (19%)	0·69

Data are n or n/N (%), median (IQR), or percentage (95% CI), unless otherwise stated. Visual analogue scale scores for pain ranged from 0 (no pain) to 100 (worst pain imaginable). A visual analogue scale score of more than 30 was considered moderate pain. ILD=interstitial lung disease. SLB=surgical lung biopsy. *Definition of unexpected chest tube was any chest tube after transbronchial cryobiopsy or chest tube for more than 24 h after SLB.

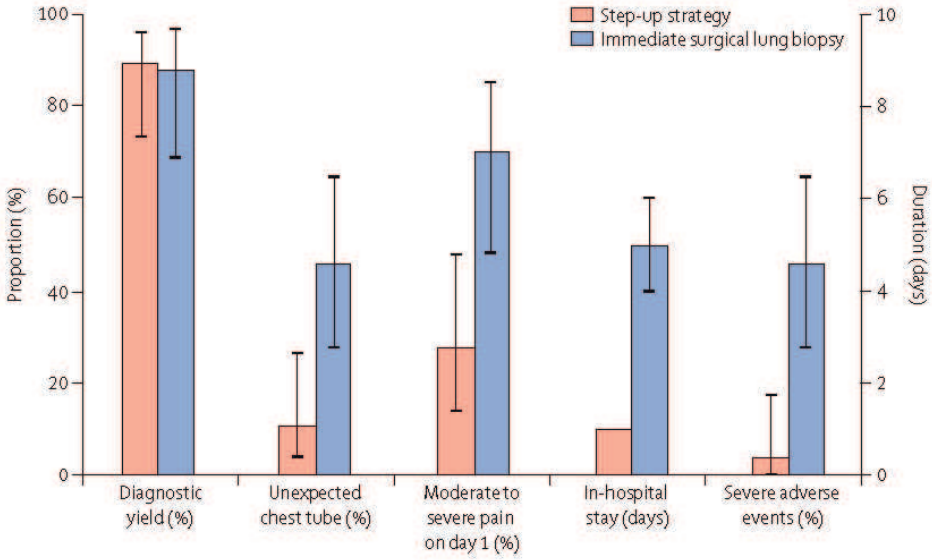


Figure 2. Primary and secondary endpoints
All outcomes are presented as percentages (left y axis), with the exception of in-hospital stay, which is presented as duration in days (right y axis). The bars represent 95% CIs (%) or IQR (days). Diagnostic yield refers to the proportion of patients in whom a classifying multi-disciplinary team diagnosis was reached. Unexpected chest tube was defined as any chest tube following transbronchial cryobiopsy or prolonged (>24 h) chest tube following surgical lung biopsy. Moderate to severe pain refers to a pain score of >30 on the visual analogue scale ranging from 0 (no pain) to 100 (worst pain imaginable). Duration of in-hospital stay included the day of hospital admission, adding 1 day per overnight stay. Severe adverse events were defined as: any medical events that occurred during the study period that resulted in death, were life-threatening (at the time of the event), or required admission to hospital or prolongation of existing inpatients' stay in hospital.

23 of 28 patients (82%) who underwent transbronchial cryobiopsy were treated in an outpatient setting. None were readmitted during the 3-month follow-up, except for the three patients who underwent subsequent SLB. The median in-hospital stay was 1 day (IQR 1–1; range 1–15 days; n=28) for the step-up strategy, versus 5 days (IQR 4–6; range 2–17 days; n=24) for the immediate SLB group (p<0·0001).

Of the 52 patients, 48 (92%) responded to the study pain-related questionnaires, although they did not always complete the questionnaire. On the first day after transbronchial cryobiopsy in the step-up strategy, 28% (n=7/25) of patients had a visual analogue scale pain score of more

than 30 versus 70% (n=14/20) after SLB in the immediate SLB strategy (p=0·0072). At day 4, this difference was reduced to 12% (n=3/25) versus 19% (n=4/21; p=0·69; table 2). During further follow-up, pain scores remained similar between the groups, and at 3 months the median visual analogue scale scores were 0 (IQR 0–25) for the step-up strategy and 1 (0–10) for the immediate SLB strategy.

Overall, 13 serious adverse events and 34 adverse events were registered (table 3). Intensive care unit admission and death did not occur. In the step-up strategy group, one patient (4%) of 28 had a serious adverse event, which was a pneumothorax with a persistent air leak requiring chest tube drainage leading to an increased hospital stay of 15 days in total. In six other patients (21%), a pneumothorax was observed but considered clinically insignificant without the need for chest tube insertion. Moderate bleeding occurred in ten patients (36%), which were all controlled by bronchoscopic procedures such as re-inflation of the balloon or instillation of cold saline. In the immediate SLB group, 11 (46%) patients had one or more serious adverse event; these events were: long-term need for chest tube drainage due to a persistent air leak leading to an increased length of in-hospital stay (n=5/24; 21%), pneumonia resulting in rehospitalisation (n=2/24; 8%), uncontrolled pain (2/24; 8%), empyema requiring surgical intervention (n=1/24; 4%), exacerbation of an underlying ILD (n=1/24; 4%), and a pneumothorax following chest tube removal (n=1/24; 4%). The patient with an exacerbation of an underlying ILD was treated with prednisolone and recovered completely.

Table 3. Adverse events

	Step-up strategy (n=28)	Immediate SLB (n=24)
Patients without adverse events	11 (39%)	6 (25%)
Patients with ≥1 adverse event	17 (61%)*	18 (75%)†
One adverse event	12 (43%)	14 (58%)
Two adverse events	3 (11%)	3 (13%)
Three adverse events	2 (7%)	1 (4%)
30-day mortality	0	0
Patients with serious adverse events‡	1 (4%)	11 (46%)
Pneumothorax in need of chest tube	1 (4%)	0
Air leak	0	5 (21%)
Pneumonia	0	2 (8%)

Table 3. Continued

	Step-up strategy (n=28)	Immediate SLB (n=24)
Uncontrolled pain	0	2 (8%)
Empyema	0	1 (4%)
Exacerbation of ILD	0	1 (4%)
Pneumothorax after chest tube removal	0	1 (4%)
Patients with non-serious adverse events	16 (57%)	9 (38%)
Moderate bleed	10 (36%)	0
Prolonged need for chest tube§	2¶ (7%)	6 (25%)
Pneumothorax without need for chest tube	6 (21%)	0
Pneumothorax after chest tube removal||	0	2 (8%)
Pneumonia	1 (4%)	1 (4%)
Laryngeal spasm	2 (7%)	0
Allergic reaction	1 (4%)	0
Uncontrolled pain	1¶ (4%)	0
Nausea	0	1 (4%)
Wound leakage	0	1 (4%)

Data are n (%). ILD=interstitial lung disease. SLB=surgical lung biopsy. *Patients with >1 adverse event consisted of only non-serious adverse events. †Patients with two adverse events consisted of one patient with one serious and one non-serious adverse event; one patient with two serious adverse events; and one patient with two non-serious adverse events; and the one patient with three adverse events had one serious and two non-serious adverse events. ‡Adverse events were considered serious adverse events if they resulted in an unexpected admission to hospital or an increased length of an existing inpatient hospital stay, in all events. The increased length of stay in hospital due to an adverse event was defined as longer than 2 days (one overnight stay) for transbronchial cryobiopsy and 4 days (three overnight stays) for SLB. §Patients in whom prolonged (>24 h) chest tube drainage did not lead to an increase in the length of hospital stay. ¶Adverse events that occurred after SLB that was performed subsequent to inconclusive transbronchial cryobiopsy results. ||Patients in whom pneumothorax did not lead to an increased length of hospital stay.

Of 52 included patients, the biopsies from 51 patients (98%) were reviewed by the reference pathologist (table 4). Biopsies from one patient (immediate SLB) were unavailable for review for logistical reasons. In four patients, the reference pathologist was also involved in the initial assessment. For 32 of 51 (63%) patients, the new histopathological diagnosis was in agreement with the histopathological pattern diagnosed by the local pathologist (κ 0·53; 95% CI 0·36–0·70): 17 of 28 patients

(61%) in the step-up strategy (0·53; 0·31–0·75) and 15 of 23 patients (65%) in the immediate SLB group (0·51; 0·26–0·76; p=0·740). Diagnostic confidence of the reference pathologist was lower for the step-up strategy than for immediate SLB: a high-confidence histopathological diagnosis was obtained in 13 of 28 patients (46%) in the step-up strategy versus 17 of 23 patients (74%) after immediate SLB (p=0·047).

Table 4. Interobserver agreement and diagnostic confidence for histopathological pattern

	Total (N=51)	Step up strategy (n=28)	Immediate SLB (n=23)	p value
Observed agreement	32 (63%)	17 (61%)	15 (65%)	0·740
Observed disagreement	19 (37%)	11 (39%)	8 (35%)	0·740
Cohens' κ for agreement, 95% CI	0·53 (0·36–0·70)	0·53 (0·31–0·75)	0·51 (0·26–0·76)	..
Diagnostic confidence of reference pathologist				
High	30 (59%)	13 (46%)	17 (74%)	0·047
Low	14 (27%)	9 (32%)	5 (22%)	0·686
Unclassifiable	7 (14%)	6 (21%)	1 (4%)	0·078

Data are n (%), unless otherwise specified. An agreement between a local pathologist and reference pathologist was required for histopathological diagnosis. In all patients, the histopathological diagnosis was reviewed on the basis of all available biopsies per patient. Diagnostic confidence in the histopathological pattern of the biopsies was obtained from the reference pathologist only. In case a patient underwent two procedures, the confidence level refers to the overall score of all biopsies per patient. SLB=surgical lung biopsy.

DISCUSSION

In patients with an undiagnosed ILD in whom the multidisciplinary team advised a lung biopsy for an accurate diagnosis, this study shows that starting with a transbronchial cryobiopsy, followed by an SLB only if the transbronchial cryobiopsy is inconclusive, appears to result in a significant reduction in patient burden. Although maintaining a similar high diagnostic yield, patients in the step-up strategy had reduced chest tube drainage, a shorter in-hospital stay, less pain, and fewer serious adverse events compared with immediate SLB.

Previous studies on transbronchial cryobiopsy and SLB were mostly single-arm, making comparisons between the tests difficult, because

outcome differences might be explained by heterogeneity in the population and methods.[3,7,8,14,25] The COLD study provides the first randomised data for two diagnostic strategies in terms of patient burden. Including diagnostic yield as a secondary outcome adds information to the existing literature on the performance of both tests, which is welcome because existing studies directly comparing transbronchial cryobiopsy and SLB are limited to a total of 123 patients across four studies.[16–19] Regarding patient burden, we observed a significant difference between strategies in favour of the step-up strategy (with an absolute risk reduction of 35%) for the need of an unexpected chest tube. In 86% (n=24/28) of patients who started with transbronchial cryobiopsy, chest tube insertion was not needed at all. Compared with immediate SLB, the step-up strategy resulted in a substantial reduction of in-hospital stay of 4 days. In fact, 82% (n=23/28) of patients in the step-up strategy underwent transbronchial cryobiopsy as an outpatient diagnostic procedure. After transbronchial cryobiopsy, patients had significantly less pain than those undergoing SLB, despite standard pain medication being given to them including an erector spinae block and opioids after SLB. Considering safety, adverse events were common for both diagnostic strategies, but were more likely to be serious in the immediate SLB group.

The observed results on patient burden are mostly in line with findings of previous observational studies and meta-analyses. A systematic review of 31 studies in patients with ILD undergoing transbronchial cryobiopsy found an overall complication rate of 23%, mostly pneumothorax (9%) and significant endobronchial bleeding (14%), and a 30-day mortality rate of 0·3%.11 A similar systematic review of 24 studies on SLB found an overall morbidity rate of 13% and a 30-day mortality rate of 2·3%.10 Ravaglia and colleagues9 compared patients with ILD undergoing transbronchial cryobiopsy (n=297) and SLB (n=150), and a long-term chest tube was required in one patient (0·3%) and five patients (3%), respectively, but was defined as lasting 5 days or longer after the procedure (as opposed to ≥24 h in our study). The mean time of hospital stay was 2·6 days versus 6·1 days, respectively, and no severe bleeding occurred in either group.[9]

In the current study, the diagnostic yield was 82% for the multidisciplinary team diagnosis after transbronchial cryobiopsy. This finding is somewhat above average as compared with findings in the previous literature, in which a systematic review of studies on transbronchial cryobiopsy found a summary diagnostic yield of 73%.[11] The diagnostic yield for

multidisciplinary team diagnosis after immediate SLB was 88% in our study, in line with the 88% found in a systematic review of studies on SLB.[26] To date, four prospective studies directly compared transbronchial cryobiopsy and SLB in the same individuals.[16–19] The diagnostic yield for multidisciplinary team diagnosis was reported by three of those studies:[16,17,19] for transbronchial cryobiopsy, it was 63%,[17] 87%,[19] and 91%,[16] whereas for SLB, this was 93%[17,19] and 95%.[16] These results indicate that SLB has a higher diagnostic yield as a single procedure. The step-up strategy was not included in previous studies. In the present study, when an SLB was done after an inconclusive transbronchial cryobiopsy, the diagnostic yield increased to 89%,with the advantage that four of five SLBs could be omitted.

In the absence of a gold standard for diagnosing ILD, comparing diagnostic tests is difficult. Although the diagnostic yield of both strategies in this study was similar, it is impossible to establish whether both strategies were equally close to the true diagnosis. The average diagnostic confidence of the reference pathologists was lower for transbronchial cryobiopsy, possibly suggesting that this is not the case. A previous study showed similar prognostic separation of transbronchial cryobiopsy-based or SLB-based idiopathic pulmonary fibrosis, suggesting a similar actual diagnostic accuracy. However, in addition to its retrospective design, the study dichotomised ILD diagnosis to idiopathic pulmonary fibrosis versus non-idiopathic pulmonary fibrosis and did not provide information on specific ILD diagnosis.[28] Therefore, more long-term data including large prospective cohorts are needed, using the final multidisciplinary team diagnosis as the diagnostic endpoint because of the uncertainty of a histopathological diagnosis alone.

The difficulty of comparing biopsy procedures was further illustrated by the fact that agreement between pathologists was only 63% (κ 0·53; 95% CI 0·36–0·70), which was similar for both transbronchial cryobiopsy and SLB and in line with other studies. Other studies showed the low agreement of histopathological diagnosis: Walsh and colleagues[22] found a κ value of 0·31 for SLB in 70 cases, and Tomassetti and colleagues28 also included transbronchial cryobiopsy, which performed slightly favourably over SLB (κ 0·52 for SLB *vs* κ 0·66 for transbronchial cryobiopsy; n=500). The COLDICE study evaluated the histopathological agreement of pathologists prospectively and found no difference between tests (transbronchial cryobiopsy κ 0·52 *vs* SLB κ 0·50; n=65) although in a post-hoc analysis it was shown that high-confidence histopathological diagnoses

were reported more often for SLB.[16,29] The present study reports a similar observation. It has been suggested that this, in part, might be because guideline definitions of histopathological patterns are based on SLBs. No formal guidelines for the assessment of usual interstitial pneumonia and hypersensitivity pneumonitis based on transbronchial cryobiopsies exist. Differences in classifications and observed confidence levels possibly highlight the need for further research and validation to formalise these findings.

The four studies directly comparing transbronchial cryobiopsy with SLB had conflicting results regarding the concordance of histopathological patterns as detected by either technique. Agreements for histological diagnosis between the two biopsy techniques ranged from 38% (κ 0·22; n=21)18 to 69% (κ 0·47; n=65).[16] Differences might be explained by the small sample sizes,16,17 differences in the number of biopsies taken, and the number of reference pathologists.[16,28]

The low agreement between not only pathologists but also ILD multidisciplinary teams[16,22] highlights difficulties and limitations in the evaluation of histopathology in ILD, which are present for both transbronchial cryobiopsy and SLB. Whether the immediate surgery strategy leads to more confident multidisciplinary team diagnoses compared with the step-up strategy could not be assessed by the present study. Nevertheless, the clinical contribution of histopathology has been shown to change the prebiopsy multidisciplinary team diagnosis,[16] and increase diagnostic confidence[3,30] and its ability to change clinical decisions.[6]

This study had several limitations. First, although adequately powered for the primary outcome, the sample size of 52 is relatively small. Second, a notable limitation is the non-masked nature of this study. Both pathologists and the multidisciplinary team discussion participants were aware of the random assignment group. It was considered not feasible to mask the pathologist because the difference between a surgical and a cryobiopsy specimen is easily recognised. Along this line, the decision was made not to mask the multidisciplinary team discussion participants, because this would limit the pathologists' ability to interactively present the biopsy during the discussion, possibly lowering the quality of the multidisciplinary team discussions. Additionally, masking the multidisciplinary team would only have affected one of our secondary outcomes (ie, diagnostic yield), but not outcomes related to patient burden (including the primary outcome). However, not masking the multidisciplinary team

might have created bias, because the multidisciplinary team might perceive transbronchial cryobiopsies with lower confidence. Given the high diagnostic yield of transbronchial cryobiopsy in our study and the resulting low proportion of patients in which subsequent SLB was advised, the effect of this bias on our study results is likely to be limited. Third, most patients had a final diagnosis of chronic hypersensitivity pneumonitis, whereas idiopathic pulmonary fibrosis accounted for less than 10% of the final diagnoses, which is less than in other studies reporting on the diagnostic yield of lung biopsy in patients with ILD.[16–19] Fourth, the baseline data of both groups showed imbalances for forced vital capacity and Hb-corrected diffusion capacity of the lungs for carbon monoxide, which were higher in the step-up group. However, when correcting for these differences in the analysis, results were similar. Fifth, although not recommended in current guidelines, it might have been of added value to record the diagnostic confidence of the multidisciplinary team diagnosis. Finally, all patients underwent an intubated surgical procedure. We are aware that surgical techniques evolve and the interest in awake, non-intubated video-assisted thoracoscopic surgery is rising.[31] It is likely that such new techniques would result in a lower patient burden, but how they compare to transbronchial cryobiopsy has yet to be established. In addition, novel endobronchial imaging techniques are being evaluated, possibly reducing the need for biopsies altogether.[32,33]

The strengths of this study include its randomised and multicentre design with recruitment of consecutive patients. Recent guidelines express the need for data from randomised trials comparing transbronchial cryobiopsy and SLB.[1,12] Additionally, the clinical importance of this study is underlined by the observation that 28% (n=34/122) of patients who were eligible for study participation declined because of a strong preference for a specific biopsy technique (either transbronchial cryobiopsy or SLB; figure 1). In addition, our design shows a strong emphasis on patient-reported outcomes, which creates the possibility to directly improve shared decision making with regard to obtaining lung tissue in patients with ILD. Unique to the study is that we compared two diagnostic strategies instead of two diagnostic techniques alone. This implies that the COLD study provides the first prospective data to support a recently advocated diagnostic strategy starting with transbronchial cryobiopsy, followed by SLB if the transbronchial cryobiopsy results are inconclusive.[12] Finally, the central training workshops allowed us to harmonise the transbronchial cryobiopsy technique, ensuring that all participating interventional pulmonologists would perform transbronchial cryobiopsy in a similar way.

In conclusion, in patients with ILD with an indication for lung biopsy, the results of our study support patient counselling towards a step-up strategy, starting with the less invasive transbronchial cryobiopsy.

CONTRIBUTORS

KAK, LW, REJ, VP, JHe, MD, DAK, PIB, and JTA were involved in study design. KAK, MKN, REJ, JMD, JRM, JHö, MK, BB, SN, EN, BM, PIB, and JTA were involved in patient recruitment. KAK, MKN, CD, JHö, MK, TR, GS, DC, JvdT, PIB, JTA, REJ, JMD, JRM, DH, BB, SN, EN, JB, BM, and DAK were involved in the data collection. KAK, MKN, JMD, CD, JHö, DH, MK, JB, BM, PIB, JTA, JRM, and GS were involved in the biopsy procedures. KAK, MD, and DAK were involved in the data management and statistical analysis. KAK, MD, DAK, and JTA had full access to the raw data in the study. MD and DAK verified the data. KAK wrote the first draft of the report with input from JTA, PIB, DAK, MKN, JHe, VP, and MD. All authors critically read the manuscript and revised accordingly. KAK, PIB, and JTA had final responsibility for the decision to submit for publication.

DECLARATION OF INTERESTS

All authors declare no competing interests. The workshop in Tübingen to assure harmonisation of the transbronchial cryobiopsy procedure was, in part, sponsored by Erbe Elektromedizin, Tübingen, Germany.

DATA SHARING

Deidentified patient data will be available after publication for researchers with a valid research question, which will be evaluated by the study board. Researchers can address these requests by email to the corresponding author (k.a.kalverda@amsterdamumc.nl).

ACKNOWLEDGMENTS

This study is funded by the Netherlands Organisation for Health Research and Development (ZonMW; 843001813) and Amsterdam University Medical Centers.

REFERENCES

1 Raghu G, Remy-Jardin M, Richeldi L, et al. Idiopathic pulmonary fibrosis (an update) and progressive pulmonary fibrosis in adults: an official ATS/ERS/JRS/ALAT clinical practice guideline. *Am J Respir Crit Care Med* 2022; **205:** e18–47.

2 Walsh SLF, Lederer DJ, Ryerson CJ, et al. Diagnostic likelihood thresholds that define a working diagnosis of idiopathic pulmonary fibrosis. *Am J Respir Crit Care Med* 2019; **200:** 1146–53.

3 Hetzel J, Wells AU, Costabel U, et al. Transbronchial cryobiopsy increases diagnostic confidence in interstitial lung disease: a prospective multicentre trial. *Eur Respir J* 2020; **56:** 1901520.

4 Poletti V, Ravaglia C, Gurioli C, et al. Invasive diagnostic techniques in idiopathic interstitial pneumonias. *Respirology* 2016; **21:** 44–50.

5 Radu D, Freynet O, Kambouchner M, et al. Diagnosis yield and safety of surgical biopsy in interstitial lung diseases: a prospective study. *Ann Thorac Surg* 2022; **114:** 1911–17.

6 Tomassetti S, Ravaglia C, Puglisi S, et al. Impact of lung biopsy information on treatment strategy of patients with interstitial lung diseases. *Ann Am Thorac Soc* 2022; **19:** 737–45.

7 Fisher JH, Shapera S, To T, Marras TK, Gershon A, Dell S. Procedure volume and mortality after surgical lung biopsy in interstitial lung disease. *Eur Respir J* 2019; **53:** 1801164.

8 Hutchinson JP, McKeever TM, Fogarty AW, Navaratnam V, Hubbard RB. Surgical lung biopsy for the diagnosis of interstitial lung disease in England: 1997–2008. *Eur Respir J* 2016; **48:** 1453–61.

9 Ravaglia C, Bonifazi M, Wells AU, et al. Safety and diagnostic yield of transbronchial lung cryobiopsy in diffuse parenchymal lung diseases: a comparative study versus video-assisted thoracoscopic lung biopsy and a systematic review of the literature. *Respiration* 2016; **91:** 215–27.

10 Sharp C, McCabe M, Adamali H, Medford AR. Use of transbronchial cryobiopsy in the diagnosis of interstitial lung disease—a systematic review and cost analysis. *QJM* 2017; **110:** 207–14.

11 Sethi J, Ali MS, Mohananey D, Nanchal R, Maldonado F, Musani A. Are transbronchial cryobiopsies ready for prime time?: a systematic review and meta-analysis. *J Bronchology Interv Pulmonol* 2019; **26:** 22–32.

12 Korevaar DA, Colella S, Fally M, et al. European Respiratory Society guidelines on transbronchial lung cryobiopsy in the diagnosis of interstitial lung diseases. *Eur Respir J* 2022; **60:** 2200425.

13 Durheim MT, Kim S, Gulack BC, et al. Mortality and respiratory failure after thoracoscopic lung biopsy for interstitial lung disease. *Ann Thorac Surg* 2017; **104:** 465–70.

14 Ravaglia C, Wells AU, Tomassetti S, et al. Diagnostic yield and risk/ benefit analysis of trans-bronchial lung cryobiopsy in diffuse parenchymal lung diseases: a large cohort of 699 patients. *BMC Pulm Med* 2019; **19:** 16.

15 Iftikhar IH, Alghothani L, Sardi A, Berkowitz D, Musani AI. Transbronchial lung cryobiopsy and video-assisted thoracoscopic lung biopsy in the diagnosis of diffuse parenchymal lung disease. A meta-analysis of diagnostic test accuracy. *Ann Am Thorac Soc* 2017; **14:** 1197–211.

16 Troy LK, Grainge C, Corte TJ, et al. Diagnostic accuracy of transbronchial lung cryobiopsy for interstitial lung disease diagnosis (COLDICE): a prospective, comparative study. *Lancet Respir Med* 2020; **8:** 171–81.

17 Wahidi MM, Argento AC, Mahmood K, et al. Comparison of forceps, cryoprobe, and thoracoscopic lung biopsy for the diagnosis of interstitial lung disease - the CHILL study. *Respiration* 2022; **101:** 394–400.

18 Romagnoli M, Colby TV, Berthet JP, et al. Poor concordance between sequential transbronchial lung cryobiopsy and surgical lung biopsy in the diagnosis of diffuse interstitial lung diseases. *Am J Respir Crit Care Med* 2019; **199:** 1249–56.

19 Fortin M, Liberman M, Delage A, et al. Transbronchial lung cryobiopsy and surgical lung biopsy: a prospective multi-centre agreement clinical trial (CAN-ICE). *Am J Respir Crit Care Med* 2023; **207:** 1612–19.

20 National Institute for Health and Care Excellence. Shared decision making. https://www.nice.org.uk/about/what-we-do/our-programmes/nice-guidance/nice-guidelines/shared-decision-making (accessed Dec 2, 2023).

21 Raghu G, Remy-Jardin M, Ryerson CJ, et al. Diagnosis of hypersensitivity pneumonitis in adults. an official ATS/JRS/ALAT clinical practice guideline. *Am J Respir Crit Care Med* 2020; **202:** e36–69.

22 Walsh SLF, Wells AU, Desai SR, et al. Multicentre evaluation of multidisciplinary team meeting agreement on diagnosis in diffuse parenchymal lung disease: a case-cohort study. *Lancet Respir Med* 2016; **4:** 557–65.

23 Travis WD, Costabel U, Hansell DM, et al. An official American Thoracic Society/European Respiratory Society statement: update of the international multidisciplinary classification of the idiopathic interstitial pneumonias. *Am J Respir Crit Care Med* 2013; **188:** 733–48.

24 Hetzel J, Maldonado F, Ravaglia C, et al. Transbronchial cryobiopsies for the diagnosis of diffuse parenchymal lung diseases: expert statement from the cryobiopsy working group on safety and utility and a call for standardization of the procedure. *Respiration* 2018; **95:** 188–200.

25 Sigurdsson MI, Isaksson HJ, Gudmundsson G, Gudbjartsson T. Diagnostic surgical lung biopsies for suspected interstitial lung diseases: a retrospective study. *Ann Thorac Surg* 2009; **88:** 227–32.

26 Raghu G, Remy-Jardin M, Myers JL, et al. Diagnosis of idiopathic pulmonary fibrosis. An official ATS/ERS/JRS/ALAT clinical practice guideline. *Am J Respir Crit Care Med* 2018; **198:** e44–68.

27 Collins SL, Moore RA, McQuay HJ. The visual analogue pain intensity scale: what is moderate pain in millimetres? *Pain* 1997; **72:** 95–97.

28 Tomassetti S, Ravaglia C, Wells AU, et al. Prognostic value of transbronchial lung cryobiopsy for the multidisciplinary diagnosis of idiopathic pulmonary fibrosis: a retrospective validation study. *Lancet Respir Med* 2020; **8:** 786–94.

29 Cooper WA, Mahar A, Myers JL, et al. Cryobiopsy for identification of usual interstitial pneumonia and other interstitial lung disease features. Further lessons from COLDICE, a prospective multicenter clinical trial. *Am J Respir Crit Care Med* 2021; **203:** 1306–13.

30 Tomassetti S, Wells AU, Costabel U, et al. Bronchoscopic lung cryobiopsy increases diagnostic confidence in the multidisciplinary diagnosis of idiopathic pulmonary fibrosis. *Am J Respir Crit Care Med* 2016; **193:** 745–52.
31 Grott M, Eichhorn M, Eichhorn F, Schmidt W, Kreuter M, Winter H. Thoracic surgery in the non-intubated spontaneously breathing patient. *Respir Res* 2022; **23:** 379.
32 Vaselli M, Kalverda-Mooij K, Thunnissen E, et al. In vivo polarisation sensitive optical coherence tomography for fibrosis assessment in interstitial lung disease: a prospective, exploratory, observational study. *BMJ Open Respir Res* 2023; **10:** e001628.
33 Wijmans L, Kalverda K, de Bruin D, et al. Bronchoscopic journey of in vivo real-time microscopic imaging in ILD: a case series. *Respiration* 2022; **101:** 1006–14.

SUPPLEMENTARY APPENDIX

Full list of in- and exclusion criteria

Inclusion: clinical and radiological data are insufficient for the establishment of a classifying ILD diagnosis and the MDT discussion advised to obtain lung tissue for ILD diagnosis. At least 18 years of age, being able to provide informed consent and be considered medically fit to undergo a SLB as assessed by the treating physician and the local MDT.

Exclusion criteria: prothrombin time international ratio >1.3, use of clopidogrel or other new anti-platelet therapy or anticoagulant drugs that could not be temporarily halted, thrombocytopenia < 70x10^9/L, history of pulmonary hypertension, diffusing capacity <30% of predicted value, forced vital capacity < 50% of predicted value, forced expiratory volume in the first second <0.8L or <50% of predicted value, body mass index >35 kg/m^2, or pregnancy.

Standard pain medication protocol

TBCB

Prior and following TBCB patients are not prescribed standard analgesics. However, are advised to take paracetamol in the case of any discomfort.

SLB

At the end of the surgical procedure patients receive an erector spinae block to reduce post-operative pain. Besides, while the chest tube is in situ, all patients are prescribed paracetamol 1000mg 4 times daily and metamizol 1000mg 4 times daily and piritramide 5-10mg subcutaneously upon request. When the chest tube is removed patients are prescribed paracetamol 1000mg 4 times daily with oxycodone 5-10mg twice daily with short acting oxynorm 5mg as needed as long as patients experience pain.

Definitions of histopathological confidence (1,2,3)

Histopathological confidence	Defined as
High	-for UIP: the coexistence of patchy fibrosis/architectural distorsion *and* fibroblastic foci with or without honeycomb changes and absence of features favouring an alternative hypothesis. -for HP: UIP like pattern associated with ancillary findings such as granulomas/giant cells; centrilobular fibrosis/bronchiolitis OR centrilobular fibrosis associated with the presence of granulomas/giant cells /organizing pneumonia. -for NSIP: areas of diffuse thickening of alveolar septa by fibrosis and/or lymphocytic infiltrate -for less common other patterns clear histopathological features consisting of specific patterns without inconsistent features
Low	-for UIP: presence of patchy fibrosis *or* honeycomb changes *or* fibrosis with isolated fibroblastic foci. -for HP: a "probable" HP pattern with criteria as above for a confident diagnosis but lacking poorly formed granulomas (2). -for NSIP: only focal changes and/or in overlap with other minor patterns -for less common other patterns histopathologic features observed in specimens with a diameter < 5 mm or mainly representative of centrilobular structures (bronchi/bronchioles) and/or in overlap with other minor patterns
Unclassifiable	-no specific histopathological pattern is recognizable or inconsistent pattern overlap is present

(1) Raghu G, Remy-Jardin M, Myers JL, Richeldi L, Ryerson CJ, Lederer DJ, Behr J,et al; American Thoracic Society, European Respiratory Society, Japanese Respiratory Society, and Latin American Thoracic Society. Diagnosis of Idiopathic Pulmonary Fibrosis. An Official ATS/ERS/JRS/ALAT Clinical Practice Guideline. Am J Respir Crit Care Med. 2018 Sep 1;198(5):e44-e68. doi: 10.1164/rccm.201807-1255ST. PMID: 30168753.
(2) Raghu G, Remy-Jardin M, Ryerson CJ, Myers JL, Kreuter M, Vasakova M, et al. Diagnosis of Hypersensitivity Pneumonitis in Adults. An Official ATS/JRS/ALAT Clinical Practice Guideline. Am J Respir Crit Care Med. 2020 Aug 1;202(3):e36-e69. doi: 10.1164/rccm.202005-2032ST. Erratum in: Am J Respir Crit Care Med. 2021 Jan 1;203(1):150-151. Erratum in: Am J Respir Crit Care Med. 2022 Aug 15;206(4):518. PMID: 32706311; PMCID: PMC7397797.
(3) Ravaglia C, Rossi G, Tomassetti S, Dubini A, Piciucchi S, Chilosi M et al. Report Standardization in Transbronchial Lung Cryobiopsy. Arch Pathol Lab Med. 2019 Apr;143(4):416-417. doi: 10.5858/arpa.2018-0438-LE. PMID: 30920865.

Table, Specifications of transbronchial cryobiopsy and surgical biopsy procedure.

	Step up strategy (n=28)	Immediate SLB (n=24)
TBCB		
Flexible endotracheal tube	27 (96%)	-
Rigid endotracheal tube	1 (3.6%)	-
Number of biopsies, median (IQR)	4 (3-5)	-
Maximum biopsy diameter in cm	0.6 (±0.25)	-
Total number of biopsies	116	-
RB 8	42 (36%)	-
RB 9	48 (41%)	-
RB 10	14 (12%)	-
LB 3	4 (3.4%)	-
LB 8	2 (1.7%)	-
LB 9	6 (5.2%)	-
SLB		
mVATS	-	13 (54%)
uVATS	3 (11%)	9 (38%)
Mini-thorocotomy	-	2 (8%)
Number of biopsies, median (IQR)	3 (3-3)	3 (2-3)
Maximum biopsy diameter in cm	4.5 (±1.0)	4.5 (±1.6)
Total number of biopsies	9	58
RUL	3 (33%)	20 (34%)
RML	3 (33%)	14 (24%)
RLL	3 (33%)	20 (34%)
LUL	-	1 (1.7%)
LLL	-	3 (5.2%)

Data is shown as n (%) or mean (SD) unless otherwise stated. TBCB= transbronchial cryobiopsy; RB= right bronchus; LB= left bronchus; SLB= surgical lung biopsy; mVATS= multi portal video assisted thoracoscopic surgery; uVATS= uniportal video assisted thoracoscopic surgery; RUL= right upper lobe; RML= right middle lobe; RLL= right lower lobe; LUL= left upper lobe; LLL= left lower lobe

Chapter 4

Transbronchial cryobiopsy followed by as-needed surgical lung biopsy *versus* immediate surgical lung biopsy for diagnosing interstitial lung disease: a cost–utility analysis

Kirsten Kalverda[1,2], Marit van Barreveld[3,4], Peter Bonta[1], Johannes Daniels[1], Chris Dickhoff[5], Daniel A. Korevaar[1], Jouke Annema[1,6] and Marcel Dijkgraaf[3,4,6]

[1]Department of Respiratory Medicine, Amsterdam University Medical Center (UMC), Amsterdam, Netherlands. [2]Department of Respiratory Medicine, Dijklander Ziekenhuis, Hoorn, Netherlands. [3]Department of Epidemiology and Data Science, Amsterdam UMC, University of Amsterdam, Amsterdam, Netherlands. [4]Methodology, Amsterdam Public Health, Amsterdam, Netherlands. [5]Department of Cardiothoracic Surgery, Amsterdam UMC, Amsterdam, Netherlands. [6]These authors contributed equally.

ERJ Open Res 2026; 12: 00629–2025

ABSTRACT

Background and objective

This study focused on the economic evaluation of the step-up diagnostic strategy (transbronchial cryobiopsy followed by surgical lung biopsy (SLB) when needed) compared with the immediate SLB strategy (immediate SLB) for diagnosing interstitial lung disease (ILD).

Methods

A cost–utility analysis was conducted from both a healthcare and a societal perspective. The societal perspective extended the healthcare perspective by including productivity losses and patient out-of-pocket expenses. This study was performed alongside a randomised controlled trial in which patients were randomised to the step-up strategy or the immediate SLB strategy, with a time horizon of 12 weeks. The primary outcome was the cost per quality-adjusted life-year (QALY). Costs were addressed irrespective of payer source and included healthcare costs by providers, costs of productivity loss by employers and disease-related out-of-pocket expenses by patients.

Results

47 patients were included: 25 patients in the step-up diagnostic strategy group and 22 in the immediate SLB strategy group. A mean difference of 0.025 (96% confidence interval (CI) 0.004–0.047; p=0.04) QALYs was found in favour of the step-up strategy. The cost per patient from the healthcare perspective was €4644 (95% CI €3683–€5803) for the step-up strategy group and €8935 (95% CI €8019–€9979) for the immediate SLB group. From a societal perspective, the cost was €6873 (95% CI €5014–€9113) in the step-up strategy group versus €12 924 (95% CI €10 745–€15 325) in the immediate SLB group.

Conclusion

The step-up diagnostic strategy is a cost-effective strategy for patients undergoing lung tissue acquisition for diagnosing ILD; therefore, implementation of this strategy is recommended.

BACKGROUND

Interstitial lung disease (ILD) comprises a heterogeneous group of diffuse parenchymal lung disorders, characterised by varying degrees of inflammation and/or fibrosis in the lung parenchyma. Accurate diagnosis is crucial for treatment decisions and prognosis, but can be challenging. In some patients, lung biopsy is required for definitive diagnosis. Historically, surgical lung biopsy (SLB) has been the standard method for obtaining lung tissue, but in the past decade, the less invasive transbronchial biopsy technique has gained acceptance. Transbronchial cryobiopsy is an endoscopic procedure and is less invasive. However, the diagnostic yield is somewhat lower than the diagnostic yield of SLB, meaning that some patients will have to undergo a step-up SLB when results from transbronchial cryobiopsy are insufficiently informative. Recently, a head-to-head comparison of the step-up strategy and immediate SLB for the diagnosis of ILD was performed (COLD study) [1]. The step-up strategy consisted of transbronchial cryobiopsy, followed by SLB if its outcome was inconclusive. The results from the randomised clinical trial showed that the step-up strategy reduced the patient burden in terms of unexpected chest tube drainages (11% versus 46%), in-hospital stay (median of 1 versus 5 days), and serious adverse events (4% versus 50%), without a loss in diagnostic yield (89% versus 88%). This means that, even when inconclusive transbronchial cryobiopsies are followed by an SLB, the step-up diagnostic strategy is less invasive while maintaining a comparably high diagnostic yield. However, full acceptance and implementation of the step-up strategy and willingness to adjust existing guidelines, in part, depends on proven cost-effectiveness. The aim of this study is to provide a cost–utility analysis (CUA) of both diagnostic strategies.

METHODS

General approach and analysis set

This economic evaluation of the step-up strategy for ILD compared with immediate SLB from a Dutch societal perspective was conducted as part of the COLD study, registered at the Dutch Trial Register (number NL7634). The study was approved by the Medical Ethics Committee of the Academic Medical Center Amsterdam (identifier number 2018_224). The primary bivariate outcome in the CUA was the cost per quality-adjusted life-year (QALY). Costs were addressed irrespective of payer source and included

healthcare costs by providers, costs of productivity loss by employers, and disease-related out-of-pocket expenses by patients. A CUA provides information for health policy decision makers to decide upon efficient and affordable healthcare in general, based on nationally accepted evaluation criteria regarding the cost ceiling level (or willingness to pay) per additional QALY in view of patients' disease burden [2, 3].

The time horizon was 12 weeks following initial biopsy procedure, allowing sufficient follow-up time after an inconclusive transbronchial cryobiopsy in the step-up strategy to conduct a subsequent SLB within 6 weeks. It was expected that complications such as pneumothorax, bleeding and infections could be handled adequately within these 12 weeks. With this limited time horizon, differential discounting of health outcomes and costs to account for time preference over years was disregarded. The current report follows the ISPOR Consolidated Health Economic Evaluation Reporting Standards 2022 [4].

An extensive report on clinical data was published separately [1]. The COLD study was a multicentre, randomised controlled trial in six hospitals across the Netherlands, including academic and general hospitals. Patients with ILD, who were fit for surgery and indicated for lung biopsy as assessed by a multidisciplinary team discussion as part of standard care (Dutch Trial Register number NL7634), were randomly allocated to the step-up strategy or immediate SLB strategy in a 1:1 ratio. Patient recruitment ran from 8 April 2019 to 24 October 2021. The planned sample size of 23 patients per group was reached, with 28 clinically evaluable patients in the step-up strategy group and 24 in the immediate SLB strategy group. Of the 56 patients who signed informed consent, one patient's lung function declined rapidly and no randomisation was performed. Three patients randomised to the immediate SLB strategy did not proceed to SLB and were excluded. Hence, the 52 remaining patients constituted the modified intention-to-treat population used for the clinical report [1]. The analysis set used in this piggyback economic evaluation included the subset of patients from this modified intention-to-treat population who completed the patient questionnaires during follow-up.

Resources and data gathering

Healthcare resource use data were gathered for 1) in-hospital diagnostic and therapeutic procedures, inpatient hospital stays, emergency care, day-care treatment, specialist consultations, rehabilitation physicians and ambulance transport; 2) other institutional care at a rehabilitation

centre, nursing home or care hotel; 3) out-of-hospital care by a general practitioner, physiotherapist, psychologist, psychiatrist or company physician; and 4) formal home care (home help, personal care, nursing). In addition, data on informal home care and health-related out-of-pocket expenses of patients for transport, over-the-counter medication and devices were gathered. Data of productivity loss resulting from absence from work due to sick leave (absenteeism) and lowered efficiency while at work (presenteeism) were also registered. Finally, data on productivity loss from unpaid work were gathered.

Clinical report forms, medical files and self-reports by patients using the Institute for Medical Technology Assessment (iMTA) Medical Consumption Questionnaire (iMCQ) [5] at 12 weeks (complemented with questions on out-of-pocket expenses) and the iMTA Productivity Cost Questionnaire (iPCQ) [6] at 4, 8 and 12 weeks after randomisation were used as data sources.

Unit costs and costs

The unit costs of (non-)hospital resources and lost working hours were obtained from the most recent Dutch Manual for Costing in healthcare research (DMC) [7]. If unit costs for laboratory analyses, diagnostics and therapeutic procedures were not listed in the DMC, they were derived from hospital unit costing sheets or tariffs for mutual services. The friction cost method [8] was applied in the case of costs of productivity loss and were based on the most recent friction period (n=115 days) as listed in the DMC. Table S1a,b shows the unit costs of the resources used. Unit costs were assumed for the base year 2022 and unit costs originating from other calendar years were price-indexed with general yearly consumer price indices from Statistics Netherlands [9].

The costs of resources were calculated by multiplying the frequency of distinct resources used by their respective unit costs. Volumes and costs are reported separately as means per patient by randomisation group. Mean subtotal costs were reported for hospital care, other healthcare, out-of-pocket expenses, productivity loss and lost unpaid work. A healthcare perspective was taken by summing the mean subtotal costs for hospital care and other healthcare, while the societal perspective was taken by summing all mean subtotal costs.

Health outcomes

The health outcome in the CUA was the number of QALYs, which was assessed using the five-level, five-dimension EuroQol questionnaire (EQ-5D-5L) as the utility measure. The EQ-5D-5L contains five items: mobility, self-care, usual activities, pain/complaints and mood (anxiety/depression). Each item has five response options: no problems, slight problems, moderate problems, severe problems and extreme problems/inability to perform. EQ-5D-5L scoring profiles at successive measurements (baseline and days 4, 14, 28, 42, 56 and 84 of follow-up) were converted into health utility scores using general population-based tariffs of time trade-off ratings of health states, with health utility scores potentially ranging between -0.44 (worst health) and 1 (best health) [10]. QALYs were calculated by first taking the average of health utility scores during follow-up, weighted by the lengths of the preceding periods in between successive measurements, and multiplying them by 12/52. Hence, the maximum achievable QALY during the 12 weeks for a patient was 0.2307.

Study population, missing data and analyses

The CUA was performed in the subset of patients of the modified intention-to-treat population who completed patient questionnaires during follow-up. Although few patients dropped out for this reason, and overlap with the published patient characteristics in the clinical report [1] can be expected, it was decided to provide an updated baseline table for the current analysis set for comparative purposes and add scores from the Eastern Cooperative Oncology Group (ECOG) performance status scale [11].

Initial data cleaning accounted for routing of questions dependent on patients' responses and for out-of-range values (such as confusing weekdays with working days). Three patients in the step-up strategy group and two patients in the immediate SLB strategy group did not respond to the invitations to complete questionnaires. These patients were excluded from the analysis, because the trial size limits the feasibility of advanced imputation approaches aimed at reducing uncertainty.

After data cleaning, missing data in the returned iMCQ and iPCQ were limited to about 1.0% of planned data points in the step-up strategy group and 2.7% in the immediate SLB group. These missing data were imputed with the mean group scores per input parameter, based on the available data. Because of the availability of, at most, seven within-patient assessments over time, missing data in the returned EQ-5D-5L questionnaires

were imputed at the level of the health utility scores following predictive mean matching with baseline predictors and the available health utility scores in the model. Five imputation sets were generated and further calculations were based on aggregated mean scores per patient over the distinct imputation sets for computational convenience. To account for the ignored variance between imputation sets by using the aggregated mean score of each patient as source data, the group mean results on health utilities were reported with 96% confidence intervals (CIs) and critical p-value of 0.04 two-sided, instead of the 95% CIs and critical p-values of 0.05 for the mean group results on costs. Uncertainty was reported with CIs of the means derived after correction for bias and using accelerated nonparametric bootstrapping [12], drawing 2500 samples of the same sizes as the original samples and with replacement. CIs were mainly used for interpretation of study results, with significance testing reluctantly reserved for the main components of total healthcare costs, total societal costs and QALYs. Differences in mean costs and QALYs were assessed using two-sample t-tests applying the abovementioned nonparametric bootstrapping procedure.

In view of the limited size of the trial, differences in QALY scores over 12 weeks may be affected by baseline health utility levels. Adjustment for baseline was done by subtracting the baseline health utilities multiplied by 12/52 from the QALYs generated during the 12 weeks of follow-up. Both, the unadjusted and baseline adjusted results were reported.

Incremental CUA was applied by relating the observed differences in costs between the step-up strategy and the immediate SLB strategy to the corresponding observed differences in QALYs. Because of a strong indication for dominance by the step-up strategy over the immediate SLB strategy based on the differences between groups in costs and QALYs, no incremental cost-effectiveness ratio was calculated and visualisations of results with cost-effectiveness planes and cost-effectiveness acceptability curves were forgone.

The observed difference in healthcare cost between the step-up strategy and the immediate SLB strategy was related to the expected yearly national number of patients with a need for diagnosis of ILD in order to forecast the budget impact for healthcare when the step-up strategy would replace the immediate SLB strategy.

Analyses were done with IBM SPSS and Microsoft Excel software.

RESULTS

Baseline characteristics

The baseline characteristics of 47 patients who participated and completed follow-up questionnaires are shown in table 1. 25 were in the step-up strategy group, and 22 in the immediate SLB strategy group. Unless otherwise stated, these patient numbers also hold for the subsequent tables with study results. For characteristics of the full clinical analysis cohort (step-up strategy, n=28; immediate SLB, n=24), see the published clinical report [1].

Table 1. Baseline characteristics by diagnostic strategy

Characteristic	Total (n=47)	Step-up strategy (n=25)	Immediate SLB (n=22)
Age, years	66 (9)	67 (8)	64 (9)
Male sex, n (%)	38 (81)	20 (80)	18 (82)
Body mass index, $kg \cdot m^{-2}$	28 (3)	28 (3)	29 (4)
Smoking status, n (%)			
Never	7 (15)	2 (8)	5 (23)
Ex-smoker	35 (74)	20 (80)	15 (68)
Active smoker	5 (11)	3 (12)	2 (9)
ECOG performance status, n (%)			
Fully active	17 (36)	9 (36)	8 (36)
Symptotic, ambulant, light work	17 (36)	10 (40)	7 (32)
>50% waking time ambulant, no work	12 (26)	6 (24)	6 (27)
>50% waking time confined to bed/chair	1 (2)	–	1 (5)
Lung function			
Forced vital capacity, % predicted value	84 (16)	91 (14)	76 (16)*
Diffusion capacity, % predicted value	55 (16)	61 (15)	48 (15)**
Health utility	0.771 (0.226)	0.757 (0.247)	0.786 (0.205)

Data are presented as mean (SD) unless otherwise stated. SLB: surgical lung biopsy; ECOG: Eastern Cooperative Oncology Group. *: p=0.001; **: p=0.005.

In this economic analysis set, the step-up strategy and immediate SLB strategy were comparable for age, sex, body mass index and smoking status. ECOG performance status was also comparable, despite significantly higher forced vital capacity and carbon monoxide diffusion capacity mean scores in the step-up strategy group. The mean baseline health utility score was 0.757 (96% CI 0.644–0.850) in the step-up strategy group and 0.786 (96% CI 0.691–0.871) in the immediate SLB strategy group, with the difference of -0.029 (96% CI -0.163 to 0.095; p=0.67).

Use and costs of hospital resources

The mean use of hospital care directly related to offering patients the step-up strategy or the immediate SLB strategy was similar for both groups (table S2). Chest computed tomography (CT) and the lung function test were standard in both strategies. Three patients (12%) received an SLB after the initial transbronchial cryobiopsy was inconclusive. The step-up strategy included a post-procedural chest X-ray and could be performed in an outpatient setting, whereas the immediate SLB strategy was associated with in-hospital stay. Medical specialists were equally frequently consulted by the patients from the two groups.

Applying the step-up strategy reduced the mean hospital healthcare cost during the first 12 weeks (table 2) by 47.7%: €4459 was spent, versus €8524 in the immediate SLB group, the difference being -€4065 (95% CI -€5642 to -€2447). The mean cost in the step-up strategy group mainly originated from the transbronchial cryobiopsy procedure itself (35.2%), inpatient hospital stay (19.1%), care by medical specialists (10.9%), day-care treatment (7.5%) and receiving SLB due to inconclusive results from transbronchial cryobiopsy (6.9%). The mean cost in the immediate SLB strategy group was mostly caused by inpatient hospital stay (43.6%), the SLB procedure itself (30.2%), need for chest tube drainage (9.3%) and care by medical specialists (5.9%).

Table 2. Mean costs (€) of hospital resources per patient by diagnostic strategy

Resource	Step-up strategy	Immediate SLB	Difference
CT-thorax	188 (–)	188 (–)	–
Lung function tests	228 (–)	228 (–)	–
Multidisciplinary team	164 (157–170)	154 (–)	9 (0–22)
Transbronchial cryobiopsy	1572 (–)	–	1572 (–)

Table 2. Continued

Resource	Step-up strategy	Immediate SLB	Difference
SLB	309 (103–515)	2574 (–)	-2265 (-2471– -1853)
Erector spinae plane block	29 (10–48)	240 (–)	-211 (-240– -173)
Chest tube drainage	127 (63–222)	793 (–)	-666 (-730– -571)
NSAIDs	17 (14–22)	22 (20–24)	-5 (-9–1)
Opioids	3 (1–5)	18 (–)	-15 (-16– -13)
Chest radiography	82 (–)	–	82 (–)
Emergency department	21 (10–31)	39 (2–80)	-18 (-122–46)
Ambulance non-acute	35 (12–59)	–	35 (12–82)
Day-care treatment	335 (281–389)	46 (15–76)	289 (207–372)
Hospital stay	850 (309–1623)	3718 (2898–4654)	-2868 (-4293– -1416)
Medical specialist	485 (327–658)	505 (397–619)	-20 (-222–199)
Rehabilitation physician	15 (0–29)	–	15 (1–43)
Total cost of hospital care	4459 (3489–5622)	8524 (7675–9547)	-4065 (-5642– -2447)

Data are presented as mean (95% confidence interval). SLB: surgical lung biopsy; CT: computed tomography; NSAID: nonsteroidal anti-inflammatory drug.

Use and costs of other healthcare resources

Use of non-hospital healthcare during the 12 weeks in both groups was limited to general practitioner, physical therapist, company physician and formal domestic help at home, while one patient in the step-up strategy group received formal nursing care at home and two patients in the immediate SLB strategy group received mental support, one from a psychologist and one from a psychiatrist (table S3). Institutionalised care in a nursing home, rehabilitation centre or care hotel was not reported in either group. The difference of -€226 in the mean total cost of healthcare other than hospital care between the groups (table S4) was non-significantly in favour of the step-up strategy, mainly driven by the SLB patient visiting the psychiatrist.

Use and costs of informal care, out-of-pocket expenses and productivity losses

Patients in the step-up strategy group reported 13.16 (95% CI 0.2–36.11) hours of informal care (mainly personal care) on average, while patients

in the immediate SLB strategy group reported 4.29 (95% CI 1.13–8.29) hours of informal care, mainly domestic help. The corresponding costs in table S5 show a cost difference of €167 at the expense of the step-up strategy group. Table S5 also shows that out-of-pocket expenses for extra domestic help at home, over-the-counter drugs and devices were limited or non-existent. The cost of health-related transport too was non-significantly increased in the step-up strategy group (€152 versus €35), contributing to the difference of €265 in total out-of-pocket expenses.

The mean productivity loss due to absence from paid work in the immediate SLB strategy group was quadruple that in the step-up strategy group (table 3). Productivity loss due to presenteeism was limited and comparable in both groups. As a result, a threefold higher productivity loss from paid work in the immediate SLB strategy group was observed, amounting to a mean additional cost of €1957. Absence from unpaid work between the groups was comparable. The mean total cost per patient of productivity loss of paid and unpaid work was €1827 (95% bias-corrected and accelerated (BCa) CI €847–€2868) in the step-up strategy group and €3852 (95% BCa CI €1823–€6388) in the immediate SLB strategy group, with a difference of -€2025 (95% BCa CI -€5155–€579) in favour of the step-up strategy.

Table 3. Mean productivity loss and related costs (€) per patient by diagnostic strategy

Resource	Step-up strategy	Immediate SLB	Difference
Paid work, hours			
Absenteeism	15.60 (1.76–32.77)	64.64 (18.91–122.98)	-49.04 (-117.52–3.71)
Presenteeism	7.13 (1.08–16.18)	7.16 (1.05–15.88)	-0.03 (-11.58–12.49)
Total, hours	22.73 (5.34–43.77)	71.79 (26.31–129.71)	-49.06 (-117.27–6.40)
Total cost of productivity loss, €	906 (213–1746)	2863 (1049–5173)	-1957 (-4677–255)
Unpaid work, hours			
Absenteeism	48.96 (17.44–87.68)	52.59 (10.77–109.08)	-3.63 (-91.58–65.01)
Total cost of lost unpaid work, €	920 (328–1648)	989 (203–2051)	-68 (-1722–1222)

Data are presented as mean (95% confidence interval). SLB: surgical lung biopsy.

Costs from healthcare and societal perspectives

From a healthcare perspective, the mean cost per patient was €4644 (95% CI €3683–€5803) in the step-up strategy group and €8935 (95% CI €8019–€9979) in the immediate SLB group. From a societal perspective, which included the healthcare costs, the productivity losses of paid and unpaid work and the out-of-pocket expenses of patients and their social networks, the mean cost per patient was €6873 (95% CI €5014–€9113) in the step-up strategy group and €12 924 (95% CI €10 745–€15 325) in the immediate SLB group.

From both a healthcare perspective and a societal perspective, significant cost savings were observed in favour of the step-up strategy, summing to -€4291 (95% CI -€5898– -€2687; p<0.001) and -€6051 (95% CI -€9749– -€2531; p=0.001).

Health outcomes

Patients in the step-up strategy group generated, on average, 0.194 (96% CI 0.177–0.209) QALYs, while patients in the immediate SLB group generated 0.176 (96% CI 0.149–0.199) QALYs, a difference of 0.018 (96% CI -0.010–0.045) in favour of the step-up strategy. Corrected for baseline health utility scores, the difference in favour of the step-up strategy was 0.025 (96% CI 0.004–0.047; p=0.04).

Incremental cost–utility and budget impact

The point estimates of differences in mean healthcare costs and mean societal costs were in favour of the step-up strategy. The same observation holds for the point-estimated mean difference in QALYs. Moreover, the observed differences in costs and (after justifiable correction for baseline health utility) in QALYs were significant and of economic relevance. The step-up strategy dominated the immediate SLB strategy regarding healthcare efficiency.

The dominance of the step-up strategy over immediate SLB suggests that replacing immediate SLB with the step-up strategy and reserving SLB only for ILD patients with inconclusive transbronchial cryobiopsy results is the most rational decision from an economical perspective. There are 31.6 (25.6–39) incident ILD cases per 100 000 Dutch inhabitants per year [13]. About a third of these patients, or 10 per 100 000, experience fibrotic ILD and an estimated 30% of that third require a histological lung biopsy. Therefore, about 560 patients in the Netherlands would be eligible for the step-up strategy. Full implementation of the step-up strategy, assuming

that approximately 12% of patients will remain in need of SLB after inconclusive transbronchial cryobiopsy, could save 560×€4291, or a total of about €2.40 million in healthcare expenditures annually.

DISCUSSION

The COLD clinical study showed that a step-up diagnostic strategy starting with transbronchial cryobiopsy (followed by SLB if results are inconclusive), versus immediate SLB, results in a significant reduction of patient burden and in-hospital stay with a similar diagnostic yield in ILD patients requiring lung tissue diagnosis [1]. The reduced patient burden was reflected in QALY gains in the first 12 weeks, we observed substantial savings in hospital costs and we noted lower productivity losses during paid work. The current report of the piggyback economic evaluation alongside the clinical study confirms and further strengthens the arguments in favour of the step-up strategy.

Previous studies, which primarily relied on retrospective data, reported comparable findings [14, 15]. However, these prior investigations focused exclusively on comparing biopsy techniques alone (either transbronchial cryobiopsy or SLB). In contrast, the present study evaluates the entire diagnostic strategy, providing a more comprehensive reflection of real-world clinical practice. The evaluation includes a societal perspective, capturing not only direct healthcare costs, but also productivity losses, informal care and out-of-pocket expenses, which are key components of the broader economic impact. The multicentre setting across both academic and general hospitals enhances the generalisability of the findings.

A methodological consideration in this evaluation is the choice of time horizon. The 12-week time horizon was chosen to capture the key short-term differences between strategies, including initial diagnostic procedures, complications such as pneumothorax and bleeding, follow-up SLB when needed, hospitalisation, recovery and changes in quality of life. Most clinically relevant effects and most of the costs of the diagnostic workup manifest within this period. Extending the analysis beyond this time horizon would require modelling long-term outcomes such as survival, which are influenced more by post-diagnostic treatment decisions than by the diagnostic pathway itself. Moreover, any long-term health benefits of avoiding unnecessary surgery would probably further strengthen the dominance of the step-up strategy. This approach

is consistent with previous trial-based cost-effectiveness evaluations within this clinical field, such as the Assessment of Surgical sTaging versus Endosonographic ultrasound in lung cancer: a Randomised clinical trial (ASTER), which concluded that long-term modelling was not necessary given the short-lived nature of utility differences observed [16].

Although long-term outcomes were not modelled, future research could consider whether the early advantages of the step-up strategy persist over time, especially in terms of survival, long-term morbidity and treatment trajectories. Nevertheless, in the Dutch context, trial-based evaluations with limited horizons are commonly used to inform reimbursement and policy decisions. Our results are informative for national health policymakers, reimbursement authorities and clinical guideline developers. Although the current analysis is based on a single trial with 47 participants and a 12-week follow-up period, its pragmatic design reflects routine clinical practice and yields timely evidence relevant for decision-making. These findings may support the national implementation of the step-up strategy and provide a foundation for future modelling or health technology assessment.

Limitations of the current study include that the current findings are specific to the Dutch healthcare context, where costs for healthcare and non-healthcare resources may differ from those in other countries, potentially limiting the generalisability of these results.

In addition, surgical approaches are evolving towards less invasive techniques, such as non-intubated video-assisted thoracoscopic surgery, resulting in shorter hospital stays. The cost-effectiveness of the step-up strategy compared with these newer surgical methods remains to be determined. Furthermore, this analysis assumes that the equipment necessary for transbronchial cryobiopsy is already available, as the purchase cost of the cryosurgery unit was not included in the evaluation. However, the initial cost of acquiring cryo equipment is relatively low and represents a one-time investment. Importantly, this equipment is increasingly utilised for other diagnostic and therapeutic bronchoscopic applications, such as cryo-endobronchial ultrasound, sampling of peripheral lung lesions and removal of foreign bodies or endobronchial blood clots, further justifying its cost. Lastly, while the trial-based approach provides robust short-term evidence, it cannot capture longer-term outcomes such as survival, diagnostic accuracy beyond 12 weeks and downstream treatment

effects. These uncertainties should be acknowledged when interpreting the cost-effectiveness results.

In conclusion, the step-up strategy proved to be superior economically over an immediate SLB strategy. It has a favourable healthcare budget impact and may support healthcare policies to contain costs and reallocate healthcare resources in the Netherlands more appropriately. Full effort should be directed at implementation of the step-up strategy, in close collaboration with lung professionals and healthcare insurers.

Data availability: Requests for data sharing should be directed to M. Dijkgraaf, who is the custodian of the complete set of data encompassing this study.

Provenance: Submitted article, peer reviewed.

This clinical trial is prospectively registered at www.onderzoekmetmensen.nl as NL7634.

Ethics statement: The study was approved by the Medical Ethics Committee of the Academic Medical Center Amsterdam (identifier number 2018_224). All patients provided written informed consent to participate.

Stakeholders: During the study's design phase, the Dutch patient organisation for individuals with pulmonary fibrosis (Longfibrose Patiëntenvereniging) and the Dutch Society for Pulmonary Medicine (Nederlandse Vereniging van Artsen voor Longziekten en Tuberculose) provided letters of support endorsing the study. Key stakeholders for the implementation of the novel diagnostic technique include patients, pulmonologists and thoracic surgeons. Study findings are disseminated to patients through the patient organisation, and to pulmonologists and surgeons via their respective professional societies. At the international level, the European Respiratory Society has established a dedicated task force on transbronchial cryobiopsy, in which the study authors have been actively involved. The results of this study are shared with key stakeholders within this task force.

Author contributions: K. Kalverda, M. Dijkgraaf, J. Annema and P. Bonta contributed to the conception and design of the study. K. Kalverda, J. Annema, P. Bonta, C. Dickhoff and D.A. Korevaar contributed to data acquisition. K. Kalverda, M. van Barreveld, D.A. Korevaar and M. Dijkgraaf

contributed to data analysis and interpretation. M. van Barreveld and M. Dijkgraaf drafted the manuscript, which was critically reviewed and textually refined by K. Kalverda and J. Annema. All authors approved the submitted manuscript. All authors agree both to be personally accountable for their own contributions and to ensure that questions related to the accuracy or integrity of any part of the work, even ones in which the author was not personally involved, are appropriately investigated and resolved, and the resolution documented in the literature.

Conflict of interest: The authors declare that they have no competing interests.

Support statement: This study was funded by the Dutch independent self-governing organisation ZonMw and Amsterdam UMC. Funding information for this article has been deposited with the Open Funder Registry.

REFERENCES

1 Kalverda KA, Ninaber MK, Wijmans L, et al. Transbronchial cryobiopsy followed by lung biopsy (when indicated) versus immediate surgical lung biopsy for diagnosing interstitial lung disease (COLD): a randomized study. Lancet Respir Med 2024; 12: 513–522.

2 Raad voor de Volksgezondheid & Zorg (RVZ). Zinnige en duurzame zorg: transparante keuze in de zorg voor een houdbaar zorgstelsel. Advies uitgebracht door de RVZ aan de minister van Volksgezondheid, Welzijn en Sport. Zoetermeer, RVZ, 2006.

3 Zaap J, Knies S, Van der Meijden C, et al. Kosteneffectiviteit in de praktijk. Diemen, Zorginstituut Nederland, 2015.

4 Husereau D, Drummond M, Augustovski F, et al. Consolidated Health Economic Evaluation Reporting Standards (CHEERS) 2022 Explanation and Elaboration: a report of the ISPOR CHEERS II Good Practices Task Force. Value Health 2022; 25: 10–31.

5 Bouwmans C, Hakkaart-van Roijen L, Koopmanschap M, et al. iMTA Medical Consumption Questionnaire. Rotterdam, Erasmus University Rotterdam, 2013.

6 Bouwmans C, Hakkaart-van Roijen L, Koopmanschap M, et al. iMTA Productivity Cost Questionnaire. Rotterdam: Erasmus University Rotterdam, 2013.

7 Hakkaart-van Roijen L, Peeters S, Kanters T. Kostenhandleiding voor economische evaluaties in de gezondheidszorg: Methodologie en Referentieprijzen. Herziene versie 2024. [Revisited costing manual for economic evaluations in healthcare: methodology and reference prices]. Rotterdam, Erasmus University Rotterdam, 2024.

8 Koopmanschap MA, Rutten FFH. A practical guide for calculating indirect costs of disease. Pharmacoeconomics 1996; 10: 460–466.

9 Centraal Bureau voor de Statistiek. Consumentenprijzen; prijsindex 2015=100. (Data source for yearly general consumer price indices.) Date last accessed: 15 December 2023. www.cbs.nl/nl-nl/cijfers/detail/83131NED

10 Versteegh M, Vermeulen K, Evers S, et al. Dutch tariff for the five-level version of EQ-5D. Value Health 2016; 19: 343–352.

11 Oken MM, Creech RH, Tormey DC, et al. Toxicity and response criteria of the Eastern Cooperative Oncology Group. Am J Clin Oncol 1982; 5: 649–655.

12 Barber JA, Thompson SG. Analysis of cost data in randomized trials: an application of the non-parametric bootstrap. Stat Med 2000; 19: 3219–3236.

13 International Respiratory Coalition. Interstitial lung disease (ILD). (Age-standardised interstitial lung disease and pulmonary sarcoidosis incidence rate in WHO European Union in 2019, Netherlands.) Date last accessed: 15 February 2019. https://international-respiratory-coalition.org/diseases/interstitial-lung-diseases

14 Sharp C, McCabe M, Adamali H, et al. Use of transbronchial cryobiopsy in the diagnosis of interstitial lung disease-a systematic review and cost analysis. QJM 2017; 110: 207–214. PMID: 27521581

15 Ravaglia C, Bonifazi M, Wells AU, et al. Safety and diagnostic yield of transbronchial lung cryobiopsy in diffuse parenchymal lung diseases: a comparative study versus video-assisted thoracoscopic lung biopsy and a systematic review of the literature. Respiration 2016; 91: 215–227.

16 Sharples LD, Jackson C, Wheaton E, et al. Clinical effectiveness and cost-effectiveness of endobronchial and endoscopic ultrasound relative to surgical staging in potentially resectable lung cancer: results from the ASTER randomised controlled trial. Health Technol Assess 2012; 16: 1–75.

SUPPLEMENTARY MATERIAL

Table S1a. Dutch unit costs (€) for used hospital resources

Resource	Unit	Unit costs in euros 2022	Source
Hospital care			
CT-thorax	procedure	188	DCM
Function tests			
Total lung capacity	test	148	Mutual services 2023 UMC
Diffusion measurement	test	81	Mutual services 2023 UMC
Multidisciplinary team	meeting	77	Hospital unit costing sheet 2018
Transbronchial cryo-biopsy	procedure^	1572	Mutual services 2023 UMC
Surgical lung biopsy	procedure^	2574	Hospitals' unit costing sheets 2017/2018
Erector spinae plane block	add-on procedure	240	Hospital unit costing sheet 2018
Chest tube drainage	procedure	793	Mutual services 2023 UMC
NSAIDs	drainage day	4	Pharmacotherapeutic Compass 2024
Opioids	SLB discharge	4	Pharmacotherapeutic Compass 2024
Chest X-ray	procedure	82	DCM
Emergency department	visit	258	DCM
Ambulance acute	ride	293	DCM
Day-care treatment	day	335	DCM
Hospital stay	day	644	DCM
Medical specialist	visit	120	DCM
Rehabilitation physician	visit	347	DCM

^ including pathological evaluation

Table S1b. Dutch unit costs (€) for used non-hospital resources

Resource	Unit	Unit costs in euros 2022	Source
Out-of-hospital consultations			
General practitioner	visit	31	DCM
Physical therapist	visit	39	DCM
Psychologist	visit	121	DCM
Psychiatrist	visit	148	DCM
Company physician	visit	120	DCM*
Other institutionalized care			
Nursing home	day	290	DCM
Rehabilitation	day	849	DCM
Care hotel	day	150	www.hotels.nl
Formal home care#			
Help at home	hour	33	DCM
Personal care	hour	58	DCM
Home nursing	hour	75	DCM
Productivity loss			
Paid work	hour	40	DCM
Unpaid work	hour	19	DCM
Out-of-pocket expenses			
Over-the-counter drugs	as reported	as reported	as reported
Devices	as reported	as reported	as reported
Domestic help	hour	19	DCM
Transport	as reported	as reported	as reported

^ including pathological evaluation *assumed equal to unit costs of medical specialist #not accounting for costs of travel expenses by professional

Table S2. Mean use of hospital resources per patient by diagnostic strategy

Resource	Step-up strategy Mean (95% CI)	Immediate SLB Mean (95% CI)	Difference Mean (95% CI)
CT-thorax	1 (-)	1 (-)	-
Lung function tests	1 (-)	1 (-)	-
Multidisciplinary team	2.12 (2.04-2.20)	2.0 (-)	0.12 (0.04 to 0.28)
Transbronchial cryo-biopsy	1 (-)	-	1 (-)
Surgical lung biopsy	0.12 (0.04-0.20)	1 (-)	-0.88 (-0.96 to -0.72)
Erector spinae plane block	0.12 (0.04-0.20)	1 (-)	-0.88 (-0.96 to -0.72)
Chest tube drainage	0.16 (0.08-0.28)	1 (-)	-0.84 (-0.92 to -0.72)
NSAIDs (days)	0.76 (0.08-1.84)	1.77 (1.41-2.18)	-1.01 (-1.97 to 0.25)
Opioids (SLB discharge)	0.16 (0.08-0.28)	1 (-)	-0.84 (-0.92 to -0.72)
Chest X-ray	1 (-)	-	1 (-)
Emergency department	0.08 (0.04-0.12)	0.15 (0.01-0.31)	-0.07 (-0.44 to 0.17)
Ambulance non-acute	0.12 (0.04-0.20)	-	0.12 (0.04 to 0.20)
Day-care treatment	1 (0.84-1.16)	0.14 (0.05-0.23)	0.86 (0.62 to 1.11)
Hospital stay	1.32 (0.48-2.52)	5.77 (4.50-7.23)	-4.45 (-6.67 to -2.20)
Medical specialist	4.04 (2.72-5.49)	4.21 (3.30-5.16)	-0.17 (-1.85 to 1.66)
Rehabilitation physician	0.04 (0.00-0.08)	-	0.04 (0.00 to 0.12)

Table S3. Mean use of other health care resources per patient by diagnostic strategy

Resource	Step-up strategy Mean (95% CI)	Immediate SLB Mean (95% CI)	Difference Mean (95% CI)
Out-of-hospital consultations			
General practitioner	1.25 (0.49-2.20)	0.84 (0.56-1.13)	0.40(-0.42 to 1.43)
Physical therapist	2.33 (0.09-5.08)	1.00 (0.14-1.95)	1.33 (-1.27 to 4.74)
Psychologist	-	0.57 (0.00-1.14)	-0.57 (-1.69 to -0.03)
Psychiatrist	-	1.43 (0.00-2.86)	-1.43 (-4.22 to -0.06)
Company physician	0.16 (0.00-0.32)	0.48 (0.16-0.84)	-0.31 (-0.73 to 0.08)
Formal home care			
Help at home	1.04 (0.00-2.08)	0.27 (0.00-0.55)	0.77 (-0.82 to 3.12)
Personal care	-	-	-
Home nursing	0.04 (0.00-0.08)	-	0.04 (0.04 to 0.16)

Table S4. Mean costs (€) of other health care resources per patient by diagnostic strategy

Resource	Step-up strategy Mean (95% CI)	Immediate SLB Mean (95% CI)	Difference Mean (95% CI)
Out-of-hospital consultations			
General practitioner	39 (15-69)	26 (17-35)	12 (-13 to 44)
Physical therapist	91 (4-198)	39 (5-76)	52 (-49 to 184)
Psychologist	-	69 (0-138)	-69 (-204 to -3)
Psychiatrist	-	211 (0-423)	-211 (-625 to -10)
Company physician	19 (0-38)	57 (19-101)	-38 (-87 to 9)
subtotal	148 (44-285)	403 (101-808)	-254 (-817 to 122)
Formal home care#	34 (0-68)	9 (0-18)	25 (-27 to 102)
Help at home Home nursing	3 (0-6)	-	3 (3 to 12)
subtotal	37 (0-74)	9 (0-18)	28 (-18 to 102)
Total costs of other health care	185 (66-336)	412 (110-829)	-226 (-802 to 166)

#Excluding costs of professional transport.

Table S5. Mean out-of-pocket expenses (€) per patient by diagnostic strategy

Resource	Step-up strategy Mean (95% CI)	Immediate SLB Mean (95% CI)	Difference Mean (95% CI)
Out-of-pocket expenses			
Informal care	247 (4-679)	81 (21-156)	167 (-107 to 629)
Extra domestic help	-	13 (0-27)	-13 (-33 to -5)
Over-the-counter drugs	3 (0-6)	7 (1-14)	-4 (-13 to 5)
Devices	-	2 (0-4)	-2 (-5 to -1)
Transport	152 (17-399)	35 (11-62)	117 (-29 to 372)
Total out-of-pocket expenses	402 (27-915)	137 (63-231)	265 (-124 to 780)

Part II

Bronchoscopic imaging techniques for the assessment of interstitial lung disease and ARDS

Chapter 5

Advances in Optical Coherence Tomography and Confocal Laser Endomicroscopy in Pulmonary Diseases

Annika Goorsenberg, Kirsten A. Kalverda, Jouke Annema, Peter Bonta

A.G. and K.A.K. contributed equally to this work.
Department of Pulmonology, Amsterdam University Medical Centers, University of Amsterdam, Amsterdam, The Netherlands

Respiration 2020;99:190–205

ABSTRACT

Diagnosing and monitoring pulmonary diseases is highly dependent on imaging, physiological function tests and tissue sampling. Optical coherence tomography (OCT) and confocal laser endomicroscopy (CLE) are novel imaging techniques with near-microscopic resolution that can be easily and safely combined with conventional bronchoscopy. Disease-related pulmonary anatomical compartments can be visualized, real time, using these techniques. In obstructive lung diseases, airway wall layers and related structural remodelling can be identified and quantified. In malignant lung disease, normal and malignant areas of the central airways, lung parenchyma, lymph nodes and pleura can be discriminated. A growing number of interstitial lung diseases (ILDs) have been visualized using OCT or CLE. Several ILD-associated structural changes can be imaged: fibrosis, cellular infiltration, bronchi(ol)ectasis, cysts and microscopic honeycombing. Although not yet implemented in clinical practice, OCT and CLE have the potential to improve detection and monitoring pulmonary diseases and can contribute in unravelling the pathophysiology of disease and mechanism of action of novel treatments. Indeed, assessment of the airway wall layers with OCT might be helpful when evaluating treatments targeting airway remodelling. By visualizing individual malignant cells, CLE has the potential as a real-time lung cancer detection tool. In the future, both techniques could be combined with laser-enhanced fluorescent-labelled tracer detection. This review discusses the value of OCT and CLE in pulmonary medicine by summarizing the current evidence and elaborating on future perspectives.

Keywords: Optical coherence tomography · Confocal laser endomicroscopy · Obstructive lung disease · Bronchoscopy · Lung cancer · Interstitial lung disease

INTRODUCTION

Diagnosing pulmonary diseases is highly dependent on imaging techniques such as high-resolution computed tomography of the chest (HRCT) or minimal invasive procedures like bronchoscopy for tissue sampling. HRCT imaging contributes to the diagnosis of many pulmonary diseases; however, spatial resolution is limited and patients are subjected to ionizing radiation. Endobronchial sampling, such as mucosal and parenchymal biopsies and needle aspiration, is associated with a complication risk, subject to sampling error and provides only information on one specific sampling site.

To diagnose and understand the pathophysiology of pulmonary diseases and monitor treatments, higher imaging resolution beyond HRCT on a histological/cellular level might be helpful. Optical coherence tomography (OCT) and confocal laser endomicroscopy (CLE) are 2 novel imaging techniques that can fill this gap between invasive and selective tissue sampling and the limited resolution of HRCT. All these techniques are complementary: from a large overview of the lung (HRCT) to near-microscopic imaging (CLE; Fig. 1). In this review, we discuss the value of bronchoscopic OCT and CLE in pulmonary diseases by summarizing OCT and CLE-based imaging studies using the anatomical compartments related to obstructive lung diseases, pulmonary malignancies and interstitial lung diseases (ILD; Fig. 2, Table 1). Furthermore, potential future clinical applications of these imaging techniques in pulmonary disease management are discussed (Table 1). The applicability of OCT in pulmonary vascular diseases has been described in a previously published review and is discussed less extensively [1].

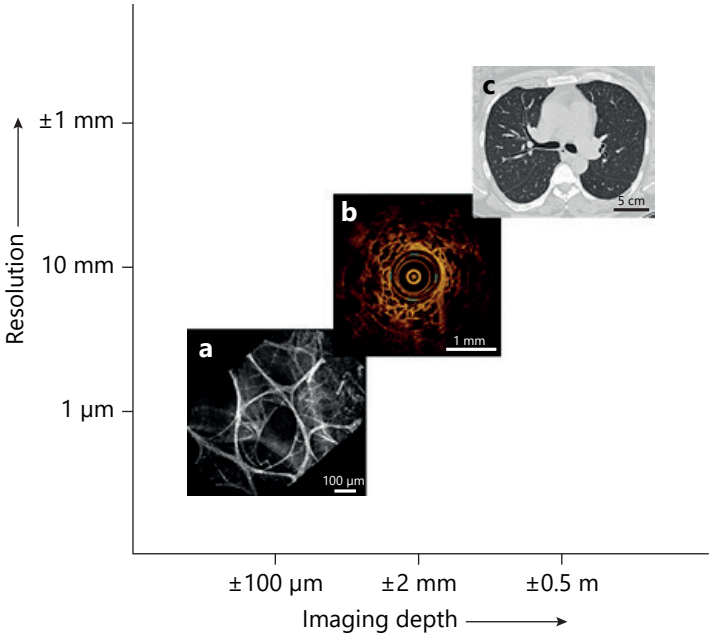


Figure 1. Imaging techniques applied to the alveolar compartment with their corresponding resolution and imaging depth. **a** CLE. **b** OCT. **c** HRCT of the chest.

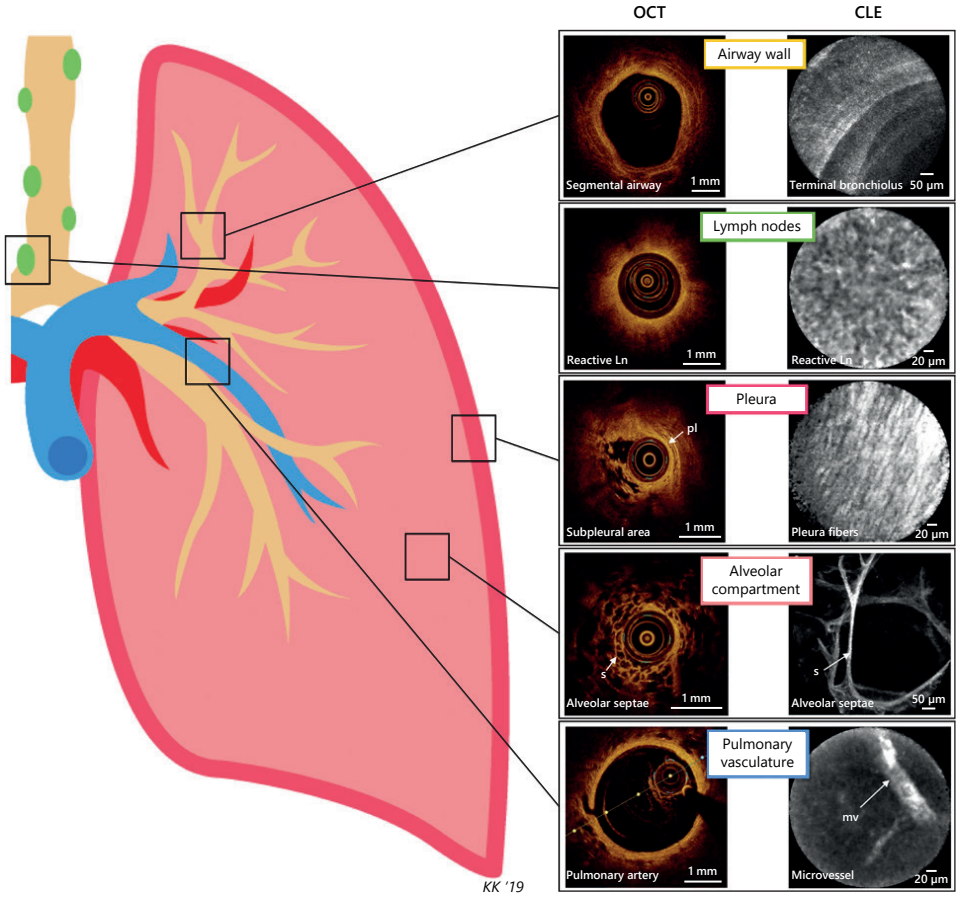


Figure 2. Overview of the pulmonary anatomical compartments with corresponding OCT and CLE images. *Airway wall:* OCT, cross-sectional view of airway wall in segmental airway; CLE, pCLE image showing a typical helical ring-like pattern of terminal bronchiole. *Lymph nodes:* OCT, image in a reactive lymph node; CLE, nCLE image showing abundant lymphocytes in a reactive lymph node. *Pleura:* OCT, image of subpleural area, pl is indicated by the white arrow; CLE, lamellar organized elastin fibres in the pl as seen with pCLE. *Alveolar compartment:* OCT, cross-sectional view of alveolar compartment with network of alveolar s; CLE, pCLE image of alveolar compartment showing alveolar septae with rectangular airspaces. *Pulmonary vasculature:* OCT, cross-sectional view from pulmonary artery; CLE, nCLE image of an mv in a lymph node. OCT, optical coherence tomography; CLE, confocal laser endomicroscopy; Ln, lymph node; pl, pleura; s, septa; mv, microvessel.

TECHNICAL BACKGROUND

Optical Coherence Tomography

OCT is an imaging technique using near-infrared light to generate high-resolution images of tissue structures with a resolution of ±10–15 µm and depth of 2–3 mm (Fig. 1) [2, 3]. The conceptual idea of OCT is comparable to ultrasound, but instead of using the reflection of acoustic waves, OCT uses the scattering of near-infrared light to generate images. An advantage of OCT over (radial) endobronchial ultrasound is that light waves do not need a transducing medium or direct contact with the tissue and therefore has excellent properties to be used in air filled anatomical compartments such as the airways. In short, in OCT, an optical beam generates near-infrared light and focuses on the tissue. The difference in time of light backscattering in structures is measured and compared with a reference beam by using principles of optical interferometry. This enables the OCT system to generate 2D cross-sectional images (Fig. 2, 3). Subsequently, consecutive 2D images generated by pullbacks can be reconstructed to 3D structures. Although many applications in medicine are explored, at first, OCT was clinically implemented in ophthalmology to image the retina [4–6]. Furthermore, OCT is nowadays applied to assess stenosis and stent apposition in coronary arteries in interventional cardiology [7–10]. For pulmonary purposes, OCT has not yet been clinically implemented. However in the last decade, studies have shown that OCT is feasible, safe and has added value in pulmonary medicine for a broad field of indications (Table 1). The studies in this review investigating the use of OCT in pulmonary medicine have used either company build OCT probes (St. Jude Medical Inc., Abbott, IL, USA; Pentax Corp., Tokyo, Japan; light-CTTM scanner, LLTech, France; LightLab Imaging Inc., Westford, USA; Niris Imaging System, Imalux Corp., Cleveland, OH, USA) or custom build devices. OCT images of the airways and/or alveolar compartment are captured during bronchoscopy (Fig. 3a–c). The OCT catheter is inserted through the working channel of a bronchoscope and advanced until the region of interest is reached. Subsequently by manual or automated pullback, the OCT catheter generates sequential cross-sectional images of segments of the anatomical compartment of interest including the airways, lung parenchyma and pulmonary arteries (Fig. 3, Table 1). This review summarizes the advances that OCT made in improving diagnosis and management of obstructive lung diseases, malignancies and ILDs.

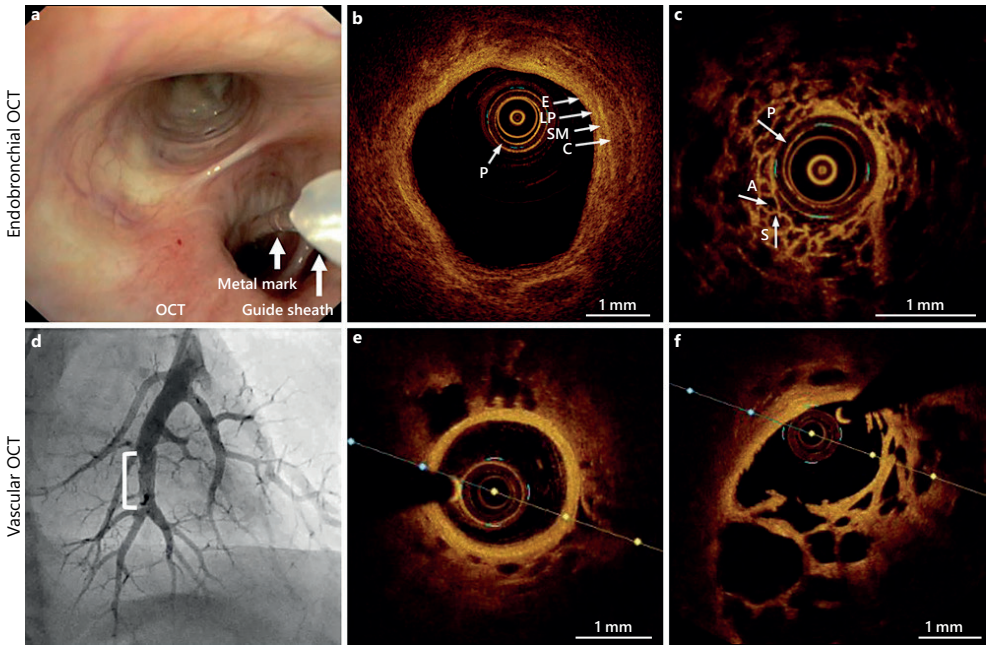


Figure 3. OCT imaging procedures of the airway wall and alveolar compartment (endobronchial OCT; **a–c**) and pulmonary artery (vascular OCT, **d–f**). **a** Bronchoscopic view of an OCT imaging procedure showing the guide sheath and the OCT catheter positioned in the right lower lobe. The metal mark guides the distance of 5.4 cm to the distal tip of the OCT catheter. **b** OCT image of a normal segmental airway wall showing the airway wall layer identification. **c** OCT image of the alveolar compartment showing normal alveoli and septae. **d** Angiography of the left lower lobe pulmonary artery with a stenosis in a chronic thromboembolic pulmonary hypertension (CTEPH) patient (white bracket). **e** OCT image of a normal proximal pulmonary artery. **f** OCT image of a pulmonary artery with webs/bands in a CTEPH patient. (Images provided by H.J. Bogaard, MD, PhD; N. van Royen, MD, PhD and M. Beijk, MD, PhD). OCT, optical coherence tomography; P, probe; A, alveolar space; S, septae; E, epithelium; LP, lamina propria; SM, submucosa; C, cartilage.

Table 1. Imaging studies in humans using OCT and CLE in respiratory medicine

Pulmonary diseases	Anatomical compartment	OCT	CLE	Potential future clinical implications
Obstructive lung diseases	Airway wall	*Asthma* – ASM detection [42] and airway wall thickness [40] – Assess airway compliance by measuring airway lumen at different pressures [39] – (Acute) BT effects: sloughing of epithelium [41], airway wall edema [40, 41] *COPD* – Evaluate airway lumen and wall thickness in different COPD stages [35, 36, 38] – Assess airway compliance by measuring airway lumen at different pressures [39]	*Asthma* – Visualization of elastin fibre pattern in airway wall [17] *COPD* – Visualization of elastin fibre pattern in airway wall [47] – Detection and quantification of emphysema [48]	– Evaluate airway remodelling including structural airway components as part of extensive phenotyping in obstructive airways disease – Evaluate effect of treatments targeting airway remodelling (e.g., Bronchial Thermoplasty, immunotherapy) – OCT combined with laser for the detection of fluorescently labelled tracers
Malignancies	Airway wall	*Lung cancer* – Detection of endobronchial neoplastic and non-neoplastic lesions [50–55]	*Lung cancer* – Detection of endobronchial neoplastic and non-neoplastic lesions [16, 58, 60, 61]	– Improvement of the (early) detection of lung cancer – Improvement of diagnostic yield of lung cancer diagnostic bronchoscopic procedures
	Mediastinal lymph nodes	*Lung cancer* – Identification of malignancies in lymph nodes (ex vivo) [57]	*Lung cancer* – Identification of malignant cells in lymph nodes [25, 26]	– Improvement of diagnostic yield for endosonographic staging in lung cancer – Differentiate malignant (subtypes), granulomatous and reactive lymph nodes

Table 1. Continued

Pulmonary diseases	Anatomical compartment	OCT	CLE	Potential future clinical implications
	Pleura	–	*Pleural lesions* – Differentiation between pleural fibrosis and mesothelioma [11] – Visualization malignant lesions during thoracoscopy [66] *Pleural effusion* – Identification of malignant cells in pleural effusion [67]	– Guidance towards (malignant) lesion – Differentiate benign versus malignant lesions
	Lung parenchyma	*Lung cancer* – Identification of malignant nodules (ex vivo) [56]	*Lung cancer* – Identification of malignant nodules: ex vivo [63] and in vivo [22, 59, 62]	– Improvement of diagnostic yield of needle aspiration – Guidance tool for transbronchial and transthoracic biopsies
Interstitial lung diseases	Lung parenchyma	*ILD* – OCT characteristics: thickening/loss of alveolar network structure (fibrosis), honeycombing, cysts and bronchiectasis [54, 71–73]	*ILD* – CLE characteristics of ILD [83, 84] – Fibrosis detection [83–85] – Identification of acute lung transplant rejection [81, 82]	– Discrimination of fibrotic versus cellular ILD – Guidance towards optimal biopsy location in ILD – Early detection of transplant rejection

Table 1. Continued

Pulmonary diseases	Anatomical compartment	OCT	CLE	Potential future clinical implications
Pulmonary vascular diseases	Pulmonary vasculature	*Pulmonary artery hypertension* – Pulmonary artery structure: thickened media [87] and intima (fibrosis) [88, 89] *Chronic thromboembolic pulmonary hypertension* – Thrombotic occlusion, luminal bands/webs [87, 89] – Visualize the effect of BPA [92] – Distinguish acute from chronic thrombi [94]	–	– Differentiation between different forms of PH, for example, PAH and CTEPH – Determine the location of pulmonary artery remodelling within the pulmonary artery system – Evaluate effects of PAH treatments on pulmonary artery remodelling

Overview of OCT and CLE literature categorized by pulmonary disease and subcategorized by anatomical compartment. All studies are performed in a research setting and are in vivo unless otherwise specified. Implementation in standard clinical care has not yet occurred. OCT, optical coherence tomography; CLE, confocal laser endomicroscopy; ASM, airway smooth muscle; BT, bronchial thermoplasty; COPD, chronic obstructive pulmonary disease; ILD, interstitial lung diseases; BPA, balloon pulmonary angioplasty; ECM, extra-cellular matrix; PH, pulmonary hypertension; PAH, pulmonary artery hypertension; CTEPH, chronic thromboembolic pulmonary hypertension.

Confocal Laser Endomicroscopy

CLE is an imaging technique compatible with bronchoscopy, thoracoscopy and transthoracic needle-based interventions [11], which provides real-time images of the airways, alveoli, lung tumours, pleura and lymph nodes with a resolution up to 3.5 µm, with a maximum depth of 70 µm and a maximum field of view of 600 µm (Fig. 1, 2). A fibre-optic probe is advanced through the working channel of a bronchoscope, thoracoscope or needle and directed to the area of interest where it illuminates tissue with laser light (most commonly used 488 nm). Reflected light is redirected back through a pinhole. Only light that is exactly in focus will pass through the pinhole, resulting in high-resolution images. Moving the laser beam vertically or horizontally enables reconstruction of 3D images by special software. In literature, CLE is also referred to as fibred confocal fluorescence microscopy, confocal micro-endoscopy or alveoloscopy. In this paper, we use the term CLE for this imaging technique. When the CLE probe is combined with a needle (CLE probe advanced through a hollow needle), the term "needle-based CLE" (nCLE) is used. "Probe-based CLE" (pCLE) refers to the technique where the CLE probe is advanced to the tissue, thereby directly omitting the need of a needle (Fig. 4).

Most evidence for the application of CLE in clinical practice is available in gastro-intestinal diseases, for instance, in the detection of neoplasia in the oesophagus [12, 13] and pancreatic cysts [14]. In non-malignant diseases like ulcerative colitis, CLE has been shown to be superior to any other imaging modality to assess mucosal healing [15].

First in vivo, in humans, reports on pCLE in the respiratory tract date back to 2007. Earliest studies showed feasibility of imaging of the airway wall and demonstrated that the images obtained by pCLE rely on the presence of elastin fibres, which is auto-fluorescent at 488 nm laser light [16, 17]. As elastin forms the backbone of structural components in the alveolar compartment including alveolar septae and microvessels [18–20] and the pleura, these can be visualized, real time and in vivo, using pCLE. Additionally, cellular components including inflammatory cells such as alveolar macrophages can be imaged based on auto-fluorescence as well [21].

Currently, in pulmonary diseases, one CLE system is commercially available (Cellvizio Endomicroscopy System, Mauna Kea Technologies, Paris, France). For pCLE, a miniprobe compatible with 1.9 mm working channel (Alveoflex™) can be used to visualize all segments of the bronchial tree

and lung parenchyma (Fig. 2). However, when reaching for the upper lobes (apical and posterior segments) a thinner, more flexible, probe (Cholangioflex™) might be advisable [22].

Imaging the bronchi and alveolar compartment with pCLE does not require additional staining. Studies have shown no advantage using fluorescein to visualize epithelial cells. Indeed, it has been reported that the visualization of alveoli is reduced using fluorescein because of a foam-like substance that appears [23, 24].

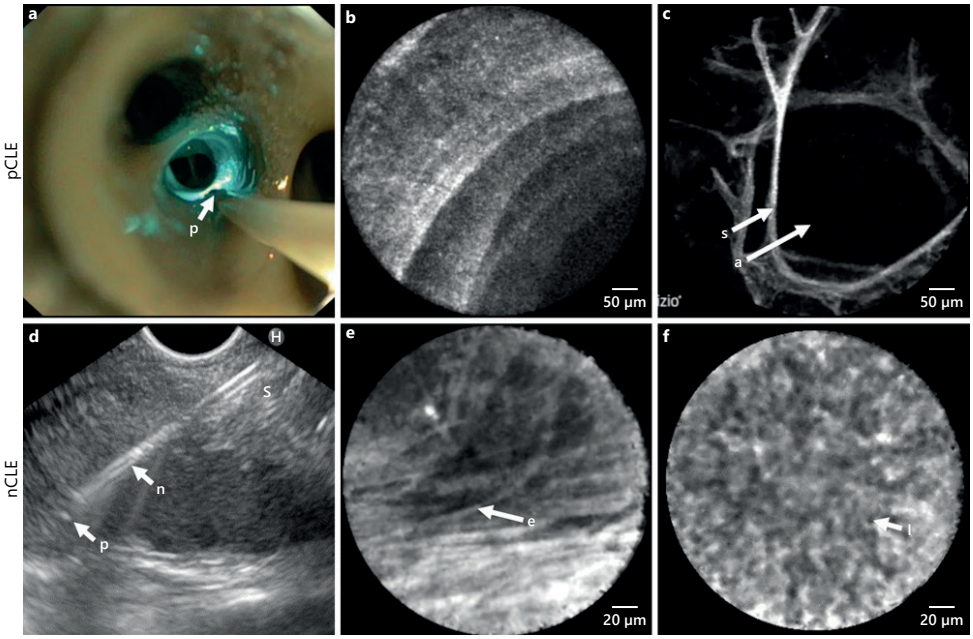


Figure 4. pCLE imaging procedures in vivo with corresponding images of the normal alveolar and airway wall compartment (**a–c**); nCLE imaging in vivo with corresponding images of reactive lymph node capsula and cortex (**d–f**). **a** pCLE with the probe (p) positioned in the central airways of the right lower lobe on its way to be advanced to the alveolar compartment. 488 nm laser light reflecting at the airway wall (blue). **b** pCLE image of the distal airway wall showing a helical ring-like pattern of the terminal bronchiole. **c** pCLE image of the alveolar compartment showing air-filled alveoli (a) and alveolar septae (s). **d** nCLE during an EUS procedure for staging of lung cancer, with the probe (p) extending 2 mm distal to the tip of the needle (n). **e** nCLE image showing elastin fibres (e) of the capsula of a lymph node. **f** nCLE image showing lymphocytes (l) in a reactive lymph node Wijmans et al. [85]. pCLE, probe based confocal laser endomicroscopy; S, septae; A, alveolar space; nCLE, needle based confocal laser endomicroscopy.

For imaging of lung masses and/or mediastinal lymph nodes, the needle-based CLE technique can be used. For this purpose, the thinnest confocal probe (AQ-flexTM) is advanced through a 19-Gauge needle. Unlike using pCLE in the respiratory tract, intravenous fluorescein-dinatrium should be administrated. Fluorescein enables the visualization of individual cells by enhancing fluorescence of the stromal background. Single cells are not stained by fluorescein, which results in a negative-like image where the individual cells are seen as dark dots on a bright background (Fig. 4f). With nCLE, different anatomical structures in lymph nodes can be identified. The capsula with auto fluorescent elastin fibres can be distinguished from the cortex in which the lymphoid cells can be identified (Fig. 4), as well as the lymphoid follicles, which appear as large dark discs [25, 26].

OBSTRUCTIVE LUNG DISEASES

Optical Coherence Tomography

Obstructive lung diseases such as asthma and chronic obstructive pulmonary disease (COPD) are characterized by airway remodelling, which includes structural changes and thickening of the airway wall [27–29]. Next to inflammation, airway remodelling is a key pathophysiological characteristic in asthma, which is associated with disease severity. Therefore, it is of importance to develop accurate tools to assess airway wall remodelling [30]. By showing a high correlation with histology for both identification (Fig. 3c) and quantification of airway wall layers in both animal studies [31] and human airways [32–34], OCT is considered a promising technique to assess airway remodelling in obstructive lung diseases.

The value of OCT is further substantiated by several studies that have correlated OCT imaging of the airway wall to HRCT and pulmonary function parameters. Coxson et al. [35] have compared HRCT with OCT imaging in a cohort of 44 current and former smokers and showed a strong correlation for airway wall thickness. In addition, in this study, forced expiratory volume in 1 second (FEV1) was measured and correlated to airway wall thickness of fifth-generation airways measured by both HRCT and OCT, with OCT showing the strongest correlation. This correlation between FEV1 and airways was confirmed in another study in which several stages of COPD patients were included and a high correlation between OCT measured airway wall dimensions and FEV1-based staging was found [36]. In allergic asthma patients, FEV1/FVC

correlated with OCT measured epithelial thickness and mucosal buckling, a potential method to assess bronchoconstriction [37]. Also with impulse oscillometry, a lung function test that uses sound waves to assess the respiratory resistance found that a correlation existed between the airway wall areas of small airways (seventh to ninth generation) assessed with OCT and respiratory resistance in heavy smokers and COPD patients [38]. Additionally, OCT can be used to assess elastic properties of the airway wall when combined with airway pressure increasing methods [39].

Next to assessing airway remodelling in patients with obstructive lung diseases, OCT might contribute in unravelling the mechanism of action of new treatment techniques and the evaluation of treatment response. In severe asthma, OCT was used in a pilot study of 2 severe asthma patients to assess the effect of bronchial thermoplasty (BT) on the airway wall up to 2 years after treatment [40]. Although the 2 included patients in this study showed similar clinical asthma symptoms and spirometry measurements, only 1 patient responded to BT. OCT was used to explore differences between these 2 patients and revealed a thickened, probably inflamed, epithelium in the non-responder patient, while the responder had a thickened airway wall without signs of inflammation. Also, after BT a difference was described: in the responder the total airway wall thickness declined, while in the non-responder, the thickness remained the same. These results suggested that OCT might have a potential role in identifying characteristics at baseline for optimal patient selection for BT.

In severe asthma, OCT has also been used to assess the acute effects of BT on the airway wall and identified acute patterns within the airway wall including epithelial sloughing and oedema (Fig. 5). Interestingly, acute BT effects extended to the distal smaller non-BT-treated airways and this suggested that BT treatment might also impact the smaller airways in severe asthmatic patients [41].

Although different airway wall layers are detectable with OCT, measuring the layers manually is time consuming and it remains difficult to identify the different structures and components within these layers such as extracellular matrix (ECM) proteins (e.g., collagen) or airway smooth muscle (ASM). By adding a birefringent platform to the OCT system, Adams et al. [42] automatically identified and quantified ASM fibres in 3 asthma patients and 3 healthy controls showing a significant difference in the thickness of ASM fibres between these 2 groups.

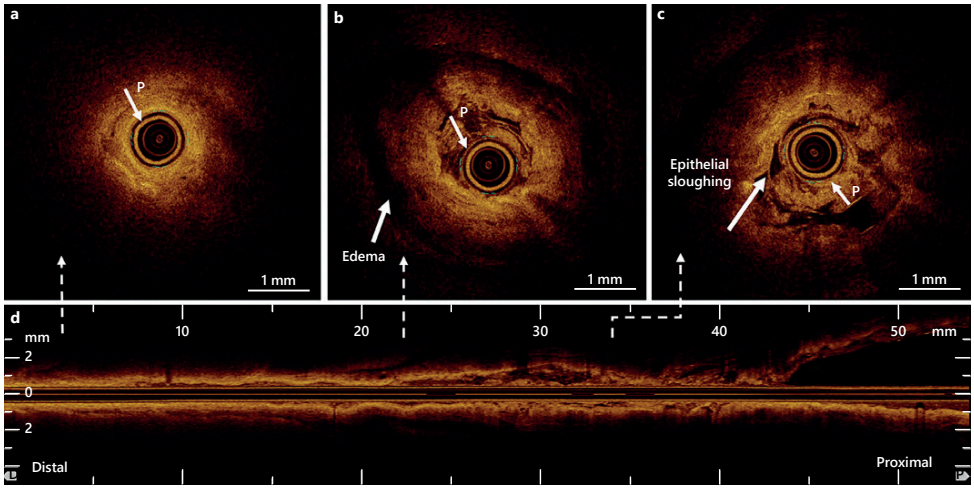


Figure 5. OCT images of the anterior segment (LB3) of the left upper lobe directly after bronchial thermoplasty (BT) treatment. **a** Normal, non-directly-BT-treated distal airway area. **b** BT-treated airway area with peribronchial oedema. **c** BT-treated airway area showing epithelial sloughing. **d** Corresponding reconstructed pullback of the airway (540 2D images, total length of 5.4 cm; Goorsenberg et al. [41]). P, probe.

Confocal Laser Endomicroscopy

Visualization of the airway wall using pCLE relies on elastin fibres in subepithelial ECM. In the bronchi, 5 different patterns can be identified, depending on the depth of the probe in the bronchial tree [16]. Ranging from dense unidirectional elastin fibres, with an occasional bronchial gland opening in proximal main bronchi, to cross-sectional fibres and loose, web-like fibres in distal, smaller airways, the distal terminal bronchiole shows a typical ring like helical pattern (Fig. 4). In patients with asthma, elastin fibres have been described to be decreased or fragmented [43]. However, in a study that focused on pCLE imaging in asthma patients and healthy controls, it was described that a dense lamellar pattern was associated with lower FEV1 [17]. In COPD, to our knowledge, only a single study imaged the airway walls with CLE. Of the different subepithelial elastin patterns, COPD patients were described to have more loose arrangements of elastin fibres, instead of a lamellar or mixed pattern of fibres, as compared to non-COPD smokers and healthy volunteers. Possibly indicating destruction of elastin fibres in the ECM of the airway wall of COPD patients, which is in line with a previous histological study by Black et al. [44].

In the alveolar compartment, animal studies have shown a correlation between pulmonary emphysema and enlarged airspaces with thinner capillaries and a loss of capillary density [45, 46]. This correlation was reproduced using pCLE in COPD patients in vivo, thus without the need for biopsy. Furthermore, COPD patients were shown to have decreased auto fluorescence intensity of alveolar septae when compared to healthy volunteers, potentially indicating destruction of these, elastin containing, alveolar septae [24, 47, 48]. Although pCLE shows specific findings in patients with COPD, the additional value of pCLE over standard chest CT and pulmonary function tests is yet to be established.

MALIGNANCIES

Optical Coherence Tomography

The detection of lung cancer tissue for diagnosis and staging purposes, but also for margin assessment in lung cancer surgery, is highly important in the management of pulmonary oncology. Several groups have investigated the use of OCT in other oncology specialties, mainly in dermatology, urology and gastroenterology [49].

The involvement of pulmonary malignancies in different anatomical compartments can be imaged with OCT including central airway endobronchial malignancies, lung parenchymal pulmonary masses or nodules and metastases in lymph nodes.

For the identification of endobronchial tumours, promising results have been published both in vivo [50– 52] and ex vivo [52–55]. In these endobronchial tumours, one study identified different characteristics for 3 subtypes of cancer: squamous cell carcinomas, adenocarcinomas and poorly differentiated carcinomas [55]. Three reviewers were trained to identify these criteria in a cohort of 82 ex vivo tumour samples that showed an average accuracy of 82.6% (range 73.7–94.7%). To the best of our knowledge, there are no studies published investigating the value of OCT in assessing the margin of the tumour-resected tissue.

In pulmonary masses, nodules and lymph node metastases, a potential use of OCT is needle-based OCT imaging in the setting of trans-bronchial needle aspiration. One research group conducted a study in pulmonary nodules showing high sensitivity and specificity (both > 95%) for ex vivo differentiation between pulmonary nodules and healthy parenchymal

tissue [56]. The same research group investigated the use of OCT for the identification of pulmonary lymph node metastases. Needle-based OCT was performed in 26 ex vivo lymph nodes, both healthy and metastatic disease [57]. The characteristics of metastatic disease were distinct from those of the lymph nodes without cancer and even had features connected with the subtype of the tumour. Both applications of needle-based OCT in pulmonary nodules and lymph nodes have not been validated in vivo yet.

Confocal Laser Endomicroscopy

Several studies have shown that pCLE has the ability to identify the abnormal area in endobronchial [16, 58– 61] and parenchymal-located malignancies (both primary lung cancer and metastatic) [58, 62, 63]. Using pCLE to image endobronchial lesions, Filner et al. [61] showed the ability to differentiate between normal versus neoplastic lesions and normal versus non-neoplastic lesions. In a study performed in 112 patients with a peripheral pulmonary nodule, pCLE was able to detect the abnormal area in 92% [64]. Additionally, Sorokina et al. [63] showed the presence of a specific pattern of alveolar dystelectasis, oedema and influx of macrophages to be present in malignant nodules in 18 lobectomy specimens. Additionally, pCLE histopathology confirmed distinctive features of adenocarcinoma, squamous cell carcinoma and small cell carcinoma. However, in a study performed by Seth et al. [64], 91 patients with peripheral lung nodule were imaged with pCLE, and although in 92% the abnormal area was identified, pCLE was not able to discriminate benign from malignant lesions. It is thought that this is due to the difficulty of staining epithelial cells of the bronchial mucosa [16, 59, 63, 64]. Unlike the mucosa of the gastrointestinal tract, fluorescein does not penetrate into the epithelial layer of the bronchi [23, 24]. Topical administrated acriflavine has shown high sensitivity and specificity to visualize malignant cells in endobronchial located tumours; however, its use is under discussion because of its potential carcinogenic properties [60].

An approach where the nodule is punctured by a needle combined with the CLE probe might resolve the problem of bronchial epithelial staining. In 2016, Wijmans et al. [65] presented a case of non-small cell lung cancer in which the primary tumour was imaged with nCLE in combination with intravenous fluorescein. Where all the previous mentioned studies for peripheral pulmonary nodules have used pCLE, Wijmans et al. [65] demonstrated in this study a case in which the primary tumour was visualized with nCLE combined with endosonography. Dark, large ag-

gregates of cells imaged with nCLE were compatible with the malignant cells of adenocarcinoma. Thereafter, a study was performed using nCLE in both centrally located primary pulmonary tumours (n = 6) and metastasis suspected lymph nodes (n = 21). Three characteristics were developed to predict malignancy: enlarged pleomorphic cells, dark clumps and directional streaming. These criteria were prospectively validated to determine malignancy of the tumours or lymph nodes with high diagnostic accuracy of 90% [26] (Fig. 6).

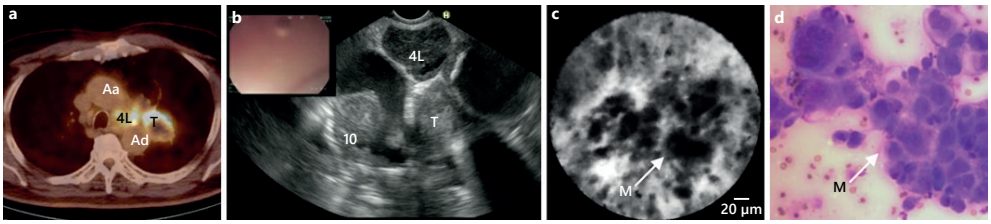


Figure 6. Endosonography guided nCLE of a mediastinal lymph node metastasis of a tumour in the left upper lobe. **a** PET-CT scan showing fludeoxyglucose-avid lymph node station 4 L, and the primary lung tumour (T). **b** EUS image showing an enlarged lymph nodes at station 4 L. **c** Real-time nCLE image of lymph node station 4 L showing large pleomorphic cells and dark clumps recognized as malignant cells (M). **d** Fine needle aspirate showing malignant cells of squamous cell carcinoma (Wijmans et al. [26]). 10, lymph node station 10 L (left); Aa, ascending aorta; Ad, descending aorta.

In pleural lesions, both pCLE and nCLE have been used to detect malignant cells. Bonhomme et al. [66] reported 3 cases with pleura imaging using pCLE. Three different images of the pleura were presented: normal pleura, pleural metastasized non-small cell lung cancer and a case of mesothelioma. pCLE of the pleura showed clear capability to differentiate normal pleura from malignant pleura in these cases. Shortly thereafter, a larger study was undertaken using both pCLE and nCLE to distinguish malignant mesothelioma from areas of pleural fibrosis. Characteristics of different pleural lesions were identified and prospectively validated in 105 pleural biopsies from 15 patients with moderate inter-observer agreement [11]. When it comes to malignant pleural effusion, one ex vivo study found high sensitivity and specificity for pleural malignancy using pCLE in pleural effusion [67].

ILDS AND OTHER PARENCHYMAL LUNG DISEASES

Optical Coherence Tomography

OCT has predominantly been used to assess abnormalities in the airway due to both obstructive airway diseases and (endobronchial) malignancies. However, recently, the use of OCT for the assessment of the alveolar compartment has been investigated [68–70]. Especially in ILDs the added value of high-resolution, near-microscopic imaging next to HRCT can be envisioned. In 2013, Hariri et al. [54] compared the histology of human lung specimens with optical frequency domain imaging in 4 patients ex vivo. Characteristics of fibrosis were identified in these OCT images. More recently, the first in vivo in human results of OCT in diagnosis of idiopathic pulmonary fibrosis has been published [71–73]. These results showed that OCT was able to identify microscopic honeycombing with alveolar OCT, while radiological honeycombing was not visible on HRCT [71]. Furthermore, characteristics for fibrotic ILDs such as thickening of alveolar septae and loss of alveolar structure, microscopic honeycombing, cysts and bronchi(ol)ectasis were identified with OCT [71–73].

Confocal Laser Endomicroscopy

Since ILD is a disease located in the alveolar compartment, CLE has been used to visualize ILD in vivo. Normal alveolar compartment images show thin alveolar septae in a round, helical or looped shape depending on the angle of penetration of the alveolar unit (Fig. 2, 4). Microvessels can be visualized and are typically thicker than the alveolar septae, and may have branches. In smoking individuals, highly fluorescent macrophages are visible throughout the alveoli, which has a positive correlation with the number of cigarettes used [21]. Also, the fluorescent intensity of alveolar structures varies: older individuals tend to have stronger fluorescent signals of alveolar elastin fibres [21, 24].

The first report of CLE in ILD was a case of pulmonary alveolar proteinosis, in which highly fluorescent globular structures were identified in vivo, compatible with globular lipoproteinaceous material in bronchoalveolar lavage. Similar findings were described in a case series of 6 patients with pulmonary alveolar proteinosis [74]. Later, case reports of amiodarone induced ILD, pulmonary alveolar microlithiasis, invasive aspergillosis, pneumocystis jiroveci pneumonia, lymphangioleiomyomatosis and metastatic pulmonary calcification were published [75–80].

In addition to the above, CLE has also been studied for the surveillance of acute cellular rejection (ACR) in lung transplant recipients. Two studies have focused on the use of pCLE in these patients and found that specific characteristics are associated with ACR. Yserbyt et al. [81] showed in 2014 the correlation between ACR and an increase in auto fluorescent alveolar cells. This finding was confirmed by Keller et al. [82] in 2019, with the addition of the perivascular distribution of the cells. Perivascular cellularity was significantly correlated with ACR.

Several studies have been performed to identify specific characteristics of pCLE images in ILD. Meng et al. [83] identified 6 different patterns to discriminate chronic fibrosing ILD from other ILDs. Salaun et al. [84] identified 9 specific CLE characteristics using data from 80 individuals (59 ILD patients, 21 healthy individuals). Based on these characteristics they were able to discriminate normal from diseased lung, and found that certain ILDs were associated with a cellular CLE pattern (presence of fluorescent bronchial and alveolar cells), while others were associated with a fibrotic CLE pattern (small alveolar mouths, disorganized dense elastin fibre network with thickened septae). They showed good reproducibility of inter-observer interpretation. In another observational study in 14 ILD patients pCLE was able to detect normal and abnormal parenchymal areas, and to discriminate mild from severe fibrosis (Fig. 7). Additionally the pleura and the adjacent subpleural alveolar space could be identified [85].

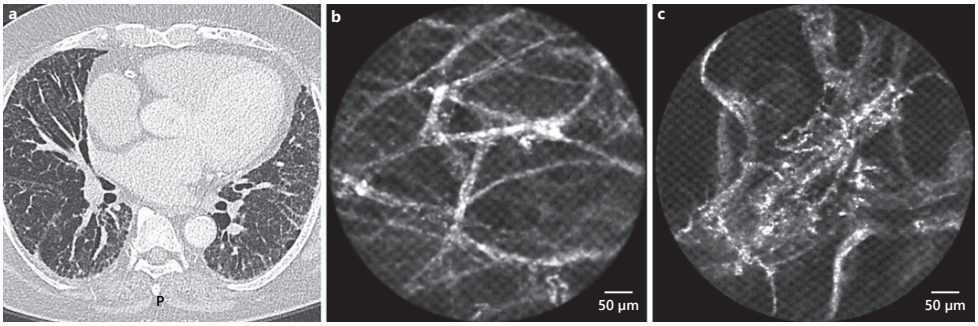


Figure 7. pCLE images of the alveolar compartment in a patient with a fibrotic NSIP. **a** HRCT image showing diffuse reticulation and bronchi(ol)ectasis. **b** pCLE image showing an increased density of alveolar elastin fibre intact network. **c** pCLE image showing an increased density of thickened alveolar elastin fibre network with loss of normal architecture. Wijmans et al. [85]. P, probe.

Based on the studies reviewed above, it seems plausible that pCLE can differentiate cellular ILDs from fibrotic ILDs; however, whether CLE can differentiate between specific subsets of ILDs remains to be established. The potential of CLE to identify these different compartments, along with an added value to characterize ILD, paves the way to use CLE as a guidance tool for endoscopic (cryo-)lung biopsies.

PULMONARY VASCULAR DISEASES

Optical Coherence Tomography

The use of OCT in pulmonary vascular diseases has been described thoroughly in previously published reviews by our group and others [1, 86]. In short, OCT has been investigated in characterizing pulmonary artery wall remodelling in pulmonary arterial hypertension [87–89]. Pulmonary artery wall thickness has been reported to correlate to hemodynamic parameters [90, 91]. In chronic thromboembolic pulmonary hypertension, OCT was able to assess thrombotic occlusion and luminal webs and/or bands [87, 89] (Fig. 3f) and has been reported to guide balloon sizing and to evaluate the effect of balloon pulmonary angioplasty treatment [92, 93]. Additionally, one study investigated the use of OCT in diagnosing peripheral pulmonary artery thrombus as compared to selective pulmonary angiography in 12 patients [94]. In this study, OCT found significantly more thrombi in the distal segments of peripheral pulmonary arteries than selective pulmonary angiography. Moreover, OCT was able to differentiate between acute "red" and chronic "white" thrombi.

Confocal Laser Endomicroscopy

To the best of our knowledge, no studies have been published regarding the use of CLE in pulmonary vascular diseases.

FUTURE PERSPECTIVES

In summary, in pulmonary medicine, OCT and CLE are promising high-resolution, real-time, in vivo imaging techniques to visualize important disease associated anatomical compartments of the respiratory tract. However, unlike in ophthalmology and cardiology, OCT and CLE have not found their implementation into standard clinical care yet.

In our opinion, the use of both CLE and OCT techniques has high potential to add to guidance and/or improvement in diagnostic yield driven by its near-microscopic resolution and real-time properties. For instance, the development of a CLE or OCT integrated cytological needle (so called smart needle) to guide the biopsy site and provide real-time feedback for the detection of lung cancer and pleura mesothelioma [11].

In addition, since advanced OCT and CLE have shown the potential of in situ cytological analysis in malignancy-suspected lymph nodes, it seems reasonable that these techniques also have the capability of detecting granulomas in, for instance, sarcoidosis.

The scope of novel imaging techniques in endoscopy may be broadened in the near future by implementing the use of fluorescently labelled tracers. In this field of imaging, optical techniques are combined with laser to detect fluorescently labelled components. In oncology, fluorescently labelled antibody detection can further boost tumour identification for cancer diagnosis, staging and assessment of tumour margins. For instance, fluorescently labelled anti-CD47 was used to detect bladder cancer [95]. Both fluorescently labelled labetuzumab and erlotinib have been used to assess colorectal cancer and EGFR- mutated lung tumours, respectively, in xenografted mouse models [96, 97]. Furthermore, to evaluate the effect of novel treatments, pCLE might be of value as was demonstrated by a study in which apoptotic cells were visualized after the administration of erlotinib in EGFR-mutated tumours in animal models [98]. In severe asthma patients, it can be envisioned that molecular labelling of monoclonal antibodies used for immunotherapy can help to visualize cellular targets and biodistribution of these antibodies with the ultimate goal to improve patient selection for these expensive therapies.

In the field of infectious diseases, efforts are made to directly visualize the presence of pathogens. So far, both in- and ex vivo studies have been published to visualize aspergillus [99–101] and staphylococcus aureus [102] in animal models using CLE.

Currently, analyzing OCT and CLE images is elaborative and this makes it a time-consuming process. The development of automated software is essential for the implementation of these techniques. Automated segmentation based on intensity analyses or deep learning techniques might prove very helpful in image analyses and will be a necessity for broader clinical application. Improvements are being made, such as automated

quantification [42] and automated mucus segmentation [37, 103]. Also, research is focused on improving the techniques, for instance, by using polarization sensitive OCT, which shows not only the structural layers of the airway wall but also the arrangement of the tissue [104]. This makes it possible to distinguish several structures in the airways such as structural airway components (e.g., ECM/ASM). Additionally, the resolution of OCT imaging might be improved by using a nano-optic endoscope: a conventional OCT system with a metalens integrated in the design [105]. Potentially these techniques can be used to assess treatment effects on airway wall structures involved in airway wall remodelling, without the need for taking a biopsy. Other factors limiting the implementation of these techniques in clinical practice are the lack of larger validation trials, costs and availability of OCT and CLE systems. Currently, pulmonary OCT and CLE have been used only in research trials in expert centres with expertise in interventional bronchoscopy with relatively small amounts of patients included.

CONCLUSION

Both OCT and CLE are complementary, high-resolution imaging techniques that have shown to be feasible and safe to use in a variety pulmonary diseases. Both techniques have considerable potential to improve diagnostics and monitoring of pulmonary diseases and their treatments; however, larger in vivo validation studies and automated software are needed before these techniques can be implemented in clinical practice.

ACKNOWLEDGEMENTS

We would like to thank J. de Boer, PhD, F. Ferold, and J. Willemse for providing polarization sensitive OCT images of an asthma patient; H.J. Bogaard, MD, PhD, N. van Rooijen, MD, PhD, and M. Beijk, MD, PhD for providing OCT images of the pulmonary vasculature and L. Wijmans for providing CLE images.

STATEMENT OF ETHICS

The authors have no ethical conflicts to disclose.

DISCLOSURE STATEMENT

The department of pulmonology received material support from St Jude Medical Inc., St. Paul, MN, USA/Abbott, Illinois and an unrestricted research grant from Mauna Kea Technologies, Paris, France.

FUNDING SOURCES

None.

AUTHOR CONTRIBUTIONS

A.G., K.A.K., P.B. and J.A. contributed to the concept and design of this review. A.G. and K.A.K. both contributed equally to data interpretation, writing the manuscript and preparing figures. P.B. and J.A. supervised the project and reviewed the manuscript. All authors approved the final version.

REFERENCES

1 Wijmans L, d'Hooghe JN, Bonta PI, Annema JT. Optical coherence tomography and confocal laser endomicroscopy in pulmonary diseases. Curr Opin Pulm Med. 2017 May; 23(3): 275–83.

2 Huang D, Swanson EA, Lin CP, Schuman JS, Stinson WG, Chang W, et al. Optical coherence tomography. Science. 1991 Nov; 254(5035): 1178–81.

3 Tearney GJ, Brezinski ME, Bouma BE, Boppart SA, Pitris C, Southern JF, et al. In vivo endoscopic optical biopsy with optical coherence tomography. Science. 1997 Jun; 276(5321): 2037–9.

4 Fercher AF, Hitzenberger CK, Drexler W, Kamp G, Sattmann H. In vivo optical coherence tomography. Am J Ophthalmol. 1993 Jul; 116(1): 113–4.

5 Swanson EA, Izatt JA, Hee MR, Huang D, Lin CP, Schuman JS, et al. In vivo retinal imaging by optical coherence tomography. Opt Lett. 1993 Nov; 18(21): 1864–6.

6 Koustenis A Jr, Harris A, Gross J, Januleviciene I, Shah A, Siesky B. Optical coherence tomography angiography: an overview of the technology and an assessment of applications for clinical research. Br J Ophthalmol. 2017 Jan; 101(1): 16–20.

7 IJsselmuiden AJ, Zwaan EM, Oemrawsingh RM, Bom MJ, Dankers FJ, de Boer MJ, et al. Appropriate use criteria for optical coherence tomography guidance in percutaneous coronary interventions : recommendations of the working group of interventional cardiology of the Netherlands Society of Cardiology. Neth Heart J. 2018 Oct; 26(10): 473–83.

8 Sotomi Y, Tateishi H, Suwannasom P, Dijkstra J, Eggermont J, Liu S, et al. Quantitative assessment of the stent/scaffold strut embedment analysis by optical coherence tomography. Int J Cardiovasc Imaging. 2016 Jun; 32(6): 871–83.

9 Bezerra HG, Costa MA, Guagliumi G, Rollins AM, Simon DI. Intracoronary optical coherence tomography: a comprehensive review clinical and research applications. JACC Cardiovasc Interv. 2009 Nov; 2(11): 1035–46.

10 Brezinski ME, Tearney GJ, Boppart SA, Swanson EA, Southern JF, Fujimoto JG. Optical biopsy with optical coherence tomography: feasibility for surgical diagnostics. J Surg Res. 1997 Jul; 71(1): 32–40.

11 Wijmans L, Baas P, Sieburgh TE, de Bruin DM, Ghuijs PM, van de Vijver MJ, et al. Confocal Laser Endomicroscopy as a Guidance Tool for Pleural Biopsies in Malignant Pleural Mesothelioma. Chest. 2019, Epub ahead of print.

12 Sharma P, Meining AR, Coron E, Lightdale CJ, Wolfsen HC, Bansal A, et al. Real-time increased detection of neoplastic tissue in Barrett's esophagus with probe-based confocal laser endomicroscopy: final results of an international multicenter, prospective, randomized, controlled trial. Gastrointest Endosc. 2011 Sep; 74(3): 465–72.

13 Shah T, Lippman R, Kohli D, Mutha P, Solomon S, Zfass A. Accuracy of probe-based confocal laser endomicroscopy (pCLE) compared to random biopsies during endoscopic surveillance of Barrett's esophagus. Endosc Int Open. 2018 Apr; 6(4):E414–20.

14 Napoleon B, Palazzo M, Lemaistre AI, Caillol F, Palazzo L, Aubert A, et al. Needlebased confocal laser endomicroscopy of pancreatic cystic lesions: a prospective multicenter validation study in patients with definite diagnosis. Endoscopy. 2019 Sep; 51(9): 825–35.

15 Mace V, Ahluwalia A, Coron E, Le Rhun M, Boureille A, Bossard C, et al. Confocal laser endomicroscopy: a new gold standard for the assessment of mucosal healing in ulcerative colitis. J Gastroenterol Hepatol. 2015 Mar; 30 Suppl 1: 85–92.

16 Thiberville L, Moreno-Swirc S, Vercauteren T, Peltier E, Cave C, Bourg Heckly G. In vivo imaging of the bronchial wall microstructure using fibered confocal fluorescence microscopy. Am J Respir Crit Care Med. 2007 Jan; 175(1): 22–31.

17 Yick CY, von der Thusen JH, Bel EH, Sterk PJ, Kunst PW. In vivo imaging of the airway wall in asthma: fibered confocal fluorescence microscopy in relation to histology and lung function. Respir Res. 2011 Jun; 12(1): 85.

18 Mercer RR, Crapo JD. Spatial distribution of collagen and elastin fibers in the lungs. J Appl Physiol (1985). 1990 Aug; 69(2): 756–65.

19 Goncalves CA, Figueiredo MH, Bairos VA. Three-dimensional organization of the elastic fibres in the rat lung. Anat Rec. 1995 Sep; 243(1): 63–70.

20 Toshima M, Ohtani Y, Ohtani O. Three-dimensional architecture of elastin and collagen fiber networks in the human and rat lung. Arch Histol Cytol. 2004 Mar; 67(1): 31–40.

21 Thiberville L, Salaun M, Lachkar S, Dominique S, Moreno-Swirc S, Vever-Bizet C, et al. Human in vivo fluorescence microimaging of the alveolar ducts and sacs during bronchoscopy. Eur Respir J. 2009 May; 33(5): 974–85.

22 Hassan T, Thiberville L, Hermant C, Lachkar S, Piton N, Guisier F, et al. Assessing the feasibility of confocal laser endomicroscopy in solitary pulmonary nodules for different part of the lungs, using either 0.6 or 1.4 mm probes. PLoS One. 2017 Dec; 12(12):e0189846.

23 Fuchs FS, Zirlik S, Hildner K, Frieser M, Ganslmayer M, Schwarz S et al. Fluoresceinaided confocal laser endomicroscopy of the lung. Respiration. 2011; 81(1): 32–8.

24 Newton RC, Kemp SV, Yang GZ, Elson DS, Darzi A, Shah PL. Imaging parenchymal lung diseases with confocal endomicroscopy. Respir Med. 2012 Jan; 106(1): 127–37.

25 Benias PC, D'Souza LS, Papafragkakis H, Kim J, Harshan M, Theise ND, et al. Needle-based confocal endomicroscopy for evaluation of malignant lymph nodes - a feasibility study. Endoscopy. 2016 Oct; 48(10): 923–8.

26 Wijmans L, Yared J, de Bruin DM, Meijer SL, Baas P, Bonta PI, et al. Needle-based confocal laser endomicroscopy for real-time diagnosing and staging of lung cancer. Eur Respir J. 2019 Jun; 53(6): 1–9.

27 Jeffery PK. Remodeling in asthma and chronic obstructive lung disease. Am J Respir Crit Care Med. 2001 Nov; 164(10 Pt 2 supplement_2):S28–38.

28 James AL, Wenzel S. Clinical relevance of airway remodelling in airway diseases. Eur Respir J. 2007 Jul; 30(1): 134–55.

29 Patel BD, Coxson HO, Pillai SG, Agusti AG, Calverley PM, Donner CF, et al.; International COPD Genetics Network. Airway wall thickening and emphysema show independent familial aggregation in chronic obstructive pulmonary disease. Am J Respir Crit Care Med. 2008 Sep; 178(5): 500–5.

30 Benayoun L, Druilhe A, Dombret MC, Aubier M, Pretolani M. Airway structural alterations selectively associated with severe asthma. Am J Respir Crit Care Med. 2003 May; 167(10): 1360–8.

31 Lee AM, Kirby M, Ohtani K, Candido T, Shalansky R, MacAulay C, et al. Validation of airway wall measurements by optical coherence tomography in porcine airways. PLoS One. 2014 Jun; 9(6):e100145.

32 Chen Y, Ding M, Guan WJ, Wang W, Luo WZ, Zhong CH, et al. Validation of human small airway measurements using endobronchial optical coherence tomography. Respir Med. 2015 Nov; 109(11): 1446–53.

33 d'Hooghe JN, Goorsenberg AW, de Bruin DM, Roelofs JJ, Annema JT, Bonta PI. Optical coherence tomography for identification and quantification of human airway wall layers. PLoS One. 2017 Oct; 12(10):e0184145.

34 Kirby M, Ohtani K, Nickens T, Lisbona RM, Lee AM, Shaipanich T, et al. Reproducibility of optical coherence tomography airway imaging. Biomed Opt Express. 2015 Oct; 6(11): 4365–77.

35 Coxson HO, Quiney B, Sin DD, Xing L, McWilliams AM, Mayo JR, et al. Airway wall thickness assessed using computed tomography and optical coherence tomography. Am J Respir Crit Care Med. 2008 Jun; 177(11): 1201–6.

36 Ding M, Chen Y, Guan WJ, Zhong CH, Jiang M, Luo WZ, et al. Measuring Airway Remodeling in Patients With Different COPD Staging Using Endobronchial Optical Coherence Tomography. Chest. 2016 Dec; 150(6): 1281–90.

37 Adams DC, Miller AJ, Applegate MB, Cho JL, Hamilos DL, Chee A, et al. Quantitative assessment of airway remodelling and response to allergen in asthma. Respirology. 2019, Epub ahead of print.

38 Su ZQ, Guan WJ, Li SY, Ding M, Chen Y, Jiang M, et al. Significances of spirometry and impulse oscillometry for detecting small airway disorders assessed with endobronchial optical coherence tomography in COPD. Int J Chron Obstruct Pulmon Dis. 2018 Oct; 13: 3031–44.

39 Williamson JP, McLaughlin RA, Noffsinger WJ, James AL, Baker VA, Curatolo A, et al. Elastic properties of the central airways in obstructive lung diseases measured using anatomical optical coherence tomography. Am J Respir Crit Care Med. 2011 Mar; 183(5): 612– 9.

40 Kirby M, Ohtani K, Lopez Lisbona RM, Lee AM, Zhang W, Lane P, et al. Bronchial thermoplasty in asthma: 2-year follow-up using optical coherence tomography. Eur Respir J. 2015 Sep; 46(3): 859–62.

41 Goorsenberg AWM, d'Hooghe JNS, de Bruin DM, van den Berk IAH, Annema JT, Bonta PI. Bronchial Thermoplasty-Induced Acute Airway Effects Assessed with Optical Coherence Tomography in Severe Asthma. Respiration. 2018; 96(6): 564–70.

42 Adams DC, Hariri LP, Miller AJ, Wang Y, Cho JL, Villiger M, et al. Birefringence microscopy platform for assessing airway smooth muscle structure and function in vivo. Sci Transl Med. 2016 Oct; 8(359): 359ra131.

43 Bousquet J, Lacoste JY, Chanez P, Vic P, Godard P, Michel FB. Bronchial elastic fibers in normal subjects and asthmatic patients. Am J Respir Crit Care Med. 1996 May; 153(5): 1648–54.

44 Black PN, Ching PS, Beaumont B, Ranasinghe S, Taylor G, Merrilees MJ. Changes in elastic fibres in the small airways and alveoli in COPD. Eur Respir J. 2008 May; 31(5): 998– 1004.

45 Yamato H, Sun JP, Churg A, Wright JL. Cigarette smoke-induced emphysema in guinea pigs is associated with diffusely decreased capillary density and capillary narrowing. Lab Invest. 1996 Aug; 75(2): 211–9.
46 Schraufnagel DE, Schmid A. Capillary structure in elastase-induced emphysema. Am J Pathol. 1988 Jan; 130(1): 126–35.
47 Cosio BG, Shafiek H, Fiorentino F, Gomez C, Lopez M, Rios A, et al. Structure-function relationship in COPD revisited: an in vivo microscopy view. Thorax. 2014 Aug; 69(8): 724–30.
48 Yserbyt J, Dooms C, Janssens W, Verleden GM. Endoscopic advanced imaging of the respiratory tract: exploring probe-based confocal laser endomicroscopy in emphysema. Thorax. 2018 Feb; 73(2): 188–90.
49 van Manen L, Dijkstra J, Boccara C, Benoit E, Vahrmeijer AL, Gora MJ, et al. The clinical usefulness of optical coherence tomography during cancer interventions. J Cancer Res Clin Oncol. 2018 Oct; 144(10): 1967–90.
50 Lam S, Standish B, Baldwin C, McWilliams A, leRiche J, Gazdar A et al. In vivo optical coherence tomography imaging of preinvasive bronchial lesions. Clin Cancer Res. 2008 Apr; 14(7): 2006–11.
51 Michel RG, Kinasewitz GT, Fung KM, Keddissi JI. Optical coherence tomography as an adjunct to flexible bronchoscopy in the diagnosis of lung cancer: a pilot study. Chest. 2010 Oct; 138(4): 984–8.
52 Tsuboi M, Hayashi A, Ikeda N, Honda H, Kato Y, Ichinose S, et al. Optical coherence tomography in the diagnosis of bronchial lesions. Lung Cancer. 2005 Sep; 49(3): 387– 94.
53 Jain M, Narula N, Salamoon B, Shevchuk MM, Aggarwal A, Altorki N, et al. Full-field optical coherence tomography for the analysis of fresh unstained human lobectomy specimens. J Pathol Inform. 2013 Sep; 4(1): 26.
54 Hariri LP, Applegate MB, Mino-Kenudson M, Mark EJ, Medoff BD, Luster AD, et al. Volumetric optical frequency domain imaging of pulmonary pathology with precise correlation to histopathology. Chest. 2013 Jan; 143(1): 64–74.
55 Hariri LP, Mino-Kenudson M, Lanuti M, Miller AJ, Mark EJ, Suter MJ. Diagnosing lung carcinomas with optical coherence tomography. Ann Am Thorac Soc. 2015 Feb; 12(2): 193–201.
56 Hariri LP, Mino-Kenudson M, Applegate MB, Mark EJ, Tearney GJ, Lanuti M, et al. Toward the guidance of transbronchial biopsy: identifying pulmonary nodules with optical coherence tomography. Chest. 2013 Oct; 144(4): 1261–8.
57 Shostak E, Hariri LP, Cheng GZ, Adams DC, Suter MJ. Needle-based Optical Coherence Tomography to Guide Transbronchial Lymph Node Biopsy. J Bronchology Interv Pulmonol. 2018 Jul; 25(3): 189–97.
58 Wellikoff AS, Holladay RC, Downie GH, Chaudoir CS, Brandi L, Turbat-Herrera EA. Comparison of in vivo probe-based confocal laser endomicroscopy with histopathology in lung cancer: A move toward optical biopsy. Respirology. 2015 Aug; 20(6): 967–74.
59 Shah PL, Kemp SV, Newton RC, Elson DS, Nicholson AG, Yang GZ. Clinical Correlation between Real-Time Endocytoscopy, Confocal Endomicroscopy, and Histopathology in the Central Airways. Respiration. 2017; 93(1): 51– 7.

60 Fuchs FS, Zirlik S, Hildner K, Schubert J, Vieth M, Neurath MF. Confocal laser endomicroscopy for diagnosing lung cancer in vivo. Eur Respir J. 2013 Jun; 41(6): 1401–8.

61 Filner JJ, Bonura EJ, Lau ST, Abounasr KK, Naidich D, Morice RC, et al. Bronchoscopic fibered confocal fluorescence microscopy image characteristics and pathologic correlations. J Bronchology Interv Pulmonol. 2011 Jan; 18(1): 23–30.

62 Hassan T, Piton N, Lachkar S, Salaun M, Thiberville L. A Novel Method for In Vivo Imaging of Solitary Lung Nodules Using Navigational Bronchoscopy and Confocal Laser Microendoscopy. Lung. 2015 Oct; 193(5): 773–8.

63 Sorokina A, Danilevskaya O, Averyanov A, Zabozlaev F, Sazonov D, Yarmus L, et al. Comparative study of ex vivo probe-based confocal laser endomicroscopy and light microscopy in lung cancer diagnostics. Respirology. 2014 Aug; 19(6): 907–13.

64 Seth S, Akram AR, McCool P, Westerfeld J, Wilson D, McLaughlin S, et al. Assessing the utility of autofluorescence-based pulmonary optical endomicroscopy to predict the malignant potential of solitary pulmonary nodules in humans. Sci Rep. 2016 Aug; 6(1): 31372.

65 Wijmans L, de Bruin DM, Meijer SL, Annema JT. Real-Time Optical Biopsy of Lung Cancer. Am J Respir Crit Care Med. 2016 Oct; 194(8):e10–1.

66 Bonhomme O, Duysinx B, Heinen V, Detrembleur N, Corhay JL, Louis R. First report of probe based confocal laser endomicroscopy during medical thoracoscopy. Respir Med. 2019 Feb; 147: 72–5.

67 Zirlik S, Hildner K, Rieker RJ, Vieth M, Neurath MF, Fuchs FS. Confocal Laser Endomicroscopy for Diagnosing Malignant Pleural Effusions. Med Sci Monit. 2018 Aug; 24: 5437– 47.

68 Quirk BC, McLaughlin RA, Curatolo A, Kirk RW, Noble PB, Sampson DD. In situ imaging of lung alveoli with an optical coherence tomography needle probe. J Biomed Opt. 2011 Mar; 16(3): 036009.

69 McLaughlin RA, Yang X, Quirk BC, Lorenser D, Kirk RW, Noble PB, et al. Static and dynamic imaging of alveoli using optical coherence tomography needle probes. J Appl Physiol (1985). 2012 Sep; 113(6): 967–74.

70 Meissner S, Knels L, Krueger A, Koch T, Koch E. Simultaneous three-dimensional optical coherence tomography and intravital microscopy for imaging subpleural pulmonary alveoli in isolated rabbit lungs. J Biomed Opt. 2009 Sep-Oct; 14(5): 054020.

71 Hariri LP, Adams DC, Wain JC, Lanuti M, Muniappan A, Sharma A, et al. Endobronchial Optical Coherence Tomography for Low- Risk Microscopic Assessment and Diagnosis of Idiopathic Pulmonary Fibrosis In Vivo. Am J Respir Crit Care Med. 2018 Apr; 197(7): 949–52.

72 Wijmans L, de Bruin DM, Bonta PI, Jonkers RE, Poletti V, Annema JT. OCT, a Valuable Novel Tool for Assessing the Alveolar Compartment in ILD? Am J Respir Crit Care Med. 2017; 197(9): 1231–2.

73 Wijmans L dBD, Jonkers R, Roelofs J, van den Berk I, Bonta P, Annema J. Visualizing the alveolar compartment in ILD patients by optical coherence tomography [abstract]. Presented at the European Respiratory Society Congress. September 10, 2017, Milan, Italy. Abstract 5061.

74 Danilevskaya O, Averyanov A, Lesnyak V, Chernyaev A, Sorokina A. Confocal laser endomicroscopy for diagnosis and monitoring of pulmonary alveolar proteinosis. J Bronchology Interv Pulmonol. 2015 Jan; 22(1): 33– 40.

75 Salaun M, Roussel F, Bourg-Heckly G, Vever- Bizet C, Dominique S, Genevois A, et al. In vivo probe-based confocal laser endomicroscopy in amiodarone-related pneumonia. Eur Respir J. 2013 Dec; 42(6): 1646–58.
76 Yserbyt J, Alame T, Dooms C, Ninane V. Pulmonary alveolar microlithiasis and probebased confocal laser endomicroscopy. J Bronchology Interv Pulmonol. 2013 Apr; 20(2): 159–63.
77 Yserbyt J, Dooms C, Ninane V, Decramer M, Verleden G. Perspectives using probe-based confocal laser endomicroscopy of the respiratory tract. Swiss Med Wkly. 2013 Mar; 143:w13764.
78 Danilevskaya O, Averyanov A, Klimko N, Lesnyak V, Sorokina A, Sazonov D, et al. The case of diagnostics of invasive pulmonary aspergillosis by in vivo probe-based confocal laser endomicroscopy of central and distal airways. Med Mycol Case Rep. 2014 Jul; 5: 35– 9.
79 Shafiek H, Fiorentino F, Cosio BG, Kersul A, Thiberville L, Gomez C et al. Usefulness of Bronchoscopic Probe-Based Confocal Laser Endomicroscopy in the Diagnosis of Pneumocystis jirovecii Pneumonia. Respiration. 2016; 92(1): 40–7.
80 Vasilev I, Mamenko I, Tabanakova I, Vikulova I, Shevel V, Ushkov A, et al. Probe-based Confocal Laser Endomicroscopy in Metastatic Pulmonary Calcification. J Bronchology Interv Pulmonol. 2018 Jan; 25(1): 60–2.
81 Yserbyt J, Dooms C, Decramer M, Verleden GM. Acute lung allograft rejection: diagnostic role of probe-based confocal laser endomicroscopy of the respiratory tract. J Heart Lung Transplant. 2014 May; 33(5): 492–8.
82 Keller CA, Khoor A, Arenberg DA, Smith MA, Islam SU. Diagnosis of Acute Cellular Rejection Using Probe-based Confocal Laser Endomicroscopy in Lung Transplant Recipients: A Prospective, Multicenter Trial. Transplantation. 2019 Feb; 103(2): 428–34.
83 Meng P, Tan GL, Low SY, Takano A, Ng YL, Anantham D. Fibred confocal fluorescence microscopy in the diagnosis of interstitial lung diseases. J Thorac Dis. 2016 Dec; 8(12): 3505–14.
84 Salaun M, Guisier F, Dominique S, Genevois A, Jounieaux V, Bergot E, et al. In vivo probebased confocal laser endomicroscopy in chronic interstitial lung diseases: specific descriptors and correlation with chest CT. Respirology. 2019 Aug; 24(8): 783–91.
85 Wijmans L, Bonta PI, Rocha-Pinto R, de Bruin DM, Brinkman P, Jonkers RE, et al. Confocal Laser Endomicroscopy as a Guidance Tool for Transbronchial Lung Cryobiopsies in Interstitial Lung Disorder. Respiration. 2019; 97(3): 259–63.
86 Jorge E, Baptista R, Calisto J, Faria H, Monteiro P, Pan M, et al. Optical coherence tomography of the pulmonary arteries: A systematic review. J Cardiol. 2016 Jan; 67(1): 6– 14.
87 Tatebe S, Fukumoto Y, Sugimura K, Nakano M, Miyamichi S, Satoh K et al. Optical coherence tomography as a novel diagnostic tool for distal type chronic thromboembolic pulmonary hypertension. Circ J. 2010 Aug; 74(8): 1742–4.
88 Domingo E, Grignola JC, Aguilar R, Montero MA, Arredondo C, Vazquez M, et al. In vivo assessment of pulmonary arterial wall fibrosis by intravascular optical coherence tomography in pulmonary arterial hypertension: a new prognostic marker of adverse clinical follow- up. Open Respir Med J. 2013 Apr; 7(1): 26–32.

89 Jiang X, Peng FH, Liu QQ, Zhao QH, He J, Jiang R, et al. Optical coherence tomography for hypertensive pulmonary vasculature. Int J Cardiol. 2016 Nov; 222: 494–8.

90 Homma Y, Hayabuchi Y, Ono A, Kagami S. Pulmonary Artery Wall Thickness Assessed by Optical Coherence Tomography Correlates With Pulmonary Hemodynamics in Children With Congenital Heart Disease. Circ J. 2018 Aug 24; 82(9): 2350–7.

91 Dai Z, Fukumoto Y, Tatebe S, Sugimura K, Miura Y, Nochioka K, et al. OCT imaging for the management of pulmonary hypertension. JACC Cardiovasc Imaging. 2014 Aug; 7(8): 843–5.

92 Sugimura K, Fukumoto Y, Satoh K, Nochioka K, Miura Y, Aoki T et al. Percutaneous transluminal pulmonary angioplasty markedly improves pulmonary hemodynamics and longterm prognosis in patients with chronic thromboembolic pulmonary hypertension. Circ J. 2012; 76(2): 485–8.

93 Roik M, Wretowski D, Łabyk A, Kostrubiec M, Rowiński O, Pruszczyk P. Optical coherence tomography of inoperable chronic thromboembolic pulmonary hypertension treated with refined balloon pulmonary angioplasty. Pol Arch Med Wewn. 2014; 124(12): 742–3.

94 Hong C, Luo FQ, Liu CL, Zhong NS, Li JY, Wang W. Clinical study of optical coherence tomography in the diagnosis of peripheral pulmonary artery thrombus. Thromb Res. 2018 Jan; 161: 52–9.

95 Pan Y, Volkmer JP, Mach KE, Rouse RV, Liu JJ, Sahoo D, et al. Endoscopic molecular imaging of human bladder cancer using a CD47 antibody. Sci Transl Med. 2014 Oct; 6(260): 260ra148.

96 Feroldi F, Verlaan M, Knaus H, Davidoiu V, Vugts DJ, van Dongen GA, et al. High resolution combined molecular and structural optical imaging of colorectal cancer in a xenograft mouse model. Biomed Opt Express. 2018 Nov; 9(12): 6186–204.

97 Patout M, Guisier F, Brune X, Bohn P, Romieu A, Sarafan-Vasseur N, et al. Real-time molecular optical microimaging of EGFR mutations using a fluorescent erlotinib based tracer. BMC Pulm Med. 2019 Jan; 19(1): 3.

98 Guisier F, Bohn P, Patout M, Piton N, Farah I, Vera P, et al. In- and ex-vivo molecular imaging of apoptosis to assess sensitivity of non-small cell lung cancer to EGFR inhibitors using probe-based confocal laser endomicroscopy. PLoS One. 2017 Jul; 12(7):e0180576.

99 Morisse H, Heyman L, Salaun M, Favennec L, Picquenot JM, Bohn P, et al. In vivo and in situ imaging of experimental invasive pulmonary aspergillosis using fibered confocal fluorescence microscopy. Med Mycol. 2012 May; 50(4): 386–95.

100 Morisse H, Heyman L, Salaun M, Favennec L, Picquenot JM, Bohn P, et al. In vivo molecular microimaging of pulmonary aspergillosis. Med Mycol. 2013 May; 51(4): 352– 60.

101 Vanherp L, Poelmans J, Hillen A, Govaerts K, Belderbos S, Buelens T, et al. Bronchoscopic fibered confocal fluorescence microscopy for longitudinal in vivo assessment of pulmonary fungal infections in free-breathing mice. Sci Rep. 2018 Feb; 8(1): 3009.

102 Mills B, Akram AR, Scholefield E, Bradley M, Dhaliwal K. Optical Screening of Novel Bacteria-specific Probes on Ex Vivo Human Lung Tissue by Confocal Laser Endomicroscopy. J Vis Exp. 2017 Nov; 129.

103 Adams DC, Pahlevaninezhad H, Szabari MV, Cho JL, Hamilos DL, Kesimer M, et al. Automated segmentation and quantification of airway mucus with endobronchial optical coherence tomography. Biomed Opt Express. 2017 Sep; 8(10): 4729–41.

104 Feroldi F, Willemse J, Davidoiu V, Grafe MG, van Iperen DJ, Goorsenberg AW, et al. In vivo multifunctional optical coherence tomography at the periphery of the lungs. Biomed Opt Express. 2019 May; 10(6): 3070– 91.

105 Pahlevaninezhad H, Khorasaninejad M, Huang YW, Shi Z, Hariri LP, Adams DC, et al. Nano-optic endoscope for high-resolution optical coherence tomography in vivo. Nat Photonics. 2018 Sep; 12(9): 540–7.

Chapter 6

In vivo polarisation sensitive optical coherence tomography for fibrosis assessment in interstitial lung disease: a prospective, exploratory, observational study

Margherita Vaselli [1], Kirsten Kalverda-Mooij[2], Erik Thunnissen[3], Michael W T Tanck[4], Onno M Mets[5], Inge A H van den Berk [5], Jouke T Annema[2], Peter I Bonta[2], Johannes F de Boer[1]

[1]Department of Physics and Astronomy, Vrije Universiteit Amsterdam, Amsterdam, The Netherlands
[2]Respiratory Medicine, Amsterdam University Medical Centres, Amsterdam, The Netherlands
[3]Department of Pathology, Amsterdam University Medical Centra, Amsterdam, The Netherlands
[4]Department of Epidemiology and Data Science, University of Amsterdam, Amsterdam, The Netherlands
[5]Department of Radiology and Nuclear Medicine, Amsterdam UMC Location AMC, Amsterdam, The Netherlands

BMJ Open Respir Res 2023;**10**:e001628

ABSTRACT

Introduction

Endobronchial polarisation sensitive optical coherence tomography (EB-PS-OCT) is a bronchoscopic imaging technique exceeding resolution of high-resolution CT (HRCT) by 50-fold. It detects collagen birefringence, enabling identification and quantification of fibrosis.

Study aim

To assess pulmonary fibrosis in interstitial lung diseases (ILD) patients with in vivo EB-PS-OCT using histology as reference standard.

Primary objective

Visualisation and quantification of pulmonary fibrosis by EB-PS-OCT.

Secondary objectives

Comparison of EB-PS-OCT and HRCT detected fibrosis with histology, identification of ILD histological features in EB-PS-OCT images and comparison of ex vivo PS-OCT results with histology.

Methods

Observational prospective exploratory study. Patients with ILD scheduled for transbronchial cryobiopsy or surgical lung biopsy underwent in vivo EB-PS-OCT imaging prior to tissue acquisition. Asthma patients were included as non-fibrotic controls. Per imaged lung segment, fibrosis was automatically quantified assessing the birefringent area in EB-PS-OCT images. Fibrotic extent in corresponding HRCT areas and biopsies were compared with EB-PS-OCT detected fibrosis. Microscopic ILD features were identified on EB-PS-OCT images and matched with biopsies from the same segment.

Results

19 patients were included (16 ILD; 3 asthma). In 49 in vivo imaged airway segments the parenchymal birefringent area was successfully quantified and ranged from 2.54% (no to minimal fibrosis) to 21.01% (extensive fibrosis). Increased EB-PS-OCT detected birefringent area corresponded to increased histologically confirmed fibrosis, with better predictive value than HRCT. Microscopic ILD features were identified on both in vivo and ex vivo PS-OCT images.

Conclusions

EB-PS-OCT enables pulmonary fibrosis quantification, thereby has potential to serve as an add-on bronchoscopic imaging technique to diagnose and detect (early) fibrosis in ILD.

WHAT IS ALREADY KNOWN ON THIS TOPIC

⇒ In patients with an interstitial lung disease (ILD), accurate diagnosis and early recognition of progressive pulmonary fibrosis is challenging but important for classification, treatment and prognosis. Endobronchial optical coherence tomography (OCT) is a minimally invasive, bronchoscopic, imaging modality to generate volumetric images of the lung parenchyma with microscopic resolution. Polarisation sensitive OCT (PS-OCT) is an extension of conventional OCT that adds birefringence detection. With fibrosis being highly birefringent, PS-OCT may enable fibrosis detection in the lung parenchyma.

WHAT THIS STUDY ADDS

⇒ In this study, we show that in vivo endobronchial PS-OCT can automatically quantify fibrosis and detect ILD features in patients with ILD by minimally invasive bronchoscopy.

HOW THIS STUDY MIGHT AFFECT RESEARCH, PRACTICE OR POLICY

⇒ Endobronchial PS-OCT has potential to serve as an add-on bronchoscopic imaging technique to diagnose and assess (progressive) fibrosis in patients with ILD.

INTRODUCTION

Interstitial lung diseases (ILDs) include a large group of different diseases, characterised by inflammation and pulmonary fibrosis.[1] Treatment consists of anti-inflammatory and/or antifibrotic medication. ILD diagnosis and identification of patients with ILD with a (progressive) fibrotic phenotype is challenging, but of key importance for treatment decisions and prognosis.[2–4]

For ILD diagnosis, no single diagnostic test exists. Guidelines recommend evaluating all available diagnostic information during a multidisciplinary team (MDT) discussion to establish a high confident diagnosis.[5] To identify the fibrotic phenotype, pulmonary function testing and high-resolution CT (HRCT) are used as diagnostic parameters. However, changes in pulmonary function tests can be non-specific and HRCT has limitations in fibrosis detection and in differentiating fibrotic from inflammatory progression. Indeed, a weak correlation exists between fibrotic extent as detected by HRCT and prognosis.[6 7] For disease pattern identification, lung biopsy is considered to be the reference standard, but is associated with morbidity and in rare case mortality. Lung tissue acquisition is, therefore, only performed in highly selected patients with ILD and is not appropriate for longitudinal measurements to evaluate fibrotic progression. Thus, there is an unmet need in fibrotic ILD diagnostics and ILD progression detection.

Conventional optical coherence tomography (OCT) is an imaging technique that uses near-infrared light to provide structural images of tissue with a resolution of ~10 µm.[8] Endobronchial OCT (EB-OCT) refers to a technique in which a thin flexible OCT probe is advanced through the working channel of the bronchoscope to the periphery of the lung. The procedure is minimally invasive, can be performed under conscious sedation and can easily be combined with the standard diagnostic techniques including bronchoalveolar lavage. In the last decade, EB-OCT emerged as a bronchoscopic imaging modality to generate cross-sectional images of the airways and lung parenchyma. Several studies reported EB-OCT in obstructive lung diseases,[9–12] detection of malignancies[13– 15] and ILDs.[16 17] Conventional EB-OCT provides volumetric reconstructions of lung tissue with microscopic resolution, but has limitations in fibrotic tissue-specific contrast.[18] Polarisation sensitive OCT (PS-OCT) is an extension of conventional OCT that adds tissue-specific contrast by assessing presence of birefringence. Birefringence is an optical property exhibited by collagen

in fibrous tissues including muscle, connective tissue and nerve fibres.[19] As pulmonary fibrosis is characterised by an increase in collagen, PS-OCT can visualise pulmonary fibrosis. To date, the potential of EB-PS-OCT in pulmonary medicine has been demonstrated in vivo in a canine model[20] and in asthma patients[21 22] to detect airway smooth muscle reduction after bronchial thermoplasty. Recently, Nandy *et al* performed EB-PS-OCT in patients with ILD and manually quantified birefringence across tissue types including destructive and interstitial fibrosis.[23]

In this study, we use in vivo EB-PS-OCT to automatically quantify the area of birefringent tissue to assess fibrotic content in patients with ILD. For the first time, we compare the ability of EB-PS-OCT and HRCT for fibrosis detection and quantification using histopathology as reference standard. Additionally, we retrieve the orientation of birefringent tissues fibres, which provides a valuable tool to distinguish fibrous tissue from other birefringent tissues such as airway smooth muscle and perichondrium.

METHODS

Study design and patient enrolment

This imaging study is a substudy of a randomised controlled trial comparing transbronchial cryobiopsy (TBCB), followed by surgical lung biopsy (SLB) and immediate SLB for ILD (COLD-study NTR NL7634). In this study, we aim to assess pulmonary fibrosis using in vivo EB-PS-OCT. The primary objective is to visualise and automatically quantify pulmonary fibrosis with in vivo EB-PS-OCT. Secondary study objectives are as follows: (1) compare EB-PS-OCT detected fibrosis with the extent of fibrosis as detected by HRCT and histology and (2) the identification of ILD hallmarks in PS-OCT images acquired both in vivo and ex vivo.

Considering this is an exploratory study no formal sample size calculation was performed.

Each subject provided separate written informed consent for this substudy. Patients with an undiagnosed ILD scheduled for lung biopsy in Amsterdam UMC were eligible for study participation. A full list of inclusion and exclusion criteria for this substudy are provided in online supplemental e-Table 1. For non-fibrotic controls, we used EB-PS-OCT

measurements of asthma patients included in the EB-PS-OCT asthma study.[21]

Patient and public involvement

For this exploratory study, patients were not involved in the design, conduct, reporting or dissemination plans.

EB-PS-OCT imaging and fibrosis quantification

Prior to cryobiopsy or SLB, EB-PS-OCT measurements were performed by pulmonologists experienced in EB imaging techniques (PB, JTA and KK-M). Regions of interest (airway segments) for EB-PS-OCT imaging were identified by the pulmonologists based on HRCT scan and planned biopsy location. Patients were deeply sedated, remaining spontaneous breathing and intubated (cryobiopsy procedure) or under full anaesthesia (SLB procedure). In each patient, three different segments were imaged with EB-PS-OCT, and each segment was imaged at least twice. Volumetric EB-PS-OCT images were acquired by advancing the EB-PS-OCT probe through the working channel of the bronchoscope to the periphery of each lung segment until pleural resistance (online supplemental e-figure 1). The probe was then manually pulled back over a length of ~5–6cm and three-dimensional volumetric images were acquired.

EB-PS-OCT measurements were performed through a distal scanning catheter, with a diameter of 1.35 mm, rotating at 52 rotations/s and protected by a medical grade pebax sheath.[24] The probe was connected to a PS-OCT system, previously described,[24] with an axial and lateral tissue resolution of 12 µm and 13 µm, respectively (refractive index n=1.4), and an imaging depth of 1.4 mm. Postprocessing analysis of the acquired EB-PS-OCT raw-data generated conventional OCT intensity images and EB-PS-OCT (optic axis orientation) images, in which birefringent structures and their fibres orientation were visualised and segmented.

For each airway segment imaged, fibrosis was automatically quantified in postprocessing as mean percentage of birefringence area in EB-PS-OCT cross-sectional images of the parenchymal (distal) part of all pullbacks acquired in that segment. EB-PS-OCT images of the proximal part of each pullback imaging the airway were not included in the fibrosis quantification given the prevalence of other birefringent structures in the proximal airway (eg, airway smooth muscle, perichondrium). Detailed information on EB-PS-OCT data processing and fibrosis quantification is provided in online supplemental e-appendix 1.

Radiological and histological evaluation

HRCT scans were evaluated by two ILD-specialised radiologists (OMM and IB) (blinded for EB-PS-OCT results and to each other). Per EB-PS-OCT imaged and biopsied segment, a fibrosis score on HRCT was determined ranging from 0 to 3 (0=no fibrosis, 1=mild fibrosis, 2=moderate fibrosis, 3=severe fibrosis). In a consensus meeting, inconsistencies were discussed, and a final score was obtained. A lung specialised pathologist (ET), blinded for clinical information including HRCT and EB-PS-OCT results, evaluated the acquired biopsies for the presence of fibrosis on a 0–3 scale. Following a 6-week wash-out period, histological evaluation was repeated evaluating the biopsies for the presence of fibrosis in a different order, and blinded for previous evaluation. When a segment was biopsied twice, the overall score included both biopsies. In case of inconsistent scores, a third evaluation was performed 2 weeks after the last histological evaluation, and a final score was obtained. Criteria for the categorical fibrosis scoring system for HRCT and histology are provided in online supplemental e-appendix 2.

Histology matching

Ex vivo PS-OCT measurements of the resected biopsies (11 SLB from 4 patients) were performed immediately after tissue extraction on the unprocessed specimen by pulling back the catheter while pressing it to the biopsy surface. All the biopsies were processed according to local standard practice. The histology sections were cut perpendicularly to the probe pullback direction. Ex vivo EB-PS-OCT images were compared with histology by the OCT expert (MV) and the pathologist (ET) for one-to-one matching of PS-OCT cross-sectional images with the histology sections obtained.

Statistical analysis

Statistical analysis to compare accuracy of fibrosis classification between EB-PS-OCT versus histology and HRCT versus histology was performed on segments from which biopsies were obtained. Asthmatic controls with normal lung parenchyma on HRCT and normal diffusion capacity on pulmonary function test served as control.

Ordinal logistic regression was chosen to model the relationship between the response ordinal variable (histological fibrosis score) and the explanatory variables (EB-PS-OCT and HRCT detected fibrosis).

To correct for multiple segments within the same patient, the ordinal logistic regression was used with a random patient effect (cumulative link mixed model). The performance of the two models (EB-PS-OCT and histology vs HRCT and histology) was compared using the area under the receiver operating characteristic curve (generalised AUROC or c-index, specific measure for ordinal outcomes[25]) and the overall accuracy (calculated using a confusion matrix). Weighted kappa was used to evaluate inter and intra observer variability between radiologists evaluating HRCT scans and the pathologist evaluating histology slides. All analyses were carried out in R (V.4.1.3).

RESULTS

Study cohort

Between January 2020 and July 2021, 16 patients with ILD who underwent lung biopsy were included (12 TBCB, 3 SLB and 1 both). Moreover, three asthma patients from a historical cohort were included as a non-fibrotic control group. These three patients were imaged with EB-PS-OCT 6 months following bronchial thermoplasty to assess airway smooth muscle thickness in the proximal airways, but EB-PS-OCT pullbacks imaged both airways and lung parenchyma.[21] Baseline characteristics and final MDT-ILD diagnoses are represented in table 1. EB-PS-OCT imaging added ~5–10 min to the biopsy procedure without any procedure-related adverse events.

Table 1. Baseline characteristics and final diagnosis of patients with ILD

	ILD patients n=16	Asthma patients n=3
Gender		
M	11 (69)	1 (33)
F	5 (31)	2 (67)
Age	64±8	46±15
BMI	28±3	31±5
Smoking status		
Never smokers	2 (12.5)	3 (100)
Ex-smokers	12 (75)	
Current smoker	2 (12.5)	
Packyears (current and ex-smokers)	21±11	

Table 1. Continued

	ILD patients n=16	Asthma patients n=3
Pulmonary function test		
FVC, % of predicted value	86±14	94±2
DLCOc, % of predicted value	58±15	92±8
Final ILD diagnosis		
cHP	7 (44)	
IPF	4 (25)	
srILD	1 (6)	
IPAF-fNSIP	1 (6)	
Idiopathic fNSIP	1 (6)	
Sarcoidosis	1 (6)	
Unclassifiable ILD	1 (6)	
Non-fibrotic asthma controls		3 (100)

Data are shown as N (%) or mean (±SD). BMI, body mass index; cHP, chronic hypersensitivity pneumonitis; DLCOc, diffusing capacity of the lung for carbon monoxide corrected for haemoglobin; F, female; fNSIP, fibrotic non-specific idiopathic pneumonitis; FVC, forced vital capacity; ILD, interstitial lung disease; IPAF, interstitial pneumonia with autoimmune features; IPF, idiopathic pulmonary fibrosis; M, male; srILD, smoking-related ILD.

Out of 19 included patients, 17 (14 ILD and 3 asthma patients) underwent in vivo EB-PS- OCT imaging of 3 different lung segments. Each segment was imaged at least 2 times, resulting in a total of 128 in vivo pullbacks (400–800 frames per pullback). Two SLB ILD patients in which in vivo EB-PS-OCT was not performed for logistical reasons, were only included for ex vivo PS-OCT imaging.

In vivo EB-PS-OCT imaging was performed in a total of 55 individual segments. Six segments were excluded: n=5 segments, due to the pullback being too proximal and not containing alveolar tissue, and n=1, due to probe malfunction. Since in one patient all pullbacks were too proximal, this led to the exclusion of this patient.

In 49 in vivo imaged lung segments from 16 patients (13 ILD and 3 asthma patients) fibrosis was quantified based on EB-PS-OCT detected birefringent area (figure 1, primary objective: visualisation and quantification of pulmonary fibrosis by EB-PS-OCT). For secondary objectives, in total 35 segments were analysed: 8 segments from asthma patients and 27 from patients with ILD as only those segments for which

corresponding biopsies were available were included (in 24 segments TBCB's were acquired (n=47 cryobiopsies) and in 3 segments SLB's were acquired (n=3 surgical biopsies)) (figure 1).

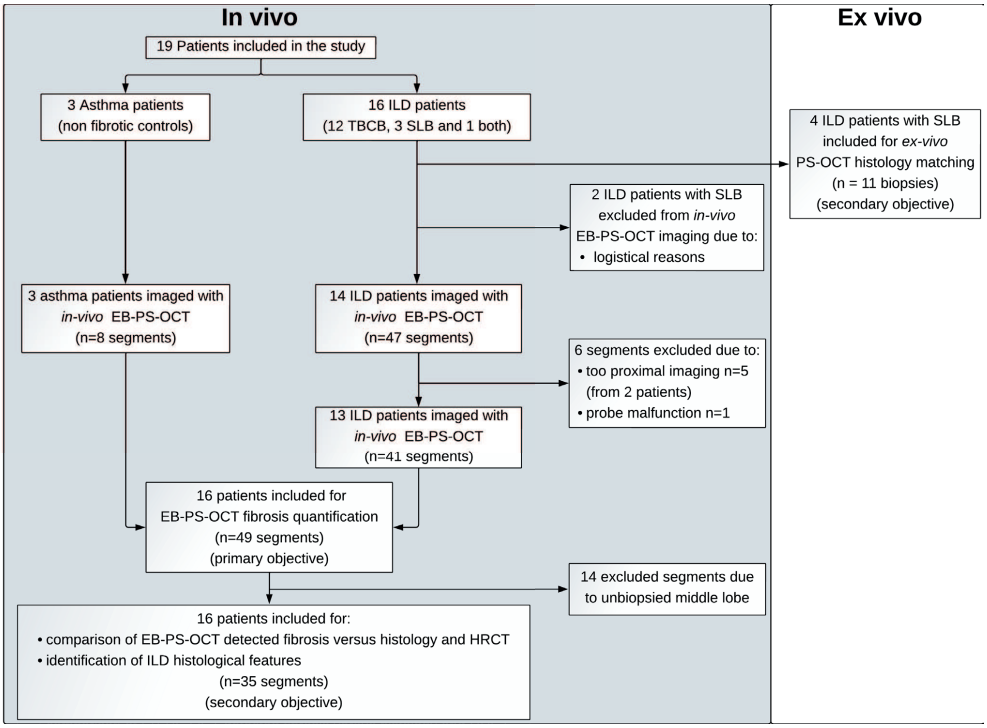


Figure 1. Flow chart of the EB-PS- OCT imaging study. Flow chart shows how patients relate to EB-PS- OCT objectives allocation both in vivo and ex vivo. Nineteen patients were included in the study (3 asthma and 16 ILD). Sixteen patients with ILD underwent lung biopsy: 12 TBCB, 3 SLB and 1 patient underwent both. Only SLB was included for ex vivo analysis. Two patients with ILD undergoing SLB were excluded from in vivo EB-PS- OCT for logistical reasons and were only included for ex vivo PS-OCT imaging. A total of 55 segments were imaged in vivo (8 from 3 asthma controls and 47 from 14 patients with ILD). After exclusion of segments in which no peripheral lung parenchyma was visualised (n=5, from 2 patients) or unable to be analysed due to probe malfunction (n=1), 49 segments were included for primary objective analysis (8 from 3 asthma patients and 41 from patients with ILD). For secondary objectives, only segments with corresponding histology were included (35 segments from 16 patients). EB-PS-OCT, endobronchial polarisation sensitive optical coherence tomography; HRCT, high-resolution CT; ILD, interstitial lung disease; SLB, surgical lung biopsy; TBCB, transbronchial cryobiopsy.

EB-PS-OCT fibrosis quantification

In 49 segments, parenchymal fibrosis was quantified based on in vivo EB-PS-OCT detected birefringence. Birefringence from the peripheral lung parenchyma ranged from 2.5% in patients without fibrosis up to 21.0% in a patient with extensive fibrosis. In non-fibrotic asthma controls, birefringence ranged from 3.3% to 6.8%.

In line with our previous study,[26] pullbacks acquired in the same segment showed good reproducibility of the EB-PS-OCT detected birefringence content (online supplemental e-Figure 2).

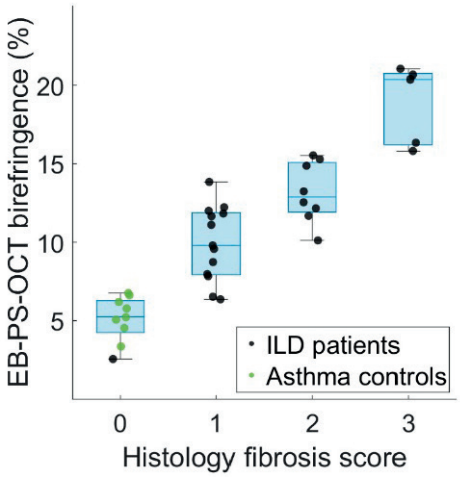


Figure 2. Quantitative measurement of birefringence % as detected by EB-PS-OCT (y-axis) compared with the histology fibrosis score (x-axis). Comparing the continuous data from EB-PS-OCT detected birefringence to the histology-based fibrosis score, higher EB-PS-OCT birefringence % corresponded to higher histological fibrosis scores. Each dot represents an EB-PS-OCT imaged and biopsied segment (n=35) from patients with ILD (black dots) and asthma controls (green dots). Birefringence from the peripheral lung parenchyma ranged from 2.5% in a patient with non-fibrotic ILD up to 21.0% in a patient with IPF. EB-PS-OCT, endobronchial polarisation sensitive optical coherence tomography; ILD, interstitial lung diseases; IPF, idiopathic pulmonary fibrosis.

In patients with ILD, 63% (n=60 pullbacks) of EB-PS-OCT imaging was performed in the lower lobes, 4% (n=4 pullbacks) was performed in the upper lobes and 33% of the pullbacks (n=31) were obtained from the middle lobe. The birefringence extent detected by EB-PS-OCT in the lower lobe and in the middle lobe of each patient were compared. Lower lobes consistently showed more birefringence than the middle lobes, especially

in idiopathic pulmonary fibrosis (IPF) and chronic hypersensitivity pneumonitis (cHP) patients (online supplemental e-Figure 3).

EB-PS-OCT detected fibrosis versus HR-CT detected fibrosis compared with histology

Comparing the continuous data from EB-PS-OCT detected birefringence to the histology-based fibrosis score (n=8 Asthma, n=27 ILD), higher EB-PS-OCT birefringence values corresponded to higher histological fibrosis scores (figure 2). Lowest fibrosis scores were obtained from the asthma controls and a non-fibrotic ILD patient, and highest scores originate from an IPF and fibrotic cHP patient.

Current diagnostic tools including pulmonary function tests and HRCT have significant limitations in detection of fibrosis and are considered insufficient to detect subtle (progression of) fibrosis. To determine if EB-PS-OCT has added value over HRCT we compared EB-PS-OCT performance with HRCT to predict the fibrotic extent in histology. As histology was used as a reference standard, we included only the imaged segments for which histology was obtained (figure 1, secondary objective). Both HRCT and biopsies were analysed for extent of fibrosis by independent and blinded radiologists (Cohen's kappa for interobserver agreement: 0.67 (95% CI 0.54 to 0.83) weighted kappa: 0.75) and a pathologist (Cohen's kappa for intraobserver agreement: 0.88 (95% CI 0.76 to 0.99); weighted kappa of 0.91), respectively.

Based on an ordinal regression model, EB-PS-OCT shows higher discriminating performance than HRCT in predicting the histology fibrosis classification (AUROC (95% CI)) 0.96 (0.92 to 1.00) vs 0.83 (0.73 to 0.93) and overall accuracy (95% CI) 0.77 (0.60 to 0.90) vs 0.60 (0.42 to 0.76).

In vivo EB-PS-OCT identified ILD hallmarks

Conventional EB-OCT enables identification of histological features of ILD.[16 23] Additionally, EB-PS-OCT can distinguish fibrosis from other aetiologies of loss of aeration and provides information on fibrotic distribution. Representative EB-PS-OCT results acquired in the asthma controls and patients with ILD are shown in figures 3 and 4. Videos of EB-PS-OCT pullbacks corresponding to figures 3 and 4 are provided as online supplemental videos 1–5. Conventional EB-OCT intensity images (grey scale) have been overlapped with EB-PS-OCT optic axis orientation images (colour scale). In asthmatic controls, the added information of optic axis orientation images to EB-OCT intensity images confirmed the

absence of fibrosis in the distal parenchymal area by the low amount of detected birefringence, although, as expected, in the proximal airway it revealed a large amount of birefringent airway smooth muscle as a sign of airway remodelling (figure 3, panel B1–B3). In fibrotic ILD cases, optic axis orientation images confirmed the presence of fibrotic tissue in the distal parenchymal area (figure 3, panel D1,2) by increasing amount of birefringence. Results show that in optic axis orientation images, fibrotic tissue fibres orientation varies significantly from region to region, as is indicated by the different colours present in fibrotic areas (figure 3, panel D1,D2). In contrast, non-pathological birefringent structures (eg, airway smooth muscle layers, perichondrium) are characterised by fibres highly organised in the same direction (figure 3, panel B1, B3, D1, D3).

Furthermore, EB-PS-OCT pullbacks acquired in vivo in patients with ILD identified fibrotic distribution and specific histological ILD hallmarks of different ILD subsets, which were visualised in the histology from the corresponding biopsies (figure 4).

In our cohort, all four IPF patients showed a subpleural distribution of fibrotic changes (figure 4A). For other, non-usual interstitial pneumonia patients, an airway centred (fibrotic cHP) or a more diffuse (fibrotic non-specific interstitial pneumonia) distribution of the fibrotic changes were noted (figure 4B,C). A patient with smoking-related abnormalities without fibrosis showed very little parenchymal birefringence, but mainly enlarged alveolar (EA) spaces with some mucus filling corresponding with emphysema (figure 4D). The ILD hallmarks visualised by EB-PS-OCT that were histologically confirmed included: dense destructive fibrosis, interstitial fibrosis and traction bronchiectasis in the IPF cohort. In this IPF cohort, no microscopic honeycombing was detected in EB-PS-OCT images, nor was it found in histology. In fibrotic cHP, we identified enlarged alveolar spaces among airway centred fibrosis. In one cHP patient, microscopic honeycombing was detected adjacent to the airway, indicating the airway centred rather than a subpleural oriented disease (online supplemental e-Figure 4). None of the above-mentioned hallmarks was visualised in any of the asthma controls. Thus, EB-PS-OCT identified characteristic features which were exclusively present in certain ILD subsets.

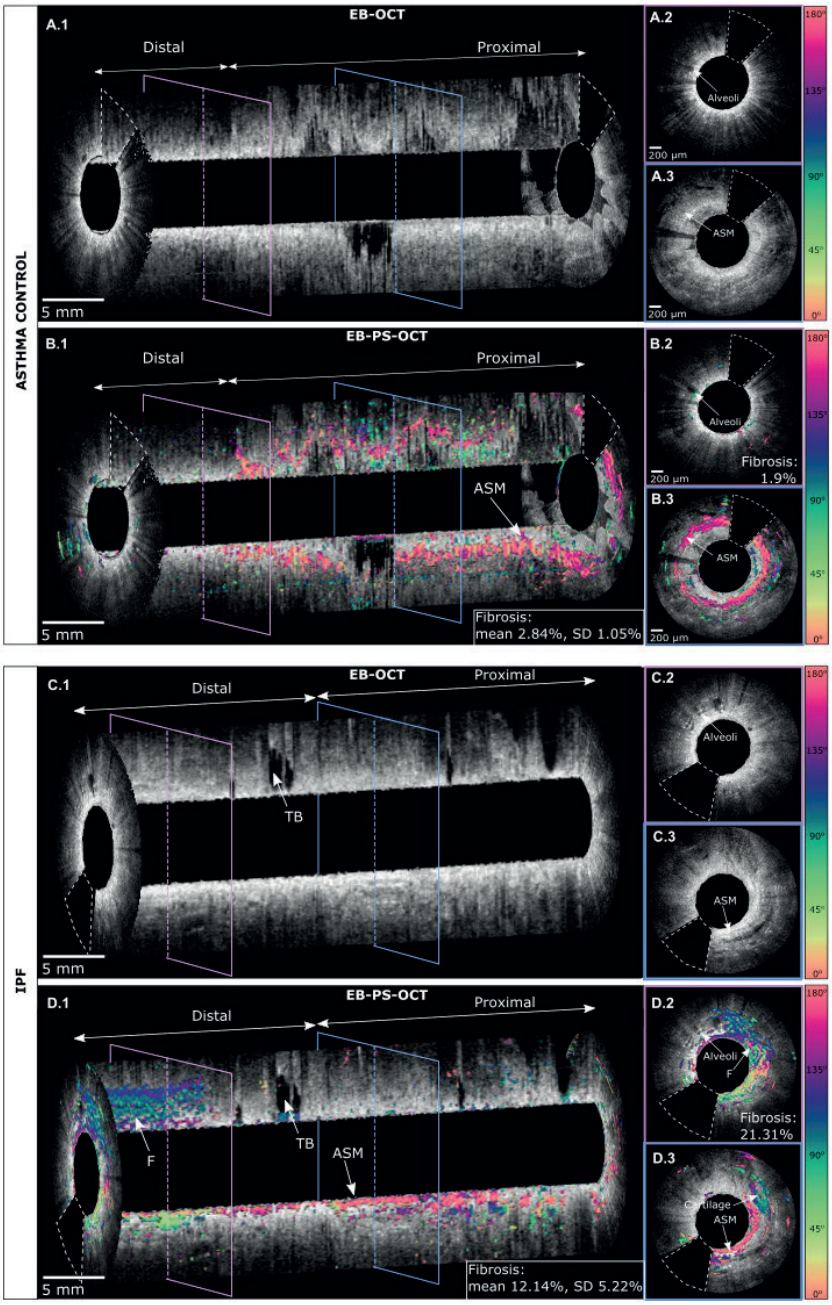


Figure 3. Conventional EB-OCT and EB-PS-OCT images of right lower lobe from an asthma patient (A, B), respectively and from an IPF patient (C, D), respectively. In the asthma patient, conventional EB-OCT visualises lattice-like signal-void areas recognised as normal alveoli in the lung parenchyma (A1) and in the cross-sectional image from the distal part of the pullback (A2). Cross-sectional image from the proximal part of the pullback shows airway smooth

muscle layer structure (A3). The additional use of polarisation properties of light to the conventional EB-OCT image results in the EB-*PS*-OCT pullback image, where birefringent structures are visible in the different colours (B1). Each colour indicates a different orientation of the tissue optic axis (right sided colour scale). The absence of birefringence in the distal airway is shown by the absence of colours in the cross-sectional image of the distal part of the EB-PS-OCT pullback (B2). In the proximal part of the pullback a thick birefringent layer (in pink) indicates the presence of an airway smooth muscle layer (B3). In the IPF patient, conventional EB-OCT pullback (C1) shows the presence of a dilated, signal-void area connected to the main airway compatible with a traction bronchiectasis. The two cross-sectional images visualise alveolar tissue in the distal part of the pullback (C2) and in the proximal part of the pullback hypodense tissue representing airway smooth muscle (C3). Additionally, EB-PS-OCT enables the visualisation of regions of dense subpleural fibrosis indicated by the presence of highly birefringent areas with random optic axis orientation in the distal end of the pullback (D1) and in a cross-sectional image from the same area (D2). A cross-sectional image from the proximal part of the pullback (D3) shows the presence of airway smooth muscle (in pink) and of a cartilage structure surrounded by a birefringent perichondrium layer (in green). Optic axis orientation images have been calibrated using the birefringent catheter sheath; this enabled to determine that birefringent structures in pink are circumferentially oriented, while birefringent structures in green are longitudinally oriented. The white dotted lines in OCT and PS-OCT images delineate the tissue area not optically accessible because of the presence of the wires feeding current to the motor. ASM, airway smooth muscle; EB-PS-OCT, endobronchial polarisation sensitive optical coherence tomography; F, fibrosis; IPF, idiopathic pulmonary fibrosis; TB, traction bronchiectasis.

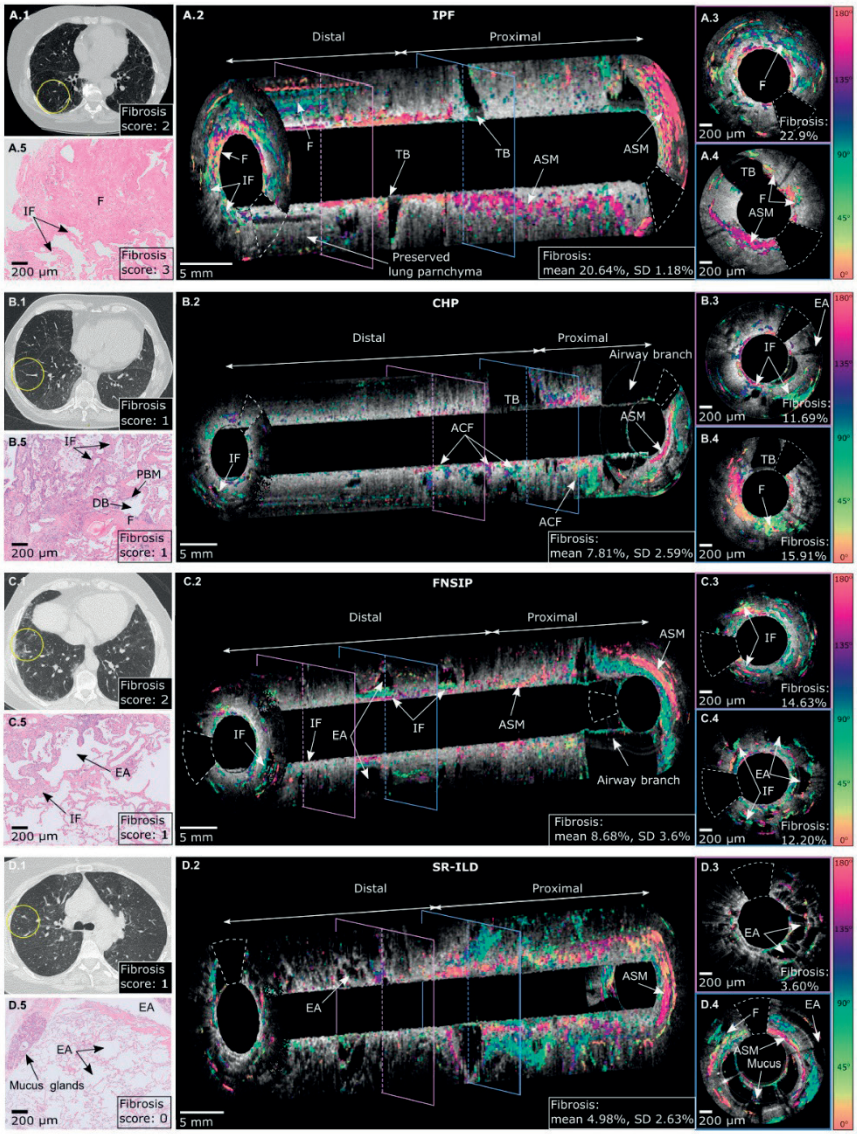


Figure 4. High-resolution CT (HRCT), H&E-stained histological section images and EB-PS-OCT images from patients diagnosed with IPF (A), cHP (B), fNSIP (C) and SR-ILD (D). Per pullback distal (parenchymal) part and proximal (airway) part are differentiated. For the evaluation of the amount of fibrosis in the lung parenchyma, only the distal part was analysed, as in the proximal part the amount of birefringence is higher due to other structures (eg, airway smooth muscle and cartilage). HRCT section indicates the segment where the EB-PS-OCT pullback was obtained (yellow circle) and the radiological fibrosis score (A1, B1, C1, D1). (A) IPF: regions of interstitial fibrosis and dense fibrosis alternate with regions of preserved lung parenchyma (A3). Traction bronchiectasis and airway smooth

muscle are visible. The overall fibrosis of the distal area of the pullback is 20.64%. (A2). Proximal cross-sectional image shows little fibrosis and airway smooth muscle (A5). H&E-stained histology slide from the biopsied segment shows combination of dense fibrosis and interstitial fibrosis. (A5). (B) cHP: Interstitial fibrosis is noted subpleurally, most fibrotic changes are in the proximal part of the distal area, indicating airway centred fibrosis (B2). Overall fibrosis of the lung parenchyma was 7.81%. In areas of interstitial fibrosis and airway centred fibrosis enlarged alveolar spaces and traction bronchiectasis are visible (B3 and B4). Corresponding H&E histology shows interstitial fibrosis, peribronchial metaplasia and distal bronchiole (B5). (C) NSIP throughout the entire distal part of the pullback interstitial fibrosis is identified in a homogeneous pattern (C2). In areas of fibrosis enlarged alveolar spaces are visible (C2 and C4). Airway smooth muscle is identified, in the proximal part of the pullback (C2). Overall fibrosis in the distal part of the pullback was 8.68%. H&E histology shows mild fibrotic changes consisting of interstitial fibrosis (C5). (D) srILD: hardly any fibrosis visible in the parenchymal part of the pullback (D2) (EB-PS- OCT detected fibrosis in the distal part of the pullback is 4.98%) (D2). The extensive amount of birefringence in the proximal part of the pullback is compatible with airway remodelling (D2). Enlarged alveolar spaces indicate emphysema in this patient (D3). Presence of mucus is noted (D4). Corresponding H&E histology shows no signs of fibrosis but enlarged alveolar spaces compatible with emphysema (D5). ACF, airway centred fibrosis; ASM, airway smooth muscle; cHP, chronic hypersensitivity pneumonitis; DB, distal bronchiole; EA, enlarged alveolar spaces; EB-PS- OCT, endobronchial polarisation sensitive optical coherence tomography; EM, emphysema; F, fibrosis; IF, interstitial fibrosis; ILD, interstitial lung diseases; IPF, idiopathic pulmonary fibrosis; NSIP, non-specific interstitial pneumonia; PBM, peribronchial metaplasia; srILD, smoking-related ILD; TB, traction bronchiectasis.

Ex vivo PS-OCT results

One-to-one matches of fibrotic structures as visualised by PS-OCT and histological images were performed by ex vivo measurements on the resected SLB. Resulting PS-OCT ex vivo pullbacks were visually inspected and 21 confident matches between PS-OCT cross-sections and histology from 8 lung segments were found. The predominant features in these matches are regions of dense fibrotic tissue as visualised in histology that were identified by highly birefringent areas in PS-OCT cross-sectional images. PS-OCT images visualised superficial birefringent areas that were histologically confirmed as thickened pleura in the matching histology (figure 5A,B).

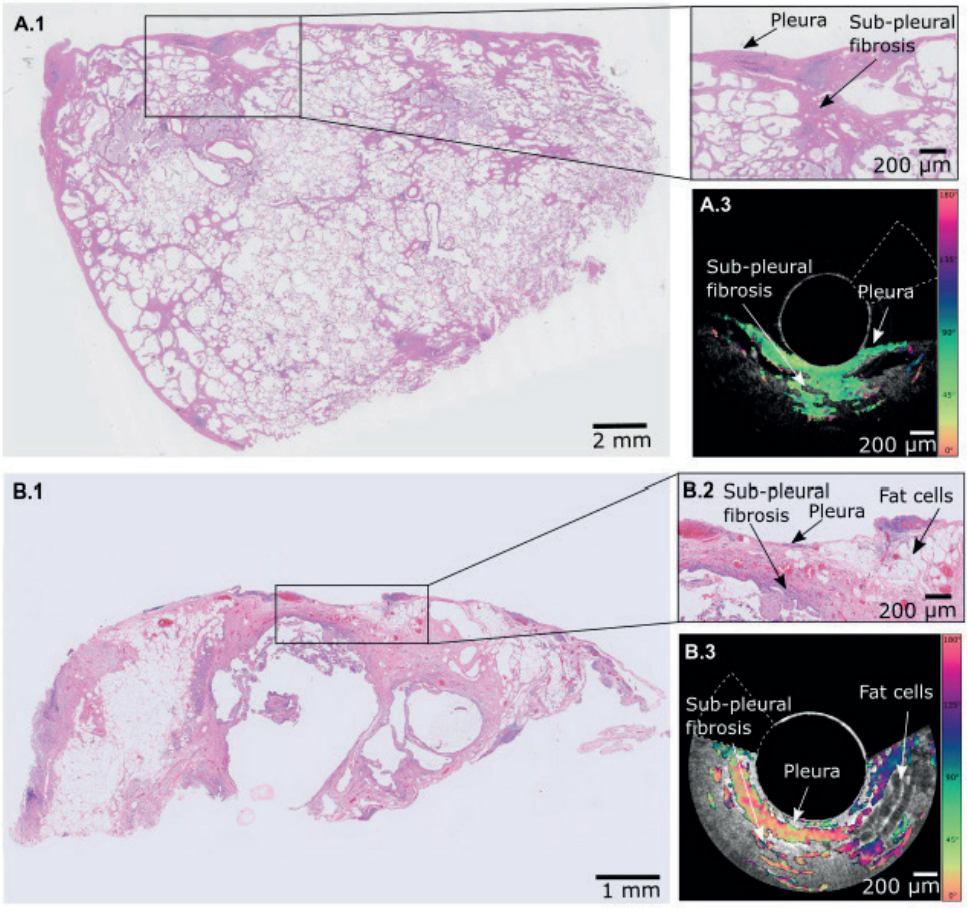


Figure 5. Matching histology of SLB and ex vivo EB-PS-OCT imaging. EB-PS-OCT imaging was performed pulling back the catheter along the surface of surgical lung biopsies from a patient with unclassified ILD (A) and a cHP patient (B). The specimens were cut perpendicular to the probe direction allowing for EB-PS- OCT and histology matching. In panel A) histology shows focal subpleural fibrosis (A1 and A2) and the cross-sectional image of the EB-PS- OCT shows birefringence in the same area, consistent with the presence of subpleural fibrosis (A3). In B, histology shows the presence of thickened pleura, subpleural fibrosis and fat cells (H&E stain B1 and B2). Corresponding to these structures, in the matching EB-PS-OCT cross-section are visualised birefringent areas and signal void cystic spaces (B3). Optic axis orientation images have been calibrated using the birefringent catheter sheath; this enabled to determine that birefringent structures in pink are circumferentially oriented, while birefringent structures in green are longitudinally oriented. The white dotted lines in OCT and PS-OCT images delineate the tissue area not optically accessible because of the presence of the wires feeding current to the motor. EB-PS- OCT, endobronchial polarisation sensitive optical coherence tomography; cHP, chronic hypersensitivity pneumonitis; ILD, interstitial lung diseases; OA, optic axis; SLB, surgical lung biopsy.

DISCUSSION

We found in vivo EB-PS-OCT to be a feasible, safe and minimally invasive imaging technique in patients with ILD. By using the fibrotic tissue specific-contrast provided by EB-PS-OCT, we demonstrated the ability of EB-PS-OCT to detect and quantify pulmonary birefringence. Results show differences in the mean birefringence area detected by EB-PS-OCT in the lung parenchyma from non-fibrotic cases (2.54%–6.75% range, in non-fibrotic ILD and asthma patients) and fibrotic cases (up to 21.01% in an IPF patient). The use of lung biopsies from corresponding lung segments confirmed that an increase in EB-PS-OCT detected birefringence corresponded to higher fibrosis extent in the biopsies. The ability of in vivo EB-PS-OCT to detect fibrosis is in line with a recent study by Nandy *et al*,[23] in which quantitative birefringence measurements were compared across tissue types in patients with ILD. Unique to EB-PS- OCT in this study, is that besides the ability to detect birefringent structures, the orientation of fibres is identified in optic axis orientation images. This enables to distinguish different highly birefringent tissues such as airway smooth muscle and perichondrium from fibrotic parenchymal areas. Moreover, the identification of fibres orientation helps identifying the transition between distal and proximal airway and assists the distinction of specific ILD subsets based on the distribution of birefringence in the airways. We envision the use of EB-PS-OCT as an add-on diagnostic technique when HRCT is non-diagnostic or to evaluate whether fibrosis is present or progressive over time. To this end, we compared the ability of EB-PS-OCT to predict the extent of fibrosis in histology with HRCT. Although HRCT has a central role in ILD diagnosis, it has limitations in the distinction between inflammation and identification of fibrosis due to similar HRCT findings (ie, ground glass opacities) or very subtle radiological changes.[6 7 27–29] Currently, the assessment of progressive pulmonary fibrosis relies on deterioration of clinical symptoms, pulmonary function tests or identification of progression on HRCT.[30] This warrants a certain amount of irreversible damage before antifibrotic treatment can be initiated. Our findings show that EB-PS-OCT, with a resolution ~50 times higher than HRCT and with unique specific contrast for fibrosis, has better discriminative ability to evaluate the extent of fibrosis. Furthermore, in addition to conventional EB-OCT, by identifying birefringent areas EB-PS-OCT may distinguish areas of fibrosis from areas with a loss of aeration due to other factors such as atelectasis or inflammation.

In this study, ex vivo PS-OCT measurements on resected lung biopsies validated the potential of PS-OCT in identifying fibrotic tissue through one-to-one matches between PS-OCT cross-sections and histology. The presence of characteristic ILD features in EB-PS-OCT images was confirmed with corresponding histopathology. The absence of these hallmarks in EB-PS-OCT images from the asthma controls substantiates EB-PS-OCT ability in discriminating pathological features specific for ILD subsets.

This study has several limitations. Although our findings originate from a relatively high number of pullbacks, we recognise the number of patients included represents a limitation of this study and implicates the need for prospective validation in a larger patient cohort.

Additionally, the reported study population includes patients with ILD with an inconclusive clinicoradiological diagnosis, and therefore, extrapolation of the added value of EB-PS-OCT in cases with classifying HRCT pattern remains to be established.

Currently, no universally accepted method is available for the quantification of fibrosis in HRCT and in histopathology. The radiological and histological four-class fibrosis score of each segment was provided based on a pragmatic visual interpretation of the HRCT and lung biopsies rather than a validated scoring tool. Thus, a method which reflects daily practice of ILD-MDT sessions in which radiologists and pathologists evaluate the presence or progression of fibrosis based on their visual assessment was chosen for being feasible and reproducible as shown by the high weighted kappa score.

In the absence of healthy volunteers, we included three asthma patients who underwent bronchial thermoplasty as non-fibrotic controls. As bronchial thermoplasty was performed in the proximal airways, we do not expect the amount of birefringence in the distal lung parenchyma to be affected by it, which is in line with normal HRCT and normal lung diffusion capacity. We recognise that asthma patients are not necessarily free from parenchymal fibrotic changes. However, normal diffusing capacity of the lungs for carbon monoxide and HRCT without parenchymal abnormalities suggest absence of fibrosis. In non-fibrotic patients (asthma and non-fibrotic ILD), detected birefringence ranged from 2.54% to 6.75%, meaning that a certain amount of birefringence should be considered as normal and reflects the normal architecture of the lung

parenchyma and its connective tissue. Based on the current study, we cannot establish the optimal threshold to differentiate fibrosis from non-fibrotic areas, including normal alveolar tissue or areas with an increased birefringent signal due to other reasons than fibrosis (ie, atelectasis). More research is needed to establish such a threshold.

As a reference standard for EB-PS-OCT detected fibrosis and ILD hallmarks, we included TBCB besides SLB as histological reference, which considering its limitation in size may increase the risk of sampling error. However, a growing body of evidence shows adequate diagnostic performance of TBCB as is illustrated by the recent guideline recommendations for the use of TBCB as a first step diagnostic approach for tissue diagnosis.[30–33] Our study adds to the hypothesis that EB-PS-OCT can potentially prevent invasive tissue acquisition by providing 'optical' histological ILD features and extent of fibrosis without the need for tissue extraction. Furthermore, due to its minimally invasive character, longitudinal measurements may identify presence and/or progression at an early stage or when HRCT is inconclusive.

In conclusion, EB-PS-OCT is feasible and safe and enables accurate in vivo quantification of fibrosis and identification of ILD features/hallmarks in the lung parenchyma of patients with ILD in a minimally invasive way. On further validation, this novel imaging technique has potential to influence ILD diagnostic, therapeutic and monitoring strategies omitting the need for tissue acquisition with added value to the currently widely used and accepted HRCT.

Contributors: Conception and design: JTA, PB and JFdB. Data acquisition: MV, KK-M, PB and JTA. Analysis and interpretation: MV, KK-M, ET, OMM, IAHvdB, PB, JTA and JFdB. Statistical analysis: MWTT, MV and KK-M. Drafting the manuscript: MV and KK-M. Revising it critically for important intellectual content: MV, KK-M, JTA, PB and JFdB. JFdB is responsible for the overall content as guarantor.

Funding: This study was funded by the Netherlands Organisation for health Research and Development (ZonMW) (843001813). This work is part of the MedPhot research programme 00770372 with project number 00770384, which is (partly) financed by the Dutch Research Council (NWO). This project has received funding from the European Union's Horizon 2020 research and innovation programme under grant agreement no. 871124 and 654148.

Competing interests: JFdB reports grants from the Dutch National Science foundation (NWO, Medphot consortium grant), LaserLab Europe, the Dutch science foundation in collaboration with industry (Heidelberg Engineering) and research institutes (TNO) and from Health Holland and is an inventor on patents related to OCT technology. All other authors have no conflict of interest.

Patient and public involvement: Patients and/or the public were not involved in the design, or conduct, or reporting, or dissemination plans of this research.

Patient consent for publication: Not applicable.

Ethics approval This study involves human participants and was approved by Medisch Ethische Toetsingscommissie AMC, 2018_208#C2021856TK0-270. Participants gave informed consent to participate in the study before taking part.

Provenance and peer review: Not commissioned; externally peer reviewed.

Data availability statement: Data are available on reasonable request. Data are available by sending a request to j.f.de.boer@vu.nl.

Supplemental material: This content has been supplied by the author(s). It has not been vetted by BMJ Publishing Group Limited (BMJ) and may not have been peer-reviewed. Any opinions or recommendations discussed are solely those of the author(s) and are not endorsed by BMJ. BMJ disclaims all liability and responsibility arising from any reliance placed on the content. Where the content includes any translated material, BMJ does not warrant the accuracy and reliability of the translations (including but not limited to local regulations, clinical guidelines, terminology, drug names and drug dosages), and is not responsible for any error and/or omissions arising from translation and adaptation or otherwise.

REFERENCES

1 Huapaya JA, Wilfong EM, Harden CT, *et al*. Risk factors for mortality and mortality rates in interstitial lung disease patients in the intensive care unit. *Eur Respir Rev* 2018;27:180061.

2 Raghu G. Idiopathic pulmonary fibrosis: new evidence and an improved standard of care in 2012. *Lancet* 2012;380:699–701.

3 Nunes H, Schubel K, Piver D, *et al*. Nonspecific interstitial pneumonia: survival is influenced by the underlying cause. *Eur Respir J* 2015;45:746–55.

4 Flaherty KR, Wells AU, Cottin V, *et al*. Nintedanib in Progressive Fibrosing interstitial lung diseases. *N Engl J Med* 2019;381:1718–27.

5 Raghu G, Remy-Jardin M, Myers JL, *et al*. Diagnosis of idiopathic pulmonary fibrosis. an official ATS/ERS/JRS/ALAT clinical practice guideline. *Am J Respir Crit Care Med* 2018;198:e44–68.

6 Humphries SM, Swigris JJ, Brown KK, *et al*. Quantitative high-resolution computed tomography fibrosis score: performance characteristics in idiopathic pulmonary fibrosis. *Eur Respir J* 2018;52:1801384.

7 Taha N, D'Amato D, Hosein K, *et al*. Longitudinal functional changes with clinically significant radiographic progression in idiopathic pulmonary fibrosis: are we following the right parameters? *Respir Res* 2020;21:119.

8 Huang D, Swanson EA, Lin CP, *et al*. Optical coherence tomography. *Science* 1991;254:1178–81.

9 Ding M, Chen Y, Guan W-J, *et al*. Measuring airway remodeling in patients with different COPD staging using Endobronchial optical coherence tomography. *Chest* 2016;150:1281–90.

10 Adams DC, Miller AJ, Applegate MB, *et al*. Quantitative assessment of airway remodelling and response to allergen in asthma. *Respirology* 2019;24:1073–80.

11 Goorsenberg AWM, d'Hooghe JNS, Srikanthan K, *et al*. Bronchial Thermoplasty induced airway smooth muscle reduction and clinical response in severe asthma. The TASMA randomized trial. *Am J Respir Crit Care Med* 2021;203:175–84.

12 Goorsenberg AWM, d'Hooghe JNS, de Bruin DM, *et al*. Bronchial thermoplasty-induced acute airway effects assessed with optical coherence tomography in severe asthma. *Respiration* 2018;96:564–70.

13 Lam S, Standish B, Baldwin C, *et al*. In vivo optical coherence tomography imaging of preinvasive bronchial lesions. *Clin Cancer Res* 2008;14:2006–11.

14 Michel RG, Kinasewitz GT, Fung K-M, *et al*. Optical coherence tomography as an adjunct to flexible bronchoscopy in the diagnosis of lung cancer: a pilot study. *Chest* 2010;138:984–8.

15 Tsuboi M, Hayashi A, Ikeda N, *et al*. Optical coherence tomography in the diagnosis of bronchial lesions. *Lung Cancer* 2005;49:387–94.

16 Nandy S, Raphaely RA, Muniappan A, *et al*. Diagnostic accuracy of endobronchial optical coherence tomography for the microscopic diagnosis of usual interstitial pneumonia. *Am J Respir Crit Care Med* 2021;204:1164–79.

17 Hariri LP, Adams DC, Wain JC, *et al*. Endobronchial optical coherence tomography for low-risk microscopic assessment and diagnosis of idiopathic pulmonary fibrosis in vivo. *Am J Respir Crit Care Med* 2018;197:949–52.

18 Carpaij OA, Goorsenberg AWM, d'Hooghe JNS, *et al*. Optical coherence tomography intensity correlates with extracellular matrix components in the airway wall. *Am J Respir Crit Care Med* 2020;202:762–6.

19 de Boer JF, Hitzenberger CK, Yasuno Y. Polarization sensitive optical coherence tomography - a review [Invited]. *Biomed Opt Express* 2017;8:1838–73.

20 Adams DC, Holz JA, Szabari MV, *et al*. In vivo assessment of changes to canine airway smooth muscle following bronchial Thermoplasty with OR-OCT. *Journal of Applied Physiology* 2021;130:1814–21.

21 Vaselli M, Wijsman PC, Willemse J, *et al*. Polarization sensitive optical coherence tomography for bronchoscopic airway smooth muscle detection in bronchial Thermoplasty-treated patients with asthma. *Chest* 2021;160:432–5.

22 Adams DC, Hariri LP, Miller AJ, *et al*. Birefringence microscopy platform for assessing airway smooth muscle structure and function in vivo. *Sci Transl Med* 2016;8.

23 Nandy S, Berigei SR, Keyes CM, *et al*. Polarization-sensitive Endobronchial optical coherence tomography for microscopic imaging of fibrosis in interstitial lung disease. *Am J Respir Crit Care Med* 2022;206:905–10.

24 Feroldi F, Willemse J, Davidoiu V, *et al*. In vivo Multifunctional optical coherence tomography at the periphery of the lungs. *Biomed Opt Express* 2019;10:3070–91.

25 Harrell FE Jr, Califf RM, Pryor DB, *et al*. Evaluating the yield of medical tests. *JAMA* 1982;247:2543–6.

26 Willemse J, Wener RR, Feroldi F, *et al*. Polarization-sensitive optical coherence tomography in end-stage lung diseases: an ex vivo pilot study. *Biomed Opt Express* 2021;12:6796–813.

27 Gotway MB, Freemer MM, King TE. Challenges in pulmonary fibrosis. 1: use of high resolution CT scanning of the lung for the evaluation of patients with idiopathic interstitial Pneumonias. *Thorax* 2007;62:546–53.

28 Remy-Jardin M, Remy J, Giraud F, *et al*. Computed tomography assessment of ground-glass opacity: semiology and significance. *J Thorac Imaging* 1993;8:249–64.

29 Hansell DM, Bankier AA, MacMahon H, *et al*. Fleischner society: glossary of terms for thoracic imaging. *Radiology* 2008;246:697–722.

30 Raghu G, Remy-Jardin M, Richeldi L, *et al*. Idiopathic pulmonary fibrosis (an update) and progressive pulmonary fibrosis in adults: an official ATS/ERS/JRS/ALAT clinical practice guideline. *Am J Respir Crit Care Med* 2022;205:e18–47.

31 Troy LK, Grainge C, Corte T, *et al*. Cryobiopsy versus open lung biopsy in the diagnosis of interstitial lung disease (COLDICE): protocol of a Multicentre study. *BMJ Open Respir Res* 2019;6:e000443.

32 Maldonado F, Danoff SK, Wells AU, *et al*. Transbronchial Cryobiopsy for the diagnosis of interstitial lung diseases: CHEST guideline and expert panel report. *Chest* 2020;157:1030–42.

33 Korevaar DA, Colella S, Fally M, *et al*. European respiratory society guidelines on Transbronchial lung Cryobiopsy in the diagnosis of interstitial lung diseases. *Eur Respir J* 2022;60:2200425.

SUPPLEMENTARY

e-Table 1. In- and exclusion criteria for study participation.

Inclusion criteria
• >18 years of age
• ILD on HR-CT
• No classifying diagnosis based on clinical data including laboratory results and HR-CT
• ILD-MDT panel indication for histology by lung biopsy
Exclusion criteria
• **Inability and unwillingness to provide informed consent**
• Inability to comply with study protocol
• Prothrombin time international normalized ratio (INR) >1.3
• Use of clopidogrel, or other new anti-platelet therapy, or anticoagulant drugs that cannot be stopped temporarily
• Thrombocytopenia <70x10^9/L
• History of pulmonary hypertension (systolic pulmonary artery pressure > 50 mmHg)
• Diffusing capacity < 30%
• Forced vital capacity <50%
• Forced expiratory volume in the first second (FEV1) <0,8L or <50% of predicted value
• Body mass index >35
• Pregnancy

e-Appendix 1: EB-PS-OCT data processing and fibrosis quantification:

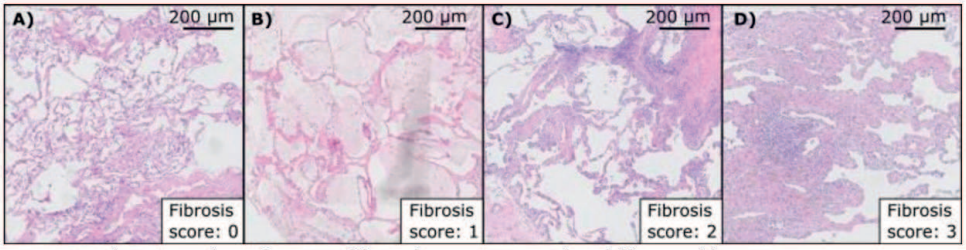
Analysis of the acquired EB-PS-OCT raw-data was performed in MATLAB R2021a (MathWorks) in post-processing. Conventional OCT intensity images were generated from raw data and displayed in grayscale with 55 dB dynamic range. For all the acquired frames, after compensating for the polarization mode dispersion induced by the optical fibers in the system [1], birefringence properties of tissue were extracted using the differential Mueller matrix algorithm developed by Villiger et al [2]. To retrieve depth-resolved optic axis orientation images, the presence of preceding birefringent layers of tissue with a different optic axis was compensated [3]. Moreover, the variation of the incident polarization state induced by the rotation of the motor at the tip of the catheter was corrected. Absolute orientation of the tissue optic axis was extracted using the catheter sheath, made of homogenously oriented birefringent material, as calibration tool [4]. This enabled the discrimination of parallel and circumferentially oriented birefringent tissue structures. Birefringent structures

were automatically segmented by thresholding optic axis orientation images based on optic axis uniformity over a small region (threshold value of 0.55) [5]. The optic axis uniformity was calculated over a two-dimensional spatial kernel (4x18 pixels), which correspond to 26 µm in depth and 7° along the azimuthal direction. In each frame the percentage of birefringent area over the total OCT cross section was calculated, extending from the outer sheath of the catheter to an imaging depth of 790 µm. To quantify fibrosis in the lung parenchyma, a distinction between peripheral parenchymal (distal) area of the pullback imaging the alveolar compartment and proximal part of each pullback imaging the airways was made. The peripheral parenchymal area of the pullback (100–350 adjacent frames per pullback) was identified in post-processing by i) the presence of alveoli adjacent to the EB-PS-OCT probe and ii) the absence of birefringent airway smooth muscle. This distinction was performed by a reader with expertise in EB-PS-OCT who manually assessed individual cross-sectional images based on the above criteria.

e-Appendix 2

Criteria for the categorical fibrosis scoring system for histology:

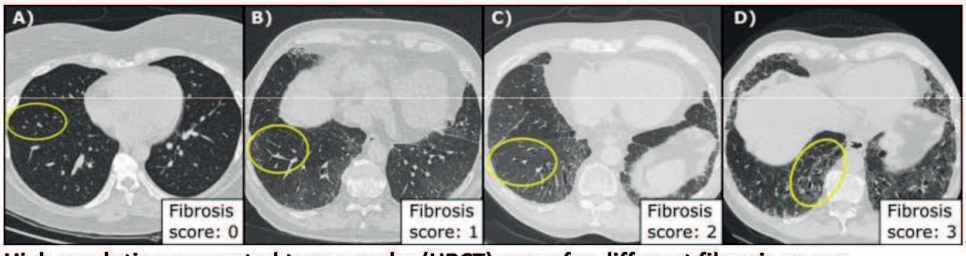
Fibrosis score 0: No fibrosis	Fibrosis score 1: Mild fibrosis	Fibrosis score 2: Moderate fibrosis	Fibrosis score 3: Severe fibrosis
Normal lung parenchyma without presence of fibrosis	Focal slight increase of alveolar wall thickness by collagen	Moderate, focal, increase in alveolar wall thickness by collagen	Diffuse prominent increase in thickness of alveolar walls by collagen



Hematoxylin-eosin (H&E) stained histologic sections for different fibrosis scores.
A) fibrosis score 0= no fibrosis. The image shows prominent collapse of thin alveolar walls, B) fibrosis score 1= mild fibrosis, C) fibrosis score 2= moderate fibrosis, C) fibrosis score 3= severe fibrosis)

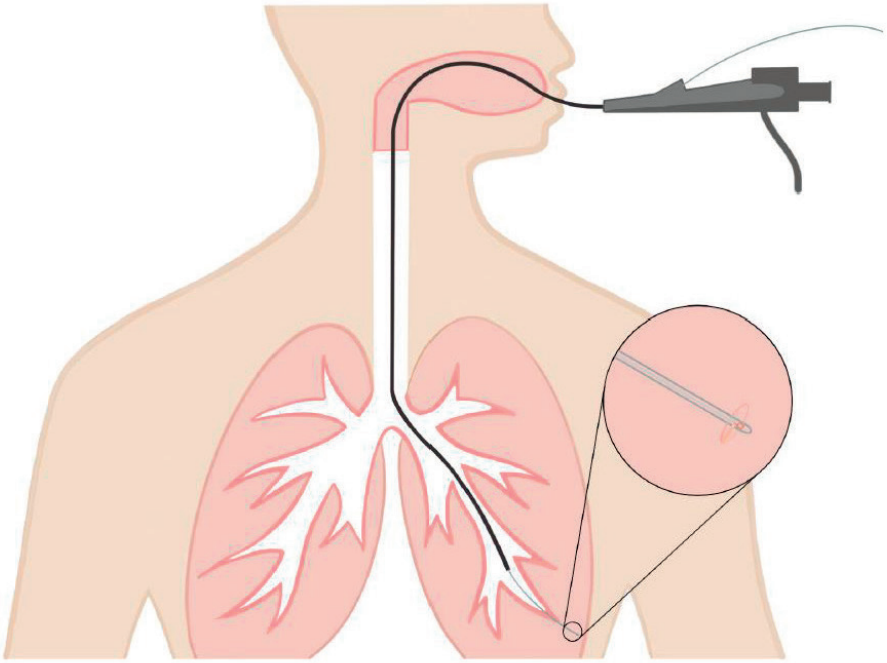
Criteria for the categorical fibrosis scoring system for HRCT:

Fibrosis score 0: No fibrosis	Fibrosis score 1: Mild fibrosis	Fibrosis score 2: Moderate fibrosis	Fibrosis score 3: Severe fibrosis
lung parenchyma without reticulation or anatomical distortion	some reticulation with very little to none architectural distortion	reticulation with clear but limited signs of distortion and traction bronchiectasis	Reticulation with extensive distortion and traction bronchiectasis

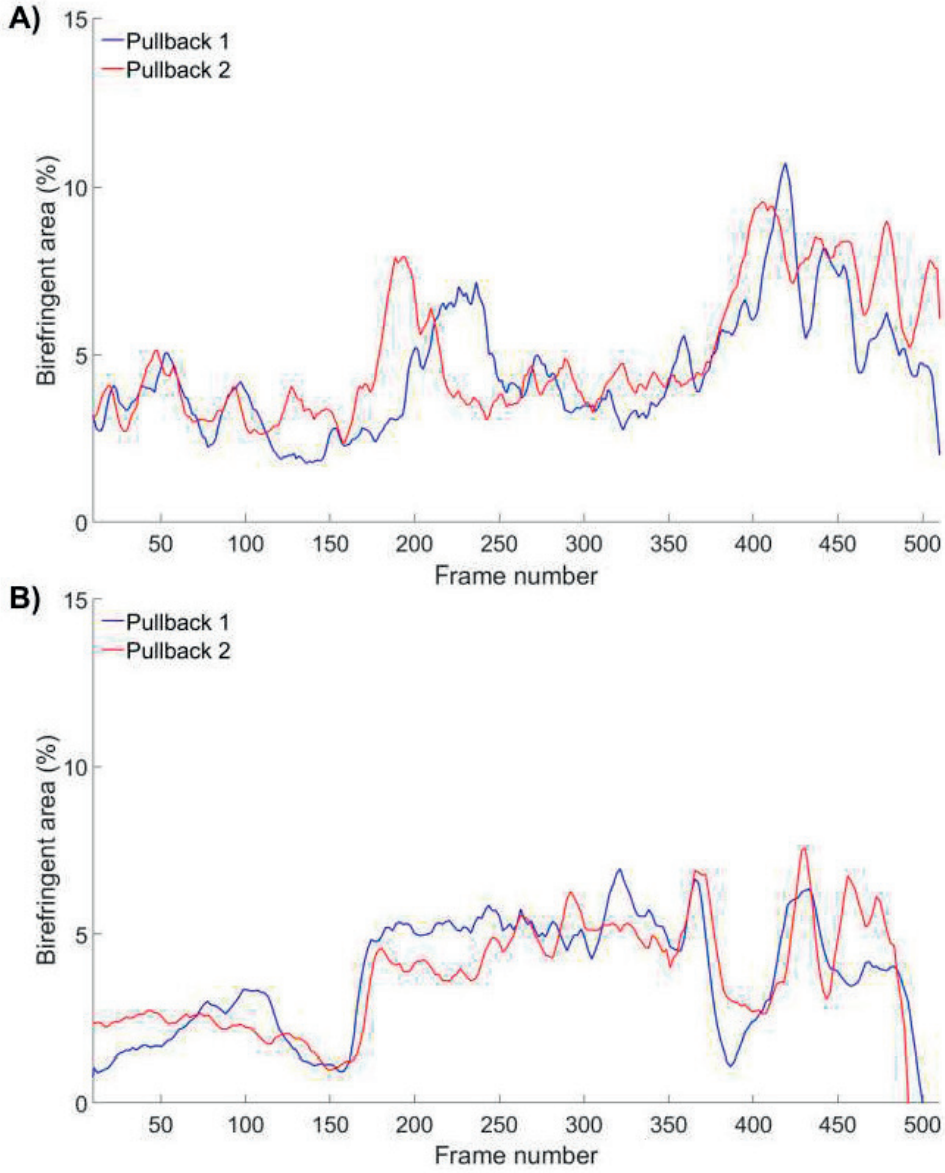


High resolution computed tomography (HRCT) scans for different fibrosis scores.
A) fibrosis score 0= no fibrosis, B) fibrosis score 1= mild fibrosis, C) fibrosis score 2= moderate fibrosis, C) fibrosis score 3= severe fibrosis). For each panel the yellow circle in the HRCT section indicates the segment for which the fibrosis score is assessed.

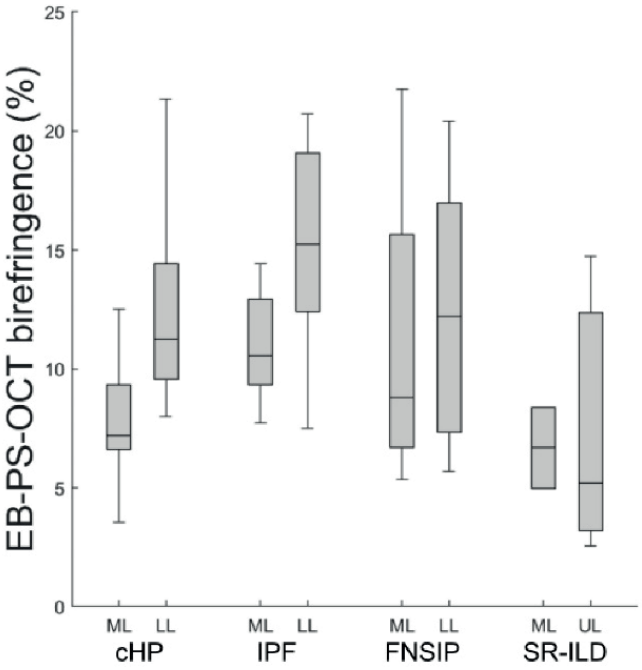
Figures



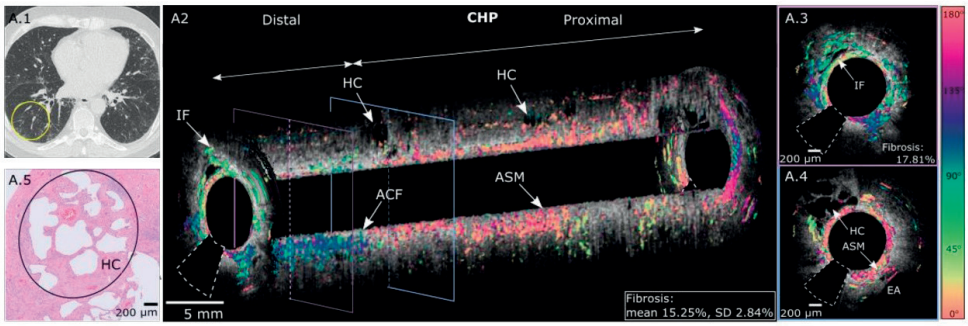
e-Figure 1. Schematic drawing of the *in-vivo* endobronchial polarization sensitive optical coherence tomography (EB-PS-OCT) procedure. Volumetric EB-PS-OCT images were acquired by advancing the EB-PS-OCT probe through the working channel of the bronchoscope to the periphery of each lung segment until pleural resistance.



e-Figure 2. Reproducibility of the birefringent content detected by *in-vivo* endobronchial polarization sensitive optical coherence tomography (EB-PS-OCT). **A**) EB-PS-OCT detected birefringent content in two consecutive pullbacks (pullback 1 in blue and pullback 2 in red) acquired in segment RB10 from a cHP patient. **B**) EB-PS-OCT detected birefringent content in two consecutive pullbacks (pullback 1 in blue and pullback 2 in red) acquired in segment RB9 from a different cHP patient. EB-PS-OCT detected birefringent content is expressed as percentage of birefringence over the total PS-OCT cross-section extending from the catheter sheath.



e-Figure 3. ILD patients with inconclusive or inconsistent HRCTs, EB-PS-OCT detected fibrosis in the alveolar compartment of the lower lobe (LL), resulted to be consistently higher than in the alveolar compartment of the middle lobe (ML) in patients diagnosed with IPF and FNSIP. In patients diagnosed with cHP, EB-PS-OCT detected fibrosis in the alveolar compartment of the lower lobe (LL), resulted to be significantly higher than in the alveolar compartment of the middle lobe (ML) (p value=0.069). In SR-ILD the EB-PS-OCT detected fibrosis in the alveolar compartment of the middle lobe resulted to be higher than in the alveolar compartment of the upper lobe (UL).



e-Figure 4. High resolution computed tomography (HRCT), Hematoxylin-eosin (H&E) stained histologic section images and PS-OCT images of lung segment RB9 from a patient diagnosed with chronic hypersensitivity pneumonitis (cHP). The PS-OCT pullback illustrates presence of airway centered fibrosis (ACF) around the airways proximal to regions with preserved alveolar architecture. A.1) HRCT image, the yellow circle indicates the region of interest (segment RB9) in which the biopsy from figure A.5 and PS-OCT images from figure A.2-4 were acquired. A.2) Volumetric PS-OCT pullback shows the presence of airway centred fibrosis (ACF). A.3,4) OCT and OA cross sectional images, taken from the locations of the PS-OCT pullback (A.2) show presence of interstitial fibrosis (IF), microscopic honeycombing (HC) and airway smooth muscle (ASM). A.5) Hematoxylin-eosin (H&E) stained histologic section from transbronchial cryobiopsy of corresponding lung segment confirmed presence of microscopic honeycombing (marked with a black circle).
The white dotted lines in PS-OCT images delineate the tissue area not optically accessible because of the presence of the wires feeding current to the motor.

Extended Data References:

References:

[1] Braaf, B., et al. (2014). "Fiber-based polarization-sensitive OCT of the human retina with correction of system polarization distortions." Biomed Opt Express **5**(8): 2736-2758.

[2] Villiger, M., et al. (2016). "Deep tissue volume imaging of birefringence through fibre-optic needle probes for the delineation of breast tumour." Sci Rep **6**: 28771.

[3] Willemse, J., et al. (2020). "In Vivo 3D Determination of Peripapillary Scleral and Retinal Layer Architecture Using Polarization-Sensitive Optical Coherence Tomography." Transl Vis Sci Technol **9**(11): 21.

[4] Villiger, M., et al. (2018). "Optic axis mapping with catheter-based polarization-sensitive optical coherence tomography." Optica **5**(10): 1329-1337.

[5] Feroldi, F., et al. (2019). "In vivo multifunctional optical coherence tomography at the periphery of the lungs." Biomed Opt Express 10(6): 3070-3091.

Chapter 7

Endobronchial Optical Coherence Tomography: Shining New Light on Diagnosing Usual Interstitial Pneumonitis?

Kirsten A. Kalverda, M.D[1], Margherita Vaselli, M.Sc.[2], Lizzy Wijmans, M.D.[1], Daniel M. de Bruin, M.Sc., Ph.D.[1], Renée E. Jonkers, M.D., Ph.D.[1], Venerino Poletti, M.D., Ph.D.[3,4], Johannes de Boer, M.Sc., Ph.D.[2], Jouke T. Annema, M.D., Ph.D.[1], Peter I. Bonta, M.D., Ph.D.[1]

[1]Amsterdam University Medical Centers, Amsterdam, the Netherlands
[2]Vrije Universiteit de Boelelaan, Amsterdam, the Netherlands
[3]Ospedale GB Morgagni Forli, Italy
[4]Aarhus University Hospital, Aarhus, Denmark

American Journal of Respiratory and Critical Care Medicine Volume 205 Number 8

To the Editor:

In 15–30% of patients with a fibrotic interstitial lung disease (ILD), tissue acquisition is indicated, as the diagnostic confidence based on clinical and radiological investigations does not justify a specific treatment allocation (1). However, surgical lung biopsy and transbronchial cryobiopsy are associated with considerable risks of morbidity and even mortality (2). Minimally invasive imaging techniques have the potential to obviate the need for tissue biopsy in at least a proportion of these patients (3).

Therefore, we are excited by the work of Nandy and colleagues and congratulate them on their work on endobronchial optical coherence tomography (EB-OCT) in fibrotic ILD (3). With histopathology of surgical lung biopsy as reference standard, EB-OCT convincingly distinguished usual interstitial pneumonitis (UIP) from non-UIP disease in patients with unclassifiable ILD. In addition, non-UIP ILD diagnoses were identified with EB-OCT with high concordance with histopathological diagnosis (3).

To fully appreciate the added value of EB-OCT to the current diagnostic workup (clinical evaluation, high-resolution computed tomography, and BAL), it is important to have additional insights in patient characteristics and selection. A description of the high-resolution computed tomography patterns and a clinical-radiological diagnosis, as assessed by a multidisciplinary discussion, in Table 3 would have been helpful. Can the authors provide more details on this aspect?

Our study group has EB-OCT experience from more than 50 patients, and we have learned that adequate and reproducible EB-OCT imaging can be challenging. First, subpleural probe placement is of key importance to differentiate between UIP and non-UIP disease. Nandy and colleagues report that the presence of pleural resistance confirmed subpleural positioning. In our experience, especially in patients with extensive fibrotic changes, it can be difficult to reach the subpleural space, and in general when the OCT probe hits a carina, this can resemble pleural resistance. Therefore, a validated method for correct EB-OCT probe positioning seems needed. We have noticed that in a subset of patients, we were able to visualize the pleura and/or thoracic wall and thereby confirmed subpleural placement of the EB-OCT probe (4). We question if this "subpleural sign" could be used for probe positioning. Second, in our experience, EB-OCT alveolar image quality improves when flushing with saline just before the OCT pullback; do the authors have a similar

experience? Third, it is not clear whether the same airway segments were measured multiple times, and therefore image reproducibility is not addressed. Furthermore, can the authors comment on image interpretation: was it based on all cross-sectional images (1,340 images per pullback) or on the three-dimensional reconstructions of the entire pullback, or both? In this respect, what were the EB-OCT image interpretation training requirements?

For future direction, the authors postulate that EB-OCT, given the low-risk nature of the procedure, can be used for longitudinal measurements. Indeed, in addition to identification of EB-OCT patterns, quantifying the amount of fibrosis would be helpful to evaluate treatment response or disease progression. Polarization-sensitive OCT (PS-OCT) could provide the contrast to quantify fibrosis; this is currently being explored by our study group to strengthen the potential of EB-(PS)OCT in respiratory diseases (5, 6). We warmly encourage further studies investigating the diagnostic potential of EB-(PS)OCT, with the aim of improving safe and minimally invasive diagnostics for the vulnerable population of patients with ILD.

REFERENCES

1. Raghu G, Remy-Jardin M, Myers JL, Richeldi L, Ryerson CJ, Lederer DJ, et al.; American Thoracic Society, European Respiratory Society, Japanese Respiratory Society, and Latin American Thoracic Society. Diagnosis of idiopathic pulmonary fibrosis: an official ATS/ERS/JRS/ ALAT clinical practice guideline. Am J Respir Crit Care Med 2018;198: e44–e68.
2. Ravaglia C, Bonifazi M, Wells AU, Tomassetti S, Gurioli C, Piciucchi S, et al. Safety and diagnostic yield of transbronchial lung cryobiopsy in diffuse parenchymal lung diseases: a comparative study versus video-assisted thoracoscopic lung biopsy and a systematic review of the literature. Respiration 2016;91:215–227.
3. Nandy S, Raphaely RA, Muniappan A, Shih A, Roop BW, Sharma A, et al. Diagnostic accuracy of endobronchial optical coherence tomography for the microscopic diagnosis of usual interstitial pneumonia. Am J Respir Crit Care Med 2021;204:1164–1179.
4. Wijmans L, de Bruin D, Jonkers R, Roelofs J, van den Berk I, Bonta P, et al. Visualizing the alveolar compartment in ILD patients by optical coherence tomography [abstract]. Eur Respir J 2017;50:OA1467.
5. Vaselli M, Wijsman PC, Willemse J, Goorsenberg AWM, Feroldi F, d'Hooghe JNS, et al. Polarization sensitive optical coherence tomography for bronchoscopic airway smooth muscle detection in bronchial thermoplasty-treated patients with asthma. Chest 2021;160:432–435.
6. Vaselli M, Mooij-Kalverda KA, Bonta P, De Boer J, Annema J. In vivo PS-OCT to detect fibrotic lung disease [abstract]. Eur Respir J 2021;58:OA234.

Chapter 8

Confocal laser endomicroscopy in patients with acute respiratory failure

Kirsten A. Kalverda[1], Lizzy Wijmans1, Lieuwe D.J. Bos[2], Mary R. Smit[2], Inge A.H. van de Berk[3], Daniel M. de Bruin[4], Paul Bloemen[4], Teodora Radonic[5], Marcus J. Schultz[6,7,8,9] Peter I. Bonta[1], Jouke T. Annema[1]

Authors' affiliation(s):
1. Department of Respiratory Medicine, Amsterdam UMC, University of Amsterdam, Amsterdam, The Netherlands
2. Department of Intensive Care Medicine, Amsterdam UMC, University of Amsterdam, Amsterdam, The Netherlands
3. Department of Radiology, Amsterdam UMC, University of Amsterdam, Amsterdam, The Netherlands
4. Department of Biomedical Engineering and Physics, Amsterdam UMC, University of Amsterdam, Amsterdam, The Netherlands
5. Department of Pathology, Amsterdam UMC, University of Amsterdam, Amsterdam, The Netherlands
6. Department of Anesthesia, General Intensive Care and Pain Management, Division of Cardiothoracic and Vascular Anesthesia & Critical Care Medicine, Medical University Wien, Vienna, Austria
7. Department of Anesthesiology, Rescue– and Pain Medicine, Cantonal Hospital St. Gallen, HOCH Health Ostschweiz, St. Gallen, Switzerland
8. Mahidol-Oxford Tropical Medicine Research Unit (MORU), Mahidol University, Bangkok, Thailand
9. Nuffield Department of Medicine, Oxford University, Oxford, UK

Corresponding author:
Name: Kirsten Kalverda, MD

Email: k.a.kalverda@amsterdamumc.nl
Keywords: ARDS, confocal laser endomicroscopy, mechanical ventilation, fibroproliferation

Accepted for publication by Intensive Care Medicine Experimental

ABSTRACT

Background:

Survivors of the early exudative phase of acute respiratory distress syndrome (ARDS) may develop a fibroproliferative repair response and persistent microstructural remodeling associated with adverse outcomes. Conventional imaging, including chest computed tomography (CT), has limited biological specificity for early microscopic remodeling. Confocal laser endomicroscopy (CLE) enables real-time bronchoscopic imaging of the alveolar compartment with near-histologic resolution. We evaluated the feasibility and safety of bedside bronchoscopic CLE in invasively ventilated ICU patients with acute respiratory failure and explored whether in vivo CLE provides microscopic alveolar information complementary to chest CT.

Methods:

In this single-center observational pilot study, mechanically ventilated adult ICU patients with a clinical indication for bronchoalveolar lavage (BAL) underwent additional bedside bronchoscopic CLE. Primary endpoints were feasibility (≥1 interpretable alveolar video with visible septal architecture per procedure) and safety (CLE-related adverse events within 24 hours). Secondary exploratory endpoints were dominant in vivo CLE patterns of alveolar filling (air, fluid, cells) and architecture (thin elastin fibers with hexagonal architecture; increased elastin with preserved architecture; increased elastin with distortion) and qualitative comparison with CT abnormalities in the imaged segments. As an exploratory additional analysis, ex vivo CLE was performed in a single autopsy case and compared with histopathology.

Results:

Thirty-three patients were included (median age 64 years; 61% male); 31/33 met Berlin ARDS criteria. Forty-one CLE procedures were performed, all yielding high-resolution alveolar imaging (procedural feasibility 100%). A total of 150 videos were acquired (mean acquisition time 46 seconds per video), with a mean of three bronchial segments imaged per procedure. No CLE-related adverse events occurred. Patterns that were recognized by CLE were: alveolar filling with air (n=94, 63%), fluid (n=18, 12%), cells (n=38, 25%); alveolar architecture was described as thin elastin fibers with hexagonal architecture (n=37; 25%), increased elastin fibers with preserved architecture (n=80; 53%) or distorted architecture (n=29; 19%). Architecture was undeterminable in 4 (3%) videos.

CLE detected abnormalities in 6/7 CT-normal appearing segments and demonstrated architectural changes in 60/78 segments with ground-glass opacities. In the autopsy case, ex vivo CLE was concordant with histopathology: regions with increased and distorted CLE signal corresponded to thickened alveolar septa and fibrotic remodeling.

Conclusion:
Bedside bronchoscopic CLE is feasible and safe in mechanically ventilated ICU patients with ARDS. CLE provides complementary microscopic information on alveolar filling and architecture beyond chest CT, including features compatible with early structural remodeling.

BACKGROUND

Patients with severe acute respiratory failure requiring invasive ventilation are frequently classified as having acute respiratory distress syndrome (ARDS) (1). ARDS, however, is a heterogeneous clinical syndrome. It is likely that this heterogeneity contributes to the repeated failure of interventions to improve clinical outcomes in unselected patients. Several approaches to identify more homogeneous ARDS subgroups have been proposed, including subphenotyping based on etiology, systemic inflammatory profiles, and radiological characteristics(2).

A direct histopathological approach to subphenotyping is rarely feasible, because surgical lung biopsy in these critically ill patients entails substantial procedural risk. Nevertheless, while diffuse alveolar damage (DAD) is classically linked to ARDS, autopsy data and limited open lung biopsy data indicate that DAD is present in only ~45% of patients fulfilling clinical ARDS criteria, underscoring the biological heterogeneity within the syndrome (3, 4). Importantly, in selected cohorts undergoing surgical lung biopsy, histological information frequently leads to changes in clinical management, suggesting that distinct underlying pathological patterns are clinically meaningful (5). Another clinically relevant aspect of heterogeneity is how lung injury evolves over time. Following an early exudative phase, some patients transition into fibroproliferative repair and, in a subset, ongoing microstructural remodeling, which has been associated with worse outcomes(6). Chest CT and lung ultrasound are increasingly used in acute respiratory failure, but their ability to capture microscopic injury and repair is limited.

Confocal laser endomicroscopy (CLE) is a minimally invasive bronchoscopic imaging technique. CLE enables real-time imaging of the alveolar compartment with near histology resolution by visualization of the elastin fiber scaffold. In healthy volunteers the alveolar area is characterized by thin elastin fibers interconnected in hexagonal architecture with air-filled alveolar spaces(7). An overview, including technical aspects and clinical implications, of this novel technique was published previously(8).

On a microscopic level, fibrotic remodeling is characterized by excessive extracellular matrix deposition, with collagen as a key component. However, increased and distorted elastin fibers within the alveolar network have also been described in fibrotic lung disease and in non-resolving fibroproliferative ARDS. Since structural remodeling can affect respiratory mechanics, bedside assessment of the elastin scaffold may provide clinically meaningful information beyond conventional imaging(9-11).

Given the marked biological heterogeneity underlying the clinical ARDS syndrome and the limited feasibility of obtaining histology in invasively ventilated ICU patients, bedside in vivo microscopy may provide complementary biological information to conventional imaging. We therefore conducted a single-center observational pilot study of bronchoscopic CLE in mechanically ventilated patients with acute respiratory failure. The primary aim was to assess procedural feasibility and safety. Secondary, exploratory aims were to describe the spectrum of in vivo CLE patterns of alveolar filling and architecture encountered at the bedside, and to explore whether these patterns show qualitative concordance with CT abnormalities in the CLE-imaged segments. We expected CLE to demonstrate distinct patterns of alveolar filling and architectural change, potentially beyond what CT can detect. We therefore explored qualitative concordance between CLE patterns and CT abnormalities within the same imaged segments. Data from this study have been presented in part as a conference abstract (12).

METHODS

Study design and study cohort

This single-center observational pilot study was approved by the institutional review board of Amsterdam University Medical Center (NL61112.018.17) and subsequently extended under a follow-up protocol (NL76007.018.20). The extension enabled inclusion of patients with CO-

VID-19 and allowed inclusion of an autopsy case for exploratory ex vivo measurements. Written informed consent was obtained from patients' legal representatives prior to study procedures.

Eligible participants were adult ICU patients receiving invasive mechanical ventilation with a clinical indication for diagnostic bronchoscopy (including bronchoalveolar lavage). Patients were excluded if informed consent could not be obtained from legal representatives or if extracorporeal membrane oxygenation (ECMO) was in use.

Final clinical diagnosis of respiratory failure was established in a multidisciplinary meeting (including intensivists, pulmonologists, and a radiologist) using all available clinical data, excluding CLE images.

Bronchoscopic CLE imaging

CT scanning was performed prior to bronchoscopic CLE imaging and was used as guidance towards location of the CLE imaging, based on most prominent abnormalities.

Following diagnostic bronchoscopy, CLE imaging was performed using the Cellvizio® 100 Series with the 1.4-mm AlveoFlex Confocal Miniprobe™ (Mauna Kea Technologies, Paris, France), providing real-time autofluorescence imaging (488-nm excitation, >500-nm emission) with a field of view of 600 µm, lateral resolution up to 3.5 µm, and imaging depth up to 70 µm. The probe was advanced through the bronchoscope working channel until the alveolar compartment was reached, defined by visualization of alveolar septae. Videos were acquired per imaged segment and stored for offline analysis.

CT and CLE image assessment

All CLE videos were analyzed at the video level. Each video was linked to a CT-defined segment based on the bronchoscopic location where CLE imaging was performed.

CT evaluation

A chest radiologist assessed the dominant CT pattern in the imaged lung segments according to the Fleischner glossary of terms for thoracic imaging(13).

CLE assessment
Videos were scored for dominant patterns of alveolar filling and architecture. Alveolar architecture was categorized as: (1) thin elastin fibers with hexagonal architecture, (2) increased elastin fibers with preserved architecture, or (3) increased elastin fibers with distortion of normal alveolar architecture. Alveolar filling was classified as: air, fluid, or cells. Cellular alveolar filling' was defined as intra-alveolar cellularity. As CLE does not permit definitive cell identification, this pattern was not subclassified by cell type.

Dominant alveolar filling and architecture patterns on CLE were assessed by two respiratory physicians experienced in CLE (KK and LW), who were blinded to CT findings.

Ex vivo CLE–histology comparison
In the event of a clinical autopsy, ex vivo CLE imaging was first performed on unprocessed excised lung tissue. The specimen was subsequently formalin-fixed and paraffin-embedded, sectioned, and the CLE probe was used to acquire images directly from the unstained tissue sections on glass slides, before hematoxylin and eosin (H&E) staining.

To enable 1:1 correlation, an overview 'map' of the unstained section was generated using confocal laser scanning microscopy (Leica SP-8; excitation 488 nm, emission 505–554 nm; resolution 2 × 2 µm; scan area 17 × 24 mm). This was needed to relocate the exact CLE-imaged regions after staining. The overview scan was used solely for navigation and not for pattern classification. After H&E staining of the same section, histopathological findings were compared with the corresponding ex vivo CLE images to assess concordance, including features compatible with fibrotic remodeling.

Study endpoints

The primary endpoints were feasibility and safety.

Feasibility was defined as the proportion of CLE procedures in which at least one interpretable alveolar video with septal architecture was successfully acquired.

Safety was defined as the occurrence of any adverse event judged to be related to CLE within 24 hours after the procedure. Predefined events of

interest included pneumothorax and clinically relevant airway bleeding or desaturation.

Secondary exploratory endpoints were (1) identification of dominant in vivo CLE patterns of alveolar filling and architecture and (2) qualitative comparison of CLE patterns with CT abnormalities in the imaged segments. An additional exploratory endpoint was ex vivo CLE–histopathology concordance in a single autopsy case.

Table 1: Patient characteristics

	N=33
Age years (median; range)	64; 25-78
Male (N; %)	20; 61%
Smoking status at the time of hospital admission	
Active smoker (N; %)	**5; 15%**
Non-smoker (N; %)	26; 84%
Not reported (N; %)	2; 6%
Cause for acute respiratory failure	
ARDS (N; %)	31; 94%
Cardiogenic pulmonary edema (N; %)	1; 3%
Sputum plugging (N; %)	1; 3%
ARDS etiology (N=31)	
Pneumonia (N; %)	25; 76%
COVID	18; 72%
Influenza	3; 9%
Other	4; 12%
Sepsis (N; %)	1; 3%
Severe Trauma (N; %)	2; 6%
Mimick: panbronchiolitis (N; %)	1; 3%
Mimick: acute interstitial pneumonia (N; %)	1; 3%
Mimick: Aspergillus pneumonia (N; %)	1; 3%
ARDS severity at the time of CLE procedure (N=41)	
Mild (N; %)	5; 12%
Moderate (N; %)	19; 46%
Severe (N; %)	15; 37%
Not applicable* (N; %)	2; 5%
30-day mortality (N; %)	11; 33%

Sample size and statistical analysis

Given the exploratory pilot design, no formal sample size calculation was performed; a convenience sample of up to 35 inclusions was planned. Recruitment occurred when trained personnel and CLE equipment were available; apart from these operational constraints, no additional preselection criteria were applied.

Given the exploratory design, analyses were primarily descriptive. Continuous variables are reported as median (range) or mean (±SD), as appropriate; categorical variables as counts and percentages. CLE outcomes were analyzed at the video level and linked to the CT-defined segment in which imaging was performed. Cross-tabulations were used to summarize the distribution of dominant CLE alveolar filling and architectural patterns across dominant CT patterns. No formal hypothesis testing was planned and no adjustment for repeated procedures within patients was performed; results should therefore be interpreted as descriptive.

RESULTS

Study cohort

Between October 11, 2017 and January 24, 2022, we enrolled 33 mechanically ventilated ICU patients with acute respiratory failure in a convenience sample. Inclusion depended on the on-site availability of trained staff and CLE equipment and recruitment was intermittently paused due to ICU operational constraints, including the early phase of the COVID-19 pandemic. Thereby, inclusion was primarily constrained by staff and equipment availability. The cohort had a median age of 64 years and was 61% male. All had bilateral opacities on chest CT. Thirty-one patients met the Berlin criteria for ARDS(14); the remaining two had cardiogenic pulmonary edema (n=1) and sputum plugging (n=1). ARDS was predominantly pulmonary infection-related. Thirty-day ICU-mortality was 33% (11/33). Baseline characteristics are summarized in Table 1.

At the time of imaging, patients had typically been ventilated for approximately one week , and CT was performed a median of 1 day before CLE (Table 2).

Feasibility and safety

CLE imaging was feasible in all included patients and 6 patients underwent repeated imaging procedures (Table 2). One planned CLE procedure

was cancelled due to oxygen desaturation during bronchoalveolar lavage (BAL) prior to CLE; this patient underwent three other successful CLE imaging procedures.

In total, 150 CLE videos were obtained (Figure 1). Mean acquisition time per video was 46 seconds (range 11–222). A mean of three lung segments per patient were imaged, resulting in <5 minutes additional bronchoscopy time.

One patient developed a right-sided pneumothorax within 24 hours after CLE. After multidisciplinary review, this was considered to be unrelated to the CLE as the pneumothorax occurred directly after central venous line placement, a more likely explanation.

No clinically relevant bleeding occurred, and no procedure was terminated due to desaturation.

CLE imaging assessment

Videos were scored for alveolar filling and architecture and linked to the corresponding CT pattern in the sampled segment (Table 3). In CT-normal segments (n=7 videos), CLE showed fluid filling in 4, cellular filling in 2, and predominantly air-filled alveoli in 1. Alveolar architecture was largely preserved; increased elastin signal was observed in two videos, and architecture could not be assessed in one due to extensive cellular filling (Figure 1, Panel 1).

In segments with ground-glass opacity as the dominant CT pattern (n=78), CLE showed predominantly air-filled alveoli in 55 (71%), cellular filling in 16 (21%), and fluid filling in 7 (9%) (Figure 1, Panels 2–4). Among air-filled videos, 49/55 (89%) showed architectural abnormalities. The dominant architectural patterns were increased elastin fibers with preserved architecture (50/78; 64%) and increased elastin fibers with distortion (10/78; 13%) (Figure 1, Panels 4–5). Normal architecture was observed in 18/78 (23%) videos; 12/18 (67%) of these still demonstrated alveolar filling.

In segments with dominant reticulation on CT (n=28), all videos showed increased elastin signal. Increased elastin fibers with distortion was the dominant pattern in 17/28 (61%) videos(Figure 1, Panel 6); in the remaining 11/28 (39%), increased elastin with relatively preserved architecture was dominant, although focal distortion was still present.

Table 2: CLE imaging procedures, CT patterns and CLE patterns

	N=33
Number of patients, with at least 1 CLE imaging procedure (N)	33
Patients with 1 CLE procedure	27
Patients with 2 CLE procedures	4
Patients with 3 CLE procedures	2
Total number of in vivo CLE procedures (N)	41
Duration of invasive mechanical ventilation at CLE imaging days (median; range)	3 (0–24)
1st CLE procedure (n=33)	5 (0–37)
2nd CLE procedure (n=6)	12 (9–18)
3rd CLE procedure (n=2)	25 (24–26)
Time between last CT scan and CLE imaging days (median; range)	1 (0–3)
Dominant CT pattern in successfully CLE imaged segments (N=150)	
Normal (N; %)	7 (4.7%)
Ground glass (N; %)	78 (52%)
Consolidation (N; %)	28 (19%)
Reticulation (N; %)	28 (19%)
Tree in bud (N; %)	5 (3.3%)
Atelectasis (N; %)	4 (2.7%)
Dominant CLE imaged alveolar filling pattern (N=150)	
Air (N; %)	94 (63%)
Cells (N; %)	38 (25%)
Fluid (N; %)	18 (12%)
Dominant CLE imaged alveolar architecture (N=150)	
Thin elastin fibers with hexagonal architecture (N; %)	37 (25%)
Increased or thickened fibers with preserved architecture (N; %)	80 (53%)
Increased fibers with distortion of architecture (N; %)	29 (19%)
Undeterminable (N; %)	4 (2.6%)

In consolidated segments (n=28), CLE most often showed air-filled alveoli (15/28; 54%) or cellular filling (10/28; 36%). Architecture was classified as normal in 13/28 (46%) videos, of which 8/13 (62%) showed alveolar filling (cells n=6; fluid n=2). Five videos (5/28; 18%) demonstrated both predominantly air-filled alveoli and normal architecture. Increased elastin with preserved architecture was observed in 13/28 (46%) con-

solidation videos and distortion in 2/28 (7%) (Figure 1, Panel 7). A full overview of CLE patterns stratified by CT pattern is provided in table 3.

Of the videos showing cellular alveolar filling (38/150, 25%), 15 (39%) were obtained from patients who were active smokers at hospital admission, 21 (55%) from non-smokers, and 2 (5%) from patients whose smoking status was not reported (Table 1).

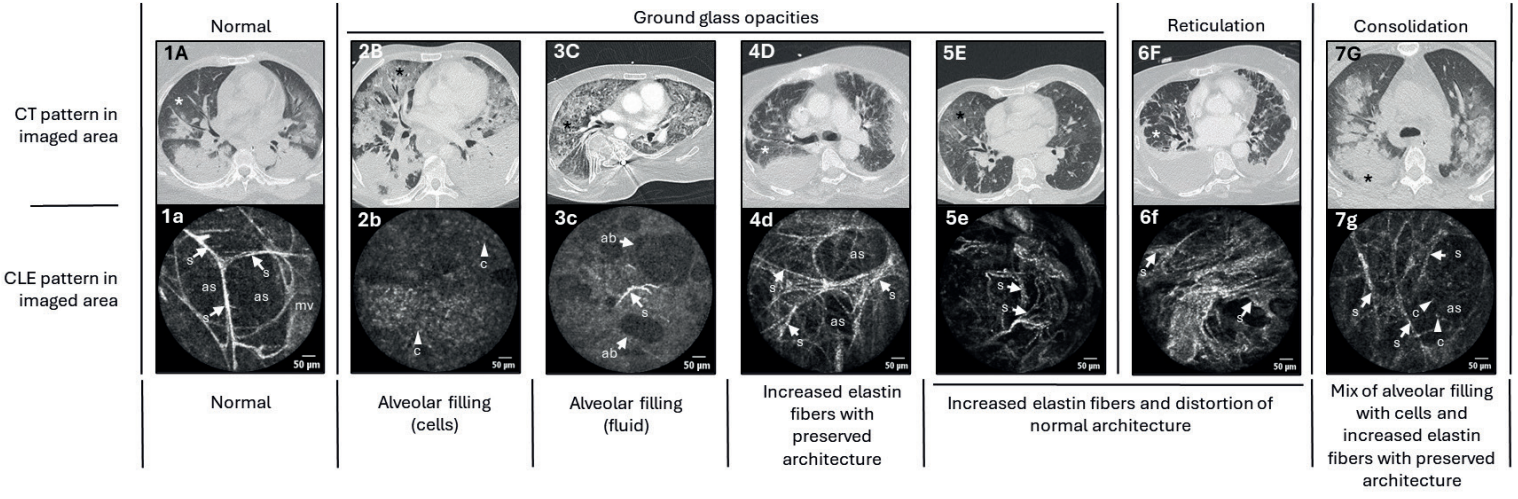


Figure 1. Thoracic CT scans showing the area of CLE imaging (asterisk, upper panel) and different corresponding CLE patterns (lower panel).

1A: CT scan showing bilateral consolidations, CLE imaging in normal area of lung parenchyma. 1a: corresponding CLE image showing elastin fibers which correspond with intact architecture of thin alveolar septae (white arrows) and rectangular airspaces (as), additionally an alveolar microvessel (mv) is partially visible. 2B: CT scan showing consolidation and ground glass opacities, in the imaged area ground glass is the dominant pattern. 2b: CLE showing an abundance of cellular alveolar filling, individual cells are indicated with white arrow head. 3C: CT scan showing a predominant pattern of bilateral ground glass opacities. 3c: CLE showing alveolar filling with fluid and air bubbles (white arrows). 4D:CT scan showing a predominant ground glass pattern. 4d: CLE showing increased elastin fibers (arrows), normal architecture with rectangular airspaces (as) are recognizable. 5E: CT scan showing bilateral ground glass opacities. 5e: CLE image with increased elastin fibers and distortion of normal architecture of alveolar septae (white arrows). 6F: CT scan showing a predominant pattern of reticulation in imaged segment. 6f: CLE image with increased elastin fibers and distortion of normal architecture of alveolar septae (white arrows). 7G: CT scan showing bilateral consolidations. 7g: CLE image showing a combined pattern of some alveolar filling with cells (white arrowhead) and increased elastin fibers with normal recognizable architecture of alveolar septae (white arrows).

Serial CLE imaging

Of the 150 videos, 126 were obtained during the first CLE procedure per patient, 13 during a second procedure, and 11 during a third. Alveolar filling decreased across follow-up procedures (first: 53/126 [42%]; second: 3/13 [23%]; third: 0/11 [0%]). Architectural abnormalities were common at all time points with increasing incidence over time (88/126 [70%], 11/13 [85%], and 10/11 [91%] for first, second, and third procedures, respectively). The proportion of videos showing increased elastin with distortion increased across procedures (20/126 [16%], 3/13 [23%], and 6/11 [55%]).

Ex vivo CLE–histopathology comparison

In one patient with COVID-19–associated ARDS, autopsy tissue enabled qualitative comparison of in vivo and ex vivo CLE with histopathology. In vivo CLE on day 12 after intubation (one day prior to death) showed prominently thickened elastin fibers with areas of preserved alveolar architecture and regions of distortion (Figure 2A). Ex vivo CLE mosaics from the autopsy specimen demonstrated similar heterogeneity, with preserved areas alongside regions of increased signal and architectural distortion (Figure 2B). Histopathology confirmed corresponding abnormalities, and areas of fibrotic remodeling on H&E aligned with regions of increased CLE signal, with fluorescence outlining thickened alveolar septa (Figure 2C; Figure 3). Although the in vivo and ex vivo images were obtained from the same specimen and likely represented overlapping regions, they did not provide an exact 1:1 spatial match. Using a slide-based mapping approach (Methods; Figure 3A), ex vivo CLE acquired of an unstained tissue section could be matched 1:1 to H&E findings after staining of the same section (Figure 3B–C). In these co-localized regions, areas showing fibrotic remodeling on histology corresponded to increased CLE signal outlining thickened alveolar septa. In addition to structural abnormalities, individual intra-alveolar cells could be identified (arrowheads; Figure 3A and 3C).

Table 3 CLE patterns stratified by CT pattern

		CLE pattern (N=150)						
		Filling			Architecture			
		Air N=94	Cells N=38	Fluid N=18	Thin elastin fibers preserved architecture N=37	Increased elastin fibers preserved architecture N=80	Increased elastin fibers distorted architecture N=29	Undeterminable N=4
CT pattern (N=150)	**Normal (N=7)**	1	2	4	4	2	0	1
	Ground glass (N=78)	55	16	7	18	50	10	0
	Reticulation (N=28)	21	5	2	0	11	17	0
	Consolidation (N=28)	15	10	3	13	13	1	1
	Tree in bud (N=5)	0	4	1	1	2	0	2
	Atelectasis (N=4)	2	1	1	1	2	1	0

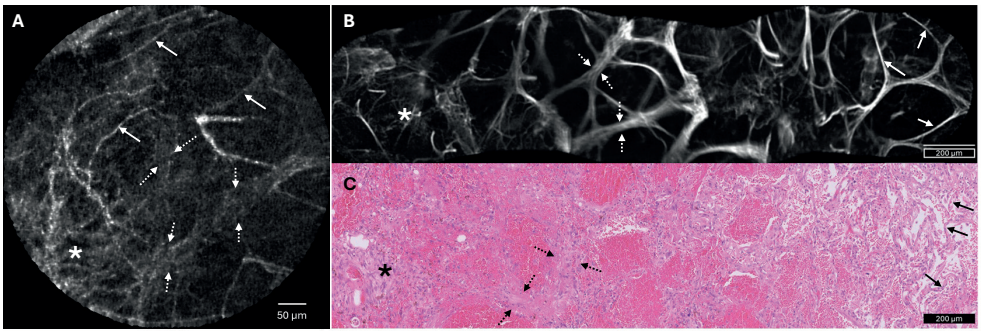


Figure 2. In vivo and ex vivo CLE imaging in COVID-19 ARDS with histologic correlation.

Symbols are consistent across panels: solid arrows indicate thin alveolar septa; dotted arrows indicate septal thickening/increased elastin signal consistent with fibrotic remodeling; the asterisk marks an area with loss of recognizable alveolar architecture. (A) In vivo CLE acquired one day prior to death. (B) Ex vivo CLE mosaic from autopsy lung tissue. (C) Corresponding hematoxylin and eosin–stained section from the same specimen, also demonstrating intra-alveolar hemorrhage with airspaces filled by erythrocytes.

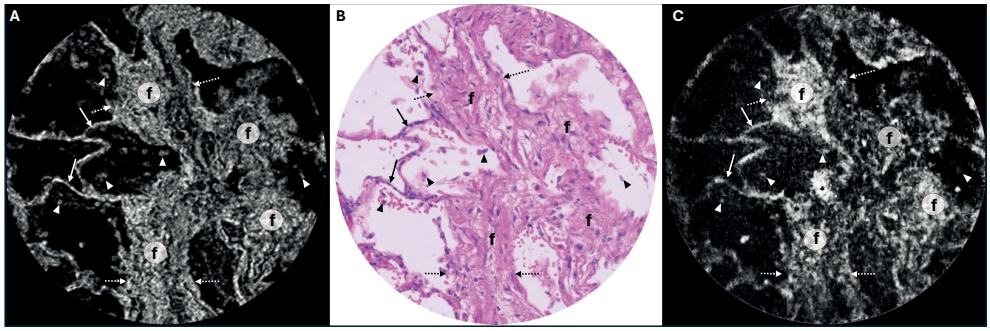


Figure 3. 1:1 mapping of ex vivo confocal autofluorescence imaging to histology in autopsy lung tissue from fatal COVID-19 ARDS.

Symbols are consistent across panels: arrowheads indicate individual intra-alveolar cells; solid arrows indicate thin alveolar septa; dotted arrows indicate septal thickening/increased elastin signal consistent with fibrotic remodeling (f). (A) Overview confocal laser scanning microscopy autofluorescence map of an unstained formalin-fixed paraffin-embedded tissue section (Leica SP-8; 488-nm excitation), used as a navigation map to relocate regions of interest for probe-based CLE. (C) Probe-based CLE image (Cellvizio® 100 Series) acquired from the mapped region on the same section, demonstrating increased signal along thickened septa in areas corresponding to fibrosis. (B) Subsequent H&E staining of the same section confirms fibrotic remodeling (increased collagen deposition and fibroblasts) in regions of increased autofluorescence/CLE signal. Together, the panels illustrate concordant spatial localization of fibrotic areas and the visualization of intra-alveolar cells.

DISCUSSION

This single-center observational pilot study demonstrates that confocal laser endomicroscopy (CLE) can be integrated into routine diagnostic bronchoscopy to provide real-time bedside imaging of the alveolar compartment in mechanically ventilated ICU patients with acute respiratory failure. In line with our primary aims, procedural feasibility was 100% and CLE acquisition added less than five minutes to standard bronchoscopy, without CLE-related adverse events in this cohort. As secondary, exploratory findings, CLE revealed distinct patterns of alveolar filling and architecture, and these patterns showed qualitative concordance with CT abnormalities in the imaged segments. Taken together, these data extend the limited ICU literature on CLE by linking in vivo alveolar micro-imaging to CT-defined segments and support the concept that bedside "alveolar microscopy" can complement conventional imaging in a biologically heterogeneous syndrome where histology is rarely available.

Compared with CT, CLE identified microscopic abnormalities in most CT-normal appearing segments that were sampled, and revealed architectural changes consistent with remodeling in many segments with ground glass opacities. Together, these observations support prior reports suggesting that CT scans are often non-specific for early fibroproliferation in ARDS(15). Although ground-glass opacities on CT are commonly attributed to edema, inflammation, or partial alveolar collapse, our CLE patterns suggest that microscopic architectural remodeling may already be present in a subset of these regions. Within CT-defined consolidations, a minority of sampled regions demonstrated preserved aeration and normal architecture on CLE, which may reflect atelectasis rather than parenchymal disease, although CLE sampling error cannot be excluded.

Beyond adding microscopic information to CT findings, CLE has practical advantages in the ICU. Lung ultrasound is an important bedside tool because it is non-invasive and radiation-free, but it remains limited to macroscopic patterns and cannot visualize alveolar microstructure. On the other hand, CLE requires bronchoscopy; however, in mechanically ventilated patients with acute respiratory failure, bronchoscopy with BAL is often clinically indicated, allowing CLE to be integrated into the same procedure with limited additional invasiveness and minimal prolongation. In this setting, CLE provides a direct, high-resolution view of the alveolar compartment, enabling assessment of septal architecture and intra-alveolar contents beyond the scope of ultrasound.

The present work primarily visualized the autofluorescent elastin scaffold, which is considered the dominant source of signal in CLE(16). Although pulmonary fibrosis is classically characterized by collagen deposition, alterations of the elastin network accompany fibrotic remodeling and may explain why fibrotic change is detectable with CLE(9-11). In the autopsy case, areas with increased or distorted CLE signal corresponded to thickened septa and fibrotic regions on histology. Ex vivo imaging of histology sections further suggested that collagen contributes to tissue autofluorescence, albeit likely to a lesser extent than elastin, supporting the concept that CLE can capture composite microstructural remodeling in vivo.

Cellular or fluid alveolar filling observed on CLE may be compatible with barrier disruption and distal airspace exudation in the exudative/inflammatory phase of ARDS, when neutrophils and macrophages

are prominent drivers of injury. Previous in vivo CLE reports in ARDS and COVID-19 have described highly fluorescent floating structures, which were hypothesized to represent inflammatory cells containing protein–lipid components (17-19). Interestingly, in patients with repeat procedures we observed less alveolar filling over time, alongside more architectural distortion and increased elastin signal. Although based on few follow-up procedures and susceptible to selection and survivor bias, this pattern is biologically plausible and may indicate a shift from inflammatory alveolar flooding toward fibroproliferative remodeling that may be difficult to appreciate on CT alone.

Regarding safety, no CLE-attributed complications were observed, which is in line with previous studies of CLE in patients with chronic lung disease(7, 20). One patient developed a pneumothorax within 24 hours; however, causality was considered unlikely in the context of concurrent procedures with a known pneumothorax risk. Nonetheless, given the small sample size and the vulnerability of this ICU population, definitive conclusions regarding safety require larger studies.

Several limitations merit consideration. Most of these limitations primarily affect the interpretation of the exploratory pattern and CT-comparison analyses rather than the primary feasibility and safety endpoints. This was an exploratory single-center study with a small convenience sample. Segment selection was CT-guided and therefore not random, enriching for abnormal regions; as a result, the study cannot reliably quantify specificity or false-positive rates in CT-normal lung. In addition, multiple videos and procedures per patient were analyzed without adjustment for within-patient clustering. CLE interpretation relied on expert consensus without formal inter-observer variability testing, and histopathological correlation was available only in a single autopsy case.

Importantly, these limitations should be interpreted in the context of the novelty of this work. To our knowledge, this is the first report of bedside CLE at this scale in mechanically ventilated patients. Clinically, bedside CLE may complement conventional imaging by adding microstructural and cellular information that otherwise would require high-risk bronchoscopic cryo- or surgical biopsy. As a future perspective CLE-based ARDS phenotyping has potential to add bedside microstructural information to support risk stratification and trial enrichment, but this needs prospective validation against outcomes. Given the pathological heterogeneity of clinical ARDS and the prognostic relevance of fibroprolifera-

tion(4, 21), improved bedside phenotyping could help identify patients with early structural remodeling or alternative injury patterns and guide escalation to further diagnostics or targeted therapies in selected non-resolving cases. Prospective studies should evaluate reproducibility, define standardized descriptors, and test whether CLE-informed alveolar phenotyping improves clinical decision-making.

In conclusion, bedside bronchoscopic CLE is feasible and safe in mechanically ventilated ICU patients and provides a novel window into alveolar microstructure and filling patterns. Larger studies should evaluate whether CLE-derived descriptors can reproducibly phenotype acute respiratory failure and inform personalized management.

LIST OF ABBREVIATIONS

ARDS – acute respiratory distress syndrome

BAL – bronchoalveolar lavage

CLE – confocal laser endomicroscopy

COVID-19 – coronavirus disease 2019

CT – computed tomography

ECMO – extracorporeal membrane oxygenation

H&E – hematoxylin and eosin

ICU – intensive care unit

SD – standard deviation

SP-8 – confocal laser scanning microscope (Leica SP-8)

DECLARATIONS

Ethics approval and consent to participate

Study was approved by the institutional review board (Medical Ethics Review Committee) of Amsterdam University Medical Center (NL61112.018.17) and subsequently extended under a follow-up protocol (NL76007.018.20). Written informed consent was obtained from patients legal representatives. Study was performed in accordance with Good Clinical Practice guidelines and the Declaration of Helsinki.

Consent for publication

Not applicable

Competing interests

L.D.B. reports grants from Dutch lung foundation and Health Holland (Public-Private Partnership grant), grants from IMI COVID19 initiative, grants from Amsterdam UMC fellowship, grants from ZonMW (VIDI & COVID19 Urgency grant), grants from ERS Gold Metal for ARDS. He also reports advisory boards or consultancy fees, paid to the institution, for: Santhera, Astra Zeneca, Aptarion, all outside the submitted work. MR.S. is supported by a personal grant from NWO (Veni, paid to the institution). J.T.A. has received research grants from Mauna Kea Technologies. All other authors declare no conflicts of interest.

Authors contributions

K.A.K., L.W., L.D.J.B, M.J.S., P.I.B and J.T.A. were involved in study design and writing the protocol. K.A.K., L.W., L.D.J.B, M.R.S, M.J.S., P.I.B, J.T.A were involved in patient recruitment. K.A.K., L.W., L.D.J.B, M.R.S, P.I.B, J.T.A were involved in the data collection and bronchoscopy procedures. I.A.H.B. was responsible for CT interpretation. K.A.K., L.W., D.M.B and P.B. were involved in image acquisition and analysis. T.R. was involved in pathology interpretation. All authors critically read the manuscript and revised accordingly. K.A.K., L.D.J.B, M.J.S, P.I.B, J.T.A had final responsibility for the decision to submit for publication.

Funding

This study was sponsored by Amsterdam University Medical Centers, and in part funded through a research grant from Mauna Kea Technologies.

Availability of data and material

Data will be available after publication for researchers with a valid research question, which will be evaluated by the study board. Researchers can address these requests by email to the corresponding author.

Acknowledgments

Not applicable

REFERENCES

1. Bellani G, Laffey JG, Pham T, Fan E, Brochard L, Esteban A, et al. Epidemiology, Patterns of Care, and Mortality for Patients With Acute Respiratory Distress Syndrome in Intensive Care Units in 50 Countries. Jama. 2016;315(8):788–800.
2. Bos LDJ, Ware LB. Acute respiratory distress syndrome: causes, pathophysiology, and phenotypes. Lancet. 2022;400(10358):1145–56.
3. Thille AW, Penuelas O, Lorente JA, Fernandez-Segoviano P, Rodriguez JM, Aramburu JA, et al. Predictors of diffuse alveolar damage in patients with acute respiratory distress syndrome: a retrospective analysis of clinical autopsies. Crit Care. 2017;21(1):254.
4. Cardinal-Fernández P, Lorente JA, Ballén-Barragán A, Matute-Bello G. Acute Respiratory Distress Syndrome and Diffuse Alveolar Damage. New Insights on a Complex Relationship. Ann Am Thorac Soc. 2017;14(6):844–50.
5. Mir T, Regmi N, Saydain G, Kaul V, Soubani AO, Qureshi WT. Outcome and Post-Surgical Lung Biopsy Change in Management of ARDS: A Proportional Prevalence Meta-Analysis. Adv Respir Med. 2022;90(4):267–78.
6. Thompson BT, Chambers RC, Liu KD. Acute Respiratory Distress Syndrome. N Engl J Med. 2017;377(6):562–72.
7. Salaün M, Guisier F, Dominique S, Genevois A, Jounieaux V, Bergot E, et al. In vivo probe-based confocal laser endomicroscopy in chronic interstitial lung diseases: Specific descriptors and correlation with chest CT. Respirology. 2019;24(8):783–91.
8. Goorsenberg A, Kalverda KA, Annema J, Bonta P. Advances in Optical Coherence Tomography and Confocal Laser Endomicroscopy in Pulmonary Diseases. Respiration. 2020;99(3):190–205.
9. Negri EM, Montes GS, Saldiva PH, Capelozzi VL. Architectural remodelling in acute and chronic interstitial lung disease: fibrosis or fibroelastosis? Histopathology. 2000;37(5):393–401.
10. Mecham RP. Elastin in lung development and disease pathogenesis. Matrix Biol. 2018;73:6–20.
11. Wijmans L, Bonta PI, Rocha-Pinto R, de Bruin DM, Brinkman P, Jonkers RE, et al. Confocal Laser Endomicroscopy as a Guidance Tool for Transbronchial Lung Cryobiopsies in Interstitial Lung Disorder. Respiration. 2019;97(3):259–63.
12. Mooij - Kalverda KA, Wijmans L, Bos L, Smit M, Van Den Berk I, De Bruin D, et al. Confocal laser endomicroscopy (CLE) in patients with acute respiratory failure on the ICU. European Respiratory Journal.54(suppl 63):PA3170.
13. Bankier AA, MacMahon H, Colby T, Gevenois PA, Goo JM, Leung ANC, et al. Fleischner Society: Glossary of Terms for Thoracic Imaging. Radiology. 2024;310(2):e232558.
14. Ranieri VM, Rubenfeld GD, Thompson BT, Ferguson ND, Caldwell E, Fan E, et al. Acute respiratory distress syndrome: the Berlin Definition. Jama. 2012;307(23):2526–33.
15. Hamon A, Scemama U, Bourenne J, Daviet F, Coiffard B, Persico N, et al. Chest CT scan and alveolar procollagen III to predict lung fibroproliferation in acute respiratory distress syndrome. Ann Intensive Care. 2019;9(1):42.

16. Thiberville L, Moreno-Swirc S, Vercauteren T, Peltier E, Cavé C, Bourg Heckly G. In vivo imaging of the bronchial wall microstructure using fibered confocal fluorescence microscopy. Am J Respir Crit Care Med. 2007;175(1):22–31.
17. Danilevskaya O, Sazonov D, Klypa T, Zabozlaev F, Popova E. Confocal Laser Endomicroscopy in a Critically Ill COVID-19 Patient. Tuberc Respir Dis (Seoul). 2022;85(3):273–5.
18. Lesur O, Chagnon F, Lebel R, Lepage M. In Vivo Endomicroscopy of Lung Injury and Repair in ARDS: Potential Added Value to Current Imaging. J Clin Med. 2019;8(8).
19. Craven TH, Walton T, Akram AR, Scholefield E, McDonald N, Marshall ADL, et al. Activated neutrophil fluorescent imaging technique for human lungs. Sci Rep. 2021;11(1):976.
20. Wijmans L, Kalverda K, de Bruin D, Brinkman P, van den Berk I, Roelofs J, et al. Bronchoscopic Journey of in vivo Real-Time Microscopic Imaging in ILD: A Case Series. Respiration. 2022;101(11):1006–14.
21. Gerard L, Bidoul T, Castanares-Zapatero D, Wittebole X, Lacroix V, Froidure A, et al. Open Lung Biopsy in Nonresolving Acute Respiratory Distress Syndrome Commonly Identifies Corticosteroid-Sensitive Pathologies, Associated With Better Outcome. Crit Care Med. 2018;46(6):907–14.

PART III

Novel imaging technique for rapid assessment of lung tissue in interstitial lung disease

Chapter 9

Rapid on-site histology of lung biopsies in ILD using higher harmonic generation microscopy: a proof of concept and image atlas

Laura M. G. van Huizen*[a], Kirsten A. Mooij Kalverda*[b], Jan von der Thüsen[c], Venerino Poletti[d,e], Teodora Radonic[f], Chris Dickhoff[g], Johannes M.A. Daniels[b], Peter I. Bonta[b], Jouke T. Annema[b$], Marie Louise Groot[a$]

*These authors contributed equally
$ shared senior author ship
[a] LaserLab Amsterdam, Dept. of Physics, Faculty of Science, Vrije Universiteit Amsterdam, Amsterdam, The Netherlands
[b] Dept. of Pulmonary diseases, Amsterdam Universities Medical Center, University of Amsterdam, Amsterdam, The Netherlands
[c] Dept. of Pathology and Clinical Bioinformatics, Erasmus MC, Rotterdam, The Netherlands
[d] Dept. Medical Specialities, DIMEC, University of Bologna- Ospedale GB Morgagni, Forlì, Italy
[e] Dept. of Respiratory Diseases & Allergy, Aarhus University Hospital, Aarhus, Denmark
[f] Dept. of Pathology, Amsterdam Universities Medical Center, Amsterdam, The Netherlands
[g] Dept. of Cardiothoracic Surgery, Amsterdam Universities Medical Center, Amsterdam, The Netherlands

Short Title: Rapid on-site histology of ILD

Corresponding Author:
Laura van Huizen
E-mail address: l.m.g.van.huizen@vu.nl

Keywords: transbronchial cryobiopsy, third harmonic generation microscopy, multiphoton microscopy, label-free histology, rapid on-site evaluation

submitted for publication

ABSTRACT

Rationale: Diagnosing interstitial lung diseases (ILD) can be challenging and lung biopsy assessment is regularly indicated. Conventional evaluation of lung histology is constrained by manual, time-consuming sample preparation. Higher harmonic generation (HHG) microscopy allows for rapid imaging of fresh, unprocessed biopsies. It combines three imaging modalities: third harmonic generation (THG) representing cellular structures, second harmonic generation (SHG) representing collagen, and two-photon excited auto-fluorescence (2PEF) representing elastin.

Objectives: 1) Assess feasibility of HHG microscopy for on-site imaging of fresh lung biopsies in ILD; 2) provide an image atlas with matching conventional histology; 3) explore the added value of HHG to conventional microscopy.

Methods: Observational study in ILD patients scheduled for lung biopsy. Fresh, unprocessed, biopsies were imaged on-site with a mobile HHG microscope. Two pathologists compared HHG images to corresponding histology to identify key ILD features. Signal intensities for THG, SHG, and 2PEF were quantified in regions classified as normal, fibrotic, or inflammatory. Depth scans up to 100 µm were acquired for three-dimensional (3D) reconstructions.

Measurements and Main Results: 65 biopsies (53 transbronchial cryobiopsies; 12 surgical biopsies) from 18 patients were obtained. All (100%) biopsies were successfully imaged with HHG microscopy. For analysis, 97 context mosaic images (maximum 5x5mm^2) and 86 targeted higher-magnification mosaic images were selected. Acquisition time for a context image was 2.2 (± 0.6) minutes. HHG microscopy enabled simultaneous visualization of collagen, elastin, and cellular structures without staining. Pathologists were, independently, able to identify a range of key ILD features which clearly resembled conventional microscopy. Signal quantification differentiated inflammatory from fibrotic regions, with increased THG and SHG contributions, respectively. 46 depth stacks enabled 3D biopsy evaluation.

Conclusions: HHG microscopy enables rapid on-site imaging of fresh, unprocessed lung biopsy samples, providing visualization of tissue architecture and key microstructures relevant to identification of ILD patterns, 3D assessment, and potential quantification of major tissue components.

INTRODUCTION

Interstitial lung disease (ILD) is an umbrella term referring to a wide variety of diffuse parenchymal lung diseases with varying degrees of inflammation, fibrosis, or both, of the lung parenchyma. Early and adequate diagnosis is of key importance for correct treatment allocation and prognosis, but this can be challenging and may require tissue sampling[1-3]. For histological examination of lung tissue, conventional bright-field microscopy of stained tissue slides is the reference standard. However, this technique has several limitations: it requires manual and time-consuming sample preparation; each additional stain requires a separate tissue section, which can be problematic when tissue is limited; and digitization requires dedicated slide scanning systems. Moreover, histological sections provide an inherently two-dimensional representation of tissue that is structurally interconnected in three dimensions.

Higher harmonic generation (HHG) microscopy is a laser-based, label-free imaging technique that provides images of freshly excised unprocessed tissue with subcellular detail, within minutes[4-7]. HHG refers to the integration of three different imaging modalities in one image: third harmonic generation (THG), which reveals tissue interfaces and this provides morphological information of cellular structures and their nuclei; second harmonic generation (SHG) reveals mainly collagen fibers; and two-photon excited auto-fluorescence (2PEF) reveals auto-fluorescent signals from auto-fluorescent molecules in cellular cytoplasm and elastin fibers in extra cellular matrix and connective tissue. When using HHG microscopy to assess human lung tissue, various relevant tissue structures can be visualized including alveoli, bronchi, pleura, blood vessels, and cellular structures such as respiratory epithelium, pneumocytes and inflammatory cells[7-11]. In diseased lung tissue, areas of fibrosis could be identified[8, 9, 12].

Building on these observations, we designed a study with three aims: (1) to assess the feasibility of obtaining high-quality HHG images of fresh, unprocessed lung biopsies from patients with ILD; (2) to create an image atlas pairing HHG images with conventional hematoxylin and eosin (H&E) stained slides; and (3) to explore the potential added value of HHG microscopy beyond conventional histological work-up. Importantly, the primary goal of this study is not to replace conventional histology, but to demonstrate that HHG microscopy enables rapid on-site visualization of biopsy architecture and key ILD features in fresh tissue, potentially

supporting biopsy adequacy assessment and enabling future quantitative tissue analysis. A subset of the transbronchial cryobiopsy data from this prospective cohort was previously published as a research letter addressing rapid on-site biopsy adequacy classification using HHG microscopy[13]. The present manuscript substantially extends that work by including surgical lung biopsy specimens, providing a broader atlas of ILD-relevant histopathological features with matched conventional histology, and adding exploratory analyses that leverage HHG's multimodal signals (THG/SHG/2PEF) for quantification and depth-resolved (3D) assessment of inflammatory and fibrotic remodeling.

METHODS

This study was part of the COLD study, in which patients were randomized towards immediate surgical lung biopsy or transbronchial cryobiopsy, followed by surgical lung biopsy when needed, for diagnosing ILD [13]. In the current study, for which separate written informed consent was obtained from all participants, we prospectively compared HHG with conventional histological evaluation of lung biopsies. Considering the explorative nature of this study, no formal sample size calculation was performed. The full in- and exclusion criteria are presented in Online Data Supplement. To support interpretation and illustration of normal lung microanatomy, we additionally used representative images from a separate cohort of 2 patients without ILD undergoing lobectomy for lung cancer. Lobectomy specimens were imaged using the same HHG workflow and paired with conventional histology. These images were used for reference purposes and were not included in the primary feasibility analyses.

Sample handling

Immediately after tissue extraction, each freshly excised lung biopsy was placed in a glass sample holder and imaged by the mobile HHG microscope (Figure 1A-B). Subsequently, tissue was fixed in 4% formaldehyde, embedded in paraffin, cut in 3 µm sections and routinely stained with hematoxylin and eosin (H&E) for the primary histopathological assessment. Upon indication, additional staining (Elastica van Gieson and CD68 staining) was performed. Digitized H&E stained slides were made available through scanning (Philips UPS scanner) and pathology viewer software (Philips, version 3.2). Further details on sample handling are described in the Online Data Supplement.

Image acquisition

HHG imaging was performed using a transportable Flash Scanner microscope (Flash Pathology B.V.; dimensions 0.6 × 0.8 × 1.5 m^3), of which the details were described in our previous study[7] (Figure 1A and 1B). A 50-femtosecond laser beam centered at 1070 nm was used to generate nonlinear signals in unprocessed tissue. Induced signals were detected simultaneously: third harmonic generation (THG) at 349 to 361 nm, second harmonic generation (SHG) at 530 to 540 nm, and two-photon excited autofluorescence (2PEF) at 562 to 665 nm (Figure 1C). A low laser power of ~5 mW on the sample was used. Individual image tiles (maximum field of view: 500 × 500 μm^2) were acquired by raster-scanning the laser beam across the specimen. To generate larger images, the sample was translated in the lateral (x–y) and axial (z) directions using a motorized stage, after which adjacent tiles were stitched to form two-dimensional mosaics and three-dimensional depth stacks. All images were acquired as tiled mosaics. We distinguished a "context mosaic" covering a large field-of-view for anatomical orientation (sampling resolution of 1 µm, covering areas up to 5 × 5 mm^2) and a "targeted mosaic" acquired within a preselected region of interest (ROI) for detailed assessment (sampling resolution up to 0.25 µm covering areas up to 2.5 × 2.5 mm^2). Depth stacks were acquired to a maximum imaging depth of 100 µm. ROIs and imaging depths were selected at the discretion of the HHG operator or pulmonologists based on suspected histological hallmarks. Images were gamma-corrected (gamma 0.7) and saved as 24-bit RGB BMP files using the acquisition software (Flash Pathology B.V.), with THG displayed in green, SHG in red, and 2PEF in blue (Figure 1C). Local contrast enhancement was applied per channel. Images were assembled into 2D mosaics and 3D stacks in ImageJ/Fiji (v1.53f, NIH), and 3D reconstructions were generated using Imaris Viewer (v10.0.0).

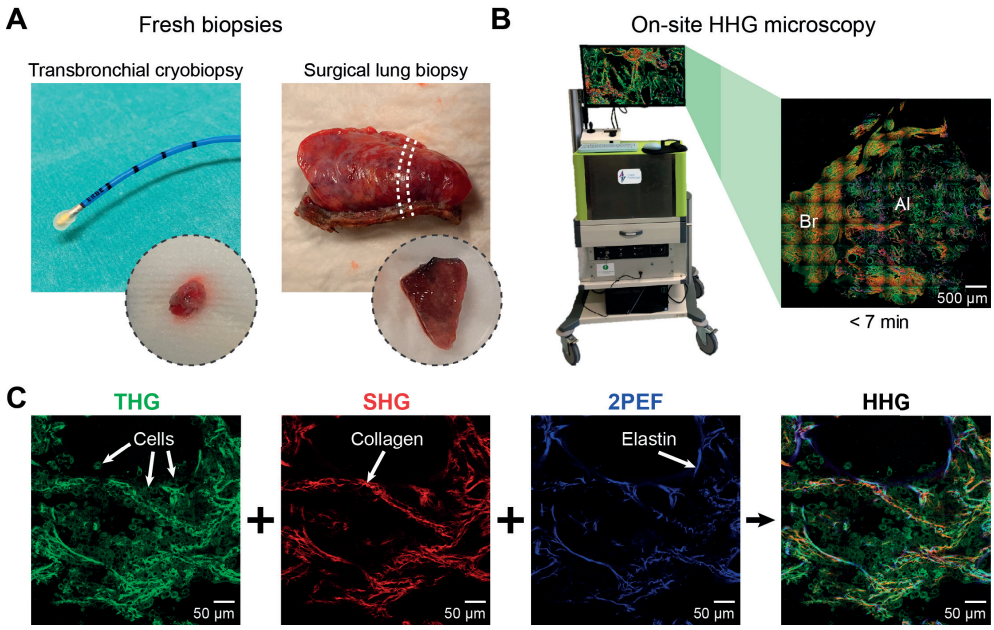


Figure 1 Technique overview. (A) Macroscopic view of imaged biopsies. Transbronchial cryobiopsies were imaged immediately following tissue extraction and were placed as a whole in the HHG microscope. Imaged surgical lung biopsies were cut from the extracted biopsy to fit in the sample holder and to allow for parenchymal imaging. (B) Biopsies were imaged on-site using the mobile HHG microscope (Flash Pathology B.V.) HHG images are obtained in mosaic tiles, covering a maximum field of view of 500 x 500 mm2 per tile. To generate a larger context mosaic image measuring up to 5x5 mm2, tiles were stitched together. This example shows a biopsy with a bronchiole (Br) surrounded by alveolated (Al) tissue . (C) The HHG images consist of three simultaneously detected signals: third harmonic generation (THG, in green), second harmonic generation (SHG, in red), and two-photon excited autofluorescence (2PEF, in blue) which provide complementary information of, respectively, tissue interfaces including cell morphology, collagen fibers and autofluorescent cell cytoplasm and elastin fibers. Note that the combined HHG images contain a broader color spectrum due to overlapping signals, e.g. yellow composed of SHG (red) and THG (green).

Pathological assessment

In accordance with international guidelines on ILD diagnosis, all biopsies were discussed during a multidisciplinary team (MDT) meeting for histopathological interpretation and consensus of ILD diagnosis[1]. Obtained HHG images were coded per biopsy in numerical order and were paired with corresponding histopathology slides. For each biopsy, the best context mosaic images and targeted mosaic images were selected for interpretation; if both sides of a biopsy were imaged, two

images were provided. Both HHG images and H&E slides were available digitally via WebMicroscope. Two ILD-expert pathologists (JT and VP) independently reviewed the HHG images, blinded to clinical data and the local ILD diagnosis. They recorded predefined tissue and ILD features; only features reported by both reviewers were included.

Statistical analysis and HHG signal quantification

Descriptive statistics were used to characterize the cohort and summarize identifiable parenchymal structures. For signal quantification, image regions representing normal alveolar tissue, inflammatory areas, or fibrotic areas were selected. THG, SHG, and 2PEF channels were separated, and each channel underwent Gaussian filtering ($\sigma x,y = 3$) and background subtraction (rolling-ball radius 11) to reduce noise. Mean pixel intensity per channel was calculated, and relative channel contributions were visualized using a ternary plot.

RESULTS

Study cohort

Between January 2020 and October 2021, 18 ILD patients who underwent lung biopsy at the Amsterdam UMC were included. Patient characteristics are summarized in Table 1. Fourteen patients underwent transbronchial cryobiopsy, 3 patients underwent surgical lung biopsy, and 1 patient underwent both. This resulted in 19 biopsy procedures in 18 patients and a total of 65 biopsy specimens (53 transbronchial cryobiopsies; and 12 surgical biopsies). Per cryobiopsy procedure, at least 2 biopsies (range 2-5) from 2 different segments were obtained, with a mean maximum diameter of 0.7 (± 0.3) cm per biopsy specimen. In all surgical biopsy procedures, 3 biopsies were obtained from 3 different lobes, with a mean maximum diameter of 5.7 (± 0.9) cm. Final ILD-MDT diagnosis included hypersensitivity pneumonitis (n = 9), idiopathic non-specific interstitial pneumonia (n = 3), idiopathic pulmonary fibrosis (n = 2) and 4 other diagnoses (Table 1).

Table 1. Patient characteristics.

Total number of ILD patients	**18**
Male sex	14 (78%)
Age, years	64 (± 9)
Pulmonary function test	
FVC, % predicted	**82 (± 10)**
DLCOc, % predicted	56 (± 14)
Final ILD-MDT diagnosis	
fHP	9 (50%)
iNSIP	3 (17%)
IPF	2 (11%)
CTD-ILD	1 (5.5%)
SR-ILD	1 (5.5%)
Sarcoidosis	1 (5.5%)
Unclassifiable	1 (5.5%)

Acquired and selected HHG images

From all biopsies (n=65), subcellular resolution HHG microscopic images were obtained. 121 rapid on-site context mosaic images were obtained, of which 97 were selected for histological assessment. 102 more detailed targeted mosaic images were obtained, of which 86 were included (Table 2). Images were excluded due to duplication (n=17; >50% overlap with a previous image), technical artifacts (n=12; e.g., air bubbles between the objective and sample-holder glass or suboptimal positioning relative to the scanning beam), or tissue-related artifacts (n=11; e.g., extensive air within the tissue or insufficient contact between tissue and glass).

Median turnaround time from placing the specimen in the holder to a first context mosaic image was 7 ± 1.8 minutes, this includes 2.2 ± 0.6 minutes for image acquisition (maximum 5 × 5 mm^2) and 4.9 ± 1.7 minutes for sample loading and positioning. Targeted mosaic images (maximum 2.5 × 2.5 mm^2) were acquired in 2.3 ± 0.5 minutes, and depth scans (maximum depth 100 µm) for 3D reconstruction were acquired in 1.9 ± 0.8 minutes. No tissue damage or reduced histological quality attributable to HHG imaging was noted on subsequent routine pathology review.

Table 2. Higher harmonic generation (HHG) for imaging of transbronchial cryobiopsies and surgical lung biopsies.

Data are shown as n (%) or mean (± SD).

Total number of biopsies imaged with HHG microscopy	**65**
Transbronchial cryobiopsies	53 (82%)
Surgical lung biopsies	12 (18%)
Number of acquired HHG images	269
Rapid on-site context mosaic images	**121**
(sampling resolution: 1 µm, max 5 x 5 mm^2)	97 (80%)
Selected for image analysis*	102
Targeted mosaic images	86 (84%)
(sampling resolution: up to 0.25 µm, max 2.5 x 2.5 mm^2)	46
Selected for image analysis*	
Depth scan stacks for 3D reconstruction	7.0 (± 1.8)
(sampling resolution: up to 0.25 µm, max 100 µm deep)	2.2 (± 0.6)
Acquisition time (minutes)	2.3 (± 0.5)
From placing sample in tissue holder to first context mosaic image	1.9 (± 0.8)
Rapid on-site context mosaic image	
Higher resolution targeted mosaic image	
Depth scan stack for 3D reconstruction	

* Reasons for excluding images for pathological assessment from both context mosaic (n=24) and targeted mosaic (n=16) images, included: duplicates (n=17), technical artifacts (n=12), and tissue artefacts (n=11)

Identification of histopathological features on HHG microscopy

Across all biopsies, both reference pathologists recognized fundamental parenchymal structures and distinguished broadly normal, inflammatory, and fibrotic regions on HHG images. Normal structures identifiable on HHG included alveolar septa, pleura, blood vessels, and bronchioles (Figure 2). Cellular structures were predominantly visualized via THG (green), enabling identification of bronchiolar epithelium, pneumocytes (type II), and endothelial cells. Multiple inflammatory cell types were distinguished, including alveolar macrophages, lymphocytes, and granulocytes (Figure 3). Extracellular matrix components were readily differentiated because collagen generated SHG signal (red) and elastin generated 2PEF signal (blue), facilitating interpretation of alveolar architecture and aiding, for example, in differentiating blood-vessel wall layers (Figure 2E). A range of ILD-relevant histological features were

identified, including inflammatory regions with increased cellularity (increased THG), fibrotic regions with increased collagen (increased SHG), elastotic regions with increased elastin (increased 2PEF), and mixed regions (Figure 4A–L). Fibrosis ranged from mild to extensive and could be patchy or homogeneous, with variable architectural distortion. Microscopic honeycombing was recognized as dense fibrosis with cystic change (Figure 4M). Inflammatory findings included giant cells, granulomas and lymphocytic infiltrates (Figure 3A–F, K; Figure 4O). Oedema (Figure 4A), areas with extensive intra-alveolar macrophages accumulation (Figure 4C), and Masson bodies consistent with organizing pneumonia (Figure 3G) were also identified.

Depth scanning and 3D reconstructions

In addition to 2D imaging, 46 z-stacks were acquired from 33 biopsies, with imaging depths ranging from 30 to 100 µm. Depth imaging enabled identification of structures and cells not apparent within a single 2D plane and improved visualization of alveolar architecture. Three-dimensional reconstructions demonstrated the alveolar network in a single view; separation of SHG and 2PEF further delineated 3D collagen and elastin architecture (Figure 5).

Quantification of THG, SHG and 2PEF signals

Based on HHG images, the pathologists distinguished normal from inflammatory and fibrotic regions, reflecting increased cellularity and collagen content, respectively (Figure 6I–III). Quantitative analysis of mean signal intensities demonstrated clustering of normal, inflammatory, and fibrotic alveolar regions on ternary plots (Figure 6IV). In normal alveolar tissue, relative signal contributions were balanced (~30–35% each), whereas inflammatory regions showed increased THG contribution and fibrotic regions showed increased SHG contribution.

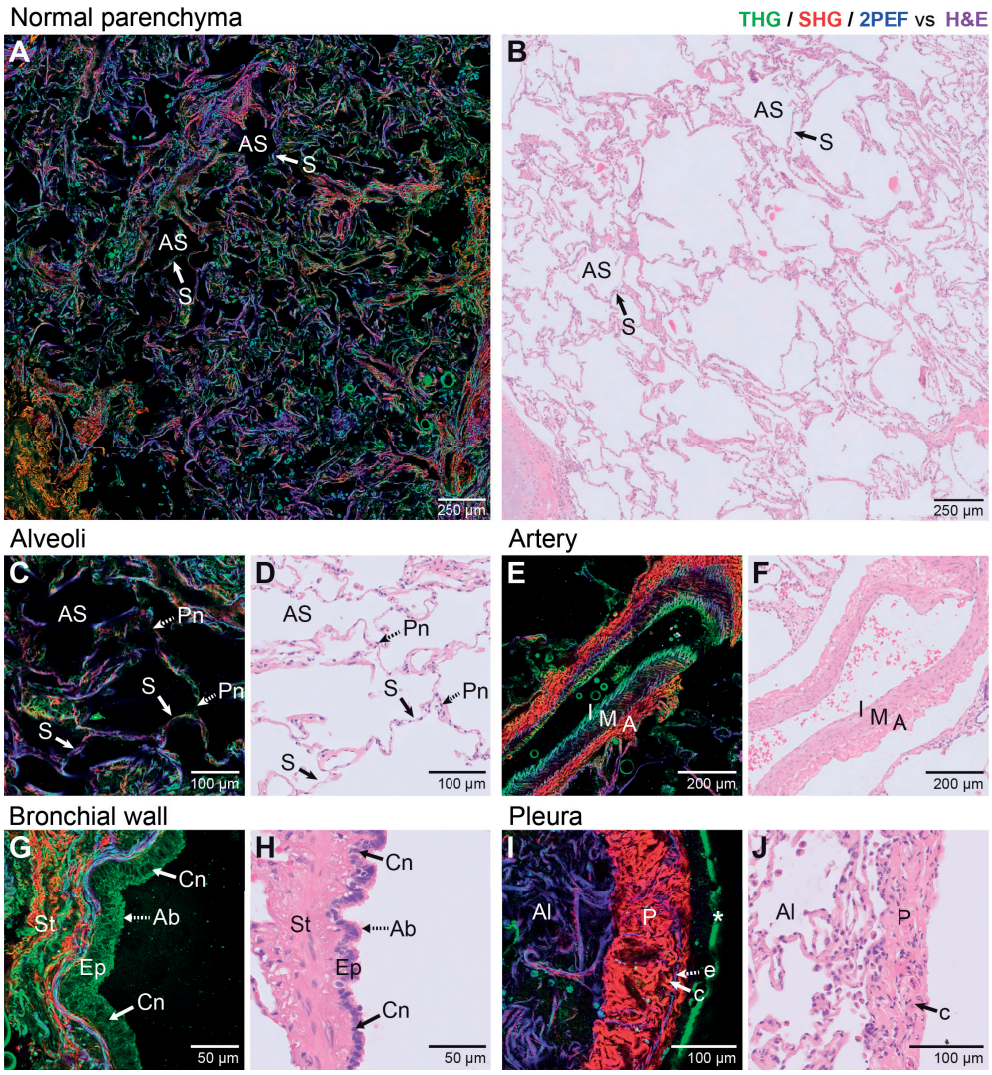


Figure 2. HHG microscopy images of lung structures with corresponding histology. (A,B) Image of transbronchial cryobiopsy showing alveolar tissue including alveolar space (AS) and alveolar septa (S). (C–J) Magnified targeted mosaic images showing the architecture of various lung structures. (C,D) Alveoli including alveolar space (AS), alveolar septa (S), and pneumocyte (Pn). (E,F) Pulmonary artery showing the layers of adventitia (A), media (M), and intima (I). (G,H) Bronchiolar wall with respiratory epithelium (Ep) and their cell nuclei (Cn), apical bar (Ab)) and underlying stroma (St). (I,J) Visceral pleura (P) consisting of collagen (c) and elastic (e) fibers merged with the fibroelastic framework of the lung alveoli (Al). (*) Interface of liquid with air, revealed by THG microscopy.

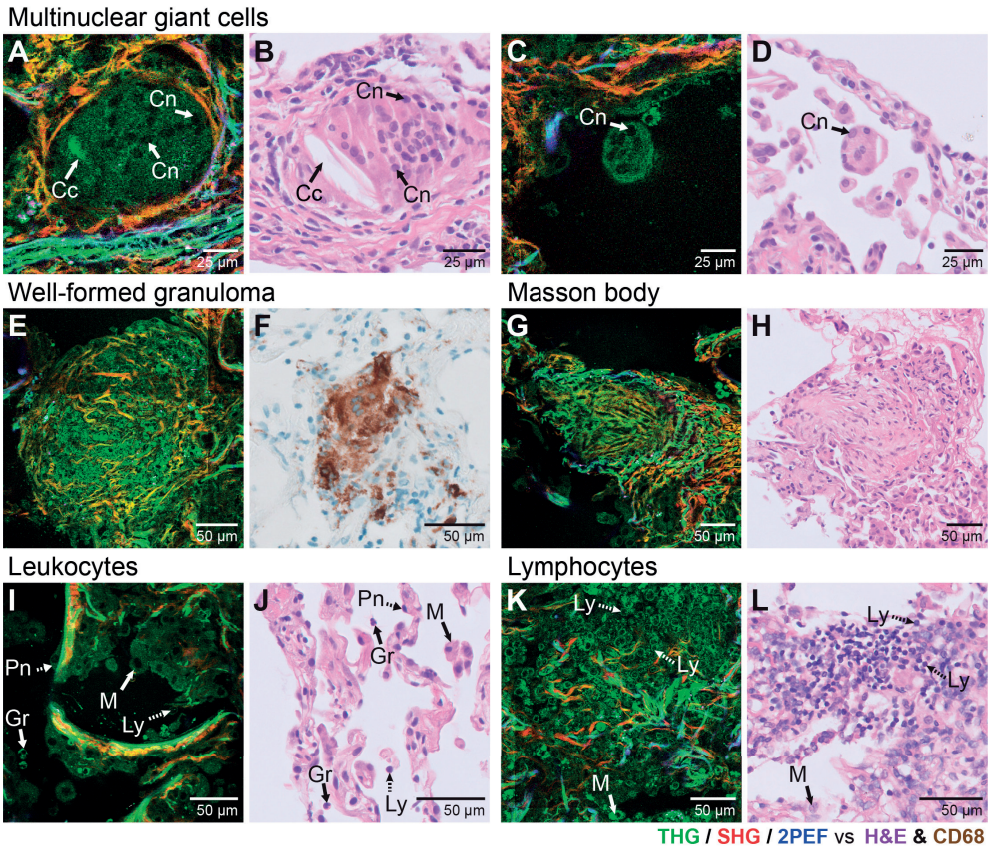


Figure 3. HHG microscopy images of cellular features with corresponding histology. (A–D) Giant cells with multiple cell nuclei (Cn) and a cholesterol cleft (Cc) visualized by THG microscopy. (E,F) Well-formed granuloma, consisting of aggregates of mature mononuclear phagocytes (macrophages and/or epithelioid cells). (G,H) Masson body: an alveolar plug consisting of loose fibrosis in which spindle shaped fibroblast are embedded. (I,J) Different types of leukocytes including granulocytes (Gr) with multilobular nuclei, mononuclear lymphocytes (Ly) and macrophages (M). Also, pneumocytes (Pn) lining the alveolar septa are identified. (K,L) Magnified image of Figure 3O–P showing the infiltration of lymphocytes (Ly) and surrounding macrophages (M). Corresponding histology are hematoxylin and eosin (H&E) stained slides and in case of granuloma (F) stained with CD68.

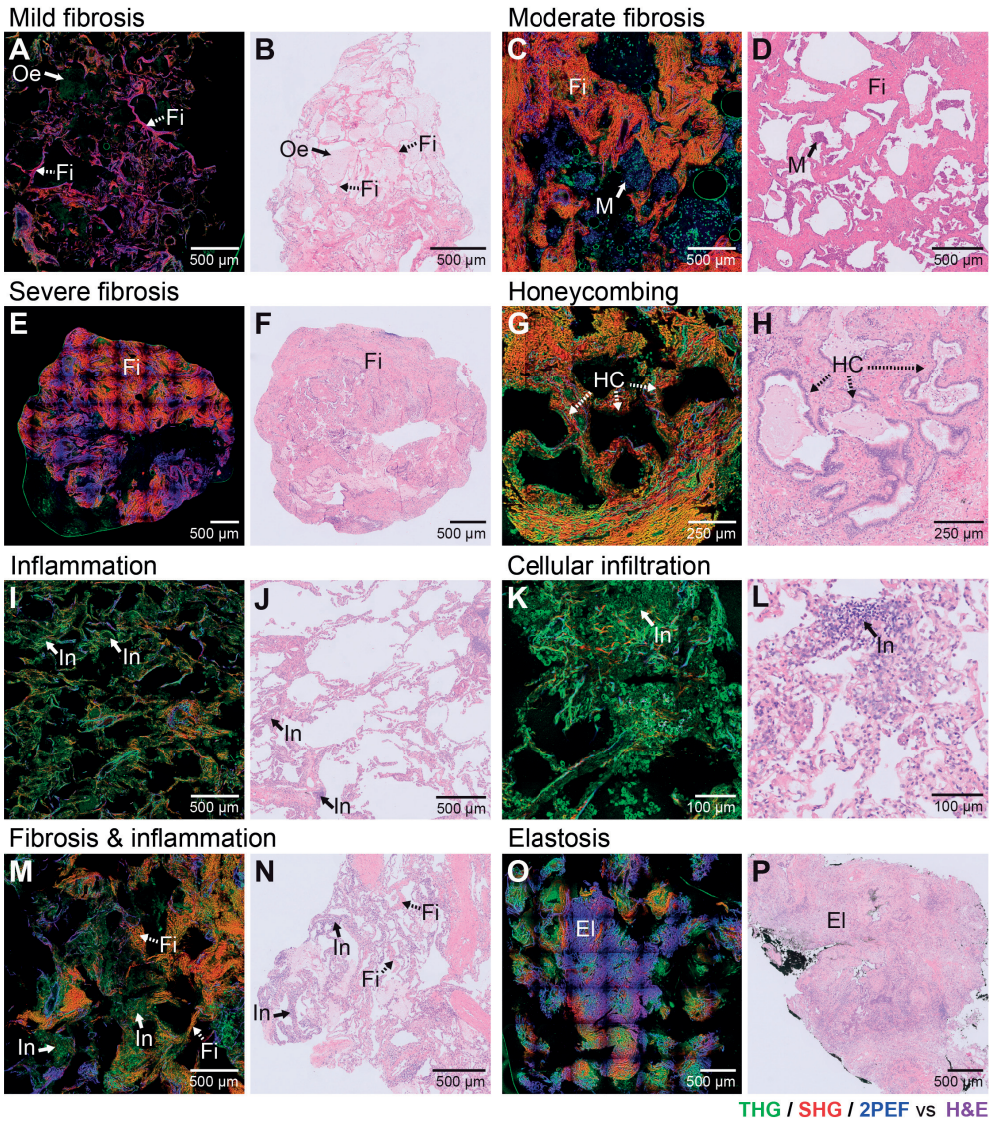


Figure 4. HHG microscopy images of ILD characteristics with corresponding histology. (A–F) Various stages of fibrosis (Fi) with an increased amount of collagen revealed by SHG microscopy: (A,B) mild fibrosis with thickened alveolar septa, but preserved alveolar architecture, (C,D) moderate fibrosis with thickened alveolar septa consistent with fibrotic NSIP pattern(E,F) severe fibrosis with distorted, unrecognizable architecture. (A,B) Oedema (Oe) could be visualized by THG. (C,D) Extensive alveolar infiltration of macrophages (M), a characteristic of alveolar macrophage pneumonia was identified. (G,H) Honey combing (HC) recognized as an area of dense fibrosis with cystic change. (I,J) Thickened alveolar septa by cellular infiltration of lymphocytes (In) revealed by THG microscopy of a patient diagnosed with hypersensitivity pneumonitis. (K,L) Magnified image of cellular infiltration of lymphocytes (In) in alveolar septa. (M,N) A mixed pattern

was observed by thickened alveolar septa due to both fibrosis (Fi) and cellular infiltration (In) of a patient diagnosed with cellular non-specific interstitial pneumonia. (O,P) Area of elastosis (El) was recognized by an increased 2PEF signal. (C,D,G,H) Images of surgical lung biopsies, while the rest are images from transbronchial cryobiopsies. (E,O) Context mosaic images, while the rest are targeted mosaic images.

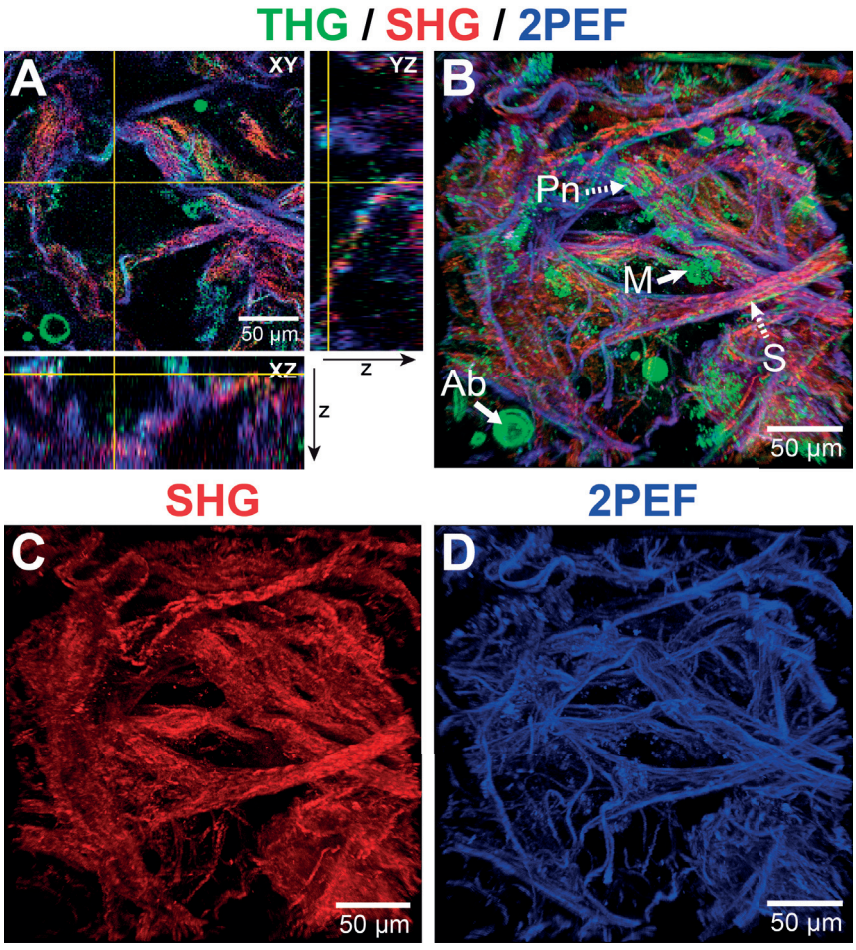


Figure 5. HHG microscopy 3D imaging shows the 3D architecture of alveolar tissue. Depth scan of 95 µm with step size of 5 µm. (A) Orthogonal views. (B) 3D reconstructed image. (C,D) SHG and 2PEF modalities separated showing the collagen (C) and elastin (D), respectively. The 3D image visualizes the 3D architecture of alveolar septa (S) that consist of collagen, elastin and pneumocytes (Pn), and structures in alveolar spaces, including macrophages (M) and air bubbles (Ab). Videos of the depth scan and the 3D rotating image can be found in the Online Data Supplement (Video E1 and E2).

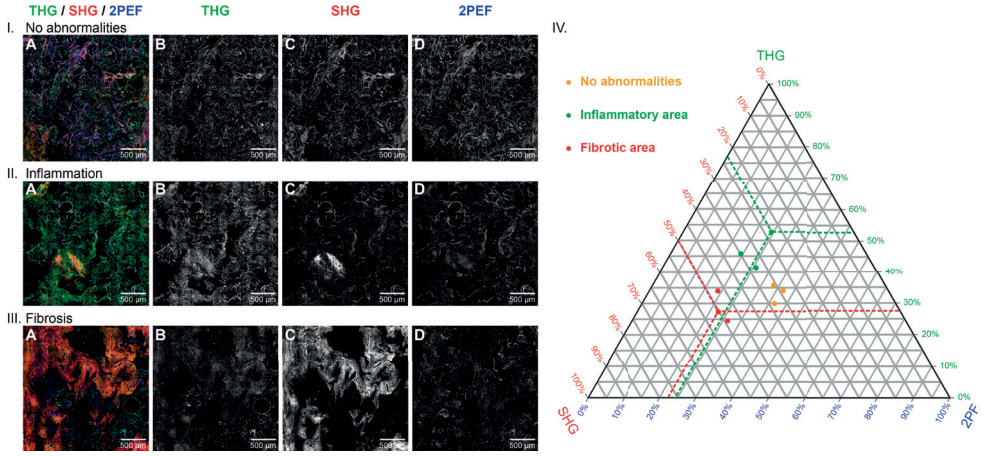


Figure 6. Quantification of HHG signals for normal, fibrotic and inflammatory areas. (I-III) HHG microscopy images from targeted mosaic images of normal (A-I), fibrotic (A-II) and inflammatory (A-III) areas, separated by THG (panel B), SHG (panel C) and 2PEF (panel D). (IV) The relative percentages of THG, SHG and 2PEF signal intensities plotted in a ternary plot. Every dot corresponds to a selected area of a different patient, with the fibrotic areas in red, inflammatory areas in green and normal areas in orange. The dotted lines are an indicator how to read the different signal ratios (in this example the fibrotic case: 28 % THG; 50 % SHG; 22 % 2PEF, and inflammatory case: 53 % THG; 23 % SHG; 24 % 2PEF). The normal areas were selected from biopsies classified as normal alveolar tissue with one case from this study cohort and two cases from a cohort where the patient underwent lobectomy for lung cancer treatment.

DISCUSSION

We demonstrate the feasibility of HHG microscopy for on-site imaging of fresh, unprocessed lung biopsies from patients with ILD. Within minutes, HHG provided highly detailed, subcellular-resolution images in which key histological features relevant to ILD evaluation were recognized. Notably, HHG enabled integrated visualization and quantitative distribution analysis of collagen, elastin, and multiple inflammatory cell types in a single image without fixation, sectioning, or staining, and images were immediately available in digital format for sharing and review.

Prior work using two modalities (two-photon fluorescence and SHG) demonstrated detection of fibrotic changes in animal models and in prepared human lung tissue from patients with idiopathic pulmonary fibrosis[9]. Similar approaches have shown that increased collagen content in fibrotic ILD corresponds to increased SHG signal[12, 14]. Interestingly,

although available in some of these systems, none of the previous work on HHG microscopy included THG to assess tissue from ILD patients. In ILD diagnostics, inflammatory response is a critical dimension alongside fibrosis[1, 15]. THG has been reported to enable identification of specific inflammatory cell types[11], which we confirm here (Figures 3 and 4). These findings support the value of integrating THG within HHG microscopy for ILD tissue evaluation.

The combination of THG, SHG, and 2PEF yields composite images that closely resemble conventional H&E appearance, as reflected by the ability of two ILD-expert pathologists to identify architectural changes and characteristic ILD features. With this study we contribute to building an image atlas pairing HHG with conventional histology across a broad spectrum of ILD findings, including areas of healthy lung tissue for comparison.

Consistent with earlier work, SHG and 2PEF revealed fibrotic remodeling and architectural distortion, with increased SHG:2PEF ratios in the most fibrotic regions. By incorporating THG, we extended this concept to a three-component assessment including inflammatory regions. These analyses are exploratory and intended to demonstrate signal separability rather than provide clinically applicable thresholds. Although the study was not designed to draw conclusions from these ratios, the proof-of-concept supports further study to evaluate whether relative signal ratios could assist in differentiating predominantly fibrotic from more inflammatory-driven ILD phenotypes, potentially informing prognostication and treatment response.

This study has limitations. First, the image-review design was not fully independent: while the two pathologists were blinded to clinical data and to each other, they were allowed to compare HHG images and corresponding H&E slides iteratively. This may have introduced confirmation bias. We mitigated this by using two independent reviewers and reporting only features concordantly identified by both. Second, formal interobserver agreement analysis was not performed, as the study aimed at feasibility and atlas construction rather than diagnostic reproducibility. Third, given the novelty of the technique and absence of a formal training set, we focused on recognition of structures and features rather than pattern-based diagnosis or disease classification. Fourth, while the number of biopsies was substantial (n=65), the number of patients was limited. Approximately 20% of acquired images were excluded, largely reflecting an operator learning curve in ROI selection

and specimen positioning relative to the scanning beam, which increased duplicate acquisition and overall imaging time. In addition, to prevent alveolar collapse in cryobiopsies, some specimens were stored in formalin; when imaging was prolonged, longer fixation led to tissue stiffening and reduced contact with the sample-holder glass, contributing to suboptimal imaging. In a minority of cases, air-bubble artifacts were observed; this was partially mitigated by washing the biopsy in a saline solution.

While recognizing the limitations, HHG microscopy has multiple potential clinical and research applications. The total time from biopsy acquisition to interpretable HHG imaging was typically below 10 minutes, making integration into procedural workflows feasible without prolonging procedures. Given its rapid acquisition and high interpretability of both normal and diseased lung features, HHG microscopy may enable real-time on-site assessment of biopsy adequacy. In a recent pilot study from our group, HHG microscopy differentiated adequate from inadequate transbronchial cryobiopsies (based on biopsy size and the presence of abnormal alveolar tissue) with 86.1% sensitivity and 76.9% specificity, suggesting potential to improve diagnostic yield by reducing sampling error[13]. In conventional workflows, additional stains are required to visualize extracellular matrix components and assess their relative proportions. HHG provides label-free, integrated digital images in which the three modalities correspond to different components, potentially complementing routine pathology by providing broader, more detailed, and quantifiable information on fibrosis and inflammation. Depth scanning enables three-dimensional tissue assessment, which may partially mitigate inherent limitations of conventional two-dimensional histology in spatially heterogeneous ILD. By providing volumetric context within the same biopsy region, 3D HHG may reduce 'cutting plane' effects and help distinguish true architectural distortion from sectioning-related appearances, potentially improving confidence in subtle structural abnormalities. Future integration of HHG into an endoscope might reduce or obviate the need for tissue sampling. Given that *in vivo* fluorescence-based endomicroscopy is already clinically available, this may be feasible[16]. For research, HHG may support studies in fibrotic models, drug development and testing, and prognostic or predictive biomarker development. Finally, digital acquisition facilitates rapid remote consultation, education, and data storage.

In conclusion, on-site HHG microscopy enables integrated visualization of ILD-relevant microstructures in fresh, unprocessed lung biopsies,

supports 3D assessment, and may facilitate quantification of key tissue components such as fibrosis, inflammation and elastin accumulation. With further refinement and validation in larger cohorts, HHG microscopy may help guide clinical procedures and complement current histopathological assessment of ILD.

STATEMENTS

Acknowledgement (optional)

We thank Maret Heems and Yael Rip for their help during the experiments, and Maret in particular for providing a literature review and partial analysis of the data. Also, we thank Frank van Mourik (Flash Pathology B.V.) for the technical support and Albert Stoop for the transport of the mobile HHG microscope to Amsterdam UMC location AMC.

Statement of Ethics

The study was approved and monitored by the medical ethical committee of the Amsterdam UMC (identifier: 2018_208) and was performed in accordance with good clinical practice guidelines and the declaration of Helsinki.

Conflict of Interest Statement

M.L.G. declares to have indirect interest in Flash Pathology B.V. L.M.G.v.H. received technical support from Flash Pathology. Flash Pathology was not involved in the design of the study and data acquisition and analysis. Other authors have no conflict of interest.

Funding Sources

This publication is part of the project Instant Pathology (with project number 15825) of the research program Open Technology, by the domain which is (partly) financed by the Dutch Research Council (NWO- Applied and Engineering Sciences) and Horizon 2020 Framework Program grants 654148 and 871124. This study was also, in part, funded by Netherlands Organisation for Health Research and Development (ZonMW), project number 843001813. Technical support is provided by Frank van Mourik (Flash Pathology B.V.).

Author Contributions

Conception or design; L.H., K.K., P.B., J.A., M.G.

Acquisition, analysis, or interpretation of data: L.H., K.K., J.T., P.B., V.P., T.R., C.D., J.D, J.A.

Drafting or revising the manuscript: L.H., K.K., J.T., V.P., T.R., C.D., P.B., J.A., M.G.

Final approval and accountable for all aspects of the work: L.H., K.K., J.T., V.P., T.R., C.D., J.D., P.B., J.A., M.G.

Data Availability Statement

The data that support the findings of this study are available in this article. Further inquiries can be directed to the corresponding author on reasonable request.

REFERENCES

1. Raghu, G., et al., *Idiopathic Pulmonary Fibrosis (an Update) and Progressive Pulmonary Fibrosis in Adults: An Official ATS/ERS/JRS/ALAT Clinical Practice Guideline.* Am J Respir Crit Care Med, 2022. **205**(9): p. e18–e47.
2. Ryerson, C.J., et al., *Update of the international multidisciplinary classification of the interstitial pneumonias: an ERS/ATS statement.* Eur Respir J, 2025. **66**(6).
3. Mor, E., et al., *Clinical utility of lung biopsy in fibrotic interstitial lung disease.* American Journal of Respiratory and Critical Care Medicine, 2026.
4. Kuzmin, N.V., et al., *Third harmonic generation imaging for fast, label-free pathology of human brain tumors.* Biomed Opt Express, 2016. **7**(5): p. 1889–904.
5. van Huizen, L.M.G., et al., *Second and third harmonic generation microscopy visualizes key structural components in fresh unprocessed healthy human breast tissue.* J Biophotonics, 2019. **12**(6): p. e201800297.
6. Sun, Y., et al., *Intraoperative visualization of the tumor microenvironment and quantification of extracellular vesicles by label-free nonlinear imaging.* Sci Adv, 2018. **4**(12): p. eaau5603.
7. van Huizen, L.M.G., et al., *Compact portable multiphoton microscopy reveals histopathological hallmarks of unprocessed lung tumor tissue in real time.* Transl Biophotonics, 2020. **2**(4): p. e202000009.
8. van Huizen, L.M.G., et al., *Rapid On-Site Pathology Visualization of COVID-19 Characteristics Using Higher Harmonic Generation Microscopy.* Am J Respir Crit Care Med, 2023. **208**(2): p. 199–200.
9. Pena, A.M., et al., *Three-dimensional investigation and scoring of extracellular matrix remodeling during lung fibrosis using multiphoton microscopy.* Microsc Res Tech, 2007. **70**(2): p. 162–70.
10. Filippi, A., et al., *Multimodal label-free ex vivo imaging using a dual-wavelength microscope with axial chromatic aberration compensation.* J Biomed Opt, 2018. **23**(9): p. 1–9.
11. van Huizen, L.M.G., et al., *Leukocyte differentiation in bronchoalveolar lavage fluids using higher harmonic generation microscopy and deep learning.* PLoS One, 2023. **18**(6): p. e0279525.
12. Tilbury, K., et al., *Second harmonic generation microscopy analysis of extracellular matrix changes in human idiopathic pulmonary fibrosis.* J Biomed Opt, 2014. **19**(8): p. 086014.
13. Kalverda, K.A., et al., *Rapid On-Site Evaluation of Cryobiopsies in Interstitial Lung Disease Using Higher Harmonic Generation Microscopy.* Am J Respir Crit Care Med, 2025. **211**(10): p. 1876–1879.
14. Kottmann, R.M., et al., *Second harmonic generation microscopy reveals altered collagen microstructure in usual interstitial pneumonia versus healthy lung.* Respir Res, 2015. **16**(1): p. 61.
15. Mikolasch, T.A., H.S. Garthwaite, and J.C. Porter, *Update in diagnosis and management of interstitial lung disease* Clin Med (Lond), 2017. **17**(2): p. 146–153.
16. Wijmans, L., et al., *Bronchoscopic Journey of in vivo Real-Time Microscopic Imaging in ILD: A Case Series.* Respiration, 2022. **101**(11): p. 1006–1014.

ONLINE DATA SUPPLEMENT

Rapid on-site histology of lung biopsies in ILD using higher harmonic generation microscopy: a proof of concept and image atlas

Laura M. G. van Huizen*[1], Kirsten A. Mooij Kalverda*[2], Jan von der Thüsen[3], Venerino Poletti[4,5], Teodora Radonic[6], Chris Dickhoff[7], Johannes Daniels [2], Peter I. Bonta[2], Jouke T. Annema[2 $], Marie Louise Groot[1 $]

*These authors contributed equally

$ shared senior author ship

1. Inclusion and exclusion criteria

No specific exclusion criteria for this study participation were formulated. However, as this study was a sub study of a randomized trial comparing transbronchial cryobiopsy (TBCB) followed by surgical lung biopsy (SLB) versus SLB alone for ILD diagnosis (COLD-study NTR NL7634), the in- and exclusion criteria for that study were also applicable for the current study (Table E1).

Table E1: Inclusion and exclusion criteria for study participation

Inclusion criteria
· >18 years of age · ILD on HR-CT · No classifying diagnosis based on clinical data including laboratory results and HR-CT · ILD-MDT panel indication for histology by lung biopsy
Exclusion criteria
· Inability and willingness to provide informed consent · Inability to comply with study protocol · Prothrombin time international normalized ratio (INR) >1.3 · Use of clopidogrel, or other new anti-platelet therapy, or anticoagulant drugs that cannot be stopped temporarily · Thrombocytopenia <70x10^9/L · History of pulmonary hypertension (systolic pulmonary artery pressure > 50 mmHg) · Diffusing capacity < 30% · Forced vital capacity <50% · Forced expiratory volume in the first second (FEV1) <0,8L or <50% of predicted value · Body mass index >35 · Pregnancy

2. Sample handling

In case of transbronchial cryobiopsy (TBCB), the obtained tissue was defrosted in saline following extraction. To keep the samples hydrated and to avoid alveolar collapse, the biopsies were put on a NaCl 0.9% wetted gauze, or the specimen was briefly fixed in formaldehyde (for specific sample handling per case see Table E2). Each lung tissue biopsy was labeled separately in chronological order, after which each lung biopsy was placed in a separate sample holder (35 mm diameter µ-Dish with 0.17 mm thick glass bottom, Ibidi GmbH), and placed in the mobile HHG microscope which was stationed in the bronchoscopy suite (Figure 1B).

Table E2 – Sampling handling per case of the transbronchial cryobiopsies and surgical lung biopsies.

Case	Number of biopsies	Type of biopsy	Fresh	Gaze with NaCl	In PFA	In PBS
LI001	4	TBCB			All*	
LI002	3	TBCB			All*	
LI003	4	TBCB			All*	
LI004	2	TBCB			All*	
LI005	4	TBCB			All*	
LI006	4	TBCB			All*	
LI007	4	TBCB			All*	
LI008	3	TBCB	1st		2nd – 3rd	
LI009	3	SLB	All			
LI010	4	TBCB	1st		2nd – 4th	
LI011	4	TBCB	1st		2nd – 4th	
LI012	3	SLB				All
LI013	3	SLB				All
LI014	3	SLB				All
LI015	3	TBCB	1st	2nd	3rd	
LI016	4	TBCB		1st – 2nd	3rd – 4th	
LI017	5	TBCB		1st – 2nd	3rd – 5th	
LI018	2	TBCB		1st	2nd	
LI019	3	TBCB		1st – 2nd	3rd	

TBCB= transbronchial cryobiopsy, SLB= surgical lung biopsy, PFA = paraformaldehyde solution, 4%, PBS = phosphate-buffered saline solution
* The first biopsy was in PFA for ~ 1 minute.

In case of a surgical lung biopsy, the resected lung tissue was transported to the pathology department where small pieces of lung tissue were excised (max 1 × 1 × 1 cm^3) and except for the first case submerged in phosphate-buffered saline to avoid alveolar collapse. To achieve the best one-to-one comparison as possible with the histopathology slides, the specimens were cut in the same orientation as imaged by the HHG microscope. Hereafter, the samples were placed in the sample holder and imaged with the mobile HHG microscope located at the pathology department.

3. Image acquisition

Of every biopsy an initial context mosaic image of maximum 5 × 5 mm^2 was acquired with a sampling resolution of 1 µm. In case the biopsy exceeded 5 mm, in diameter, multiple mosaic images, adjacent to each other, were combined to 1 image. An exception is case 1, where no context mosaic image was acquired, but instead an overview was created by scanning over the tissue with a joystick and stitching those images together.

Based on the context mosaic image, regions of interest (ROI) were indicated at the discretion of the HHG expert or pulmonologists, to acquire targeted mosaic 2D ROI images of maximum 2.5 × 2.5 mm^2 with a sampling resolution of 0.5 µm, and 2 targeted mosaic images with a sampling resolution of 0.25 µm. Only of case 1 and 2, no targeted mosaic images were acquired.

In 33 (51%) biopsies additional 3D depth scans were acquired of maximum 100 µm deep, with a sampling resolution of either 0.5 µm (n = 10) or 0.25 µm (n = 36).

4. 3D imaging

Video E1: Depth scan of alveolar tissue to a depth of 95 µm and steps of 5 µm.

Video E2: 3D reconstruction of a scan of 95 µm in depth with steps of 5 µm, showing the alveolar 3D architecture.

Chapter 10

Rapid On-Site Evaluation of Cryobiopsies in Interstitial Lung Disease Using Higher Harmonic Generation Microscopy

Kirsten A. Kalverda[1]*, Laura M.G. van Huizen[4]*, Jan von der Thüsen[5], Venerino Poletti[6,7], Teodora Radonic[2], Chris Dickhoff[3], Johannes M.A. Daniels[1], Peter I. Bonta[1], Jouke T. Annema[1]‡, and Marie Louise Groot[4]‡

*These authors contributed equally to this work.

‡Co-senior authors

[1]Department of Pulmonary Diseases, [2]Department of Pathology, and [3]Department of Cardiothoracic Surgery, Amsterdam University Medical Center, Amsterdam, the Netherlands; [4]LaserLab Amsterdam, Department of Physics, Faculty of Science, Vrije Universiteit Amsterdam, Amsterdam, the Netherlands; [5]Department of Pathology, Erasmus MC, Rotterdam, the Netherlands; [6]Department of Medical and Surgical Sciences, Bologna University–Forlí Campus, Forlì, Italy; and [7]Department of Respiratory Diseases and Allergy, Aarhus University Hospital, Aarhus, Denmark

American Journal of Respiratory and Critical Care Medicine Volume 211 Number 10

To the Editor:

"Interstitial lung disease" (ILD) is an umbrella term referring to diffuse parenchymal lung disorders that exhibit varying degrees of inflammation and fibrosis. Diagnosing ILD can be challenging and may require invasive lung biopsy procedures such as transbronchial cryobiopsy or surgical lung biopsy (1). Guidelines recommend starting with the less invasive transbronchial cryobiopsy technique, followed by surgical lung biopsy in case of an uninformative cryobiopsy procedure (step-up strategy) (2, 3). To date, no technique exists to provide immediate feedback on alveolar sample adequacy, which, if available, could reduce the need for repeat procedures, thereby minimizing patient burden and diagnostic delays.

Higher harmonic generation (HHG) microscopy, a laser-based, label-free imaging technique, enables the rapid imaging of freshly excised tissue with subcellular resolution. HHG integrates three imaging modalities: third-harmonic generation, which delineates tissue interfaces and cellular morphology; second-harmonic generation, highlighting collagen fibers; and two-photon excited autofluorescence, visualizing autofluorescentmolecules in the cytoplasm and extracellular matrix. Previous studies demonstrated HHG's ability to visualize relevant lung structures, including alveoli, bronchi, pleura, blood vessels, pneumocytes, inflammatory cells, and areas of fibrosis (4–6). Furthermore, its potential to identify representative tissue in lung cancer was recently reported (7). We hypothesized that HHG microscopy could identify representative transbronchial cryobiopsy samples suitable for diagnosing ILD. Some of the results of this study has been previously reported in conference abstract form (8).

We conducted a prospective study at AmsterdamUniversity Medical Centers (UMC) as part of the COLD (Transbronchial cryobiopsy followed by as-needed surgical lung biopsy versus immediate surgical lung biopsy for diagnosing interstitial lung disease) study (3), recruiting consecutive patients with ILD scheduled for transbronchial cryobiopsy. Written informed consent was obtained fromall participants, and the study was approved by the AmsterdamUMC Medical Ethics Committee (identifier 2018_208) and conducted in accordance with Good Clinical Practice guidelines and the Declaration of Helsinki.

Freshly excised transbronchial cryobiopsy specimens were immediately placed in a glass sample holder and imaged using a transportable HHG

microscope (FD1070; Flash Pathology B.V.) (7). HHG images were obtained in mosaic tiles, each covering amaximum field of view of 500×500 mm^2. These tiles were stitched together to create a largermosaic image-measuring up to 5×5mm^2 using Flash Pathology software. After imaging, samples were fixed, paraffin embedded, sectioned (3 μm), and stained with hematoxylin and eosin (H&E) for histopathological evaluation. Digital H&E slides were reviewed using Philips pathology viewer software (version 3.2).

All biopsies were assessed during multidisciplinary discussion for histopathological interpretation and diagnostic consensus. Adequacy criteria included a biopsy sample size of >5mm, alveolar tissue proportion >40%, and representation of abnormalities identified on high-resolution computed tomography. Two experienced ILD pathologists (J.v.d.T. and V.P.) independently evaluated the H&E and HHG images. Both were familiar with HHG imaging fromprior work in coronavirus disease (COVID-19)–related pulmonary fibrosis and lung cancer (5, 7). Assessments were separated by a six-month washout period, with blinding to both the final clinical diagnosis and each other's evaluations. Discrepancies were resolved through a consensusmeeting, and consensus evaluations were used to determine the sensitivity and specificity of HHG adequacy assessment, using conventional histological analysis as the reference standard.

Between January 2020 and June 2021, 15 patients with ILD undergoing transbronchial cryobiopsy at Amsterdam UMC provided informed consent. The first patient was excluded from analysis because of the unavailability of HHG mosaic imaging software at the time. Thus, 49 biopsies from14 patients (mean age, 64±8 yr; 10 men, 4 women) were included in the final analysis. Final ILD multidisciplinary discussion diagnoses included fibrotic hypersensitivity pneumonitis (n = 6), idiopathic nonspecific interstitial pneumonia (n = 3), idiopathic pulmonary fibrosis (n = 2), connective tissue disease–related ILD (n = 1), smoking-related ILD (n = 1), and sarcoidosis (n = 1). A minimum of 2 biopsy samples per procedure (range, 2–5) were obtained from different lung segments, with an average diameter of 0.7±0.3 cm. HHG imaging did not compromise tissue quality, as confirmed by histological evaluation.

The mean turnaround time from sample placement to completion of the HHG mosaic image was 7±1.8 minutes. This included 4.9±1.7 minutes for sample loading and positioning and 2.1±0.6 minutes for imaging.

On the basis of H&E slides, 36 biopsies (73%) were deemed adequate, while 13 (27%) were inadequate. Interrater agreement for H&E adequacy assessment was substantial (κ = 0.748 [95% confidence interval (CI), 0.545–0.950]). Using HHG images, 34 biopsies (69%) were classified as adequate, with a similar interrater agreement (κ = 0.820 [95% CI, 0.652–0.988]). Reasons for inadequacy included proximal sampling (bronchus or vessel-dominant tissue), advanced fibrosis, or the presence of only normal lung tissue. The sensitivity and specificity of HHG-based adequacy were 86.1% (95% CI, 70.5–95.3%) and 76.9% (95% CI, 46.2–94.7%), respectively. Representative HHG images of adequate and inadequate samples are shown in Figure 1.

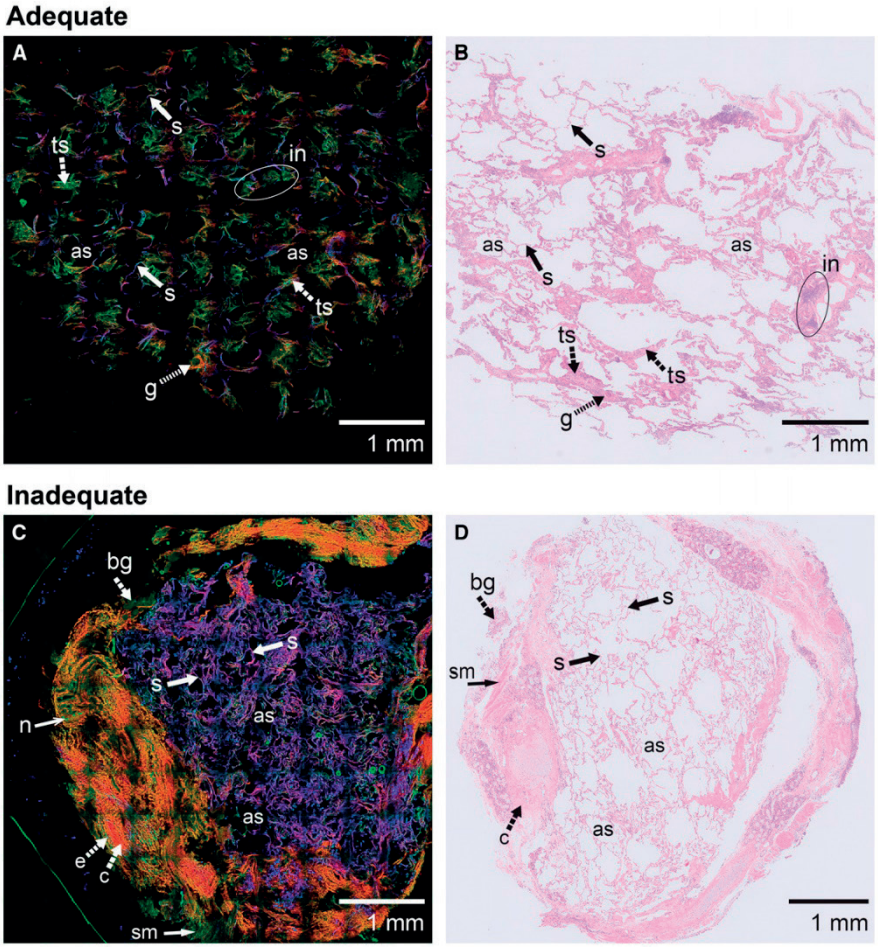


Figure 1. Adequacy assessment of transbronchial cryobiopsies. (A and C) Images obtained by higher harmonic generation microscopy of freshly obtained, unprocessed, transbronchial cryobiopsy samples. Three imaging modalities

are integrated: third-harmonic generation (green), revealing tissue interfaces and cellular morphology; second-harmonic generation (red), highlighting collagen fibers; and two-photon excited auto-fluorescence (blue), visualizing autofluorescent molecules in the cytoplasm and extracellular matrix. (B and D) Corresponding hematoxylin and eosin–stained biopsy samples. (A and B) Example of an adequate peripheral lung biopsy as indicated by the presence of alveolar septa and alveolar spaces. A patchy distribution of thickened septa with cellular infiltrates and granulomas (g) is seen. The multidisciplinary discussion diagnosis of this patient was hypersensitivity pneumonitis. (C and D) Inadequate biopsy containing mainly normal parenchymal lung tissue as indicated by the presence of thin alveolar septa and alveolar spaces (as), without the influx of inflammatory cells or the presence of fibrotic tissue. The presence of bronchial wall tissue—bronchial glands, airway smooth muscle, a small neural branch, and airway wall tissue consisting of collagen and elastin—indicates that the biopsy was taken too proximally. as=alveolar space; bg=bronchial glands; c=collagen; e=elastin; g=histiocytic aggregate/granuloma; in=cellular infiltrate; n=small neural branch; s=alveolar septa; sm=airway smooth muscle; ts=thickened septa.

Our findings highlight the potential of HHG microscopy as an innovative tool for rapid on-site biopsy adequacy assessment in transbronchial cryobiopsy procedures. The high sensitivity observed suggests a low false-negative rate, indicating that biopsies deemed inadequate on HHG microscopy are unlikely to be sufficient on histopathological analysis. This capability could enable clinicians to obtain additional biopsies during the same procedure when initial samples are insufficient, thereby improving diagnostic yield and minimizing the need for repeat procedures.

Currently, rapid on-site evaluation is routinely used for cytology specimens during endoscopic procedures but is unavailable for histological specimens because of time-consuming processing steps. HHG microscopy, which analyses unprocessed samples, has the potential to bridge this gap by offering near instantaneous evaluation of histological biopsy samples.

The strengths of this study are its innovative concept, prospective design, inclusion of various ILD diagnoses, and blinded assessments by two experienced pathologists. High interrater agreement underscores the reproducibility of HHG image interpretation. However, the study's small sample size limits generalizability. In absence of formal criteria to define transbronchial cryobiopsy adequacy, we used criteria based on expert consensus and supporting literature (9–11). Accordingly, we included biopsies with a reasonable likelihood of contributing to ILD diagnosis and excluded those unlikely to be diagnostically useful, such as samples

consisting predominantly of central airway tissue, end-stage fibrosis, or entirely normal lung parenchyma. This pragmatic approach provided a feasible framework for on-site assessment; however, further refinement and formal validation are warranted. Although the current turnaround time of approximately 7 minutes may be considered lengthy compared with rapid on-site evaluation, ongoing refinements, including automation and artificial intelligence integration, have already reduced this to approximately 3 minutes in our latest workflow. In addition, HHG's imaging depth is currently restricted to 100 µm, which may necessitate manual sample rotation to obtain comprehensive assessments, increasing imaging time.

Our experience is that HHG image evaluation by the pathologists was rapid (1–2 min per biopsy sample). Although assessments in this study were done after the procedure, the digital format and short interpretation time, make (remote) real-time use feasible, regardless of the location of the pathologist.

HHG microscopy's potential extends beyond adequacy assessment. Its ability to visualize extracellular matrix components (collagen, elastin) and inflammatory cells without the need for staining, as demonstrated in Figure 2, may enhance understanding of respiratory pathophysiology. Furthermore, HHG microscopy's ability to perform in-depth tissue scanning facilitates generating three-dimensional reconstructions, enabling the assessment of the biopsy within its intrinsic architectural organization. Digital imaging capabilities allow remote consultation, education, and data storage, offering opportunities for global collaboration.

This pilot study highlights HHG microscopy as a feasible method for rapid on-site evaluation of transbronchial cryobiopsy adequacy.With further refinement and validation in larger cohorts, HHG microscopy has the potential to improve diagnostic yield and enhance the histopathological assessment of ILD.

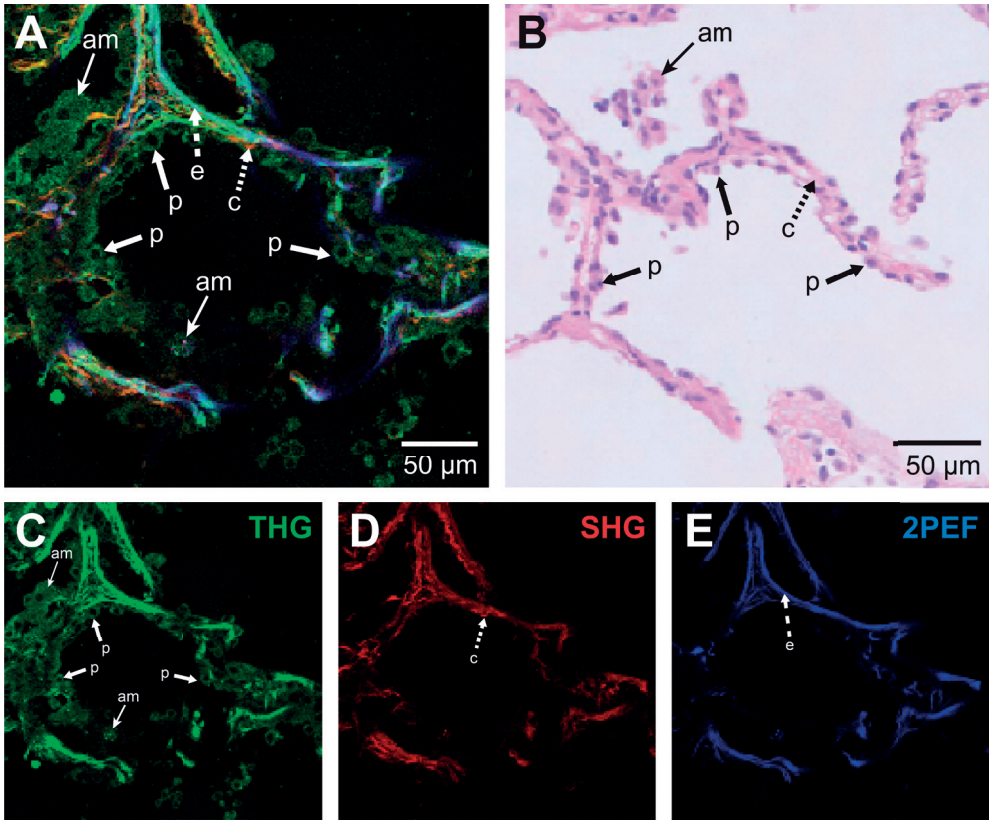


Figure 2. High-resolution imaging of alveolar tissue using HHG microscopy. (A) Integrated HHG image of alveolar tissue, where individual cells, such as type II pneumocytes and alveolar macrophages can be identified alongside extracellular matrix components, collagen and elastin, in the alveolar septa. (B) Corresponding H&E–stained biopsy sample. (C–E) Individual imaging components contributing to the integrated HHG image: (C) THG imaging, which highlights structural interfaces and cellular morphology in green; (D) SHG imaging, visualizing collagen fibers in red; and (E) 2PEF, which captures elastin fibers in blue. Interestingly, HHG clearly shows the presence of elastin fibers, which are not visible with the standard H&E stain. 2PEF=two-photon excited auto-fluorescence; am=alveolar macrophage; c=collagen; e=elastin; H&E=hematoxylin and eosin; HHG=higher harmonic generation; p=pneumocyte; SHG=second-harmonic generation; THG=third-harmonic generation.

Author disclosures are available with the text of this letter at www.atsjournals.org.

Acknowledgment: The authors thank Frank van Mourik (Flash Pathology B.V.) for technical support and Albert Stoop for transport of the mobile HHG microscope to Amsterdam UMC location AMC.

REFERENCES

1. Raghu G, Remy-Jardin M, Richeldi L, Thomson CC, Inoue Y, Johkoh T, et al. Idiopathic pulmonary fibrosis (an update) and progressive pulmonary fibrosis in adults: an official ATS/ERS/JRS/ALAT clinical practice guideline. Am J Respir Crit Care Med 2022;205:e18–e47.
2. Korevaar DA, Colella S, Fally M, Camuset J, Colby TV, Hagmeyer L, et al. European Respiratory Society guidelines on transbronchial lung cryobiopsy in the diagnosis of interstitial lung diseases. Eur Respir J 2022;60:2200425.
3. Kalverda KA, Ninaber MK, Wijmans L, von der Thusen J, Jonkers RE, Daniels JM, et al. Transbronchial cryobiopsy followed by as-needed surgical lung biopsy versus immediate surgical lung biopsy for diagnosing interstitial lung disease (the COLD study): a randomised controlled trial. Lancet Respir Med 2024;12:513–522.
4. van Huizen LMG, Radonic T, van Mourik F, Seinstra D, Dickhoff C, Daniels JMA, et al. Compact portable multiphoton microscopy reveals histopathological hallmarks of unprocessed lung tumor tissue in real time. Transl Biophotonics 2020;2:e202000009.
5. van Huizen LMG, Kalverda KA, Bugiani M, Poletti V, Bonta PI, Annema JT, et al. Rapid on-site pathology visualization of COVID-19 characteristics using higher harmonic generation microscopy. Am J Respir Crit Care Med 2023;208:199–200.
6. Tilbury K, Hocker J, Wen BL, Sandbo N, Singh V, Campagnola PJ. Second harmonic generation microscopy analysis of extracellular matrix changes in human idiopathic pulmonary fibrosis. J BiomedOpt 2014;19:086014.
7. van Huizen LMG, Blokker M, Daniels JMA, Radonic T, von der Thüsen JH, Veta M, et al. Rapid on-site histology of lung and pleural biopsies using higher harmonic generation microscopy and artificial intelligence analysis. Mod Pathol 2025;38:100633.
8. Van Huizen L, Mooij- Kalverda K, Poletti V, Bonta P, Daniels J, Groot M, et al. Instant pathology of transbronchial cryobiopsies (TBCB) for sample adequacy in ILD patients. Eur Respir J 2022;60:3701.
9. Colby TV, Tomassetti S, Cavazza A, Dubini A, Poletti V. Transbronchial cryobiopsy in diffuse lung disease: update for the pathologist. Arch Pathol Lab Med 2017;141:891–900.
10. Mehrad M, Colby TV, Rossi G, Cavazza A. Transbronchial cryobiopsy in the diagnosis of fibrotic interstitial lung disease. Arch Pathol Lab Med 2020;144:1501–1508.
11. Ravaglia C, Rossi G, Tomassetti S, Dubini A, Piciucchi S, Chilosi M, et al. Report standardization in transbronchial lung cryobiopsy. Arch Pathol Lab Med 2019;143:416–417.

Chapter 11

Rapid On-Site Pathology Visualization of COVID-19 Characteristics Using Higher Harmonic Generation Microscopy

Laura M. G. van Huizen[1], Kirsten A. Kalverda[2], Marianna Bugiani[3], Venerino Poletti[4], Peter I. Bonta[2], Jouke T. Annema[2], and Marie Louise Groot[1]

[1]LaserLab Amsterdam, Vrije Universiteit Amsterdam, Amsterdam, the Netherlands; [2]Department of Pulmonology and [3]Department of Pathology, Amsterdam University Medical Centers, Amsterdam, the Netherlands; and [4]Dipartimento di Medicina Specialistica Diagnostica e Sperimentale, University of Bologna/Pulmonology, Ospedale G.B.Morgagni, Forli, Italy

American Journal of Respiratory and Critical Care Medicine Volume 208 Number 2

A 61-year-old man without a relevant past medical history presented with cough and dyspnea and tested positive for severe acute respiratory syndrome coronavirus 2 (SARS-CoV-2) by PCR testing. Twelve days after disease onset, his condition deteriorated clinically, with respiratory failure requiring invasive mechanical ventilation. Chest computed tomography showed bilateral pulmonary embolism, diffuse ground-glass opacities, consolidations, and subpleural reticulation (Figure 1A). Infection other than COVID-19 was excluded with BAL. After 16 days of mechanical ventilation, he died of COVID-19 acute respiratory distress syndrome.

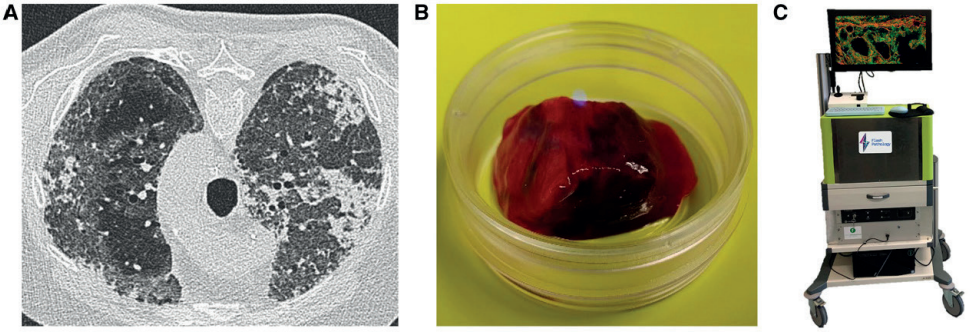


Figure 1. ICU chest computed tomography of a patient with coronavirus disease (COVID-19) shows diffuse ground-glass opacities, upper-lobe consolidations, and subpleural reticulation. The centrally located lung parenchyma appears relatively spared (A). Fresh, unprocessed autopsy lung tissue from the right upper lobe (B) was imaged with a mobile higher harmonic generation microscope (HHGM) (C). Technical details of the HHGM are described in our previous study (4).

Twenty hours after the time of death, an autopsy was performed. Resected unprepared lung tissue (1×2 cm^2) from the right upper lobe (Figure 1B), excised perpendicular to the bronchial tree, was immediately placed on a mobile higher harmonic generation microscope (HHGM) (Figure 1C). HHGM is a laser-based imaging technique that provides on-site images of unprocessed samples as large as 2 cm. Two-dimensional images and three-dimensional depth scans (up to 100 µm) can be acquired. HHGM images consist of three different signals visualizing cellular structures (green), collagen (red), and elastin fibers (blue). Earlier studies demonstrated the visualization of histological hallmarks of cancer in HHGM images (1–5).

Here, HHGM single images (0.5×0.5 mm^2) were acquired within 1–3 seconds, and "overview" images (2.5×2.5 mm^2) within 40 seconds to 2.5 minutes, depending on the image quality. HHGM images could be

interpreted immediately and showed lung architecture including alveolar septa, alveolar spaces, interlobular septa, blood vessels, and fibrin networks; cellular structures including pneumocytes, lymphocytes, and macrophages; and squamous metaplasia, in agreement with standard histology (Figure 2). Pathologists were able to identify COVID-19 characteristics, including inflammation with septal leukocyte infiltration, alveolar architecture distortion, and fibrosis with alveolar septa thickening due to an increased amount of collagen.

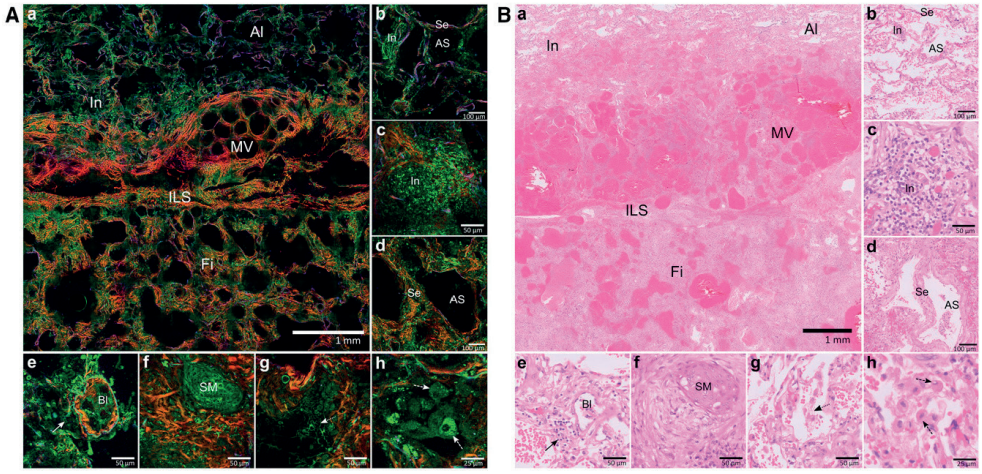


Figure 2. Higher harmonic generation microscope (HHGM) images of unprepared autopsy lung tissue of a deceased patient with coronavirus disease (COVID-19) show histopathological features (A) comparable to the corresponding standard histology images (B). HHGM visualizes lung architecture, including ILS (a), alveolar septa (Se), and alveolar spaces (AS) (b and d). Also, HHGM reveals Bl (e) and cellular elements, including lymphocytes (solid arrow) (e), SM (f), macrophages in fibrin (dotted arrow, g), and pigmented macrophages (striped arrow, h). This enables identification of normal Al and areas with different COVID-19–related pathologic features (a): In, Fi by thickening of the Se (d), and area showing dilated and partially destroyed ASs consistent with barotrauma induced by MV. The acquisition time of the 5κ5–mm² HHGM "overview" image (a) was 2.7 minutes (with 1 pixel per micrometer), and the acquisition time of the 0.5κ0.5–mm² magnified images (b–h) was 3.5 seconds (with 2 pixels per micrometer). Al= alveolar architecture; ASs= alveolar spaces; Bl= blood vessels; Fi= fibrosis; ILS= interlobular septa; In= inflammation; MV= mechanical ventilation; Se= alveolar septa; SM=squamous metaplasia.

This report shows that HHGM is able to rapidly visualize disease characteristics in fresh, unprepared lung tissue on site. Hence, HHGM has the potential to improve rapid diagnosis and understanding of lung diseases.

Author disclosures are available with the text of this article at www.atsjournals.org.

REFERENCES

1. Kuzmin NV, Wesseling P, Hamer PC, Noske DP, Galgano GD, Mansvelder HD, et al. Third harmonic generation imaging for fast, label-free pathology of human brain tumors. Biomed Opt Express 2016;7: 1889–1904.
2. van Huizen LMG, Kuzmin NV, Barbé E, van der Velde S, Te Velde EA, Groot ML. Second and third harmonic generation microscopy visualizes key structural components in fresh unprocessed healthy human breast tissue. J Biophotonics 2019;12:e201800297.
3. Zhang Z, de Munck JC, Verburg N, Rozemuller AJ, Vreuls W, Cakmak P, et al. Quantitative third harmonic generation microscopy for assessment of glioma in human brain tissue. Adv Sci (Weinh) 2019;6:1900163.
4. van Huizen LMG, Radonic T, van Mourik F, Seinstra D, Dickhoff C, Daniels JMA, et al. Compact portable multiphoton microscopy reveals histopathological hallmarks of unprocessed lung tumor tissue in real time. Transl Biophotonics 2020;2:e202000009.
5. You S, Sun Y, Chaney EJ, Zhao Y, Chen J, Boppart SA, et al. Slide-free virtual histochemistry (part II): detection of field cancerization. Biomed Opt Express 2018;9:5253–5268.

Part IV

Discussion

Chapter 12

General discussion

DISCUSSION

The overarching aim of this thesis was to evaluate how innovations in bronchoscopic techniques can contribute to the diagnostic work-up and assessment of interstitial lung disease (ILD) while reducing patient burden. The thesis is organized into three parts. The introduction (Chapter 1) provides background on ILD and current diagnostic bronchoscopic tissue sampling methods, including endosonography and transbronchial lung cryobiopsy. Also, three novel imaging technologies are introduced. Two in vivo techniques that can be used during bronchoscopy: polarization-sensitive endobronchial optical coherence tomography (PS-EB-OCT) and confocal laser endomicroscopy (CLE). A third technique called higher harmonic generation (HHG) microscopy; is used ex -vivo to asses biopsy specimens.

Part I (Chapters 2–4) addresses bronchoscopic sampling strategies. First, intrathoracic lymph node sampling comparing endobronchial ultrasound (EBUS) and esophageal ultrasound using an EBUS scope (EUS-B) for diagnosing stage I–II pulmonary sarcoidosis was investigated in a randomized controlled trial (RCT). In addition, patients were randomized between two different needle types (standard 22G needle and 25G core biopsy needle). Second, in suspected ILD patients with an indication for lung biopsy, a step-up strategy starting with transbronchial lung cryobiopsy is compared to immediate surgical lung biopsy. An accompanying economic evaluation assesses the cost-effectiveness of this step-up approach. **Part II** (Chapters 5–8) explores bronchoscopic imaging as an adjunct to conventional diagnostics, reporting exploratory findings on PS-EB-OCT for fibrosis quantification and detection of tissue specific features in ILD and on bedside CLE in acute respiratory failure. **Part III** (Chapters 9–11) focuses on ex vivo HHG microscopy applied to lung biopsy material, including transbronchial cryobiopsy specimens, with a particular emphasis on rapid tissue visualization and workflow support. The last part (Chapters 12–15) comprises the general discussion and Dutch and English summaries.

BACKGROUND

ILD comprises a broad and heterogeneous spectrum of diffuse parenchymal lung disorders with overlapping presentations but divergent prognosis and treatment, making accurate ILD classification essential (1-3).

While clinical data including HRCT discussed in a multidisciplinary discussion are central to diagnosis, tissue is considered helpful in a relevant subset of patients (4, 5). The preferred bronchoscopic approach depends on the suspected disease and procedural risk. In stage I–II pulmonary sarcoidosis, intrathoracic lymph nodes are an accessible target using endosonography and is recommended in international guidelines (6). However, whether a transbronchial (EBUS) or transesophageal (EUS-B) route is preferable remains debated. In other ILDs, decisions between transbronchial lung cryobiopsy and surgical lung biopsy involve trade-offs between diagnostic yield, safety, and resource use, and uncertainty persists in these vulnerable patient populations (7, 8). In addition, ARDS represents an acute diffuse parenchymal lung disease in which histologic heterogeneity may be clinically relevant, yet tissue is rarely obtained in the ICU, supporting interest in less invasive approaches to obtain microscopic lung tissue information.

PART I BRONCHOSCOPIC SAMPLING TECHNIQUES FOR DIAGNOSING INTERSTITIAL LUNG DISEASE

Chapters 2–4 focus on tissue acquisition techniques: endosonographic route and needle type selection in sarcoidosis (**Chapter 2**) and step-up lung biopsy versus immediate surgery, including cost–utility, in ILD (**Chapters 3–4**).

In **Chapter 2** (ISA trial), we compared trans bronchial needle aspiration (TBNA) by EBUS with fine needle aspiration (FNA) through EUS-B for granuloma detection in consecutive patients with suspected stage I and II pulmonary sarcoidosis. The study was built on the landmark GRANULOMA trial, which shifted practice toward endosonography-guided nodal sampling as a high-yield, less invasive, single diagnostic test. The GRANULOMA trial found that, in patients suspected of sarcoidosis stage I and II, endosonography (either by EBUS or EUS) has a higher diagnostic yield for granuloma detection than transbronchial mucosa- or lung biopsies(9).

The ISA trial in this thesis addressed a practical next step. Specifically, if endosonography is performed, does the route of access, endobronchial versus esophageal, matter? The study was performed in a global randomized 2×2 factorial design (14 hospitals, 9 countries; n=358). Granuloma detection rate was high and similar for both routes: 70% for EBUS versus

68% for EUS-B (p=0.67), with comparable sensitivity for sarcoidosis at 6-month follow-up (78% vs 82%, p=0.46). Adverse events were generally mild and comparable for both groups. These results indicate that both routes can be used safely and effectively, and that route selection can be guided by practical considerations (expertise, patient tolerance, and nodal accessibility) rather than expected yield. Within the ISA trial (**Chapter 2**), patients were additionally randomized to a standard 22G needle or a 25G ProCore needle use. Granuloma detection and sample representativeness were similar for both needles. This suggests that in stage I–II sarcoidosis, needle type does not affect diagnostic performance.

Although the sensitivity of EBUS and EUS-B for diagnosing sarcoidosis in the ISA trial was high (≈80%) and consistent with prior literature, a substantial minority of patients still remains without a pathology confirmed diagnosis (6). Moreover, within ISA, needle type (standard 22G vs 25G ProCore) did not improve granuloma detection rate, suggesting that simply changing needles is unlikely to close this diagnostic gap. Recent meta-analyses suggest that approaches aimed at obtaining larger core specimens, such as EBUS-guided transbronchial node biopsy compared with conventional TBNA, can improve diagnostic yield in mediastinal lymphadenopathy. Meta-analyses of dedicated FNB tip designs also suggest a potential yield benefit, although results are mixed and sarcoidosis-specific head-to-head data remain limited (10, 11). In the last decade, EBUS-guided transbronchial mediastinal cryobiopsy (cryo-EBUS) has emerged as a potential way to increase diagnostic yield. After an initial TBNA puncture creates a tract into the lymph node, a cryoprobe is advanced through this tract to obtain a frozen tissue core. In a recent randomized trial in suspected stage I–II sarcoidosis, Deng et al. reported a higher sensitivity for diagnosis sarcoidosis with cryo-EBUS compared with conventional TBNA (95% vs 84%) (12). Together with the growing literature on cryo-EBUS, this raises the question of how to position the technique in clinical practice (13, 14). At present, cryo-EBUS is still considered more invasive than TBNA, requires dedicated training and equipment, and is not widely available yet. Besides, as with any emerging procedure, early reports on cryo-EBUS may overestimate diagnostic performance due to selective reporting and center expertise, and the safest way to overcome the learning curve has not yet been clearly defined. The added value of cryo-EBUS to conventional EBUS-TBNA for granuloma detection remains to be established. The availability of rapid on-site evaluation (ROSE) may be of importance, in terms of when to escalate to

mediastinal cryobiopsy, as it can enable same-session decision making after a non-diagnostic TBNA sample.

In **Chapter 3** (the multicenter randomized COLD trial, performed in six Dutch hospitals), we compared a step-up strategy (transbronchial cryobiopsy, followed by surgical lung biopsy when needed) with immediate surgical lung biopsy in ILD patients with an indication for tissue sampling. The step-up strategy substantially reduced patient burden: unexpected chest tube drainage occurred in 11% (3/28) versus 46% (11/24) after immediate surgical lung biopsy (absolute risk reduction 35%, p=0.0058), hospital stay was shorter (median 1 vs 5 days), and post-procedural pain was lower in the step-up group. Overall diagnostic yield was similar between strategies (89% step-up vs 88% immediate surgical lung biopsy), while only 3/28 patients required subsequent surgical lung biopsy. Importantly, this is the first randomized trial comparing of these two diagnostic strategies, and it demonstrates that a less invasive-first approach can meaningfully reduce patient burden maintaining a high diagnostic yield. Limitations of the study include that although powered adequately for the primary endpoint the trial was not powered for smaller differences in diagnostic yield or diagnosis-specific effects. Blinding was not feasible, and knowledge of biopsy type may have influenced multidisciplinary decision-making, particularly since reference-pathologist confidence was lower in the step-up group. However, inter-observer variability was similar between groups, indicating that lower confidence did not translate into poorer agreement. This may reflect that current criteria for "high-confidence" diagnoses are largely derived from surgical lung biopsy–based definitions.

In **Chapter 4**, we performed a cost–utility analysis alongside the COLD trial, comparing the step-up strategy with immediate surgical lung biopsy from both health-care and societal perspectives over 12 weeks. In 47 patients (25 step-up; 22 immediate surgical lung biopsy), the step-up strategy was economically dominant, combining lower costs with better health outcomes. Mean health-care costs were €4,644 versus €8,935 (difference -€4,291; p<0.001) and societal costs were €6,873 versus €12,924 (difference -€6,051; p=0.001), largely driven by shorter inpatient stay and fewer surgical procedures, as well as higher productivity losses after immediate surgical lung biopsy. The step-up strategy also yielded a small but significant QALY gain after baseline adjustment (Δ0.025; 96% CI 0.004–0.047; p=0.04), supporting implementation of the step-up strategy as the preferred diagnostic approach when lung tissue is

required. Limitations should be considered when interpreting these economic findings. First, the analysis was trial-based with a 12-week time horizon, and therefore does not capture longer-term outcomes or downstream effects on treatment trajectories. Second, costs and resource use reflect the Dutch healthcare setting, which may limit generalizability to countries with different unit costs and pathways. However, it is not expected that the overall conclusions will change substantially with a longer follow-up or in a different country, because the observed differences were primarily driven by short-term, procedure-related factors that occur early after biopsy, most notably the need for inpatient hospital stay and chest tube drainage after surgical lung biopsy. Moreover, most relevant complications and recovery-related quality-of-life effects manifest within weeks of the procedure, which are captured within the 12-week horizon.

Overall, the results, from **Chapter 3 and 4**, support the step-up strategy as the preferred approach when histology is indicated.

However, surgical approaches are becoming less burdensome, which may shift the balance between diagnostic yield and patient burden. In this context, non-intubated thoracoscopic surgery (NITS), also known as awake or spontaneously breathing VATS, is gaining interest as an alternative to conventional VATS for surgical lung biopsies. NITS a surgical technique in which patient are not intubated and ventilated. This is of interest as it is suggested that an exacerbation of the underlying ILD, which is very serious adverse event sometimes leading to death, may be due to acute lung injury from mechanical ventilation (15, 16). In addition, NITS is associated with reduced post-operative pain and shorter recovery period (17). As the chest tube is usually removed within 2 hours following surgery, patients can be discharged the same day (18). When these techniques become reproducible outside expert centers, they could shift the balance in fibrotic ILD back toward surgical biopsy in selected patients and, in doing so, reshape how the COLD step-up strategy should be interpreted in contemporary practice.

This highlights that the optimal biopsy technique is dynamic and context dependent, and should be revisited as both bronchoscopic and surgical techniques evolve. In this setting, a recent expert statement emphasize that lung biopsy should be considered a selective test, best discussed in an MDT discussion, and pursued when histology is expected to add meaningful information beyond clinical and radiologic data. Technique

selection should be tailored to the differential diagnosis, local expertise and facilities, and the anticipated balance between diagnostic gain, patient burden, and the risk of adverse events (8). At the same time, increasing caution around biopsy also has potential downsides. A highly restrictive tissue policy may normalize diagnostic uncertainty, increase reliance on imperfect HRCT based categorization, and promote "lumping" into broad labels such as unclassifiable fibrotic ILD or progressive pulmonary fibrosis, even when histology could meaningfully influence early treatment choices or prognostic counselling in carefully selected patients. Furthermore, it provides biological reference material that is essential to validate emerging tools such as quantitative imaging analytics, molecular profiling, and novel bronchoscopic imaging techniques and develop novel treatments that specifically impact on lung tissue molecular signatures. These considerations support a strategy that is neither biopsy by default nor biopsy avoidance, but a deliberate effort to maximize clinical value while minimizing harm, supported by continued development of less invasive methods that provide biological information.

PART II BRONCHOSCOPIC IMAGING TECHNIQUES FOR THE ASSESSMENT OF INTERSTITIAL LUNG DISEASE AND ARDS

In **Chapters 5-8**, we demonstrate that minimally invasive bronchoscopic novel imaging techniques can add microscopic tissue specific information beyond conventional CT.

Chapter 5 provides an overview of bronchoscopic optical coherence tomography (OCT) and confocal laser endomicroscopy (CLE), and discusses their applications for diagnosis and monitoring across a variety of pulmonary diseases, including ILD.

In **Chapter 6**, it was shown that polarization sensitive endobronchial optical coherence tomography (PS-EB-OCT) was able to detect and quantify fibrotic changes in the lung. In a prospective exploratory study of 19 patients (16 ILD patients; 3 asthma controls), PS-EB-OCT was feasible and safe, added ~5–10 minutes without procedure-related adverse events, and enabled automated quantification of birefringent area in 49 lung segments. Birefringent area correlated with histologically confirmed fibrosis and discriminated histological confirmed extend of fibrosis better than HRCT (AUROC 0.96 vs 0.83; accuracy 0.77 vs 0.60).

In addition, PS-EB-OCT visualized ILD-relevant microfeatures (e.g. interstitial and destructive fibrosis including microscopic honeycombing, traction bronchiectasis, and airway-centered fibrosis in patient with fibrotic HP), suggesting potential clinical value when conventional imaging is inconclusive. Our findings are in line with a landmark study by Nandy et al., suggesting that certain microstructural signatures may be detectable without a biopsy (19). Nevertheless, some issues need to be resolved before this technique can be clinically implemented, some of which were discussed through a correspondence letter (**Chapter 7**). In short, larger cohorts with longer follow-up are required to validate robustness across diagnoses and to determine how birefringence relates to clinically meaningful outcomes, including progression and treatment response. Second, clinically interpretable thresholds remain unknown. It is unclear what constitutes "high" birefringence in an individual patient and how this may vary with age, smoking status, or other exposures. Third, blinded and standardized interpretation frameworks are needed, ideally including studies that assess whether independent observers can reliably recognize and classify specific OCT patterns.

In the coming years, the broader applicability of PS-EB-OCT may become increasingly relevant. For example, the expected rise in incidentally detected interstitial lung abnormalities (ILAs) will likely intensify the need to distinguish minimal radiologic change from true early fibrotic remodeling (20). In this setting, bronchoscopic tissue-level microscopic imaging could offer a way to test whether subtle HRCT abnormalities correspond to microscopic fibrosis, and longitudinal measurements might allow earlier detection of progression than currently feasible with standard imaging alone.

Confocal laser endomicroscopy (CLE) offers a complementary view to OCT by visualizing the alveolar compartment at an even higher, subcellular resolution. **In Chapter 8**, we assessed whether bedside CLE can be incorporated into routine ICU bronchoscopy and whether it provides microscopic information beyond chest CT. In this single-center pilot study, 33 mechanically ventilated patients underwent 41 CLE procedures. Feasibility was 100%, the procedure added less than five minutes to bronchoscopy, and no CLE-attributed adverse events occurred. CLE enabled a systematic assessment of alveolar filling and architecture. Abnormalities were frequently seen in CT-normal segments, and in a subset of CT ground-glass segments CLE showed architectural remodeling that resembled patterns seen in areas with overt reticulation. Together with ex vivo–validated

fibrotic features, these findings suggest that CLE may detect early fibroproliferative microstructural changes that can be underestimated on CT. Although we acquired a substantial number of videos (n=150), they were obtained from a limited number of patients (n=33), and analyses did not adjust for within-patient clustering. In addition, CLE image assessment was performed by expert consensus without formal inter-observer variability testing, limiting conclusions on reproducibility.

The clinical rationale for studies like these in ARDS is underscored by the observation that among patients who meet clinical ARDS criteria, only about half show diffuse alveolar damage (DAD) on histology (21). This distinction is clinically relevant, as DAD is associated with worse outcomes (22). The desire to identify DAD and alternative causes of respiratory failure is reflected in centers that perform lung biopsies in non-resolving ARDS, which often lead to changes in therapy (23). However, surgical biopsy in this population carries substantial morbidity and mortality, and published series are strongly affected by selection and indication bias. Transbronchial cryobiopsy may offer a less invasive alternative, but current evidence is limited and adverse events remain common, even though management changes are frequent after biopsy (24-26).

More evidence is needed, ideally with histology as a reference standard in well-designed validation studies. In practice, obtaining matched histology in critically ill ARDS patients will remain challenging. One pragmatic approach could be validation against autopsy material, at least to establish whether endobronchial microscopic tissue imaging patterns can reliably identify DAD and key alternative pathologies. If such validation is achieved, endoscopic microscopic tissue imaging could offer a safer way to better characterize ARDS patients at the bedside, while reducing reliance on high-risk tissue biopsy. Future work should include blinded image assessment by multiple raters, developing AI algorithms for image interpretation, study structured CLE correlation with clinical ARDS phenotypes, and evaluation of associations with longer-term outcomes.

Future work should include blinded image assessment by multiple raters, structured correlation with clinical phenotypes, and evaluation of associations with longer-term outcomes. Because CLE is a point-sampling technique with a limited field of view, multimodal integration may add value. Combining CLE with PS-EB-OCT could connect alveolar-level detail to a broader spatial context and to fibrosis-related signals.

Building on the above, minimally invasive bronchoscopic "optical biopsy" approaches such as OCT and CLE, could be positioned as an intermediate step between CT-based assessment and tissue biopsy in ILD and ARDS. To date, these add-on imaging techniques have not been associated with reported adverse events, although published experience is largely limited to expert centers.

Endobronchial imaging is most logically positioned as an add-on to bronchoscopic procedures that are already routinely performed. In contemporary ILD diagnostics, bronchoalveolar lavage (BAL) is often performed in the work-up of ILD patients that remain unclassified. BAL is performed by wedging the bronchoscope in a subsegmental bronchus, instilling sterile saline into the distal airspaces, and retrieving the fluid for analysis of inflammatory cells and soluble components. Although BAL is rarely diagnostic on its own, a marked lymphocytosis can substantially increase diagnostic confidence, particularly when hypersensitivity pneumonitis, alveolar sarcoidosis, or cellular NSIP are considered. In a smaller subset of conditions, BAL findings may be directly diagnostic, including pulmonary Langerhans cell histiocytosis, pulmonary alveolar proteinosis and diffuse alveolar hemorrhage (27-29). In addition, there is growing interest in BAL profiling beyond diagnosis. With antifibrotics now available for progressive pulmonary fibrosis, there is an increasing need to identify patients at risk of progression early and to move toward biomarker guided prognostication and treatment selection. Several candidate biomarkers are being explored in BAL based analyses, but robust and widely validated markers are not yet available (30-32). Therefore, combining endobronchial imaging techniques with BAL is an attractive strategy, as BAL is widely available, familiar, and generally safe, and it would allow direct correlation between imaging features and local cellular or inflammatory profiles obtained from the same lung region. In addition to BAL, OCT and CLE provide microstructural information rather than cellular or soluble marker data, and could therefore complement BAL based profiling within the same minimally invasive procedure.

PART III NOVEL IMAGING TECHNIQUE FOR RAPID ASSESSMENT OF LUNG TISSUE IN INTERSTITIAL LUNG DISEASE

Despite the promise of bronchoscopy-facilitated microscopic tissue specific *in vivo* imaging, tissue sampling remains indicated when

non-invasive evaluation does not yield a classifying diagnosis and the MDD expects added value from histopathology. In ILD, our work supports a step-up approach starting with transbronchial cryobiopsy. However, transbronchial cryobiopsy performance varies across centers and operators, in part due to differences in experience, technique, and sampling error (33-35). This variability strengthens the case for improving biopsy workflows to reduce inconclusive samples and avoid additional invasive procedures. Within this context, higher harmonic generation (HHG) microscopy may be a useful addition to the biopsy workflow.

In **Chapter 9**, we evaluated HHG microscopy on fresh, unprocessed lung tissue. We report 65 biopsies from 18 ILD patients imaged on site. HHG images could be interpreted by two ILD-expert pathologists and showed close agreement with matched conventional histology. Key ILD-relevant features were recognized, including inflammatory and fibrotic regions, architectural distortion, and microscopic honeycombing. A further advantage is that HHG provides simultaneous, label-free visualization of multiple microstructural components within a single image (e.g., collagen, elastin, and cellular structures), whereas conventional pathology typically requires multiple stains for different components. This is relevant because it enables quantitative analysis of signal intensities and component ratios, which may help distinguish more inflammatory from more fibrotic ILD patterns. Furthermore, 3D reconstruction enables depth-resolved tissue assessment beyond conventional 2D sections, which may reflect in vivo architecture more closely. Besides the limited sample size, an important limitation of this study includes that although the pathologists were blinded for clinical data and to each other, they had access to both the HHG images and H&E stained slides. This may have introduced confirmation bias. We tried to overcome this limitation by only including features that both pathologists had identified.

The rapid on-site tissue visualization was further illustrated in **Chapter 11**, where HHG imaging of fresh autopsy lung tissue from a patient with COVID-19 ARDS immediately revealed inflammation, alveolar architectural distortion and fibrosis with increased collagen, consistent with standard histology.

Because HHG is rapid and can be performed on site, it may support procedural feedback during biopsy. In **Chapter 10**, we prospectively evaluated HHG for rapid on-site adequacy assessment of TBLC in ILD. In 14 patients

(49 biopsies), HHG mosaics were generated within 7 ± 1.8 minutes. Two ILD-expert pathologists independently assessed adequacy on H&E and HHG with substantial agreement (κ 0.748 for H&E; κ 0.820 for HHG), supporting reproducible HHG interpretation. Using H&E as the reference, HHG adequacy assessment showed 86.1% sensitivity and 76.9% specificity. These results support HHG as a practical tool for rapid adequacy feedback during transbronchial cryobiopsy. However, this was a small pilot study, and biopsy adequacy performance estimates depend on the adequacy definition used. In addition, although imaging was rapid, adequacy assessment was performed offline after the procedure rather than truly in real time on site, meaning that direct workflow impact was not tested. These findings nevertheless support a prospective workflow study in which HHG is embedded during TBLC to evaluate whether real-time adequacy feedback reduces sampling error, increases diagnostic yield, and lowers the need for additional surgical biopsy.

A central limitation in ILD diagnostics is variability: interpretation differs between observers and between centers, and sampling error contributes to inconclusive results. HHG microscopy produces rapid, label-free images directly from fresh biopsy tissue and generates a consistent digital format. This makes it a good match for computer-assisted analysis. In a clinical workflow study in lung and pleural biopsies, van Huizen et al. showed that on-site HHG imaging can deliver a biopsy overview within minutes and that both pathologists and an AI algorithm could classify malignancy versus non-malignancy on HHG images with high feasibility, illustrating how HHG can turn “fresh tissue” into immediate, standardized digital information that is amenable to automated support (36).

In ILD specifically, Lami et al. demonstrated that a multimodal AI model combining histopathology with CT improved performance for UIP versus non-UIP and, importantly, substantially increased agreement and confidence among general pathologists. This supports the idea that AI can reduce interobserver variability when it is fed with complementary signals rather than a single modality (37).

FUTURE PERSPECTIVES

Ultimately, the goals of ILD care remain clear: to prolong survival, preserve quality of life, counsel patients honestly about prognosis, and move toward therapies that can stop, reverse, or even cure disease. Yet despite

major progress, including advancements in HRCT, the introduction of antifibrotics, and expanding treatment options for progressive fibrosing phenotypes, outcomes remain heterogeneous and many trials still show modest effects (38). This highlights that current diagnostic classification and CT patterns do not fully reflect the processes that drive disease progression. In that context, this thesis shows how novel imaging techniques may contribute to improve the diagnostic work up while reducing patient burden. It does so by adding approaches that aim lung tissue level assessment and by improving how tissue is obtained and evaluated when it is still required.

When lung tissue is indicated, randomized data show that starting with transbronchial cryobiopsy and reserving surgical lung biopsy for selected cases reduces procedure related burden while maintaining overall diagnostic yield, with favorable short term economic benefits. At the same time, recent expert guidance emphasizes that biopsy decisions and technique selection is complex and should be made in an MDT setting. The decision should be based on the differential diagnosis, local expertise and facilities, and the balance between expected diagnostic benefit and procedural risk (8). Looking forward, progress is most likely to come from a stepwise diagnostic strategy in which CT, bronchoscopic tissue-level microscopic imaging, and tissue based evaluation each contribute, rather than from a single replacement for histology. In future studies, PS-EB-OCT as add-on to standard immune-BAL bronchoscopy should be advanced into prospective multicenter ILD studies with standardized acquisition and blinded assessment. These studies should link fibrosis quantification and histologic patterns to ILD classification, progression, treatment response, and longer term outcomes in progressive pulmonary fibrosis. They should also focus on whether these measures are informative in earlier disease stages, such as interstitial lung abnormalities. In ARDS, future studies should validate bedside CLE patterns against robust reference standards and outcomes, to determine whether bronchoscopic tissue-level microscopic imaging can help identify DAD and key alternative pathology.

For patients who still require biopsy, the transbronchial lung cryobiopsy workflow can be improved. HHG microscopy can provide rapid, label free, digital visualization of fresh biopsy tissue, which may reduce sampling error and the rate of inconclusive procedures by enabling immediate feedback on specimen adequacy. Future studies should evaluate HHG in a prospective multicenter workflow design in which real time HHG

adequacy feedback guides additional sampling during TBLC, with endpoints including adequacy and diagnostic yield and confidence. In parallel, future studies may develop and validate straightforward quantitative measures from the different HHG image channels (THG, SHG, and 2PEF) and test whether these measures, potentially supported by artificial intelligence, can make biopsy interpretation more consistent.

Implementation research of any of the mentioned techniques should define training requirements, reproducibility across centers, and real world impact, including whether adding microscopic imaging to routine bronchoscopy can increase management confidence and diagnostic yield. Together, these future steps build on the findings of this thesis and may move ILD diagnostics toward greater precision with lower patient burden, while supporting earlier risk stratification and more targeted treatment decisions.

KEY FINDINGS

- Both endobronchial ultrasound (EBUS) and esophageal ultrasound using the EBUS scope (EUS-B) provide comparable diagnostic performance for stage I–II sarcoidosis; sampling route choice can be pragmatic (patient tolerance, anatomy, type of anesthesia, logistics, expertise).

- Both standard 22G TBNA needle and 25G ProCore needle provide comparable diagnostic performance for stage I–II sarcoidosis. Choice can be made upon availability and preference.

- When lung biopsy is indicated for diagnosing interstitial lung disease (ILD), a step-up strategy starting with transbronchial lung cryobiopsy and reserving surgical biopsy for inconclusive cases preserves overall diagnostic yield while reducing patient burden and complications.

- The step-up -cryobiopsy first- strategy is cost-effective, supporting broader implementation as standard care where expertise exists.

- In vivo polarization sensitive endobronchial optical coherence tomography (PS-EB-OCT) is feasible and safe and enables detection and quantification of fibrotic extent in the lung parenchyma. In addition, PS-EB-OCT identifies microscopic ILD tissue features, suggesting value as an add-on to CT when ILD detection and classification are challenging.

- Bedside confocal laser endomicroscopy (CLE) during routine ICU bronchoscopy is feasible and safe and adds alveolar-level information that can complement CT in ARDS patients.

- Higher harmonic generation microscopy can image fresh, unprocessed ILD biopsy tissue on site and allows ILD-expert pathologists to recognize key structures and patterns with close agreement to conventional histology

- HHG microscopy allows rapid on-site assessment of cryobiopsy adequacy with high sensitivity, with conventional histology as the reference standard

REFERENCES

1. Wijsenbeek M, Suzuki A, Maher TM. Interstitial lung diseases. Lancet. 2022;400(10354):769–86.
2. Ryerson CJ, Adegunsoye A, Piciucchi S, Hariri LP, Khor YH, Wijsenbeek MS, et al. Update of the international multidisciplinary classification of the interstitial pneumonias: an ERS/ATS statement. Eur Respir J. 2025;66(6).
3. Travis WD, Costabel U, Hansell DM, King TE, Jr., Lynch DA, Nicholson AG, et al. An official American Thoracic Society/European Respiratory Society statement: Update of the international multidisciplinary classification of the idiopathic interstitial pneumonias. Am J Respir Crit Care Med. 2013;188(6):733–48.
4. Hetzel J, Wells AU, Costabel U, Colby TV, Walsh SLF, Verschakelen J, et al. Transbronchial cryobiopsy increases diagnostic confidence in interstitial lung disease: a prospective multicentre trial. Eur Respir J. 2020;56(6).
5. Tomassetti S, Ravaglia C, Puglisi S, Ryu JH, Colby TV, Cavazza A, et al. Impact of Lung Biopsy Information on Treatment Strategy of Patients with Interstitial Lung Diseases. Ann Am Thorac Soc. 2022;19(5):737–45.
6. Crouser ED, Maier LA, Wilson KC, Bonham CA, Morgenthau AS, Patterson KC, et al. Diagnosis and Detection of Sarcoidosis. An Official American Thoracic Society Clinical Practice Guideline. Am J Respir Crit Care Med. 2020;201(8):e26–e51.
7. Raghu G, Remy-Jardin M, Richeldi L, Thomson CC, Inoue Y, Johkoh T, et al. Idiopathic Pulmonary Fibrosis (an Update) and Progressive Pulmonary Fibrosis in Adults: An Official ATS/ERS/JRS/ALAT Clinical Practice Guideline. Am J Respir Crit Care Med. 2022;205(9):e18–e47.
8. Mor E, Piciucchi S, Ravaglia C, Aronson K, Poletti V, Hariri LP, et al. Clinical utility of lung biopsy in fibrotic interstitial lung disease. American Journal of Respiratory and Critical Care Medicine. 2026.
9. von Bartheld MB, Dekkers OM, Szlubowski A, Eberhardt R, Herth FJ, in 't Veen JC, et al. Endosonography vs conventional bronchoscopy for the diagnosis of sarcoidosis: the GRANULOMA randomized clinical trial. Jama. 2013;309(23):2457–64.
10. Yang W, Yang H, Zhang Q, Herth FJF, Zhang X. Comparison between Endobronchial Ultrasound-Guided Transbronchial Node Biopsy and Transbronchial Needle Aspiration: A Meta-Analysis. Respiration. 2024;103(12):752–64.
11. Gupta N, Goel AD, Agrawal S, Juvva KS, Prasad VP, Maturu VN. Comparison of Diagnostic Yield and Performance of Franseen Tip Needle Versus Non-Franseen Tip Needle in Patients Undergoing Endobronchial Ultrasound-Guided Transbronchial Needle Sampling for Undiagnosed Mediastinal Lymphadenopathy: A Systematic Review and Meta-Analysis. J Bronchology Interv Pulmonol. 2026;33(1).
12. Deng M, Tang F, Chen Y, Zhao S, Tong R, Yang Z, et al. Endobronchial ultrasound-guided transbronchial mediastinal cryobiopsy versus transbronchial needle aspiration for diagnosing sarcoidosis: A randomized controlled trial. Endosc Ultrasound. 2025;14(5):266–73.
13. Zhang J, Guo JR, Huang ZS, Fu WL, Wu XL, Wu N, et al. Transbronchial mediastinal cryobiopsy in the diagnosis of mediastinal lesions: a randomised trial. Eur Respir J. 2021;58(6).

14. Fan Y, Zhang AM, Wu XL, Huang ZS, Kontogianni K, Sun K, et al. Transbronchial needle aspiration combined with cryobiopsy in the diagnosis of mediastinal diseases: a multicentre, open-label, randomised trial. Lancet Respir Med. 2023;11(3):256–64.
15. Lohser J, Slinger P. Lung Injury After One-Lung Ventilation: A Review of the Pathophysiologic Mechanisms Affecting the Ventilated and the Collapsed Lung. Anesth Analg. 2015;121(2):302–18.
16. Ferrando C, Carramiñana A, Piñeiro P, Mirabella L, Spadaro S, Librero J, et al. Individualised, perioperative open-lung ventilation strategy during one-lung ventilation (iPROVE-OLV): a multicentre, randomised, controlled clinical trial. Lancet Respir Med. 2024;12(3):195–206.
17. Guerrera F, Costardi L, Rosboch GL, Lyberis P, Ceraolo E, Solidoro P, et al. Awake or intubated surgery in diagnosis of interstitial lung diseases? A prospective study. ERJ Open Res. 2021;7(3).
18. Nguyen A, Jouitteau T, Bourdin A, Gamez AS, Solovei L, Molina J, et al. Exploring Benefits of Non-Intubated Surgery for Lung Biopsy in Interstitial Lung Disease. Respirology. 2025;30(10):949–56.
19. Nandy S, Raphaely RA, Muniappan A, Shih A, Roop BW, Sharma A, et al. Diagnostic Accuracy of Endobronchial Optical Coherence Tomography for the Microscopic Diagnosis of Usual Interstitial Pneumonia. Am J Respir Crit Care Med. 2021;204(10):1164–79.
20. Hatabu H, Hunninghake GM, Richeldi L, Brown KK, Wells AU, Remy-Jardin M, et al. Interstitial lung abnormalities detected incidentally on CT: a Position Paper from the Fleischner Society. Lancet Respir Med. 2020;8(7):726–37.
21. Thille AW, Penuelas O, Lorente JA, Fernandez-Segoviano P, Rodriguez JM, Aramburu JA, et al. Predictors of diffuse alveolar damage in patients with acute respiratory distress syndrome: a retrospective analysis of clinical autopsies. Crit Care. 2017;21(1):254.
22. Cardinal-Fernández P, Lorente JA, Ballén-Barragán A, Matute-Bello G. Acute Respiratory Distress Syndrome and Diffuse Alveolar Damage. New Insights on a Complex Relationship. Ann Am Thorac Soc. 2017;14(6):844–50.
23. Mir T, Regmi N, Saydain G, Kaul V, Soubani AO, Qureshi WT. Outcome and Post-Surgical Lung Biopsy Change in Management of ARDS: A Proportional Prevalence Meta-Analysis. Adv Respir Med. 2022;90(4):267–78.
24. Eisenmann S, Lambrecht N, Diessel L, Busse C, Nuding S, Vogt A. Transbronchial cryobiopsy in unexplained, severe ARDS: a single center retrospective case series. BMC Pulm Med. 2023;23(1):5.
25. Zhou G, Feng Y, Wang S, Zhang Y, Tian Y, Wu X, et al. Transbronchial lung cryobiopsy may be of value for nonresolving acute respiratory distress syndrome: case series and systematic literature review. BMC Pulm Med. 2020;20(1):183.
26. Li Q, Lafrance D, Liberman M, Leduc C, Charbonney E, Titova P, et al. Transbronchial Lung Cryobiopsies, Transbronchial Forceps Lung Biopsies, and Surgical Lung Biopsies in Mechanically Ventilated Patients with Acute Hypoxemic Respiratory Failure: A Retrospective Cohort Study. J Intensive Care Med. 2024;39(10):985–93.

27. Raghu G, Remy-Jardin M, Ryerson CJ, Myers JL, Kreuter M, Vasakova M, et al. Diagnosis of Hypersensitivity Pneumonitis in Adults. An Official ATS/JRS/ALAT Clinical Practice Guideline. Am J Respir Crit Care Med. 2020;202(3):e36–e69.
28. Ng MHV, Wettesinghe PV, Ryerson CJ, Khor YH. Clinical care in interstitial lung disease: a critical appraisal of clinical guidance documents. Eur Respir Rev. 2025;34(178).
29. Meyer KC, Raghu G, Baughman RP, Brown KK, Costabel U, du Bois RM, et al. An official American Thoracic Society clinical practice guideline: the clinical utility of bronchoalveolar lavage cellular analysis in interstitial lung disease. Am J Respir Crit Care Med. 2012;185(9):1004–14.
30. Simons IA, Korevaar DA, Denswil NP, Maitland-van der Zee AH, Nossent EJ, Duitman JW, et al. Prognostic biomarkers for the development of progressive pulmonary fibrosis in hypersensitivity pneumonitis: a systematic review. Eur Respir Rev. 2025;34(176).
31. Simons IA, Boerrigter BG, Hovestadt MCM, Mooij-Kalverda KA, Zhang S, Boers LS, et al. Alveolar cell composition in interstitial lung disease and the development of a pulmonary progressive fibrosing phenotype: a retrospective cohort study. Respir Res. 2025;26(1):164.
32. Watase M, Mochimaru T, Kawase H, Shinohara H, Sagawa S, Ikeda T, et al. Diagnostic and prognostic biomarkers for progressive fibrosing interstitial lung disease. PLoS One. 2023;18(3):e0283288.
33. Hostettler KE, Tamm M, Bubendorf L, Grendelmeier P, Jahn K, Stolz D, et al. Integration of transbronchial cryobiopsy into multidisciplinary board decision: a single center analysis of one hundred consecutive patients with interstitial lung disease. Respir Res. 2021;22(1):228.
34. Almeida LM, Lima B, Mota PC, Melo N, Magalhaes A, Pereira JM, et al. Learning curve for transbronchial lung cryobiopsy in diffuse lung disease. Rev Port Pneumol (2006). 2017.
35. Hetzel J, Maldonado F, Ravaglia C, Wells AU, Colby TV, Tomassetti S, et al. Transbronchial Cryobiopsies for the Diagnosis of Diffuse Parenchymal Lung Diseases: Expert Statement from the Cryobiopsy Working Group on Safety and Utility and a Call for Standardization of the Procedure. Respiration. 2018;95(3):188–200.
36. van Huizen LMG, Blokker M, Daniels JMA, Radonic T, von der Thüsen JH, Veta M, et al. Rapid On-Site Histology of Lung and Pleural Biopsies Using Higher Harmonic Generation Microscopy and Artificial Intelligence Analysis. Mod Pathol. 2025;38(1):100633.
37. Lami K, Ozasa M, Che X, Uegami W, Kato Y, Zaizen Y, et al. Enhancing Interstitial Lung Disease Diagnoses Through Multimodal AI Integration of Histopathological and CT Image Data. Respirology. 2025;30(8):726–35.
38. Cottin V, Valenzuela C. Evidence from recent clinical trials in fibrotic interstitial lung diseases. Curr Opin Pulm Med. 2024;30(5):484–93.

Chapter 13

English summary

ENGLISH SUMMARY

This thesis investigates how bronchoscopic techniques can improve the diagnostic work-up and assessment of interstitial lung diseases (interstitial lung disease, ILD). The central aims are to maintain (or increase) diagnostic certainty and to reduce patient burden by choosing less invasive strategies whenever possible. The thesis is built around three complementary components: (1) optimising sampling strategies when lung tissue is needed, (2) adding microscopic information through in vivo bronchoscopic imaging, and (3) improving the workflow and interpretation of biopsies through rapid ex vivo microscopy.

Part I Bronchoscopic sampling techniques for diagnosing interstitial lung disease

Chapter 2 focuses on granulomatous ILD: stage I and II sarcoidosis. In the international randomized ISA study, 358 patients from 14 centers worldwide were included with suspected stage I–II sarcoidosis. Patients were randomized between endobronchial ultrasound (EBUS) and esophageal ultrasound using an EBUS scope (EUS-B) for lymph node sampling. In addition, there was a second randomization between two needle types: a standard 22G EBUS needle and a 25G ProCore needle. The yield for detecting granulomas was comparable between both routes (70% in the EBUS group versus 68% in the EUS-B group; p=0.67). The representativeness of the lymph node material was also comparable for both needles (90.4% for 22G versus 91.1% for ProCore; p=0.829). The clinical message is that both EBUS and EUS-B achieve a high and similar diagnostic yield. Therefore, the choice of approach can mainly be made pragmatically, based on patient tolerance, type of sedation, and local expertise.

Chapters 3 and 4 focus on patients with suspected ILD in whom a biopsy is indicated. Lung tissue can be obtained by surgical lung biopsy (high diagnostic yield but invasive) or by transbronchial cryobiopsy (lower diagnostic yield but less invasive). The randomised COLD study (**Chapter 3**) compares a step-up strategy (starting with transbronchial cryobiopsy, with surgical lung biopsy only if results are inconclusive) with immediate surgical lung biopsy. In total, 55 patients were included from 6 hospitals in the Netherlands. The number of patients who required an unexpected chest drain was substantially higher in the immediate surgery group (11% in the step-up group versus 46% in the immediate surgery group; p=0.0058). Diagnostic yield was similarly high in both groups (89% in the step-up group versus 88% in the immediate surgery group; p=0.841),

while hospital stay, the amount of pain experienced, and the number of serious complications were higher in the immediate surgery group. The economic evaluation (**Chapter 4**) builds on these findings and shows that the step-up strategy is cost-effective. Taken together, these results support a "least-invasive-first" approach when histology is needed: start with cryobiopsy and reserve surgery for the minority of patients in whom this does not provide sufficient diagnostic certainty.

Part II Bronchoscopic imaging techniques for the assessment of interstitial lung disease and ARDS

Chapter 5 describes, in a review, the technical developments and clinical applications of optical coherence tomography (OCT) and confocal laser endomicroscopy (CLE) in respiratory medicine. Both techniques aim to bridge the gap between macroscopic imaging (HRCT) and invasive histology by adding microscopic in vivo information during bronchoscopy.

Chapter 6 evaluates polarization-sensitive endobronchial OCT (PS-EB-OCT) as an additional technique for fibrosis assessment in ILD, with histology as the reference. In 19 patients we show that PS-EB-OCT is feasible and able to detect and quantify fibrosis. The more fibrosis PS-EB-OCT detected, the more fibrosis was actually seen in the corresponding biopsies. Moreover, agreement with the histological fibrosis measure was better than that of CT. In addition, microscopic features relevant for ILD diagnostics could be recognized in PS-EB-OCT images. This supports the idea that PS-EB-OCT could potentially develop into an "optical biopsy", but it requires larger prospective studies for clinical validation, standardization, and interpretation frameworks.

Chapter 7 is a response to a study in which histological patterns are recognized based on endobronchial OCT. Although the results are promising, we emphasize the need for prospective validation, transparent reporting of the patient population, and especially standardization of measurements to ensure reproducibility and generalizability.

Chapter 8 brings the micro-imaging concept to the intensive care unit. We investigated bronchoscopic CLE in mechanically ventilated patients with respiratory failure. In 33 patients (41 procedures) we show that bronchoscopic CLE is feasible and safe in this setting. CLE can visualize patterns of alveolar filling (for example cells or fluid) and architectural changes that may complement conventional imaging. Therefore, bron-

choscopic CLE has the potential to add microscopic information without a biopsy, particularly in a population in whom invasive tissue sampling is often too risky.

Part III Novel imaging technique for rapid assessment of lung tissue in interstitial lung disease

In **Chapters 9–11** we introduce higher harmonic generation (HHG) microscopy as a rapid method to image fresh, unprocessed lung tissue. Normally, histological processing requires fixation, embedding, sectioning, and staining, which is time-consuming. HHG offers the possibility to obtain tissue-level structural information directly, within minutes.

Chapter 9 describes a proof-of-concept study in which we assessed 65 biopsies using HHG. Importantly, these were fresh, unprocessed biopsies that could be examined directly in the bronchoscopy suite or operating theatre. We show that images can be obtained within minutes and that two pathologists can recognize essential features of healthy and diseased lung tissue. HHG also enables simultaneous assessment of collagen, elastin, and cellular structures in a single image, without additional stains. This makes it possible to visualize their relative distribution. In addition, HHG microscopy allows depth scanning, so that 3D assessment can be added.

Chapter 10 explores clinical applicability as a "rapid on-site evaluation" (ROSE)-like tool for cryobiopsies. Because cryobiopsies sometimes contain insufficient informative tissue, rapid feedback on biopsy quality may increase diagnostic yield and may prevent additional (surgical) procedures. In this study, 49 cryobiopsies were assessed for "adequacy" based on HHG images, using conventional histology as the reference. This resulted in a sensitivity of 86.1% and a specificity of 76.9% for identifying adequate biopsies. These findings support that HHG can provide direct feedback during procedures.

Chapter 11 illustrates rapid HHG visualization in autopsy tissue from COVID-19 ARDS, demonstrating the technique in a context where rapid, label-free assessment of lung tissue can be valuable.

In **Chapter 12** the findings of this thesis are brought together and placed in clinical context, with attention to future perspectives. Overall, the results support a stepwise, patient-centered diagnostic approach: HRCT,

clinical data, and multidisciplinary discussion remain the basis. When additional certainty is needed, the data support a least-invasive-first strategy for tissue sampling. At the same time, the imaging chapters show that innovative bronchoscopic imaging and rapid ex vivo microscopy may contribute to ILD diagnostics and may improve workflow when tissue is obtained.

Chapter 14

Nederlandse samenvatting

NEDERLANDSE SAMENVATTING

Dit proefschrift onderzoekt hoe bronchoscopische technieken de diagnostische work-up en beoordeling van interstitiële longziekten (interstitial lung disease, ILD) kunnen verbeteren. Centrale uitgangspunten zijn het behouden (of vergroten) van diagnostische zekerheid én het verminderen van patiëntbelasting door waar mogelijk minder invasieve strategieën te kiezen. Het proefschrift is opgebouwd rond drie complementaire onderdelen: (1) optimaliseren van samplingstrategieën wanneer longweefsel nodig is, (2) toevoegen van microscopische informatie via bronchoscopische beeldvorming in vivo, en (3) verbeteren van workflow en interpretatie van biopten via snelle ex vivo microscopie.

Deel I Bronchoscopische samplingtechnieken om ILD te diagnosticeren

Hoofdstuk 2 richt zich op granulomateuze ILD: sarcoïdose stadium I en II. In de internationale gerandomiseerde ISA-studie werden 358 patiënten uit 14 centra wereldwijd geïncludeerd met een verdenking op sarcoïdose stadium I–II. Patiënten werden gerandomiseerd tussen endobronchiale echografie (EBUS) en oesofagiale echografie met een EBUS-scoop (EUS-B) voor lymfeklierpuncties. Daarnaast was er een tweede randomisatie tussen twee naaldtypen: een standaard 22G EBUS-naald en een 25G ProCore-naald. De opbrengst voor het aantonen van granulomen was vergelijkbaar tussen beide routes (70% in de EBUS-groep versus 68% in de EUS-B-groep; p=0,67). Ook de representativiteit van het verkregen kliermateriaal was vergelijkbaar voor beide naalden (90,4% voor 22G versus 91,1% voor ProCore; p=0,829). De klinische boodschap is dat zowel EBUS als EUS-B een hoge en vergelijkbare diagnostische opbrengst hebben. De keuze voor de benadering kan daarom vooral pragmatisch worden gemaakt, op basis van patiënttolerantie, type sedatie en lokale expertise.

Hoofdstuk 3 en 4 richten zich op patiënten met een verdenking op ILD bij wie een biopt geïndiceerd is. Het biopteren van longweefsel kan d.m.v. chirurgische biopten (hoge diagnostische opbrengst maar invasief) of middels transbronchiale cryobiopten (lagere diagnostische opbrengst maar minder invasief). De gerandomiseerde COLD-studie (Hoofdstuk 3) vergelijkt een step-up strategie (starten met transbronchiale cryobiopten, aanvullend chirurgische longbiopten alleen bij inconclusieve resultaten) met direct uitgevoerde chirurgische longbiopten. Er werden 55 patiënten geïncludeerd, afkomstig uit 6 verschillende ziekenhuizen in Nederland.

Het aantal patiënten dat een onverwachte thoraxdrain nodig had was aanzienlijk hoger in de directe chirurgie groep (11% in step-up groep versus 46% in de directe chirurgie groep (p=0.0058)). De diagnostische opbrengst tussen beide groepen was vergelijkbaar hoog (89% in step-up groep versus 88% in directe chirurgie-groep (p=0.841)), terwijl de ligduur in het ziekenhuis, de hoeveelheid pijn die mensen ervaarden en het aantal ernstige complicaties groter was in de directe chirurgie groep. De economische evaluatie (Hoofdstuk 4) bouwt hierop voort en laat zien dat de step-up strategie kosteneffectief is. Gezamenlijk ondersteunen deze resultaten een "least-invasive-first" benadering wanneer histologie nodig is: begin met cryobiopten en reserveer chirurgie voor de minderheid bij wie dit onvoldoende diagnostische zekerheid oplevert.

Deel II Bronchoscopische beeldvormende technieken voor de beoordeling van ILD en ARDS

Hoofdstuk 5 beschrijft in een review de technische ontwikkelingen en klinische toepassingen van optical coherence tomography (OCT) en confocale laser-endomicroscopie (CLE) binnen de longgeneeskunde. Beide technieken beogen een brug te slaan tussen macroscopische beeldvorming (HRCT) en invasieve histologie, door tijdens een bronchoscoop microscopische informatie in vivo toe te voegen.

Hoofdstuk 6 evalueert polarization-sensitive endobronchial OCT (PS-EB-OCT) als aanvullende techniek voor fibrosebeoordeling bij ILD, met histologie als referentie. In 19 patiënten laten we zien dat PS-EB-OCT haalbaar is en in staat is om fibrose te detecteren én te kwantificeren. Hoe meer fibrose PS-EB-OCT detecteerde, hoe meer fibrose daadwerkelijk in de corresponderende biopten werd gezien. Bovendien bleek de overeenkomst met de histologische fibrosemaat beter dan die van CT. Daarnaast konden in PS-EB-OCT-beelden microscopische kenmerken worden herkend die relevant zijn voor ILD-diagnostiek. Dit ondersteunt de gedachte dat PS-EB-OCT potentieel kan uitgroeien tot een vorm van "optisch biopt", maar vraagt om grotere prospectieve studies voor klinische validatie, standaardisatie en interpretatiekaders.

Hoofdstuk 7 is een reactie op een studie waarin histologische patronen worden herkend op basis van endobronchiale OCT. Hoewel de resultaten veelbelovend zijn, benadrukken we de noodzaak van prospectieve validatie, transparante rapportage van de patiëntpopulatie en vooral

standaardisatie van metingen om reproduceerbaarheid en generaliseerbaarheid te waarborgen.

Hoofdstuk 8 verplaatst het micro-imaging concept naar de intensive care. We onderzochten bronchoscopische CLE bij beademde patiënten met respiratoir falen. In 33 patiënten (41 procedures) tonen we dat bronchoscopische CLE haalbaar en veilig is in deze setting. CLE kan patronen van alveolaire vulling (bijvoorbeeld cellen of vocht) en veranderingen in architectuur zichtbaar maken die conventionele beeldvorming kunnen aanvullen. Daarmee heeft bronchoscopische CLE de potentie om microscopische informatie toevoegen zonder biopt, juist in een populatie waarin invasieve weefselafname vaak te risicovol is.

Deel III Nieuwe beeldvormende techniek voor snelle beoordeling van longweefsel in ILD

In **Hoofdstuk 9–11** introduceren we higher harmonic generation (HHG) microscopie als snelle methode om vers, onbewerkt longweefsel af te beelden. Normaal gesproken vereist histologische verwerking fixatie, inbedden, snijden en kleuren, wat een tijdrovend traject is. HHG biedt de mogelijkheid om direct, binnen minuten, structuurinformatie op weefselniveau te verkrijgen.

Hoofdstuk 9 beschrijft een proof-of-concept studie waarin we 65 biopten met HHG beoordeelden. Uniek is dat het om verse, onbewerkte biopten gaat, die direct op de bronchoscopie- of operatiekamer kunnen worden bekeken. We laten zien dat binnen enkele minuten beelden beschikbaar zijn en dat twee pathologen essentiële kenmerken van gezond en ziek longweefsel kunnen herkennen. HHG maakt bovendien gelijktijdige beoordeling van collageen, elastine en cellulaire structuren mogelijk in één beeld, zonder extra kleuringen. Dit maakt het mogelijk om de onderlinge verhoudingen weer te geven. Daarnaast biedt HHG microscopie de mogelijkheid tot dieptescans waardoor 3D-beoordeling kan worden toegevoegd.

Hoofdstuk 10 verkent de klinische toepasbaarheid als “rapid on-site evaluation” (ROSE)-achtig hulpmiddel voor cryobiopten. Omdat cryobiopten soms onvoldoende informatief weefsel bevatten, kan snelle terugkoppeling over bioptkwaliteit mogelijk de diagnostische opbrengst verhogen en aanvullende (chirurgische) procedures mogelijk voorkomen. In deze studie werden 49 cryobiopten op basis van HHG-beelden beoor-

deeld op “adequaatheid”, met conventionele histologie als referentie. Dit resulteerde in een sensitiviteit van 86,1% en een specificiteit van 76,9% voor het herkennen van adequate biopten. De bevindingen ondersteunen dat HHG kan bijdragen aan directe feedback tijdens procedures.

Hoofdstuk 11 illustreert de snelle HHG-visualisatie in autopsieweefsel van COVID-19 ARDS, als demonstratie van de techniek in een context waar snelle, label-vrije beoordeling van longweefsel waardevol kan zijn.

In Hoofdstuk 12 worden de bevindingen van dit proefschrift samengebracht en geplaatst in klinische context, met aandacht voor toekomstperspectieven. Overkoepelend ondersteunen de resultaten een stapsgewijze, patiëntgerichte diagnostische benadering: HRCT, klinische gegevens en multidisciplinaire bespreking blijven de basis. Wanneer aanvullende zekerheid nodig is, pleiten de data voor een least-invasive-first strategie voor weefselafname. Tegelijk laten de imaging-hoofdstukken zien dat innovatieve bronchoscopische beeldvorming en snelle ex vivo microscopie potentieel kunnen bijdragen aan ILD-diagnostiek en mogelijk de workflow kunnen verbeteren wanneer er weefsel wordt uitgenomen.

Appendices

PhD PORTFOLIO

Name PhD Student	Kirsten Alexandra Kalverda
PhD period	January 2018 – June 2026
Name PhD supervisor	Prof. dr. J.T. Annema
Name PhD co-supervisor	Dr. P.I. Bonta

PhD Training

Courses

EPIC training	2018
eBROK course	2020
Update	2023
Update	2026
Practical Biostatistics 2019	

Seminars, workshops and masterclasses

Thoracic ultrasound, yearly	2018–2020
ERS EBUS course, yearly	2018–2026
ILD course, Royal Brompton	2018
Cryobiopsy workshop, Tubingen	2019
Andreas Cursus, Amsterdam	2019
Virtual academy for ILD, ERS (online)	2020–2021
ILD Masterclass, Rotterdam	2022
Sarcoidosis Academy, Milaan	2023
Teach the teacher	2025

Presentations

Conventional Aspiration versus Biopsy needle: The International Sarcoidosis	2018
Assessment (ISA) RCT (poster discussion, ERS congress, Parijs)	
OCT and CLE in Interstitial lung disease (Oral presentation, Italian Pulmonology	2019

National Congress XLV AIPO, Florence)	
Towards real time image guided cryobiopsies (Online webinar, ERS, Amsterdam)	2019
Confocal laser endomicroscopy (CLE) in patients with acute respiratory failure on the ICU (Poster presentation, ERS congress, Madrid)	2019
Interobserver agreement on EBUS and EUS-B cytological specimens in patients with sarcoidosis (Poster presentation, ERS congress, online)	2020
Instant on site pathology of cryobiopsies in interstitial lung disease (poster presentation, ERS Congress, online)	2020
Adembenemend mooi (Oral presentation, Amsterdams longcongres, Amsterdam)	2020
Zorgpad poliklinische post-COVID (Oral presentation, Nederlandse internisten vereniging, online)	2021
Cryobiopsy and new imaging in ILD (ERS live, ERS Congress, online)	2021
In vivo PS-OCT to detect fibrotic lung disease (Oral presentation, ERS congress, online)	2021
CLE in ILD and ARDS (Workshop presentation, webinar by Mauna Kea, online)	2021–2022
Guiding techniques for cryobiopsy (Oral presentation, Transbronchial cryobiopsy in diffuse parenchymal lung disease, Ravenna)	2022
Instant pathology of transbronchial cryobiopsies (TBCB) for sample adequacy in ILD patients (Poster presentation, ERS congress, Barcelona)	2022
Cryo- versus surgical lung biopsy for diagnosing interstitial lung disease (ILD): the COLD RCT (Oral presentation, ERS congress, Milaan)	2023
Refereeravond Nieuwe diagnostische mogelijkheden bij ILD (Presentatie, regionale refereeravond, Amsterdam)	2023
Pro – Con Debat longbiopten in ILD (Debat, Amsterdams Longcongress, Amsterdam)	2023
"Trots van eigen bodem: COLD studie" (Oral presentation, symposium ILD: overview van ATS, WASOG, ERS 2024)	2024

Novel Imaging technique in ILD (Oral presentation, Landelijk pathologen congress, Den Haag)	2025

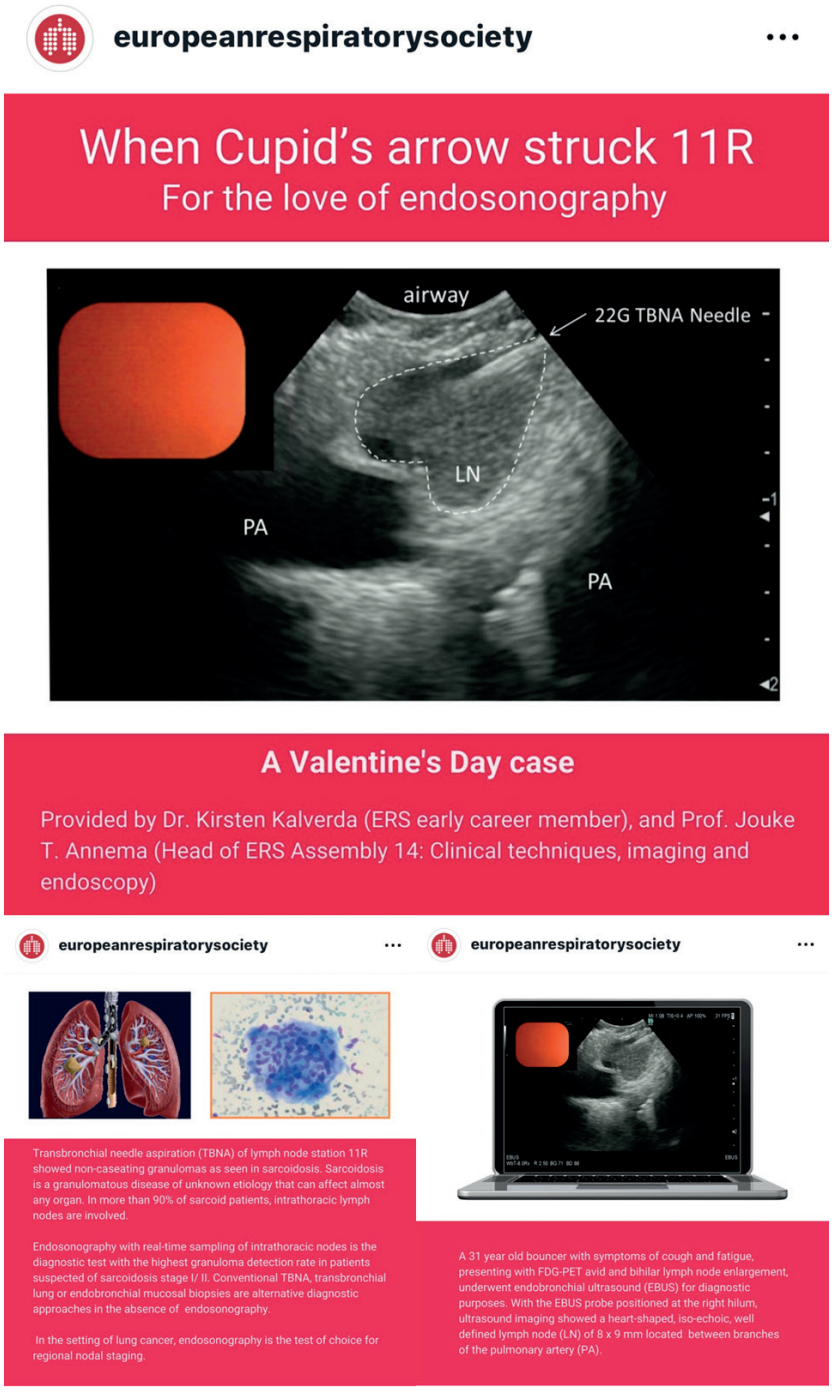
(Inter)national conferences

European Respiratory Society Congress, Parijs	2018
Italian Pulmonology National Congress XLV AIPO, Florence	2019
European Respiratory Society Congress, Madrid	2019
European Respiratory Society Congress, Online	2020
European Respiratory Society Congress, Online	2021
European Respiratory Society Congress, Barcelona	2022
Transbronchial cryobiopsy in diffuse parenchymal lung disease, Ravenna	2022
European Respiratory Society Congress, Milaan	2023
Nederlands Longartsen Congres, Papendal	2023
European Respiratory Society Congress, Wenen	2024
European Respiratory Society Congress, Amsterdam	2025

Lecturing

Longembolieën, COPD en Astma en Longfibrose (Amstel Academie)	2018–2020
Endosonography for diagnosing sarcoidosis (ERS EBUS course, Amsterdam)	2018–2019
Transbronchial cryobiopsy in ILD – How I do it (ERS congress, Vienna)	2024
Bronchoalveolaire lavage in ILD (Landelijke NVALT nascholing)	2025

This contribution was published on Valentine's Day 2022 as part of a European Respiratory Society social media campaign



LIST OF PUBLICATIONS

1. Crombag LMM, **Kalverda KA**, Szlubowski A, Gnass M, Tournoy KG, Sun J, Oki M, Ninaber MK, Steinfort DP, Jennings BR, Liberman M, Bilaceroglu S, Bonta PI, Korevaar DA, Trisolini R, Annema JT. EBUS versus EUS-B for diagnosing sarcoidosis: The International Sarcoidosis Assessment (ISA) randomized clinical trial. Respirology 2022 Feb;27(2):152-160.

2. **Kalverda KA**, Goorsenberg A, Annema J, Bonta P. Advances in Optical Coherence Tomography and Confocal Laser Endomicroscopy in Pulmonary Diseases. Respiration 2020;99(3):190-205

3. Mahomedradja RF, van den Beukel TO, van den Bos M, Wang S, **Kalverda KA**, Lissenberg-Witte BI, Kuijvenhoven MA, Nossent EJ, Muller M, Sigaloff KCE, Tichelaar J, van Agtmael MA. Prescribing errors in post - COVID-19 patients: prevalence, severity, and risk factors in patients visiting a post - COVID-19 outpatient clinic. BMC Emerg Med. 2022 Mar 5;22(1):35. doi: 10.1186/s12873-022-00588-7. PMID: 35247982; PMCID: PMC8897739.

4. **Kalverda KA**, Vaselli M, Wijmans L, de Bruin DM, Jonkers RE, Poletti V, de Boer J, Annema JT, Bonta PI. Endobronchial Optical Coherence Tomography: Shining New Light on Diagnosing Usual Interstitial Pneumonitis? Am J Respir Crit Care Med. 2022 Apr 15;205(8):967-968

5. Wijmans L, **Kalverda K**, de Bruin D, Brinkman P, van den Berk I, Roelofs JJTH, Jonkers R, Bonta PI, Annema J. Bronchoscopic Journey of in vivo Real-Time Microscopic Imaging in ILD: A Case Series. Respiration. 2022;101(11):1006-1014. doi: 10.1159/000526045. Epub 2022 Aug 31. PMID: 36044868; PMCID: PMC9811420.

6. Smesseim I, **Mooij-Kalverda K,** Hessels L, Korevaar DA, Atasever B, de Graaff H, Goorhuis A, Nossent E, Bos L, Bonta P; Amsterdam UMC HFNC study group:; van den Aardweg J, Boersma W, van der Lee I, Reesink HJ. High flow nasal cannula for acute respiratory failure due to COVID-19 in patients with a 'do-not-intubate' order: A survival analysis. Clin Respir J. 2023 Feb;17(2):115-119. doi: 10.1111/crj.13573. Epub 2022 Dec 30. PMID: 36584670; PMCID: PMC9880618.

7. Kramer T, Wijsman PC, **Kalverda KA**, Bonta PI, Annema JT. Advances in bronchoscopic optical coherence tomography and confocal laser endomicroscopy in pulmonary diseases. Curr Opin Pulm Med. 2023 Jan 1;29(1):11–20. doi: 10.1097/MCP.0000000000000929. Epub 2022 Nov 16. PMID: 36474462; PMCID: PMC9780043.

8. Chilunga FP, Appelman B, van Vugt M, **Kalverda K**, Smeele P, van Es J, Wiersinga WJ, Rostila M, Prins M, Stronks K, Norredam M, Agyemang C. Differences in incidence, nature of symptoms, and duration of long COVID among hospitalised migrant and non-migrant patients in the Netherlands: a retrospective cohort study. Lancet Reg Health Eur. 2023 Apr 7;29:100630. doi: 10.1016/j.lanepe.2023.100630. PMID: 37261215; PMCID: PMC10079482.

9. van Huizen LMG, **Kalverda KA**, Bugiani M, Poletti V, Bonta PI, Annema JT, Groot ML. Rapid On-Site Pathology Visualization of COVID-19 Characteristics Using Higher Harmonic Generation Microscopy. Am J Respir Crit Care Med. 2023 Jul 15;208(2):199–200

10. Guo L, Appelman B, **Mooij-Kalverda K**, Houtkooper RH, van Weeghel M, Vaz FM, Dijkhuis A, Dekker T, Smids BS, Duitman JW, Bugiani M, Brinkman P, Sikkens JJ, Lavell HAA, Wüst RCI, van Vugt M, Lutter R; Amsterdam UMC COVID-19 Biobank study Group. Prolonged indoleamine 2,3-dioxygenase-2 activity and associated cellular stress in post-acute sequelae of SARS-CoV-2 infection. EBioMedicine. 2023 Aug;94:104729. doi: 10.1016/j.ebiom.2023.104729. Epub 2023 Jul 26. PMID: 37506544; PMCID: PMC10406961.

11. van Huizen LMG, Blokker M, Rip Y, Veta M, **Mooij Kalverda KA**, Bonta PI, Duitman JW, Groot ML. Leukocyte differentiation in bronchoalveolar lavage fluids using higher harmonic generation microscopy and deep learning. PLoS One. 2023 Jun 27;18(6):e0279525. doi: 10.1371/journal.pone.0279525. PMID: 37368904; PMCID: PMC10298778.

12. **Kalverda KA**, Vaselli M, Thunnissen E, Tanck MWT, Mets OM, van den Berk IAH, Annema JT, Bonta PI, de Boer JF. In vivo polarisation sensitive optical coherence tomography for fibrosis assessment in interstitial lung disease: a prospective, exploratory, observational study. BMJ Open Respir Res. 2023 Aug;10(1):e001628

13. Kuut TA, Müller F, Csorba I, Braamse A, Aldenkamp A, Appelman B, Assmann-Schuilwerve E, Geerlings SE, Gibney KB, Kanaan RAA, **Mooij-Kalverda K**, Olde Hartman TC, Pauëlsen D, Prins M, Slieker K, van Vugt M, Keijmel SP, Nieuwkerk P, Rovers CP, Knoop H. Efficacy of Cognitive-Behavioral Therapy Targeting Severe Fatigue Following Coronavirus Disease 2019: Results of a Randomized Controlled Trial. Clin Infect Dis. 2023 Sep 11;77(5):687-695. doi: 10.1093/cid/ciad257. PMID: 37155736; PMCID: PMC10495128.

14. **Kalverda KA**, Ninaber MK, Wijmans L, von der Thüsen J, Jonkers RE, Daniels JM, Miedema JR, Dickhoff C, Hölters J, Heineman D, Kant M, Radonic T, Shahin G, Cohen D, Boerrigter B, Nijman S, Nossent E, Braun J, Mathot B, Poletti V, Hetzel J, Dijkgraaf M, Korevaar DA, Bonta PI, Annema JT. Transbronchial cryobiopsy followed by as-needed surgical lung biopsy versus immediate surgical lung biopsy for diagnosing interstitial lung disease (the COLD study): a randomised controlled trial. Lancet Respir Med. 2024 Jul;12(7):513-522

15. Simons IA, Boerrigter BG, Hovestadt MCM, **Mooij-Kalverda KA**, Zhang S, Boers LS, van der Zee AHM, Nossent EJ, Duitman JW. Alveolar cell composition in interstitial lung disease and the development of a pulmonary progressive fibrosing phenotype: a retrospective cohort study. Respir Res. 2025 Apr 28;26(1):164. doi: 10.1186/s12931-025-03236-3. PMID: 40296077; PMCID: PMC12038994.

16. **Kalverda KA**, van Huizen LMG, von der Thüsen J, Poletti V, Radonic T, Dickhoff C, Daniels JMA, Bonta PI, Annema JT, Groot ML. Rapid On-Site Ewvaluation of Cryobiopsies in Interstitial Lung Disease Using Higher Harmonic Generation Microscopy. Am J Respir Crit Care Med. 2025 Oct;211(10):1876-1879

17. **Kalverda K,** van Barreveld M, Bonta P, Daniels J, Dickhoff C, Korevaar DA, Annema J, Dijkgraaf M. Transbronchial cryobiopsy followed by as-needed surgical lung biopsy versus immediate surgical lung biopsy for diagnosing interstitial lung disease: a cost-utility analysis. ERJ Open Res. 2026 Feb 9;12(1):00629-2025. doi: 10.1183/23120541.00629-2025. PMID: 41668879; PMCID: PMC12884382.

ABOUT THE AUTHOR

Kirsten Alexandra Kalverda was born on 28 March 1984 in Utrecht and grew up in Nieuwegein with her younger brother and parents. After graduating from secondary school (VWO) at Cals College in Nieuwegein in 2002, she moved to Wisconsin, USA, for one year. There, she lived with a host family and studied at the University of Wisconsin.

In 2003, she started medical school at the University of Amsterdam. She obtained her medical degree in 2011, after taking a gap year during which she travelled through Southeast Asia. She then worked as a resident not in training at the Rode Kruis Hospital in Beverwijk in internal medicine, gastroenterology and pulmonology.

In 2013, she started her pulmonary medicine training at Spaarne Hospital in Hoofddorp and later also in Haarlem. In 2018, she moved to the Academic Medical Center (later: Amsterdam UMC), where she combined her specialist training with a PhD trajectory under the supervision of Prof. Dr J.T. Annema. This thesis is the result of that work.

In 2020, during the first wave of the COVID-19 pandemic, she completed her training as a pulmonologist. She subsequently worked as a pulmonologist at Amsterdam UMC until 2023. In 2023, she moved to Dijklander Hospital (Hoorn and Purmerend), where she has been working as a pulmonologist since then.

Kirsten is married to Ralph Mooij. Together they have two daughters, Isabella (2014) and Eveline (2015). Thomas and Sebastiaan are, of course, part of the family as well.

DANKWOORD

Dit proefschrift had niet tot stand kunnen komen zonder de hulp van een heleboel slimme, lieve, inspirerende en behulpzame mensen. Ik ben dankbaar dat ik jullie om mij heen heb. Iedereen die heeft bijgedragen aan dit proefschrift: enorm bedankt. Zonder jullie had ik dit niet kunnen volbrengen. In het bijzonder noem ik:

Alle patiënten die aan onze studies hebben deelgenomen, zonder jullie bereidheid zouden er geen wetenschappelijke studies zijn, en geen vooruitgang in de geneeskunde.

Mijn promotor, Jouke Annema. Ik weet nog goed dat ik voor het eerst bij je op gesprek kwam; nooit had ik kunnen bedenken waar we acht jaar later zouden staan. Je hebt me warm, enthousiast en tegelijk strak begeleid, met oog voor zowel de professionele doelen als de menselijke kant. Als ik het even niet meer zag, kwam jij met een pragmatische en verhelderende oplossing. Ik heb me door jouw begeleiding altijd gehoord en geholpen gevoeld. Ook je aanstekelijke enthousiasme voor avonturen buiten de werkvloer is inspirerend gebleken.

Mijn co-promotor, Peter Bonta. Alleskunner. Altijd vrolijk, altijd bereid om te helpen en altijd vol ideeën. Ik bewonder hoeveel passie jij tegelijkertijd hebt voor de patiënten, de kliniek en de wetenschap. Het is echt mijn wens om door te gaan met waar we samen al mee begonnen zijn, want met jou samenwerken is een feest. Je kunt op de juiste momenten kritisch zijn, maar weet me tegelijk met jouw positieve energie altijd weer te motiveren.

Mijn paranimfen. Laurence Crombag, met jouw oprechte aandacht voor wie ik ben naast mijn werk voelde het meteen vertrouwd. En toen bleek dat we een ISA-baby deelden, was het natuurlijk helemaal goed. Ik bewonder je drive; je wil om het goed te doen. Maar het meest heb ik aan je relativeringsvermogen. Het is altijd zo fijn om even bij je langs te komen of je te bellen, en te kunnen kletsen over de écht belangrijke dingen van het leven.
Lianne Alink, jouw reactie toen ik vertelde dat ik ging promoveren was echt goud. Zo mooi dat ik oprecht ging twijfelen of jij of ik nou ging promoveren. Een betere paranimf kan ik me dus niet wensen. Maar nog veel belangrijker is jouw aanwezigheid als vriendin. Ook bij jou kan ik terecht voor een heerlijk potje relativeren. Ik koester alle -bijzonder

nette- avonturen die we samen hebben beleefd, en ik hoop dat er nog veel meer volgen.

Team endo! Wat een droomteam om onderdeel van te mogen zijn. Samen behaalden we mooie resultaten, gaven we internationale workshops en presentaties en deelden we vooral veel bijzondere momenten, van support tijdens presentaties tot de nodige ontspanning daarna. De avond in de wasmachine was al top, maar karaoke in een kelder in Madrid valt niet te toppen. Annika Goorsenberg, met ons gezamenlijke review, een van mijn eerste projecten, liet je me op een hele fijne manier landen in het team-endo-promotieclubje. Lizzy Wijmans, dank voor je eindeloze geduld om me alles uit te leggen, ik kwam dankzij jou in een gespreid bed van CLE-probes terecht.
Bedankt voor hulp bij projecten en gezelligheid voor Jolanda Kuijvenhoven, Julia d'Hooge, Pieta Wijsman, Tess Kramer, Tatiana Soldati, Sofi Vasilev en Saskia van Heumen.
Marianne van de Pol, onze drijvende kracht. Dank dat je me scherp hield tijdens de monitorbezoeken en tegelijk altijd praktisch meedacht.
Team-endo is niets zonder endoscopieverpleegkundigen. Dank jullie wel voor jullie eindeloze geduld en hulp als wij weer eens met een CLE of OCT probe aan kwamen zetten, of beter nog: allebei!
Margherita Vaselli, thank you for all your help and patience. And thank you for explaining the technical parts over and over again. Working with you was a pleasure, I wish you all the best for the future, both professionally and on a personal level.
Laura van Huizen, jouw bijdrage aan dit proefschrift is enorm. Het was superfijn om met je samen te werken, ook als je weer eens geduld moest hebben met mijn stukken. Ik hoop dat we ook na mijn PhD nog mooie projecten samen kunnen doen.

Marloes Groot, Johannes de Boer, Daniel de Bruin, Paul Bloemen, dank voor alle technische hulp, begeleiding, creatieve oplossingen en scherpe blik.

Jurgen Hetzel and Venerino Poletti, the godfathers of cryobiopsy. Jürgen, thank you for your inspiration and guidance throughout our COLD experience, from the memorable cryobiopsy workshops in Tübingen to our many valuable conversations. Venerino, thank you for your enthusiasm and your never-ending energy for our projects. Your knowledge has been invaluable for my thesis. I hope we will keep working together in the future.

Teodora Radonic en Jan von der Thüsen, mijn steun en toeverlaten bij de interpretatie van PA-plaatjes. Dank voor jullie scherpe blik, geduldige uitleg en het steeds weer meedenken over de HHG-beelden. Dat was enorm leerzaam en waardevol.

Marcel Dijkgraaf, de urenlange telefoongesprekken over eindpunten, vragenlijsten, statistiek en rebuttals hebben tot een prachtig eindresultaat geleid. Jouw mentorschap hierin waardeer ik enorm.

Collega's van de radiologie, in het bijzonder Inge van de Berk en Onno Mets, dank voor het herbeoordelen van CT's en voor jullie radiologische bijdragen aan verschillende artikelen.

Longartsen van het Amsterdam UMC, dank voor al jullie begeleiding en steun, de koffiemomentjes, opbeurende woorden en lieve begeleiding. In het bijzonder Els Weersink, aan wie ik veel heb gehad op moeilijke momenten. René Jonkers, dank voor de waardevolle gesprekken, je hulp en het vertrouwen dat je in mij had. Hans Daniels, dank voor je begeleiding in meerdere studies, je laagdrempeligheid en natuurlijk voor het uitkiezen van de beste borrelplek in Milaan.
Team ILD: Esther Nossent, Bart Boerrigter, Suzan Nijman en Robert-Jan Slager. Dank voor jullie hulp bij het includeren van studiepatiënten en voor de kennis die jullie met me wilden delen. Esther, jouw kennis en drive zijn bewonderenswaardig, maar de momenten tussen het werk door waardeer ik het meest.

Longartsen van het Dijklander Ziekenhuis, Dorothée de Fraiture, Duco Schippers, Geert Rootmensen, Jorn Vos, Karen Maassen, Marian Tiemessen, Marjolein van Laren, Nick Wagemaker, Roald Roeleveld en Verina van Diepen. Dank jullie wel voor jullie juichmomenten en het vertrouwen dat jullie in mij hebben als collega.

Longartsen van het Spaarne Gasthuis, bij jullie mocht ik mijn carrière als longarts starten. Dank voor jullie begeleiding, inspiratie en vertrouwen. In het bijzonder Ivo van der Lee en Frans Krouwels: Ivo, dank voor je steun om het promotiepad op te gaan, en voor het opvangen toen ik flauwviel! Frans, dank voor de fijne gesprekken en het meedenken over mijn carrière.

Een speciale dank aan mijn mede-AIOS, die inmiddels al lang geen AIOS meer zijn, en die allemaal op hun eigen manier hebben bijgedragen aan

dit proefschrift. In het bijzonder dank ik uit deze groep Lieuwe Bos en Daniel Korevaar. Daniel, jouw bijdrage aan dit proefschrift is onmisbaar. Dank voor de tijd die je hebt genomen om altijd mee te denken, en om ingewikkelde zaken goed te verwoorden en uit te leggen. Lieuwe, heel veel dank voor al jouw input in ons CLE-project op de IC, voor je snelle reacties en voor het meedenken in oplossingen.

Mijn lieve vrienden en vriendinnen. Zonder jullie support, maar vooral ook zonder de fijne gesprekken, ontspanning, humor en lichtheid die jullie brengen, was dit traject een stuk zwaarder geweest. In het bijzonder: Annemarije de Ruiter, Nienke Blokhuis, Marije Reniers en Edwin de Goey. Dank dat jullie er altijd zijn, ook als we elkaar even minder vaak zien. Kate Adams en Judith Dudok, dank voor onze vele Barbie-momenten.

Mijn familie, papa en mama, dank voor jullie grenzeloze liefde en vertrouwen in mij. Dank dat jullie altijd voor ons klaarstaan en helpen. Martha, dank voor het vertrouwen en voor de lieve en trotse woorden die nooit onder stoelen of banken worden geschoven.

Isabella en Eveline, mijn lieve meisjes. Dank voor jullie steun. Dat jullie me uren achter elkaar achter de computer hebben laten werken. Dat jullie me oneindig veel knuffels en kusjes geven. Dank voor de prachtige doctor-taart die jullie maakten om me te supporten. Isabella, dank voor jouw vragen over wat ik nou eigenlijk aan het doen ben en wat dit onderzoek betekent. En dat je ook nog aandachtig luisterde naar het antwoord. Eveline, dank voor jouw mooie regenboogtekening die ik in meerdere presentaties heb kunnen laten zien, en die geïnspireerd was op de PS-OCT-kleuren. Die regenboogkleuren zijn uiteindelijk ook inspiratie geworden voor de cover van dit proefschrift.

Ralph. Babe. Zonder jou was dit proefschrift er nooit gekomen. Ik kan niet uitspreken hoeveel jouw support voor mij betekent. Hoe vaak jij thuis dingen hebt overgenomen zodat ik een presentatie kon afmaken, een artikel kon schrijven of gewoon even door kon werken. Maar bovenal kan ik met niemand anders zoveel lol hebben en van het leven genieten als met jou en laat je me voelen hoe trots je op mij bent. Ik hou van jou.